EFFECTS OF ULTRAFINES ON THE HYDRODYNAMICS OF GAS FLUIDIZED BEDS

by

Firoozeh Zahraei

A thesis submitted for the degree of
Doctor of Philosophy
at
University College London

Department of Chemical and Biochemical Engineering
University College London
Torrington Place
London WC1E 7JE

September 1994

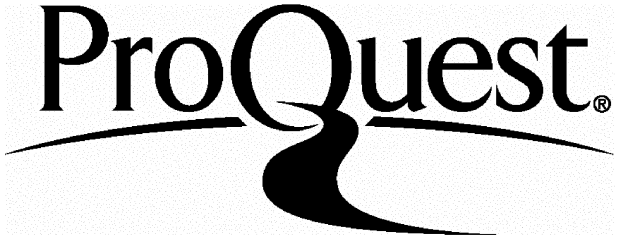

ABSTRACT

It has been reported in the literature that the addition of small quantities of so called fines (usually defined as particles less than 10μm in diameter) to Group A/C and B materials can significantly change the fluidization characteristics of the host materials; e.g. suppress bubbling, cause very large bed expansions and reduce elutriation from the bed. This change in fluidization behaviour can be linked to the physical properties of the material.

The aim of this project was to study, by a combination of experiments, the changes in fluidization behaviour of typical Group A and C materials with increasing quantities of ultrafines. The work was divided into two sections: (i) fluidization and (ii) systematic study of properties relevant to it. The fluidization experiments mainly consisted of measurements of minimum fluidization and minimum bubbling velocities as well as the bed expansion for a range of bed conditions. Bed collapse experiments were also carried out to determine the dense phase expansion together with the expansion due to bubbles. The latter basically included measurements of physical properties such as particle size and its distribution, pore size distribution and various densities of powders for several combinations of ultrafines and host materials.

Cracking catalyst (FCC), silica and kieselguhr were the host materials while a range of fumed silica were used as the ultrafine in the experiments. Additives appeared to have a considerable effect on FCC and silica by increasing the expansion up to 50%, increasing the deaeration velocity and reducing the elutriation loss while the fluidization was much smoother in general. The data obtained with kieselguhr, a typical Group C material, indicated that under some conditions, the presence of the additives resulted in significant increases in bed expansion and improved the fluidization behaviour. The extent of these effects appeared to depend on the concentration of the ultrafines.

Additives appeared to change the fluidization behaviour of the material by forming a particular network which leads to a looser bed structure. Different predictive criteria for transition from particulate to aggregate fluidization were used and compared to the experimental data. It was concluded that as well as the hydrodynamic effects, interparticle forces were of importance in the stability of the bed.

ACKNOWLEDGEMENTS

It is a pleasure to thank my supervisors Professor John G Yates and Dr Parviz Ayazi Shamlou for their expert support, guidance and advice throughout this work.

I wish to thank Dr David Newton for his contributions.

I would also like to thank BP Research for their financial support.

Special thanks are due to Mr David J Cheesman for his kind help throughout this work, specially during X–ray experiments.

I am indebted to Dr S Carrigan and Dr W Towlson, Department of Physics, UCL, for their help and advice and providing the electrometer.

I am grateful to Dr Andrzej Gierczycki for his kind assistance.

A special word of appreciation is due to all the technical staff of the Departmental Workshop for constructing the experimental apparatus and also their helpful support and advice.

Finally, I would like to express my appreciation to my family who encouraged me throughout my graduate studies. Special thanks is given to my sister, Sohayla for her love and support which made most days brighter.

To the loving memory of my mother
for her endless support, encouragement and enthusiasm
throughout my life.

TABLE OF CONTENTS

Abstract	2
Acknowledgements	4
Table of Contents	6
List of Tables	9
List of Figures	10
CHAPTER ONE: INTRODUCTION	18
CHAPTER TWO: LITERATURE SURVEY	26
2.1. General States of Fluidization	26
2.2. Minimum Fluidization Velocity	28
2.3. Bubbles	32
2.4. Entrainment and Elutriation	35
2.5. Description of Powder Groups	37
2.6. Channelling	40
2.7. Interparticle Forces	41
2.7.1. Van der Waals Forces	44
2.7.2. Electrostatic Forces	48
2.7.3. Capillary Forces	52
2.7.4. Electromagnetic Forces	53
2.7.5. Measurement of Interparticle Forces	54
2.8. Transition from Particulate to Aggregate Fluidization	61
2.9. Richardson–Zaki Parameters	68
2.10. Multicomponent Fluidized Beds	70
2.11. Effects of Fines on Fluidization	73
2.13. Conclusions	86
CHAPTER THREE: MATERIALS AND METHODS	88
3.1. Materials	88
3.2. Equipments and Methods	92

3.2.1. Obseravtion of Powders by SEM 92
3.2.2. Sample Preparation 94
3.2.3. Particle Size Measurements 95
3.2.3.1. Sieving 95
3.2.3.2. Malvern 96
3.2.3.3. Elzone 97
3.2.4. Surface Area and Porosity 98
3.2.5. Bulk Density 104
3.2.6. Skeletal Density 104
3.2.7. Particle Density 105
3.2.8. Particle Charge 106
3.2.9. Viscosity Measurement 107
3.2.10. Fluidization Experiments 110
3.2.11. Bed Collapse Experiments 112
3.3. Propagation of Errors 115

CHAPTER FOUR: RESULTS AND DISCUSSIONS 116

4.1. Morphology of Powders 116
4.2. Measurement of Physical Properties 136
4.2.1. Porosity and Surface Area 136
4.2.2. Bulk Density 144
4.2.3. Skeletal Density 147
4.2.4. Particle Density 150
4.2.5. Particle Charge 150
4.2.6. Viscosity of CAB–O–SIL 151
4.2.7. Discussions 152

4.3. Fluidization 154
4.3.1. Effect of Bed Diameter 154
4.3.2. Fluidization of Ultrafines 157
4.3.3. Fluidization of FCC 157
4.3.4. Fluidization of Silica 170
4.3.5. Fluidization of Kiesel–1 181
4.3.6. Fluidization of Kiesel–2 193
4.3.7. Discussions 199

4.4. Bed Collapse Experiments 202
4.4.1. Bed Collapse of FCC 202
4.4.2. Bed Collapse of Silica 213
4.4.3. Discussions 219

4.5. Stability of Fluidized Beds 222
4.5.1. Density and Viscosity of the Continuous Phase 222
4.5.2. Richardson–Zaki Parameters 227
4.5.3. Foscolo–Gibilaro's model 232
4.5.4. Mutsers–Rietema's model 239
4.5.5. Reiling's model 243
4.5.6. Discussions 247

CHAPTER FIVE: CONCLUSIONS AND RECOMMENDATIONS FOR FURTHER STUDY 250

5.1. Conclusions 250
5.2. Recommendations for Further Study 253
Appendix A: Derivation of Reiling's model 254A
Nomenclature 255

References 260

List of Tables

Table 3.1. Physical properties of FCC and Silica. 91

Table 4.2.1. Effect of addition of CAB–O–SIL on physical properties of FCC. 138

Table 4.2.2. Effect of addition of CAB–O–SIL on physical properties of silica. 139

Table 4.2.3. Effect of addition of S1 fumed silica on physical properties and fluidization of kiesel–1. 140

Table 4.2.4. Effect of addition of CAB–O–SIL on physical properties and fluidization of kiesel–2. 141

Table 4.3.1. Effect of addition of CAB–O–SIL on fluidization behaviour of FCC. 165

Table 4.3.2. Effect of CAB–O–SIL on the normalized pressure drop of FCC mixtures. 169

Table 4.3.1. Effect of addition of CAB–O–SIL on fluidization of silica. 176

Table 4.3.4. Effect of CAB–O–SIL on the normalized pressure drop of silica mixtures. 180

Table 4.4.1. Calculation of bed expansion and voidages of FCC with different CAB–O–SIL concentrations. 206

Table 4.4.2. Calculation of bed expansion and voidages of FCC with 2.5% CAB–O–SIL at different flow rates. 212

Table 4.4.3. Calculation of bed expansion and voidages of silica with different CAB–O–SIL concentrations. 217

Table 4.5.1. Calculation of fluid density and viscosity for mixtures of FCC and CABOSIL. 224

Table 4.5.2. Calculation of fluid density and viscosity for mixtures of silica and CABOSIL. 225

Table 4.5.3. Richardson–Zaki parameters for FCC mixtures. 228

Table 4.5.4. Richardson–Zaki parameters for Silica mixtures. 228

Table 4.5.5. Calculation of terminal velocity of FCC mixtures using Kunii–Levenspiel method and also Stoke's law. 229

Table 4.5.6. Calculation of terminal velocity of silica mixtures using Kunii–Levenspiel method and also Stoke's law. 229

Table 4.5.7. Calculation of ε_b using Foscolo–Gibilaro model for FCC. 235

Table 4.5.8. Calculation of ε_b using Foscolo–Gibilaro model for silica. 236

Table 4.5.9. Calculation of ε_b using Mutsers–Ritema model for FCC. 240

Table 4.5.10. Calculation of ε_b using Mutsers–Ritema model for silica. 241

Table. 4.5.11. Calculation of ε_b using Reiling's model for FCC. 244

Table 4.5.12. Calculation of ε_b using Reiling's model for silica. 245

List of Figures

Fig. 2.1. Pressure drop through the bed as a function of gas velocity. 28

Fig. 2.2. Variation of minimum fluidization velocity with bed thickness (Rowe and Everett, 1972). 31

Fig. 2.3. Entrainment and elutriation (Yates, 1983). 36

Fig. 2.4. Powder classification diagram for fluidization by air –ambient conditions (Geldart, 1973). 37

Fig. 2.5. Cavity structure of the dense phase suggested by Massimilla et al. (1972). 56

Fig. 2.6. Fluidized bed stabilization by interparticle forces: the full line represents the continuity wave velocity, $U\varepsilon$, and broken lines represent dynamic wave velocities, Ue, for increasing values of interparticle forces. 65

Fig. 2.7. Graphical representation of ΔP^*mb, the hypothetical bed ΔP at the incipient bubbling velocity used in the transition criterion of Reiling (1992). 67

Fig. 2.8. Relationship between bed pressure drop and gas velocity; F: fluidized, P: packed (Nienow and Chiba, 1985). 72

Fig. 3.1. Size distribution of FCC. 89

Fig. 3.2. Size distribution of silica. 89

Fig. 3.3. Size distribution of kiesel–1. 90

Fig. 3.4. Size distribution of kiesel–2. 90

Fig. 3.5. Schematic diagram of Omnisorp 100. 99

Fig. 3.6. Schematic diagram of mercury porosimeter. 102

Fig. 3.7. Schematic representation of the experimental apparatus for particle charge measurement. 107

Fig. 3.8. Stress–strain relationship for Newtonian and non–Newtonian fluids (Welty et al., 1984). 108

Fig. 3.9. Schematic diagram of the viscometer. 109

Fig. 3.10. Schematic diagram of the fluidized beds. 111

Fig. 3.11. Typical bed collapse curve; gas flow is suddenly interrupted at t = 0. 113

Fig. 3.12. Schematic diagram of the bed collapse set–up (Not to scale). 114

Fig. 4.1.1. CAB–O–SIL (× 100). 119

Fig. 4.1.2. CAB–O–SIL (× 10,000). 119

Fig. 4.1.3. FCC with no additive (× 100). 120

Fig. 4.1.4. FCC with no additive (× 3000). 120

Fig. 4.1.5. FCC with 1% CAB–O–SIL (× 100). 121

Fig. 4.1.6. FCC with 1% CAB–O–SIL (× 3000). 121

Fig. 4.1.7. FCC with 2.5% CAB–O–SIL (× 100). 122

Fig. 4.1.8. FCC with 2.5% CAB–O–SIL (× 3000). 122

Fig. 4.1.9. FCC with 5% CAB–O–SIL (× 100). 123

Fig. 4.1.10. FCC with 10% CAB–O–SIL (× 100). 123

Fig. 4.1.11. FCC with 5% CAB–O–SIL before fluidization (× 950). 124

Fig. 4.1.12. FCC with 5% CAB–O–SIL after fluidization (× 3000). 124

Fig. 4.1.13. FCC with 15% CAB–O–SIL (× 100). 125

Fig. 4.1.14. S1 fumed silica (× 10,000). 125

Fig. 4.1.15. Silica with no additive (× 100). 126

Fig. 4.1.16. Silica with no additive (× 10,000). 126

Fig. 4.1.17. Silica with 1% CAB–O–SIL (× 100). 127

Fig. 4.1.18. Silica with 1% CAB–O–SIL(× 10,000). 127

Fig. 4.1.19. Silica with 2.5% CAB–O–SIL (× 100). 128

Fig. 4.1.20. Silica with 5% CAB–O–SIL (× 100). 128

Fig. 4.1.21. Silica with 15% CAB–O–SIL (× 100). 129

Fig. 4.1.22. Silica with 15% CAB–O–SIL (× 10,000). 129

Fig. 4.1.23. Kiesel–1 with no additive (× 1000). 130

Fig. 4.1.24. Kiesel–1 with no additive (× 2000). 130

Fig. 4.1.25. Kiesel–1 with 1% S1 fumed silica (× 3000). 131

Fig. 4.1.26. Kiesel–1 with 1% S1 fumed silica (× 7000). 131

Fig. 4.1.27. Kiesel–1 with 3% S1 fumed silica (× 1000). 132

Fig. 4.1.28. Kiesel–1 with 3% S1 fumed silica (× 3500). 132

Fig. 4.1.29. Kiesel–2 with no additive (× 1000). 133

Fig. 4.1.30. Kiesel–2 with 1% CAB–O–SIL (× 1500). 133

Fig. 4.1.31. Kiesel–2 with 2% CAB–O–SIL (× 3000). 134

Fig. 4.1.32. Kiesel–2 with 3% CAB–O–SIL (× 1600). 134

Fig. 4.1.33. Kiesel–2 with 4% CAB–O–SIL (× 3000). 135

Fig. 4.1.34. Kiesel–2 with 5% CAB–O–SIL (× 1000). 135

Fig. 4.2.1. Effect of CAB–O–SIL on the total pore volume of FCC. 137

Fig. 4.2.2. Effect of CAB–O–SIL on the total pore volume of silica. 137

Fig. 4.2.3. Effect of CAB–O–SIL on the BET surface area of FCC. 143

Fig. 4.2.4. Effect of CAB–O–SIL on the BET surface area of silica. 143

Fig. 4.2.5. Effect of CAB–O–SIL on the bulk density of FCC. 145

Fig. 4.2.6. Effect of CAB–O–SIL on the bulk density of silica. 145

Fig. 4.2.7. Effect of CAB–O–SIL on the bulk density of Kiesel–1. 146

Fig. 4.2.8. Effect of CAB–O–SIL on the bulk density of Kiesel–2. 146

Fig. 4.2.9. Effect of CAB–O–SIL on the skeletal density of FCC. 148

Fig. 4.2.10. Effect of CAB–O–SIL on the skeletal density of silica. 148

Fig. 4.2.11. Skeletal density of Kiesel–1 with different CAB–O–SIL concentrations. 149

Fig. 4.2.12. Skeletal density of Kiesel–2 with different CAB–O–SIL concentrations. 149

Fig. 4.2.13. Determination of the viscosity of CAB–O–SIL. 151

Fig. 4.3.1. Fluidization of Ballotini in the 10 cm bed. 155

Fig. 4.3.2. Fluidization of Ballotini in the 5 cm bed. 156

Fig. 4.3.3. Fluidization of FCC. 159

Fig. 4.3.4. Fluidization of FCC with 1% CAB–O–SIL. 160

Fig. 4.3.5. Fluidization of FCC with 2.5% CAB–O–SIL. 161

Fig. 4.3.6. Fluidization of FCC with 5% CAB–O–SIL. 162

Fig. 4.3.7. Fluidization of FCC with 10% CAB–O–SIL. 163

Fig. 4.3.8. Fluidization of FCC with 15% CAB–O–SIL. 164

Fig. 4.3.9. Effect of CAB–O–SIL addition on U_{mf} and/or U_{mb} of FCC. 167

Fig. 4.3.10. Effect of CAB–O–SIL on the expansion of FCC. 167

Fig.4.3.11. Effect of CAB–O–SIL on the bed voidage of FCC. 168

Fig.4.3.12. Effect of CAB–O–SIL on the normalized pressure drop of FCC mixtures. 168

Fig.4.3.13. Fluidization of silica. 171

Fig.4.3.14. Fluidization of silica with 1% CAB–O–SIL. 172

Fig.4.3.15. Fluidization of silica with 2.5% CAB–O–SIL. 173

Fig.4.3.16. Fluidization of silica with 5% CAB–O–SIL. 174

Fig.4.3.17. Fluidization of silica with 10% CAB–O–SIL. 175

Fig.4.3.18. Fluidization of silica with 15% CAB–O–SIL. 176

Fig.4.3.19. Effect of CAB–O–SIL on the U_{mf} and U_{mb} of silica. 178

Fig.4.3.20. Effect of CAB–O–SIL on the bed expansion of silica. 178

Fig.4.3.21. Effect of CAB–O–SIL on the bed voidage of silica. 179

Fig.4.3.22. Effect of CAB–O–SIL on the normalized pressure drop of silica. 179

Fig.4.3.23. Fluidization of kiesel–1 with 1% S1 fumed silica in the 5 cm bed. 183

Fig.4.3.24. Fluidization of kiesel–1 with 2% S1 fumed silica in the 5 cm bed. 184

Fig.4.3.25. Fluidization of kiesel–1 with 3% S1 fumed silica in the 5 cm bed. 185

Fig.4.3.26. Fluidization of kiesel–1 with 4% S1 fumed silica in the 5 cm bed. 186

Fig.4.3.27. Fluidization of kiesel–1 with 5% S1 fumed silica in the 5 cm bed. 187

Fig.4.3.28. Fluidization of kiesel–1 with 1% S1 fumed silica in the 10 cm bed. 188

Fig.4.3.29. Fluidization of kiesel–1 with 2% S1 fumed silica in the 10 cm bed. 189

Fig.4.3.30. Fluidization of kiesel–1 with 3% S1 fumed silica in the 10 cm bed. 190

Fig.4.3.31. Fluidization of kiesel–1 with 4% S1 fumed silica in the 10 cm bed. 191

Fig.4.3.32. Fluidization of kiesel–1 with 5% S1 fumed silica in the 10 cm bed. 192

Fig.4.3.33. Fluidization of kiesel–2 with 1% CAB–O–SIL. 194

Fig.4.3.34. Fluidization of kiesel–2 with 2% CAB–O–SIL. 195

Fig.4.3.35. Fluidization of kiesel–2 with 3% CAB–O–SIL. 196

Fig.4.3.36. Fluidization of kiesel–2 with 4% CAB–O–SIL. 197

Fig.4.3.37. Fluidization of kiesel–2 with 5% CAB–O–SIL. 198

Fig.4.3.38. Effect of CAB–O–SIL on delayed bubbling of FCC. 201

Fig.4.3.39. Effect of CAB–O–SIL on delayed bubbling of silica. 201

Fig. 4.4.1. Bed collapse of FCC. 203

Fig. 4.4.2. Bed collapse of FCC with 1% CAB–O–SIL. 203

Fig. 4.4.3. Bed collapse of FCC with 2.5% CAB–O–SIL. 204

Fig. 4.4.4. Bed collapse of FCC with 5% CAB–O–SIL. 204

Fig. 4.4.5. Bed collapse of FCC with 10% CAB–O–SIL. 205

Fig. 4.4.6. Bed collapse of FCC with 15% CAB–O–SIL. 205

Fig. 4.4.7. Effect of CAB–O–SIL on different expansions of FCC. 209

Fig. 4.4.8. Effect of CAB–O–SIL on the bed voidage of FCC. 209

Fig. 4.4.9. Effect of initial flow rate on the bed collapse of FCC with 2.5% CAB–O–SIL. 210

Fig. 4.4.10. Effect of air flow rate on bed expansion of FCC with 2.5% CAB–O–SIL. 211

Fig. 4.4.11. Effect of air flow rate on the bed voidage of FCC with 2.5% CAB–O–SIL. 211

Fig. 4.4.12. Bed collapse of silica. 214

Fig. 4.4.13. Bed collapse of silica with 1% CAB–O–SIL. 214

Fig. 4.4.14. Bed collapse of silica with 2.5% CAB–O–SIL. 215

Fig. 4.4.15. Bed collapse of silica with 5% CAB–O–SIL. 215

Fig. 4.4.16. Bed collapse of silica with 10% CAB–O–SIL. 216

Fig. 4.4.17. Bed collapse of silica with 15% CAB–O–SIL. 216

Fig. 4.4.18. Effect of CAB–O–SIL on different expansions of silica. 218

Fig. 4.4.19. Effect of CAB–O–SIL on different bed voidages of silica. 218

Fig. 4.4.20. Effect of CAB–O–SIL on the deaeration velocity of FCC and silica. 220

Fig. 4.4.21. Comparison of different expansions of FCC mixtures. 221

Fig. 4.4.22. Comparison of different expansions of silica mixtures. 221

Fig. 4.5.1. Effect of CAB–O–SIL on the fluid density of continuous phase. 226

Fig. 4.5.2. Effect of CAB–O–SIL on the viscosity of continuous phase. 226

Fig. 4.5.3. Terminal velocity of FCC using different methods. 231

Fig. 4.5.4. Terminal velocity of silica using different methods. 231

Fig. 4.5.5. Comparison of Foscolo–Gibilaro's model to the experimental values of bed voidage for FCC. 233

Fig. 4.5.6. Comparison of Foscolo–Gibilaro's model to the experimental values of bed voidage for silica. 233

Fig. 4.5.7. Predicted values of bed voidage for different terminal velocities using Foscolo–Gibilaro model (n = 4.8) for FCC. 237

Fig. 4.5.8. Predicted values of bed voidage for different terminal velocities using Foscolo–Gibilaro model (n = 4.8) for silica. 237

Fig. 4.5.9. Effect of n values on terminal velocities of FCC mixtures using Foscolo–Gibilaro's model. 238

Fig. 4.5.10. Effect of n values on terminal velocities of silica mixtures using Foscolo–Gibilaro's model. 238

Fig. 4.5.11. Comparison of the experimental bed voidage to Mutsers–Rietema's model for FCC. 242

Fig. 4.5.12. Comparison of the experimental bed voidage to Mutsers–Rietema's model for silica. 242

Fig. 4.5.13. Comparison of the experimental bed voidage to Reiling's model for FCC. 246

Fig. 4.5.14. Comparison of the experimental bed voidage to Reiling's model for silica. 246

Fig. 4.5.15. Comparison of experimental bed voidage with different predictions for FCC mixtures. 249

Fig. 4.5.16. Comparison of experimental bed voidage with different predictions for silica mixtures. 249

CHAPTER ONE

INTRODUCTION

Application of fluidization to various reactions has been one of the outstanding achievements in chemical engineering in the last decades. The majority of fluidized beds involve gas–solid systems. Industrial fluidized beds operate at a wide range of bed diameters, gas velocities, temperatures and pressures. Since fluidization is possible over a wide range of gas flow rates, the optimum contact time or residence time of the fluid phase reactant in a catalyst bed can be selected.

Examples of commercial processes are manufacture of gasoline from petroleum fractions (fluid catalytic crackers), coal (fluid bed coal gasifiers), natural and synthesis gas, metallurgical processes like roasting of ore, chlorination of hydrocarbons, etc. Main applications include physical contacting processes like heat transfer, solids mixing, classification of particles, drying, food freezing, ... New applications include production of granular polyethylene by gaseous polymerization of ethylene, production of ultrapure silicon and its precursors for the semiconductor industry, cultivation of microorganisms in the food and pharmaceutical industries (Kunii and Levenspiel, 1991) and production of detergents with superb cleaning capabilities.

The first large scale application of fluidized beds was the fluid cracking process developed by Esso Research and Development in 1942 (Matheson et al., 1949). Since then, well over a thousand patents on application of the fluidized bed technique have been granted (Newton, 1984).

Fluidized beds are hydrodynamically more complex than competing gas–solid contactors like fixed bed (packed bed) and transport reactors. However, they have become more attractive in recent years based on their advantages over fixed beds reactors which include better temperature uniformity and control, good particle mixing, ability to move solids in and out of the reactor, adaptability to elevated temperature and pressure, simple equipment construction and lower capital and operating cost. Disadvantages of fluidization include the large deviation from plug flow due to bubbles. This is a significant problem for catalytic reactions where high conversion of gaseous reactors or high selectivity of intermediate product is required. On the other hand, rapid mixing of solids leads to a nonuniform residence time of solids in the reactor and difficult to describe gas flow patterns (Kunii and Levenspiel, 1991).

There are two distinct fluidization modes: (a) homogeneous or particulate fluidization which is characterized by the absence of bubbles and similar to a traditional liquid–solid system and (b) bubbling or aggregate fluidization which involves distinct pressure fluctuations (Harrison et al., 1961; Martin, 1983). Bubbles and continuous movement of porous catalyst particles contribute to the backmixing of gaseous reactant which lead to poorer performance. A particulate fluidized bed, would therefore be an ideal contacting device. However, particulate fluidization can mainly be achieved in solid–liquid systems and with gas–solid systems particulate fluidization is difficult.

According to two–phase theory (Toomey and Johnstone, 1952), all the gas in excess of that necessary to just fluidized the bed passes through in the form of bubbles, although there is continuous interchange of gas between the bubble phase and the emulsion phase. Gas is continuously flowing through bubbles or voids which causes solid movement and agitation of the bed and ensures that the particles are well mixed. Rapid mixing of solids leads to good temperature uniformity and uniform solids composition which promotes heat transfer between the bed particles

and heat transfer surfaces. Therefore fluidized beds are ideal contactors for strongly endothermic or exothermic reactions (Dry and Potter, 1986).

Finer particles can be used which have a greater amount of transfer surface area per unit volume of the fluidized bed. Hence, there is a high rate of heat and mass transfer between gas and solid particles compared with other modes of bed contacting.

A fluidized bed can be characterized by various parameters such as bed expansion, bubble size and frequency, magnitude of pressure fluctuations, gas and solid mixing and bed stability. Values of these quantities determine the *quality* of fluidization. The bed expansion is related to the emulsion phase porosity, which depends on the amount of gas dispersed in the solid phase. An increase in bed expansion implies that more gas is present in the emulsion phase and results in improved gas to solid contact. As the fluidizing gas rate is further increased, gas by-passes the bed in the form of bubbles which results in fluctuations in the pressure drop and bed height. Bubbles are advantageous in that they serve as the mechanism for gas mixing and heat transfer. However, if too large, they impede mass transfer in chemical reaction processes. Generally, it is preferred to limit the bubble size in order to lessen the degree of gas by-passing, but still maintain good gas/solid mixing. Different powders behave differently in this respect (see section 2.5 for Geldart's classification).

Various methods have been reported in the literature for controlling these parameters like bubble size which include:

a) Improving the grid design; it is believed that a greater number of smaller orifices leads to smaller bubbles and improved performance. However, even with an efficient grid design, large voids can still be present due to bubble coalescence, especially in deep beds (Geldart and Baeyens, 1984; Zenz, 1968; Yates et al., 1986).

b) Introducing internal structures into the bed to break up bubbles and increase the gas residence time and surface area. Internal structures include horizontal and vertical tubes, rods, baffles, perforated plates, screens, sieve trays, and special devices like bubble collectors and floating bubble breakers. These methods have not been altogether successful, specially in large commercial sized units. Most of the devices used inhibit heat transfer and lead to a loss of temperature uniformity; (Harrison and Grace, 1971; Mori et al., 1980; Rooney and Harrison, 1976).

c) Operating the fluid bed reactor at a gas velocity either very close to the minimum fluidization velocity or on the other hand, operate at sufficiently high gas velocities so that there is a parallel entrainment of solids (Grace, 1986). Either of these modes approximate gas piston type flow. Operating at the minimum fluidization velocity is impractical from an economic point of view and operating above the particle entrainment velocity either results in too short a contact time to achieve desired conversions, or requires an extremely active catalyst.

d) Modification of powder properties and thereby improving the fluidization quality*, gas/solid contact, and performance of the catalyst which is the subject of this thesis and will be briefly discussed here.

One way of modifying powder properties is to either use a wide size distribution (Geldart, 1972; Jean et al., 1990; Sun and Grace; 1990) or to increase the fraction of fines (Geldart and Abrahamsen, 1980; Jones et al., 1980; Newton, 1984; Pell and Jordan, 1988; Rowe and Yacono, 1976; Yates and Newton, 1986). *Fines* content is usually defined as the fraction of particles that can be separated by the smallest available screen, normally 325 or 400 mesh; i.e. 44 or 37 μm (Grace and Sun, 1991). Addition of fines improved the quality of fluidization (Jones et al., 1980), increased the conversion per unit residence time of gas (Pell and Jordan, 1988; Yates and Newton, 1986), reduced bubble flow rate (Jean et al., 1990), increased bed expansion and

* See p. 20 for quality of fluidization.and section 2.5 for Geldart's classification.

reduced particle elutriation (Kono et al, 1985; Kono et al, 1989) and changed the shape of bubbles from conventional *spherical cap* to smaller *cat's fingerprint.*

Most researchers have added particles to fluidized beds in the range of 10–45 μm. Few tried using so called superfines or ultrafines to improve performance. Particles are said to be *ultrafine* when their diameters are in the range of 0.1–10 μm, *superfine* when diameters are between 1–10 μm, *fine* when 10–100 μm and *granular* above 100 μm (Carr, 1970). Use of ultrafines in fluidization appears to be a relatively new and unique application on fluidization. Ultrafines, a class of Geldart Group C Powders, have attracted little attention due to their cohesivity and difficulty in becoming fluidized. The hydrodynamic performance of these particles by themselves are poor due to the large interfacial cohesion forces. Interest in ultrafines, has only increased recently (Dry et al., 1983) stimulated by commercial processes which wish to make use of them (Geldart et al., 1984) like production of silicon nitride. Silicon nitride has been recognized as a potential material to be used for composing future automobile engines and high temperature gas turbines to increase their thermal efficiencies (Liu and Kimura, 1993). Current processes for producing silicon nitride powder include direct nitridation of silicon powder which is projected to be most economical but is still of the costly batch type. For the continuous production of high quality silicon nitride powder at a reasonable cost, the application of fluidized bed reactors have been considered (Shimizu et al., 1991).

From a viewpoint of kinetics of silicon nitridation, the smaller the size of the silicon particles, the faster the reaction. However, because of the difficulties of fluidizing fine particles, specially prepared large silicon particles which are porous, being composed of fine silicon grains of a few microns in size, have been used as an alternative method (Shimizu et al., 1991; Jovanovic et al., 1992). Since product silicon nitride should be

fine enough to be ready for sintering ($d_p < 1\mu m$), large porous silicon nitride particles obtained from porous silicon need to be pulverized into fine powder. Hence, the direct use of fine silicon powder in a continuous fluidized bed system would be of great advantage over the use of pre–treated large particles because (a) processes to prepare large porous particles would be eliminated, (b) the conversion of silicon into silicon nitride would be faster, (c) the necessary residence time for the reactant silicon particles would be shorter leading to the reduction of reactor size and (d) product silicon nitride powder could be used as a raw material for sintering without being pulverized intensively. The experimental results by some investigators leads to the possibility of the direct use of silicon fine powder to produce silicon nitride in a fluidized bed reactor by mixing silicon powder with large inert fluidizable particles.

It has also been mentioned in literature* that there is an *optimum* additive concentration where the effective coverage of the particle surface is obtained. The optimum concentration is not necessarily fixed for a given additive and it may well be a function of the host powder and additive physico-chemical properties. It may also be influenced by segregation of the additive particles in extremely dry host powders or by its uneven distribution in case of cohesive powders. At this critical concentration parameters such as density or Hausner ratio** reach an stationary point and further addition of the additive may reverse the desirable effects.

Despite the reports in the literature on the effects of fines on fluidization, not much systematic study has been carried out on the effects of *ultrafines* on the fluidization behaviour of gas–solid systems. No rational explanation for the large bed expansions and improved contacting and particulate–like flow attributed to ultrafine particles has been offered.

* York (1975); Geldart and Wong (1987); Hollenbach et al. (1982).

** The ratio of tapped density to low packed bulk density (Geldart, 1984); see section 2.5.

This project focuses on the effect of the addition of ultrafines on the fluidization behaviour of Group A and C powders. Group A powders were fluid cracking catalyst (FCC) and silica which are widely used in industry. Group C powder used was kieselguhr, a type of silica with a mean particle size of 20–30 μm. Ultrafines were fumed silica with a primary size of 120 Å which agglomerated extensively due to their electrostatic charges. They had a low bulk density and could not be fluidized by themselves.

The aim of the work is to elucidate the mechanism(s) by which the addition of small amounts of ultrafines improve fluidizability of these powders. The work is divided into two sections: (i) systematic study of physical properties of powders and (ii) fluidization. The former basically includes measurements of particle size, size distribution and various densities of powders for several combinations of ultrafines and host materials. The fluidization experiments mainly consist of measurements of minimum fluidization and minimum bubbling velocities as well as the bed expansion for a range of bed conditions.

This thesis is presented in five chapters. Chapter 2 is a general review of recent literature and is divided into several sections. Definition of different states of fluidization, the role of bubbles in fluidization and powder classification of Geldart, common terms such as minimum fluidization velocity, entrainment, elutriation, channelling are discussed. Different interparticle forces, various methods for their measurements and their effects on fluidization are explained. Different models predicting the transition from particulate to aggregate fluidization are presented and compared. Characteristics of multicomponent fluidized beds are explained and a review of the recent literature on the effect of fines on the fluidization behaviour is given.

Chapter 3 describes different experiments which were carried out as well as the materials used and their properties. The results of the experiments are presented and discussed in Chapter 4 which is divided to various sections: measurements relating to physical properties of the powders, fluidization and bed collapse experiments followed by a comparison of results with various stability models predicting transition from particulate to aggregate fluidization. The thesis is concluded and suggestions are given for further study in Chapter 5.

CHAPTER TWO

LITERATURE SURVEY

This chapter is a general review of recent literature and is divided into several sections. Definition of different states of fluidization, the role of bubbles in fluidization and powder classification of Geldart, common terms such as minimum fluidization velocity, entrainment, elutriation, channelling are discussed in sections 2.1 to 2.6. Different interparticle forces, various methods for their measurements and their effects on fluidization are explained in section 2.7. Richardson–Zaki parameters are mentioned in section 2.8 while different models predicting the transition from particulate to aggregate fluidization are presented and compared in section 2.9. Characteristics of multicomponent fluidized beds are explained in section 2.10 and a review of the recent literature on the effect of fines on the fluidization behaviour is given in section 2.11. Finally the chapter is summarized and the reason why further study on the subject is necessary is given.

2.1. General States of Fluidization

Fluidization is the operation by which a bed of solid particles is transformed to a fluid–like state through contact with a gas or liquid. A fluidized bed is normally a cylindrical container in which solids are supported by a porous plate called the *distributor* and fluid is passed through the base in the upward direction. At relatively low flow rates or velocities, the solid particles lie on one another and on the distributor; the fluid merely percolates through the voids between stationary particles. This is the *fixed bed* state. With an increase in fluid velocity, particles move apart and the expansion

continues as the flow rate of the fluid increases until a point is reached at which particles are just suspended in the upward flowing fluid. At this point the drag (frictional) force between particles and fluid, counterbalances the weight of the particles and the bed behaves like a liquid. The bed is said to be in the state of *incipient fluidization.* The superficial gas velocity at which this occurs is called the *minimum fluidization velocity*, U_{mf}, and its value depends on the physical properties of the gas and the solid particles.

It is observed experimentally for many powders that as the velocity is further increased, gas bubbles form within the bed and rise to the surface and burst. At these velocities the bed is divided essentially into two phases; the dense or emulsion phase where gas percolates through and the lean or bubble phase where much of the gas is out of contact with the solids. A further increase in gas velocity leads to more vigorous bubbling with bigger and bigger bubbles appearing at the surface until at some velocity, U_S, the diameter of the surface bubbles becomes equal to the diameter of the containing vessel itself. The bed is then said to be *slugging* and it is characterized by a considerable heaving of the surface with many particles being thrown up into the space above the bed known as the *freeboard.*

Still higher gas velocities result in more and more particles being thrown into the freeboard, with many being transported out of the bed altogether, until at the highest velocities only a low concentration of rapidly moving particles remains in contact with the gas. This is the region of dilute–phase flow sometimes found in pneumatic conveying systems. For a finely divided powder there is evidence for the existence of yet another regime between the regions of slugging and dilute–phase flow which is the so–called *fast fluidization* regime characterized by the highly turbulent motion of the

aggregates or clusters of particles, the volume of which may be some twenty–five percent of the total bed volume.

2.2. Minimum Fluidization Velocity

The gas velocity at which a bed of powder becomes fluidized may be found by measuring the pressure drop across the bed as a function of gas velocity as shown in Fig. 2.1 while the minimum bubbling velocity, U_{mb}, is measured by noting the gas velocity at which the first bubble breaks through the surface when gas flow rate is increased, and/or the velocity at which bubbling ceases when gas flow rate is decreased.

Minimum fluidization velocity is normally found by working from the higher velocities at which the bed is vigorously fluidized down to the lower velocities in order to prevent spurious readings caused by particle interactions in the packed–bed state.

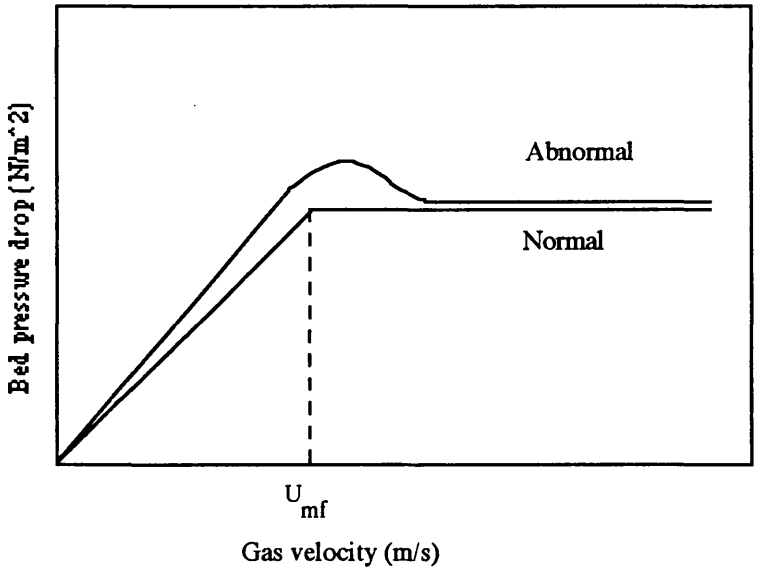

Fig. 2.1. Pressure drop through the bed as a function of gas velocity.

Many powders start to bubble as soon as they reach the minimum fluidization velocity, U_{mf}, which is considered as *normal* fluidization behaviour. Some powders, however, show *abnormal* behaviour and although fluidized, continue to expand uniformly beyond U_{mf}; when U_{mb} is reached the particles collapse and the bed begins to behave more or less normally.

There are a number of well established correlations for the prediction of U_{mf} for a particular powder in terms of the physical properties of the solid particles and the fluidizing gas. They are mostly based on the principle of taking a gas velocity–pressure drop relationship for a packed bed of particles and extending it to the point where the particles become fluidized. One of the most extensively used equations was proposed by Carman–Kozeny (Carman, 1937) as:

$$U = \frac{\varepsilon^3}{180\,(1-\varepsilon)^2}\,\frac{(\phi d_p)^2}{\mu}\,\frac{\Delta P}{H} \qquad (2.1)$$

where U is the gas velocity, ε the bed voidage, ϕ sphericity factor, d_p particle diameter, ΔP pressure drop, μ fluid viscosity and H is the bed height. Sphericity factor ϕ is defined as:

$$\phi = \frac{\text{Surface of sphere of volume equal to that of particle}}{\text{Surface area of particle}} \qquad (2.2)$$

Thus for perfect spheres $\phi = 1$ and for the other shapes $0<\phi<1$.

At the minimum fluidization point, the force applied to the bed by the fluid is equal to the gravitational force acting on the particles:

$$\frac{\Delta P}{H_{mf}} = (1-\varepsilon_{mf})(\rho_p - \rho_g)g \qquad (2.3)$$

where ε_{mf} is the void fraction at minimum fluidization velocity and ρ_p and ρ_g are the solid and gas densities respectively. Comparing equations (2.1) and (2.3) and rearranging the result, the minimum fluidization velocity may be found:

$$U_{mf} = \frac{\varepsilon_{mf}^3}{180\,(1-\varepsilon_{mf})} \frac{(\rho_p - \rho_g)(\phi d_p)^2 g}{\mu} \qquad (2.4)$$

Modified Ergun equation proposed by Wen and Yu (1966) is another well–known equation often used (Yates, 1983):

$$Re_{mf} = \sqrt{(33.7^2 + 0.0408 Ga)} - 33.7 \qquad (2.5)$$

where

$$Re_{mf} = \frac{U_{mf}\, d_p\, \rho_g}{\mu} \qquad (2.6)$$

and

$$Ga = \frac{d_p^3\, \rho_g\, (\rho_s - \rho_g)\, g}{\mu^2} \qquad (2.7)$$

Since most fluidized beds contain powders with a wide range of particle size in practice, it is necessary to define some mean dimension for characterization purposes. The most frequently used average is the surface mean diameter which is defined as (Yates, 1983):

$$\bar{d}_{sm} = \frac{1}{\sum \frac{x}{d_a}} \qquad (2.8)$$

where x is the mass fraction of particles in each size range given by the sieve aperture d_a; $\overline{d}_{sm}$ is the diameter of a particle with an external surface–to–volume ratio equal to that of the mixture average.

Although all the existing correlations for the determination of the minimum fluidization velocity are independent of bed diameter, changes in U_{mf} with the size of the bed have been reported (Ormiston et al., 1965; Rowe and Everett, 1972). Rowe and Everett measured the U_{mf} of alumina with a mean particle size of 210 μm in beds of 20 cm high by 30 cm width by t cm thickness. They observed that the slope of the pressure drop/ flow rate curve increased with bed thickness up to a limit and it then remained

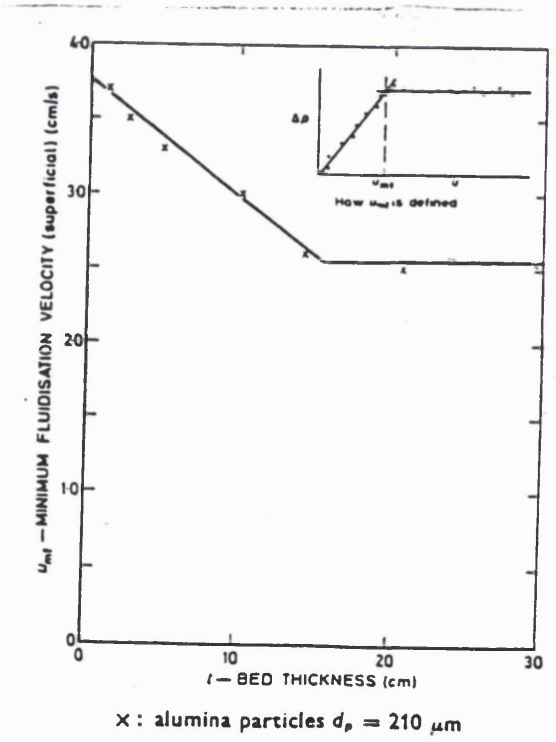

Fig. 2.2. Variation of minimum fluidization velocity with bed thickness (Rowe and Everett, 1972).

constant (Fig. 2.2); the limiting U_{mf} for the thickest sections was the true value. There was as much as a 50% increase in U_{mf} in the thinnest bed, which was an unexpectedly large variation. On the other hand, the dependence of bubble size on height and velocity changed markedly with thickness in beds less than about 5 cm. When greater than 15 cm, there was little change with thickness; and therefore between these limits there was presumably some transition. The beds above 15 cm behaved as three dimensional and below 5 cm they were two dimensional. In the latter case, the behaviour was thickness dependent.

2.3. Bubbles

According to two phase theory which was originally proposed by Toomey and Johnstone (1952), *'all the gas in excess of that necessary to just fluidize the bed passes through in the form of bubbles'*. The bubbles formed at gas velocities in excess of U_{mb} present one of the most intriguing features of fluidized beds. Although they have been the subject of many theoretical and experimental studies, the reasons for their origin and subsequent behaviour in the bed remain obscure. Bubbles appear to grow by a process of coalescence as they rise towards the surface and their rise velocity is clearly proportional to their size. They carry a cluster of particles behind them in a *wake* which fills their indented base, and as they erupt from the bed and the gas they contain escapes into the freeboard, the wake solids are dumped on to the bed surface. It has been shown conclusively that it is this transport of solids in bubble wakes that constitutes the prime mechanism by which bed particles are mixed.

Rowe et al. (1965) showed that in beds of particles of diameter greater than about 100 μm, bubbles are the main agents causing particles to move through large distances, and identified two mechanisms of their action. Firstly a drift mechanism whereby a

bubble draws up behind it a finger of underlying material rather in the manner of the displacement of an inviscid fluid by a rising sphere. Secondly a wake transport mechanism where solids in the bubble wake are carried to the surface and replaced by solids moving downwards in the emulsion phase.

Bubbles are therefore advantageous in that they serve as the mechanism for gas mixing and heat transfer. However, if too large, they can be the cause of serious gas by–passing of the solid particles and impede mass transfer in chemical reaction processes. This can lead to a lower level of conversion than would otherwise be expected. Generally, it is preferred to limit the bubble size in order to lessen the degree of gas–by–passing, but still maintain good gas/solid mixing.

In deep fluidized beds of high aspect ratio, the continuation of bubble coalescence leads eventually to the formation of bubbles whose diameter is equal to that of the bed itself. Such bubbles are called *slugs* and their hydrodynamic properties differ in many respects from those of freely moving bubbles; slugs for example rise more slowly than bubbles of equal volume. Furthermore, different types of slug can be formed depending on the type of the bed material being fluidized (Baker and Geldart, 1978). There is some evidence that fluidized beds of Group A powders have a maximum stable bubble size and this limits the formation of slugs.

Unlike gas–solid systems, however, the majority of liquid fluidized beds do not form bubbles as the liquid velocity is increased beyond U_{mf} but expand in a regular manner with the bed voidage, ε, increasing as the liquid velocity increases. Such behaviour is called *particulate* fluidization to differentiate it from the *aggregative* fluidization found in gas–solid systems. The reason for the difference in behaviour of liquids and gases have been circumstantially attributed to the greater density difference between the solid particles and the fluidizing fluid, $\rho_p - \rho$. If this is high, as with most gas–solid combinations, then aggregative behaviour is observed; if the difference is low, as with

most liquid–solid combinations, the system behaves in the particulate manner. Changing the density difference can lead to changes in behaviour irrespective of the phases involved. Bubbles can be observed when very dry dense particles, such as lead shot are fluidized by water (Harrison et al., 1961); and in the case of fine powders fluidized by gases it is observed that as the gas velocity is increased above that required for incipient fluidization, the bed expands homogeneously up to a certain point at which bubbles start to appear. This density difference therefore appears in many correlations predicting fluid bed behaviour, along with the particle diameter d_p and fluid viscosity μ as will be described in section 2.8.

The division of fluidized systems into bubbling or non–bubbling systems is too simple. Not only has the emulsion phase in bubbling gas–fluidized beds of fine particles ($d_p \leq 100$ μm) been found to have void fractions in excess of ε_{mf} (Martin, 1983), contradicting the two–phase theory, but some particles of low or moderate density ($\rho_p \approx 2500$ kg/m^3) can be fluidized as an expanded non–bubbling bed provided that the fluidizing velocity does not exceed a critical *minimum bubbling velocity* U_{mb}. For fluidization by air Geldart (1973) found empirically that this *delayed bubbling* (i.e. delayed with respect to increasing fluidizing velocity above U_{mf}) occurs if the following criterion is satisfied:

$$(\rho_p - \rho)\, d_p < 0.225 \qquad (2.9)$$

where ρ_p and ρ are in kg/m^3 and d_p is in meters. He was thus able to categorize air–fluidized beds into four groups in a now well–known plot of density difference against particle diameter to be described later in section 2.5.

2.4. Entrainment and Elutriation

In most practical applications, fluidized beds are operated at gas velocities well beyond U_{mf} and under these circumstances it is common for particles to be blown out of the bed to the freeboard space above it. This phenomenon is known as *entrainment* and it becomes more severe as the fluidizing gas velocity, U, increases. If U becomes so high that it equals the terminal–fall velocity of the bed particles, U_t, then the particles will be *elutriated*; i.e. carried out of the system completely. Normally a fluid bed consists of solid particles with a range of sizes, and as the value of U_t increases with particle diameter the smallest particles are the ones that are elutriated first although the larger ones can be entrained for a certain distance above the surface before falling back to it. Thus it is common for a particle concentration gradient to exist above the bed surface (Fig. 2.3). The height at which the particle concentration reaches a constant value is known as the *Transport Disengaging Height* or (TDH). Industrial columns are thus designed so that the gas exits above the TDH.

Many models have been proposed for the calculation of the flux of entrained solids in multisize systems. An important assumption of these models is that entrainment losses are proportionally greater for the fine particles. However, Geldart and Wong (1985) reported that the proportion of the bed particles which were smaller than 5 μm was not affected by entrainment. They also found that, with non–porous particles, the flux of entrained particles was reduced when the relative humidity of the fluidizing gas was increased past 60%. They attributed these results to the increase of the powder cohesivity with relative humidity, which they confirmed by bed expansion measurements. Electrostatic forces, which are affected by humidity, apparently had only a minor role to play in their system.

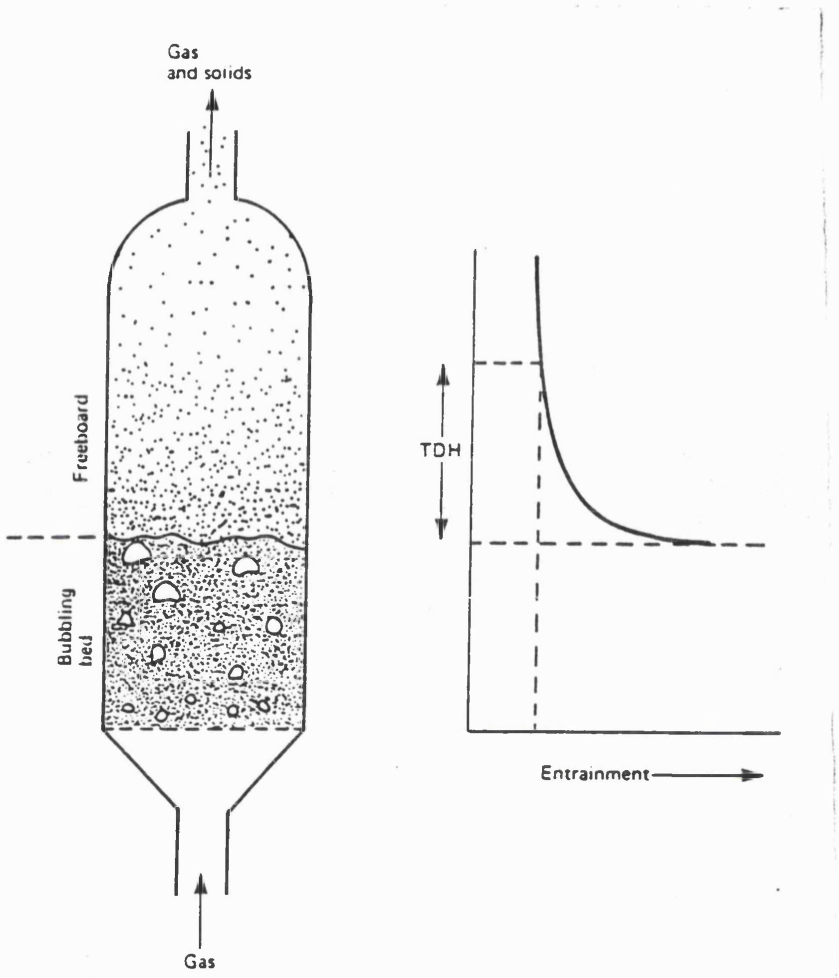

Fig. 2.3. Entrainment and elutriation (Yates, 1983).

Baron et al. (1987) reported that particle entrainment from a 61 cm i.d. bubbling fluidized bed of sand was increased with the humidity of the fluidizing gas. The gas humidity did not affect the fluidized bed behaviour, the bed expansion and the flux of particles ejected from the bed surface. They attributed the increase in particle entrainment, as the humidity was increased, to a reduction of electrostatic effects. They developed a model by assuming that the freeboard pressure drop was increased by electrostatic interactions between the column wall and the particles. It was also assumed, but not verified directly, that electrostatic effects did not affect particle agglomeration in the freeboard.

2.5. Description of Powder Groups

A convenient classification of powders was suggested by Geldart (1973) in which various powders are arranged into four groups according to their size and density to predict their fluidization behaviour; as shown in Fig. 2.4.

Group A: Beds of powders in this group expand considerably before bubbling commences. When the gas supply is suddenly cut off, the bed collapses slowly typically at a rate similar to the superficial gas velocity in the dense phase. Gross circulation of the powder occurs even when few bubbles are present, producing rapid mixing. Bubbles in a two dimensional bed appear to split and recoalesce very frequently. There is some evidence that the mean size of bubbles may be reduced in two ways; i.e. by having a wide particle size distribution and/or a small mean particle

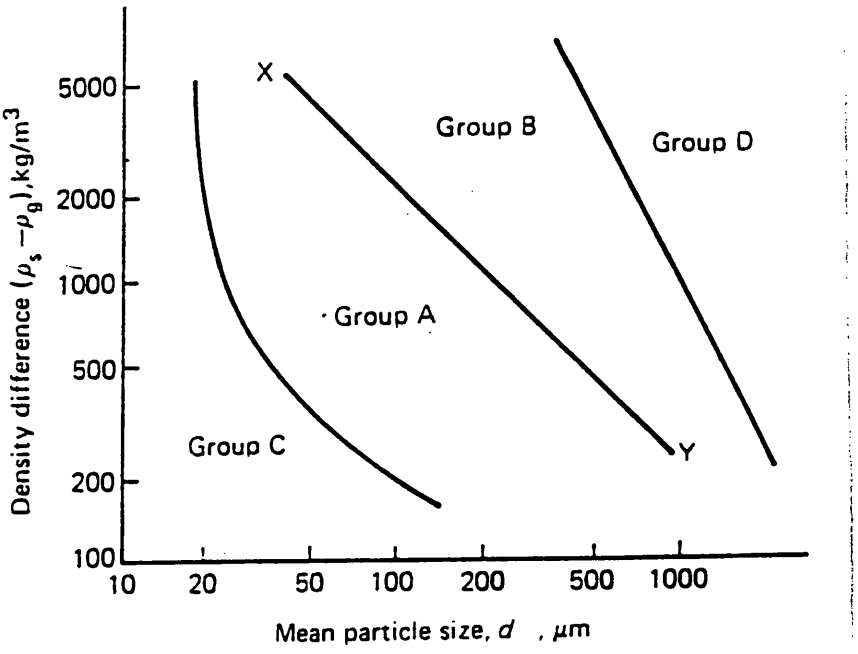

Fig. 2.4. Powder classification diagram for fluidization by air–ambient conditions (Geldart, 1973).

size. A maximum bubble size does appear to exist. When the superficial gas velocity is sufficiently high to cause the formation of slugging conditions, the slugs produced are axisymmetric; as the superficial gas velocity is further increased slug flow breaks down into a turbulent regime and the velocity at which this occurs appears to decrease with particle size.

Materials having a small mean size and/or a low particle density (less than about 1400 kg/m^3) generally exhibit this type of behaviour.

Group B: Most materials in the mean size and density ranges of 40–500 μm and 1400–4000 kg/m^3 respectively are classified as Group B. In this type of powder bubbling starts to form at or only slightly above minimum fluidization velocity. Bed expansion is small and the bed collapses very rapidly when the gas supply is cut off. There is little or no powder circulation in the absence of bubbles and bubbles burst at the surface of the bed as discrete entities. When the gas velocity is so high that slugging commences, the slugs are initially axisymmetric, but with further increase in gas velocity an increasing proportion become asymmetric, moving up the bed wall with an enhanced velocity rather than up the tube axis.

The most easily observed difference between Group A and B powders is whether the bed bubbles at or very close to minimum fluidization. If there is an appreciable bed expansion before bubbling commences, the powder belongs to Group A and is likely to have the other properties associated with that group. The boundary between Group A and Group B behaviour can be defined as the line on a particle density–diameter plot for which $U_{mb}/U_{mf}=1$. Then for Group A powders $U_{mb}/U_{mf}>1$ and for Group B material $U_{mb}/U_{mf} \leq 1$. This boundary line is plotted as XY in Fig. 2.4 for air at ambient conditions as the fluidizing gas.

Group C: Cohesive powders belong in this category. *Normal* fluidization of such powders is extremely difficult; not only because the interparticle forces are greater than the gravitational, but also because the forces which a gas can exert on these particles are not large enough for fluidization. Particle mixing is much poorer than with powders of Groups A and B. As the gas velocity is increased from zero, the powder lifts as a plug in small diameter tubes, or channels badly, i.e. the gas passes up voids extending from distributor to bed surface. Further increase in velocity enlarges the channels, and in small diameter beds, a sufficiently high velocity will carry the solids out the top in a single clump, leaving an empty vessel behind. External means such as mechanical stirrers, vibrators or fines are required to assist in their fluidization (Geldart, 1986).

Group D: This group consists of large and/or very dense particles. The largest bubbles rise more slowly than the interstitial fluidizing gas, so that gas flows into the base of the bubble and out of the top, providing a mode of gas exchange and by–passing different from that observed in Group A and B powders. The gas velocity in the dense phase is high, solids mixing relatively poor; consequently back–mixing of the gas in the dense phase is small.

Geldart et al. (1984) reported that although both aerated bulk density and tapped density varied with relative humidity, the Hausner ratio was virtually independent of RH%. Hausner ratio is the ratio of the tapped density to the low packed bulk density and is greater than unity. A drop in HR shows a decrease in the cohesiveness of the powder. According to them, powders having a HR>1.4 exhibit distinctly cohesive behaviour and should be considered as Group C; a fine powder with a ratio less than 1.25 is certainly in Group A, whilst those in the range of 1.25–1.4 may exhibit some properties of both Groups.

2.6. Channelling

Channelling leads to high values of local gas velocity, causing undesired elutriation loss of expensive bed material. If channelling is severe, fluidization is poor leading to low bed expansion and inadequate bed pressure. This problem is due to the interparticle forces (Geldart, 1973) which are greater than those which the fluid can exert on the particle, and these are generally the result of very small particle size, strong electrostatic charges or the presence of very wet and sticky material in the bed.

At present no theory on channelling is available. According to Geldart (1973), it is only certain particular powders with a very small average particle size and a high particle density which show channelling. In its generality, it is not correct. As an example, Rietema mentioned (1991) potato starch whose average particle size and particle density are similar to those of cracking catalyst; while cracking catalyst can be fluidized very well and shows high bed expansions, potato starch shows the phenomenon of channelling very seriously and gives hardly any expansion.

Liu and Kimura (1993) also reported that silicon nitride with a particle size of 0.49 μm and a particle density of 2900 kg/m^3 was easily fluidized (U_{mf} = 3.2 cm/s) while silicon with a mean size of 3.7 μm and particle density of 2400 kg/m^3 could not be fluidized at all.

Brooks and Fitzgerald (1985, 1986) found a type of fibrous carbon (TCM), 0.1–0.3 μm in diameter, which had a large bed expansion of over 100% and was free of bubbles in a gas fluidized bed which was similar to the behaviour of good quality liquid/solid fluidization.

According to Rietema (1991), it is the ratio between the elasticity modulus (to be described in section 2.7.5) and the attractive force (cohesion) which determines whether a powder will give rise to channelling or not. Soft powders such as potato starch, flour, cement, iron oxide and limestone give rise to channelling. It is remarkable that all these powders are very cohesive.

2.7. Interparticle Forces

Powder fluidization is the result of a balance between fluid–dynamic forces on one hand and gravitational forces on the other; so that the particles in the powder come into a more or less free–floating state, provided that interparticle interaction forces are at a minimum.

The dominant interaction force between particles in a powder as well as in a fluidized bed is the van der Waals force of attraction (Rietema, 1984). This interaction force includes both the forces between the fluidized particles and the wall of the apparatus in which the fluidized bed is generated. The force operates both in vacuum and in a liquid environment, although in the latter case the van der Waals force is substantially reduced.

In addition to the van der Waals force, other attraction forces may also operate between the particles in a powder, such as capillary and electrostatic forces in the case of gaseous environment. In general, these forces are smaller than the omnipresent van der Waals force.

It is assumed that at the point of minimum fluidization the particles are freely supported on the upward flowing gas stream and that there is no interaction between them

beyond U_{mf}. While this may well be true for beds of relatively large, coarse particles (Geldart Group B) it may not be so for Group A powders which contain a high proportion of fines; i.e. particles with a mean size less than about 45 μm. As was previously mentioned, these powders undergo considerable expansion in the velocity region between U_{mf} and U_{mb} and bubble formation is accompanied by bed collapse. Some researchers working with Group A powders believe that it is due to the formation and subsequent loss of a loose structure of cavities among the particles in the emulsion phase of fluid beds (Baerns, 1966; D'Amore et al., 1979; Donsi and Massimilla, 1973a and 1973b; Kono et al., 1989; Massimilla st al., 1972; Mutsers and Rietema, 1977a and 1977b; Rietema, 1967; Rietema, 1984; Yates, 1983; Zenz, 1957) and have proposed both van der Waals and capillary condensation forces as being responsible for holding particles together and preventing them from moving freely in the bed. Capillary forces can result from condensation of water vapour present in the fluidizing air and they can be an order of magnitude greater than the van der Waals forces. Both can greatly exceed the weight of individual particles.

As early as 1957, Zenz proposed that interparticle cohesion forces affect the fluidization behaviour of powders. According to Zenz, the emulsion phase of fine powders like fluid cracking catalyst consist of clusters of loosely connected *networks* of small particles that give a powder a *loose packed structure*. However, this was never verified experimentally. Meissner et al. (1964) concluded that fine particles of zinc oxide 0.25 μm agglomerated by spontaneous cohesion due to van der Waals forces. Voidages in excess of 90% were reported for fine powders due to a cohesion structure, whereas coarse particles that show no interparticle forces always pack closely with a voidage of about 35–40%. A number of authors (Baerns, 1966; Geldart, 1973; Mutsers and Rietema, 1977a and 1977b; Rietema, 1967; Rietema, 1973; Rietema, 1984; Zenz, 1957) have attributed the expansion between U_{mf}

and U_{mb} to be due to interparticle forces. They assumed that interparticle forces act even in the expanded state of homogeneous fluidization.

It has been shown (Mutsers, 1977) that the strong capillary forces are almost entirely absent from systems where powders are fluidized with air at a relative humidity of less than eighty percent and that the van der Waals forces between particles are weakened by the presence of surface irregularities and asperities (Massimilla and Donsi, 1976). Nevertheless they are considered to be strong enough to cause some cohesion and to stabilize a type of cavity structure in the powder between U_{mf} and U_{mb} which affect the corresponding expansion.

When cohesive forces start to affect the fluidization behaviour, theories based on the behaviour of a powder of one type and in one group will not be applicable to another powder of another type and class (Geldart, 1986). Nor can model studies at room temperature and a given gas type and pressure be used to predict the behaviour at higher temperatures and at other gas pressures, in particular particles classified in the transition region between class C and A. For this reason some researchers like Rietema (1984) prefer to use the term class C behaviour rather than to classify powders in class C, etc. Rietema stated that for powders showing class C behaviour, because of the relatively strong cohesive forces, as soon as the minimum fluidization rate is exceeded, more or less horizontal fractures occur in the bed. These fractures are connected by irregular vertical channels through which the excess gas seeks its way upwards. Consequently, there is hardly any movement in the bed and the pressure drop over the bed is considerably below the total weight of the bed, W, divided by the cross–sectional area, A; i.e. W/A. Grace (1986) pointed out that the boundary between C and A is strongly influenced by interparticle forces such as van der Waals, capillary, electrostatic and magnetic forces, as well as variables like size of surface

asperities, hardness of the solid material, humidity, melting or softening point, electrical conductivity and magnetic susceptibility.

Further insight into these types of cohesive forces in a more quantitative way and how they can be affected or altered is essential for understanding the fluidization of powders exhibiting class C and/or class A behaviour.

2.7.1. Van der Waals Forces

Van der Waals forces are only noticeable when the particles can come sufficiently close together, i.e. at separation distances of the order of size of a molecule, e.g. 0.2 to 1 nm. Moreover, their magnitude becomes negligible compared with that of gravitational force when the particle size exceeds a certain value. This value is of the order of a few microns. The reason is that the gravitational force is proportional to the cube of the particle diameter and the van der Waals force is proportional to the diameter.

Massimilla and Donsi (1976) gave the following equation for the attractive van der Waals force, F_w, between two non–deformable spheres of radii R_1 and R_2 separated by a distance Z:

$$F_w = \frac{h_w}{8\pi Z^2} R \qquad (2.10)$$

where

$$R = \frac{R_1 R_2}{R_1 + R_2} \qquad (2.11)$$

h_w is the Lifshitz–van der Waals constant which ranges from 1.6×10^{-19} to 16×10^{-19} J (1–10 eV) for most solids in air. For deformable solids the potential increase in area of contact leads to an increase in the cohesive force:

$$F_w = \frac{h_w}{8\pi Z^2}\left[1 + \frac{h_w}{8\pi^2 Z_o^3 h}\right]R \qquad (2.12)$$

where h represents the hardness of the more deformable solid.

Visser (1989) reported that immersion in water led to a substantial reduction in the van der Waals attraction, and the lower the individual value of the van der Waals coefficient of the material in question, the greater the reduction. Van der Waals forces only dominate over gravitational and hence over fluid–dynamic forces generated in a fluidized bed when the particles come into real contact, i.e. for separation distances of the order of a few nanometers, and have a major dimension smaller than 100 μm. For porous particles or crystals with large flattened surface areas, the region is extended to even larger particles. This is also the case for particles having a high Lifshitz–van der Waals constant. On the other hand, different means to increase the separation distance such as the addition of properly chosen fines, would substantially diminish the adhesion and hence allow the fluidization of particles normally difficult to fluidize.

Surface roughness may limit the approach of two particles and the effective separation distance will be large, thereby limiting the van der Waals attraction to almost zero when the asperities are of the order of 1 μm. In some cases

the intimate contact area may substantially increase the overall van der Waals attraction. This situation is enhanced when plastic deformation takes place, for example at high temperatures. Elastic deformation on the other hand may also increase

the contact area, but will not increase the adhesion, simply because upon separation of the adherents the particles will retain the original shape (Krupp, 1967).

The behaviour of a powder in a fluidized bed and the initial point of fluidization are both governed by van der Waals force as long as its magnitude is of the order of, or larger than, the gravitational and the fluid–dynamic forces also acting on the particles under these circumstances. Depending on the particle density, porosity and surface roughness, these cohesive forces will only be noticeable when the particle diameter is in the order of a few microns or less. Hence, following Geldart's classification, only the fluidization of powders classified as Group C may be affected by cohesive forces. Considering that, in addition to the above–mentioned restrictions, the precise particle geometry, presence of fines, particle size distribution, adsorbed molecules, etc., also determine the magnitude of the interparticle force, it is clear that no general conclusions can be drawn from fluidization experiments based on one type of particles of a given size distribution using one specific gas at a selected temperature.

As mentioned earlier, the most important parameter determining the van der Waals attraction between solids is their separation distance Z. Any means to enlarge Z will substantially reduce the adhesive force and consequently influence the fluidization behaviour of a given powder. Factors affecting the interparticle separation distance are roughening of the surface, which is mainly a question of particle preparation, and the use of spacers. In general, irregularities of particle surface will diminish adhesion, although apparent area of contact increases. Spacers can be either small molecules adsorbed onto the interacting particles, hence the influence of the type of gas used in fluidizing a powder even when no capillary condensation takes place, or small particles, e.g. fines. In the latter case the dimension of *fine* particles as compared to the host material are critical (Visser, 1989). Where additives are of the same size as

the interparticle voids, they may have no effects at all, whereas situations may also exist under which added particles can act as bridges between adjacent particles and thereby enhance their cohesiveness. The precise effect will depend entirely on the system under study, so that no general conclusions may be drawn.

Changes in surface characteristics may also diminish the particle aggregation behaviour due to the screening effect. An oxide layer on metal particles was reported (Visser, 1989) to have reduced the adhesion by a factor of up to 4.

Factors leading to an increase in cohesion are related to any effect which will increase the area of close contact between the interacting solids, provided that their separation distance is not increased at the same time. These factors are found in particular for particles having a partly flattened surface, due either to their inherent structure (as crystalline material) or to plastic deformation induced by pressure or increase in temperature. Reorientation of randomly packed particles upon fluidization may result in a more favourable configuration with respect to each other. The intimate contact area will grow and thereby increase the cohesion through the best possible fit. For example, any flat surface will try to find a matching partner. Therefore, open spaces between the particles in a fluidized bed may be created, leading to bubble formation and even channelling. The only way to minimize this effect will be to use spacers of the correct size, preferably flat on one side.

Piepers et al. (1984) reported that physically adsorbed gases increased the cohesion of powders and the cohesion further increased when the pressure of the gas was raised. Therefore the elastic modulus of the fluidized bed increased and a further increase in the maximum powder expansion became possible. The type of gas used had a large influence on the results, however, no satisfactory explanation of the results could be

given. But the increase in cohesion was probably due to an increase in gas adsorption with pressure, according to the authors. The increase in gas adsorption would have an influence not only on the van der Waals interaction between the particles in the bed, but may also have an effect on the interparticle separation distance.

2.7.2. Electrostatic Forces

Electrostatic charging of powder particles invariably arises during powder handling operations due to tribo–electrification (Bailey, 1984). Tribo–electrification is a special aspect of contact electrification which is still not fully understood. However, some general ideas are generally accepted. In practice, when particles are charged during handling, although it is impossible to theoretically predict quantitatively the charging level, it is often possible to understand the way in which the dynamic behaviour of charged particles differs from that of similar uncharged particles. Charged particles may adhere firmly to metallic surfaces, specially when powder resistivity is high, but van der Waals forces are still dominant.

Apart from the electrodynamic forces, electrostatic forces can also contribute substantially to the cohesion of particles and thereby their aggregation, as long as a gaseous environment is considered, e.g. by tribo–electric charging or by the formation of a potential difference ΔU when particles of different work functions [1] are brought into contact (Krupp, 1967). In the former case, the interaction force F_c between a spherical particle of radius R, having a particle charge q, interacting with an adjacent

[1] The basic definition of work function is 'the minimum energy required to extract the weakest bound electron from a particle surface to infinity' (Bailey, 1984)

uncharged particle at a separation distance Z due to its own image charge, is given by the classical Coulomb equation (Bailey, 1984):

$$F_c = \frac{q^2\left[1-\frac{Z}{(R^2+Z^2)^{1/2}}\right]}{16\pi\varepsilon_o Z^2} \qquad (2.13)$$

where ε_o is the permittivity of vacuum. The latter case only applies to particles of different composition, e.g. to the particles and the wall of a fluidized bed. The force of attraction F_u is given by equation (2.14); (Bailey, 1984):

$$F_u = \pi\varepsilon_o \frac{R(\Delta U)^2}{Z} \qquad (2.14)$$

In a humid environment, the Coulomb attraction is reduced to zero due to a decharging of the system.

When a particle charges during handling, the charge transferred at the particle contact point will redistribute itself over the particle surface by electrostatic forces. The rate of redistribution process depends upon the electrical relaxation time of the particle material, θ, which is a function of particle resistivity, r_p, and particle permittivity, ε; i.e. $\theta = r_p . \varepsilon$ (Bailey, 1984). Insulating materials having particle resistivities of the order of 10^{13} Ωm have relaxation times of minutes or even hours so that appreciable charge distribution does not often occur during typical industrial processing times. Semi–insulating and conducting particles attain surface charge equilibrium relatively quickly. For spherical particles the final equilibrium surface charge density is uniform, but for particles of non–spherical shape final distribution is non–uniform;

higher than average surface charge densities developing in regions of higher than average curvature.

The existence of surface charge on a particle gives rise to an electrostatic field which has a maximum intensity at the particle surface and decays inversely with the square of distance away from the surface. The maximum field that can be sustained at a particle surface depends on particle environment and particle size. For particles in an air environment, the breakdown field strength of air is a limiting factor. Harper (1967) proposed an empirical equation for maximum sustainable particle surface field, E in V/m, in terms of the radius, R, of a spherical particle as:

$$E = 9.3 \times 10^5 R^{-0.3} \qquad (2.15)$$

Therefore if in a powder handling situation electrostatic phenomena arise, they are likely to become increasingly significant as particle size is decreased. Using equation (2.15), the total charge on a particle in an air environment was given in Coulombs by Bailey (1984):

$$q = 1.03 \times 10^{-4} R^{1.7} \qquad (2.16)$$

As an example of the relative magnitudes of forces that may act upon a charged particle, consider a spherical particle of radius 10 μm and a density of 1000 kg/m^3. The gravitational force acting on this particle is about 4×10^{-11} N. The electrical force depends on both particle charge and the electrostatic field that acts on the particle. The maximum charge using equation (2.16) is 3.3×10^{-13} C. A typical field that may arise from space charge in a powder cloud is $\approx 10^5$ V/m, which results in an electrostatic force of 3.3×10^{-8} N, which is considerably larger than the gravitational force acting on the particle.

Friction causes localized heating which can have a significant effect upon tribo–electrification. Coste and Pechery studied (1977) the effect of friction on contact charging of polyethyleneglycol terephthalate (PET) and cellulose triacetate films. They observed that even at relative humidities as high as 70%, very high surface charge densities could develop. It was concluded that surface states could be significantly modified by surface friction. Their work demonstrated the fundamental role that water may play in charge transfer processes due to surface adsorption, probably at hydrophilic sites that may be present on some polymer surfaces. They also reported (1981) that smooth surfaces charged much more than rough samples.

Gallo and Lama (1976) reported that particle relative permittivity and particle size had a significant effect upon work function and contact charging. Work function decreased with an increase in particle radius and/or with particle permittivity. Therefore the work functions of large particles of a specific material would be lower than smaller particles; i.e. electron transfer from larger to smaller particles seemed to be favourable.

According to Cartwright et al. (1982), when relatively dry polyethylene powder was transferred into a silo test, bipolar charging occurred. Coarse particles charged positively. On the contrary, when relative humidity was high, all particles regardless of their size charged negatively. The influence of humidity upon powder charging is complex. It was difficult within the large scale test facility reported by Cartwright et al. to ensure that conditions were uniform throughout the system. Temperature was likely to affect the tribo–electrification process, too. However, it was clear that at high relative humidities, high levels of negative charging occured. At low values of relative humidity, although fine particles still charged negatively, the coarse particles showed a change of charging polarity such that the net charge conveyed by the powder was positive.

A charge is readily generated when dry gas is used and the particle size at which the effect becomes observable depends on the kind of solid material (Agbim et al., 1971). Charged particles experience attractive forces to metallic surfaces and may then adhere firmly to such surfaces specially if powder resistivity is high. Powder adhesive forces may be extremely high and although electrostatic effects are significant, van der Waals forces are often dominant.

2.7.3. Capillary Forces

At high humidities (≥65%), capillary condensation of the fluid in the gap between the particles in close contact may take place, resulting in a component additional to the van der Waals attraction. For two smooth spherical particles of radius R and a fluid of surface tension γ totally wetting the particle surfaces, this contribution is (Visser, 1976):

$$F_H = 2\pi \gamma R \qquad (2.17)$$

Geldart et al. (1984) reported that decreasing particle size and increasing the relative humidity of the fluidizing air decreased the ratio of the actual to the theoretical pressure drop; i.e.; $\Delta P.A/(M.g)$, which was an indication of increase in cohesiveness. Increasing the humidity of the fluidizing air decreased bed expansion at low velocities but increased it at higher flow rates. They attributed it to an increase in interparticle forces (liquid bridge in that case) which prevented the bed structure from expanding as much when the hydrodynamic drag forces were smaller (low velocities) but permitted a higher voidage at higher velocities by giving the bed structure a greater mechanical strength.

Geldart and Wong (1987) reported that the entrainment flux of non–porous fine powders decreased with an increase in relative humidity of the fluidizing gas. This effect was attributed to an increase in powder cohesiveness and was observed in particular at relative humidities above 30%. Geldart et al. (1984) stated that most Group A powders can be made to behave like Group C by fluidizing them with air of relative humidity in the range 60–90%. These results demonstrated the effect of capillary condensation on particle aggregation and hence on their fluidization behaviour.

2.7.4. Electromagnetic Forces

A rather specific additional attraction may arise when the particles can be magnetized. Depending on the degree of magnetization, p, very high attraction forces can be achieved, due to the very long range of magnetic forces; i.e. a particle may be attracted to another some distance away while capillary and/or van der Waals forces are effective only if the particles are in close proximity. Only for weakly magnetized particles such as magnetite the additional attraction forces are less pronounced but they are still noticeable (Dry et al., 1988). The corresponding force F_M is given by (Visser, 1989):

$$F_M = \frac{p^2}{6\pi \mu_o Z^2} \qquad (2.18)$$

where μ_o is the permeability of the material.

Bubbling behaviour of fine iron oxide powders in a two dimensional bed was reported (Dry et al., 1988) to be quite dissimilar to FCC or sand and bubbles appeared to shoot through the bed faster than for more commonly used materials. This effect was not

limited to two dimensional systems; in a 0.64 m i.d. unit, Dry et al. (1984) reported bubble velocities exceeding 2 m/s at a superficial velocity of just 0.4 m/s. The powder was essentially magnetite, therefore natural magnetic dipoles may be present in small particles of this material. Hence fines were more likely to participate in the formation of agglomerates which fell back into the bed. Entrainment from a bed of magnetite particles of class AC type was found by Dry et al. (1988), to be about 50% of that from the same particles demagnetized by roasting in air, as a result of a magnetic flocculation effect in the so–called lean phase. Particle shape, surface and density were not affected by roasting.

Langbein (1969) showed that the interaction between solid bodies at a separation distance Z was determined solely by the electromagnetic properties of the material contained in the surface layer of the same thickness as the separation distance Z.

Agbim et al. (1971) compared the behaviour of three grades of steel shot, two of them had become magnetized. All showed the same characteristic curve although in the case of the two magnetized materials, there was a distinct difference between the U_{mf} and U_{mb}. This difference was barely observable with the unmagnetized material and its expansion before bubbles appeared in the bed and U_{mf} was not significant. Micrographs showed that in the magnetized cases the particles were plainly adhering to one another.

2.7.5. Measurements of Interparticle Forces

Many studies on the cohesion forces between fine powder particles have shown, on the experimental (Baerns, 1966; Buysman and Peersman, 1967; Cheng, 1968) as well

as on the theoretical (Rumpf, 1970; Krupp, 1967; Dahneke, 1972) grounds, that the dimensionless cohesion number defined as:

$$Co = \frac{\text{Cohesion force between particles in contact}}{\text{Particle weight}} \qquad (2.19)$$

becomes much larger than unity when the particle diameter is decreased to below 100 μm. If such a fine powder is fluidized, the particles cannot be free–floating because each collision would lead to coherence between the colliding particles. Some researchers (Rietema, 1967; Mutsers and Rietema, 1977a; Massimilla et al., 1972, Donsi and Massimilla, 1973a) believe that the cohesion forces between the cohering particles give rise to a powder structure with a certain mechanical strength, even in the expanded state of fluidization.

Donsi and Massimilla (1973a) suggested a cavity structure of the dense phase in the expanded state of homogeneous fluidization (Fig. 2.5). It could easily be imagined that such a structure would react to compression or expansion as an elastic body. The value of the elasticity coefficient, E, depends on the bed porosity: when the bed is expanded further, the powder structure becomes looser and weaker, so that E will be reduced. This reduction will happen discontinuously since the elasticity itself resists expansion. Therefore, at increasing expansion E can remain constant only as long as the elasticity limits are not exceeded. Otherwise, some bonds between particles will be broken and the particles in the bed will rearrange themselves at a higher porosity, E being reduced stepwise.

According to Mutsers and Rietema (1977a), there was not much dependence of E on the mean particle diameter (at the same porosity). However, when the spread in particle diameter increased, E also increased. It was interesting in connection with

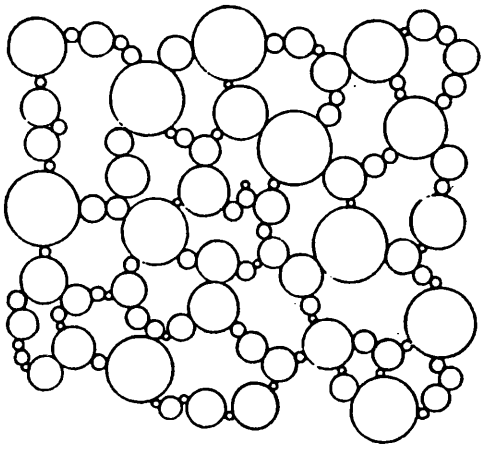

Fig. 2.5. Cavity structure of the dense phase suggested by Massimilla et al. (1972).

observations made by some researchers (de Groot, 1967; de Vries et al., 1972) that the addition of a small amount of fines improved the fluidization properties and increased the number of transfer units between rising bubbles and the dense phase. The effect of particle size distribution on the elasticity can be explained by realizing that the number of contact points increases at increasing diameter spread and assuming that the elasticity is determined by the number of contact points. At increasing porosity the number of contact points is reduced, and hence also the elasticity. The limiting value, however, is reached at higher porosity.

One of the earliest cohesion measurements was known as the centrifuge method of Boehme et al. (1962). The cohesive force of a powder was measured by rotating a plate covered with a layer of particles that came off at increasing rotational speeds. Baerns (1966), using a modified version of this method, correlated the angle of

inclination at which particles began to slide from the rotating plate to the cohesive force.

In order to measure the interparticle forces, Mutsers and Rietema (1977a) fluidized a finely dispersed solid in a square bed of 10×4 cm at such a gas rate that the bed was noticeably expanded but gas bubbles did not yet appear (homogeneous fluidization). Then the bed was tilted very slowly and without shocks about the horizontal axis. They reported that it was possible to tilt the bed through a certain angle without the powder sliding, the surface remaining perpendicular to the direction of flow. When the bed was tilted, the direction of the drag force upon the particles changed. However, as long as the surface of the bed did not slide, that change was evidently compensated by some other force which they deduced to be the result of interparticle cohesion and friction forces. They concluded that there existed a powder structure with a certain mechanical strength even in the expanded state of fluidization.

They also reported that the maximum possible tilting angle was reduced by an increase in the gas rate. In a great number of experiments this angle was found to be dependent upon both the bed porosity and the fluidizing gas that was used in the experiments. Apparently, both hydrodynamic phenomena and cohesion played a part. A bed expansion was found at which tilting without sliding was no longer possible. The porosity of the bed at that critical condition was called ε_{cr}. They observed that ε_{cr} and ε_{mb} were always approximately equal, at least within the experimental error, and that both were influenced by solids and gas properties. The degree of humidity of the powder was very important in the results.

These techniques illustrated that particle interactions were present but did not provide a scientific method of calculating the cohesive force acting between particles in a powder.

Interparticle forces have been investigated by measuring the tensile strength of powders as early as 1960's (Ashton et al., 1964; Buysman and Peersman, 1967) and more recently by several other researchers (Hartley and Parfitt, 1984; Koch and Licht, 1977; Kono et al., 1985, 1987, 1988; Seville and Clift, 1984; Tsubaki and Jimbo, 1984; Yates et al., 1984) who have made various improvements on experimental techniques. This was carried out on either some type of shear cell (Ashton et al., 1964; Carr and Walker, 1967; Hartley and Parfitt, 1984; Jenike, 1961; Jenike and Carson, 1987; Roscoe, 1953) or suspended bed experiment (Buysman and Peersman, 1967; Seville and Clift, 1984; Reiling, 1992).

A split shear cell instrument can be used to obtain the tensile strength of a powder by measuring its shear stress–strain curve. The interparticle forces are then related to the tensile strength of a powder by the classic expression derived by Rumpf (1970). The simple shear cell and the Jenike shear cell are the most well known types of shear instruments. The simple or triaxial shear cell uses a variable geometry cell so it can apply a uniform shear strain to a sample undergoing testing. The simple shear cell provides detailed stress–strain data on simple particulate solids (Cheremisinoff and Cheremisinoff, 1984; Fayed and Otten, 1984). However, the process of loading the sample into the cell is critical, since the flow properties of powders are very dependent on their stress history and uniformity of loading. So far the apparatus has only been used for sands of uniform size and clays; it has never been tried on cohesive, highly compressible powders.

The Jenike Shear cell is simpler and more versatile than the triaxial shear cell and is the most commonly accepted and widely used shear cell in industry. In a Jenike shear cell, a known amount of powder is consolidated into a shallow cylindrical chamber, which is split horizontally. The lower half of the cell is fixed and a shear force is applied to the upper, moveable half at a constant low rate. Shearing can be carried out for each of a series of normal loads on prepared samples, so that when the test is complete the relationships between the normal stress and shear stress at various bulk densities are obtained. Cohesion is defined as the shear stress for failure of a compact powder when zero stress is applied normal to the shear plane. The tensile strength is the normal stress required for failure of a powder compact at zero shear stress.

Yokoyama et al. (1982) developed a swing–type shear cell called the *Cohetester* which was similar to the Jenike shear cell in principle but was designed for very low pressures. This device was more suitable for fine, low density powders.

The annular or ringshear cell is a newer device which is quicker and easier to use (Carr and Walker, 1967) but not as well proven as the Jenike cell. The cohesion or tensile strength data from these shear cells can be used to calculate the interparticle forces using the expression proposed by Rumpf (1970). They can also be used to determine a parameter defined as *Flow Factor* which gives a good indication of the cohesiveness of the powder according to the Jenike classification (York, 1975).

A way of obtaining the interparticle forces and tensile strength of a powder in its loose–packed state is the so–called *suspended bed* experiment (Buysman and Peersman, 1967). The suspended bed operates on the principle of the pressure distribution within an inverted bed of powder suspended by an upflowing stream of gas, effecting a balance between gravity forces (weight) and hydrodynamic forces

(viscous drag). Buysman and Peersman (1967) measured gas velocities and bed pressure drops at the *rain off* points in beds of solid glass and aluminium silicate particles between 60 and 1000 μm that were inverted and suspended by an upwardly directed air flow. Their experiments were carried out in a 40 mm i.d. by 300 mm high calibrated glass tube, rotatable around a horizontal axis through its centre and fitted with porous plates on either end. The gas flow was gradually reduced until the bed *rained off* in layers. From the data at the rain off point, the interparticle forces were calculated by comparing the measured pressure drop with the theoretical bed weight per unit area. Pressure drops were considerably larger or smaller than the apparent bed weight per unit area or that predicted by the Ergun equation. The residual forces that maintain a balance of the viscous and gravity forces must be due to the interparticle effects.

Seville and Clift (1984) used the suspended bed technique to measure the interparticle capillary forces of glass ballotini particles lightly coated with non–volatile sebacite oil. The increasing interparticle forces due to the oil caused the fluidization behaviour to move from Group B through Group A to Group C.

Reiling (1992) reported that interparticle forces of Group A powders, increased by addition of Group C materials. He measured the interparticle forces using the suspension bed technique and using Rumpf's equation (1970), calculated the tensile strength of the powders. A linear relationship was found between the tensile strength and the ultrafine content.

2.8. Transition from Particulate to Aggregate Fluidization

The stability of gas fluidized beds of fine particles (homogeneous fluidization) has been studied by many investigators such as Jackson (1963), Pigford and Baron (1965), Murray (1965), Molerus (1967), Verloop and Heertjes (1970), Oltrogge (1972), Mutsers and Rietema (1977a), Foscolo and Gibilaro (1984), Reiling (1992). Some theories deny the existence of stable homogeneous fluidization (Pigford R L and Baron T, 1965; Jackson R, 1963 and Murray, 1965).

There is experimental evidence linking the system properties (particle size and density, as well as fluid viscosity and density) to the minimum bubbling conditions, U_{mb} and ε_{mb} (Godard and Richardson, 1968; Donsi and Massimilla, 1973a; Guedes de Carvalho, 1981; Rowe et al., 1982; Polletto et al., 1993); however, most reported investigations are confined to restricted ranges of operating conditions and there is a shortage of data on high pressure systems covering the full range of industrial interest, due mainly to the difficulty of observing the onset of bubbling under these conditions.

Many researchers have attempted to propose the criteria for transition from particulate to aggregate fluidization. Molerus (1967) considered a bubble to be the final result of a perturbation on an initially uniform distribution of particles and employed a stability analysis to determine under what conditions a small voidage perturbation would grow or decay. He reached a criterion where the Galileo number of the dense phase was a function of ε_{mb} ; i.e. $Ga_d = f(\varepsilon_{mb})$.

Many other models introduced later were based on the critical condition proposed by Wallis (1969) from shock wave theory. The assumption is that bubbles are in fact shock waves. Shock waves arise in a fluidized bed when the rising velocity of a porosity fluctuation exceeds the longitudinal velocity of an equilibrium disturbance: in

some respects this is analogous to the condition of a projectile reaching the velocity of sound in a fluid. Wallis stated that a bubble forms when the rising velocity of a void, U_ε, equals the propagation velocity of an elastic wave, U_e:

$$U_e = U_\varepsilon \tag{2.20}$$

For voidage propagation velocities smaller than the elastic wave velocity, $U_\varepsilon < U_e$, disturbances will be accommodated in an essentially homogeneous manner, whereas for $U_\varepsilon > U_e$ this is no longer possible and bubbles are formed.

Verloop and Heertjes (1970) and Oltrogge (1972) followed Wallis (1969) and assumed some elasticity of the bed, to be ascribed to hydrodynamic phenomena. According to their criteria, Galileo number of the dense phase was a function of bed voidage at minimum bubbling conditions, ε_{mb}, but they differed considerably from each other and Molerus' criterion.

Mutsers and Rietema (1977a) took a different approach and reached a criterion based on the importance of interparticle forces. They introduced the Fluidization Number as:

$$N_F = \frac{\rho_d^3 d_p^4 g^2}{\mu^2 E} \tag{2.21}$$

where E is the elasticity coefficient. While E includes interparticle forces, it cannot be evaluated explicitly. At the maximum stable bed expansion with porosity ε_{mb}, E could be determined as:

$$E_{mb} = \rho_p \left[\frac{U_{mb}(3-2\varepsilon_{mb})}{\varepsilon_{mb}}\right]^2 \tag{2.22}$$

The stability criterion of Mutsers and Rietema was:

$$N_F = \frac{\rho_d^3 d_p^4 g^2}{\mu^2 E} \leq \left\{\frac{150\,(1-\varepsilon)}{\varepsilon^2(3-2\varepsilon)}\right\}^2 \qquad (2.23)$$

At the bubble point velocity when $\varepsilon = \varepsilon_{mb}$, the equality would hold.

Foscolo and Gibilaro (1984) followed the approach of Verloop and Heertjes (1970) to reach the criterion for the prediction of transition from particulate to aggregate fluidization using only the hydrodynamics of fluidized bed. Considering gravitational, buoyancy and drag forces acting on a single particle, the elastic wave velocity, U_e, was determined as:

$$U_e = \sqrt{3.2\, g d_p\, (1-\varepsilon)\,(\rho_p - \rho)/\rho_p} \qquad (2.24)$$

while the voidage propagation velocity, U_ε, was obtained as:

$$U_\varepsilon = n\, U_t\, (1-\varepsilon)\, \varepsilon^{n-1} \qquad (2.25)$$

where n and U_t are the Richardson–Zaki indices to be discussed in next section. Therefore on the critical condition proposed by Wallis, the criterion for transition from particulate to aggregate fluidization is:

$$\frac{(g d_p)^{0.5}}{U_t}\left(\frac{\rho_p - \rho}{\rho_p}\right)^{0.5} \geq 0.56\, n\, (1-\varepsilon_b)^{0.5} \varepsilon_b^{n-1} \qquad (2.26)$$

where ε_b is the voidage at which the transition from particulate to aggregate fluidization occurs. For cases of practical interest, $\varepsilon_b = \varepsilon_{mb}$.

In laminar flow conditions, $Re_t < 0.2$, the terminal velocity could be determined by knowing the physical properties of the system as:

$$U_t = \frac{(\rho_p - \rho) g d_p^2}{18\mu} \qquad (2.27)$$

Substituting (2.27) in (2.26) and taking n = 4.8:

$$\frac{\mu}{\left((\rho_p - \rho)\, \rho_p\, g\, d_p^3\right)^{0.5}} \geq 0.149\, (1-\varepsilon_b)^{0.5}\, \varepsilon_b^{3.8} \qquad (2.28)$$

Gibilaro et al. later confirmed (1985) that there were undoubtedly circumstances where interparticle forces could play an important role such as the influence of electrostatic and magnetic forces and the adhesive effects of moisture in gas fluidized systems. They suggested that interparticle forces could influence the *dynamic* behaviour of the bed whilst remaining neutral to its equilibrium state. Under equilibrium conditions, all particle layers are equally attracted by the layers immediately below and above: the net force is therefore zero. Thus both the steady–state expansion characteristics and the continuity wave velocity (or voidage propagation velocity, U_ε) are unaffected by the inclusion of interparticle forces. Therefore U_ε remains as equation (2.25).

Under non–equilibrium conditions the interparticle forces can no longer be neglected; they affect the elastic modulus of the suspension and, as a result, the dynamic or elastic wave velocity U_e which now could be obtained by:

$$U_e = \sqrt{\frac{3.2 g d_p (1-\varepsilon)(\rho_p - \rho)}{\rho_p} + \frac{4mk(1-\varepsilon)^m}{\pi d_p^2 \rho_p}} \qquad (2.29)$$

where m and k are constants which should be determined for each system. This equation is very general and no method was introduced by them for evaluating the

constants explicitly. The first term under the square root sign is identical to equation (2.24) and the second term incorporates the interparticle forces. The role of interparticle attractive forces in stabilizing fluidized beds, according to the improved criterion is illustrated in Fig. 2.6: the continuity wave velocity, U_ε, is unaffected, whereas the dynamic wave velocity, U_e, increases with interparticle attraction with the consequence that it makes its first intersection with U_ε at progressively higher values of the voidage, ε. Voidages below ε_{mf} are unattainable in practice, so that an intersection in the range $\varepsilon_{mf} > \varepsilon > 0$ indicates a bed that displays aggregate behaviour from the onset of fluidization; intersections at higher voidages signify an initial range of stable particulate expansion and fully particulate behaviour is achieved where the interparticle attractive forces are sufficient to prevent any intersection occurring.

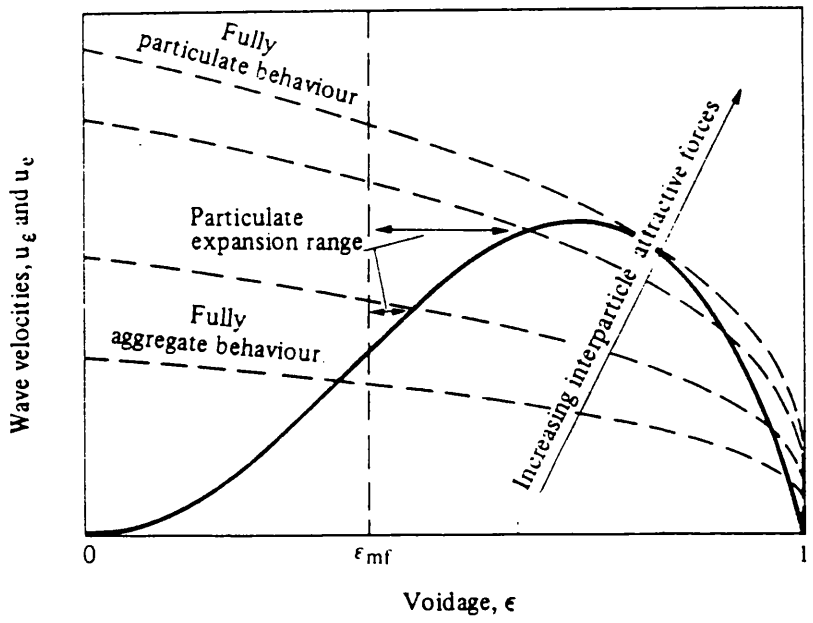

Fig. 2.6. Fluidized bed stabilization by interparticle forces: the full line represents the continuity wave velocity, U_ε and broken lines represent dynamic wave velocities, U_e, for increasing values of interparticle forces (Gibilaro et al., 1985).

Reiling (1992) took interparticle forces into account as well as the hydrodynamics to provide a more accurate criterion. The voidage propagation velocity was the same as equation (2.25) however the elastic wave velocity, considering the interparticle forces was found as (See Appendix A):

$$U_e = \sqrt{\frac{\sigma_{t,mb}}{C^* \rho_p (1 - \varepsilon_{mb}) \varepsilon_{mb}}} \qquad (2.30)$$

where $\sigma_{t,mb}$ is the tensile stress of emulsion phase at the incipient bubbling velocity and C^* is the proportionality constant defined as:

$$C^* = \frac{\text{interparticle forces across a single layer of particles}}{\text{drag force acting on a single layer of particle}} \qquad (2.31)$$

$$C^* = \frac{\delta\sigma_t}{\delta P^*} = \frac{\left(\sigma_{t,lp} - \sigma_{t,mb}\right)}{\Delta P^*_{mb}} \bullet \frac{H_{mb}}{d_p} \qquad (2.32)$$

where $\sigma_{t,lp}$ is the tensile stress of the loose packed powder and ΔP^*_{mb} is the bed pressure drop at incipient bubbling velocity. ΔP^*_{mb} is a hypothetical quantity that can be thought of as follows: As gas is passed through a bed of particles, the bed pressure increases linearly with gas velocity up to the point of minimum fluidization (Fig. 2.7). As the bed continues to expand above U_{mf} in the homogeneous region, the bed is stabilized by a sort of *cavity* structure in the region of bed expansion between U_{mf} and U_{mb}. The cohesive interparticle interactions give rise to a restoring force that counteracts the drag force. This restoring force is continuously lowered due to increase in porosity because of a reduction in the number of particle contacts. At a high enough gas velocity, the cross–linked particle networks are finally broken, there is a decrease in the internal stress of the emulsion phase. The bed reaches a maximum voidage and bubbling commences. The pressure drop at U_{mb} is ΔP^*_{mb}. This gives rise to the definition of C* in equation (2.32).

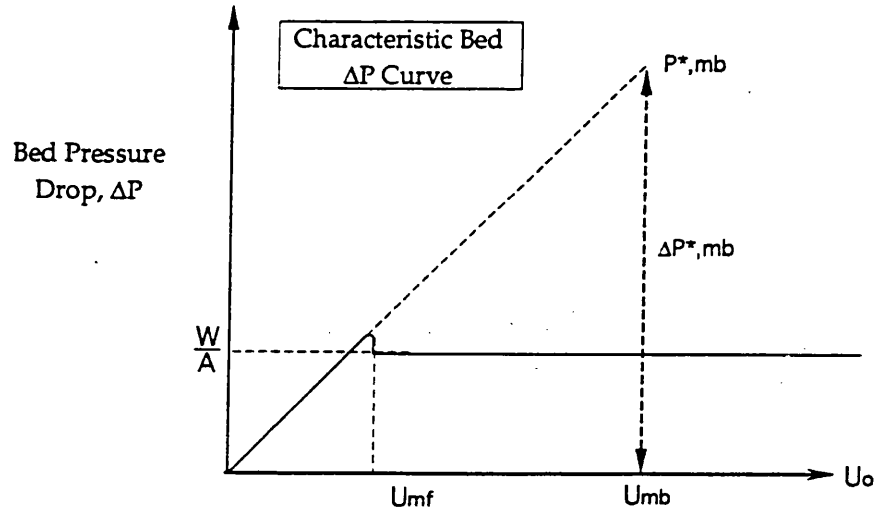

Fig. 2.7. Graphical representation of ΔP*mb, the hypothetical bed ΔP at the incipient bubbling velocity used in the transition criterion of Reiling (1992).

The tensile stress at incipient bubbling is given by:

$$\sigma_{t,mb} = \sigma_{t,lp} \frac{1-\varepsilon_{mb}}{1-\varepsilon_{lp}} \frac{\varepsilon_{lp}}{\varepsilon_{mb}} \tag{2.33}$$

Substituting (2.32) and (2.33) into (2.30) and simplifying the results yields:

$$U_e = \left[\frac{d_p . \Delta P^*_{mb}}{\rho_p . H_{mb}} \cdot \frac{\varepsilon_{lp}}{\varepsilon_{mb}\left(\varepsilon_{mb} - \varepsilon_{lp}\right)} \right]^{1/2} \tag{2.34}$$

The transition from homogeneous to heterogeneous fluidization therefore occurs when $U_e = U_\varepsilon$:

$$n\, U_t\, (1-\varepsilon)\, \varepsilon^{n-1} = \left[\frac{d_p . \Delta P^*_{mb}}{\rho_p . H_{mb}} \cdot \frac{\varepsilon_{lp}}{\varepsilon_{mb}\left(\varepsilon_{mb} - \varepsilon_{lp}\right)} \right]^{1/2} \qquad (2.35)$$

Since Richardson–Zaki indices appear in both Foscolo–Gibilaro and Reiling criteria, they will be discussed in more details in the following section.

2.9. Richardson–Zaki Parameters

The relationship between bed voidage, ε, and the superficial liquid velocity, U, is given by the Richardson–Zaki (1954) equation which describes results for both sedimentation and fluidization:

$$\frac{U}{U_i} = \varepsilon^{\,n} \qquad (2.36)$$

In equation (2.36), U_i is approximately equal to the free falling velocity, U_t, of the particles in the fluid and n is a function of Reynolds number $U_t\, d_p\, \rho/\mu$. Values of n have been given by Richardson and Zaki (1954) to be between 2.4 to 4.8 and by others (Richardson and Meikle, 1961; Jottrand 1952; Whitmore, 1957) for uniform particles, usually spheres, fluidized in a variety of liquids. As the particles deviate increasingly from spherical shape, the value of n becomes greater and Whitmore showed (1957) that while n was 4.80 for spheres, it increased to 9.5 as the particle size decreased, specially for fine irregular solids. High values of n, up to 14, were also reported by Reiling (1992).

Equation (2.36) can be rearranged as:

$$\log U = n \log \varepsilon + \log U_i \qquad (2.37)$$

Therefore a logarithmic plot of superficial fluid velocity, U, against bed voidage, ε, should be linear. The value of n is given by the slope of the line and U_i is the intercept on the U axis corresponding to $\varepsilon = 1$.

Haider and Levenspiel (1989) used a different technique for direct evaluation of terminal velocity, U_t, given particle diameter, d_p and the physical properties of the system. They introduced a dimensionless particle size d_p^* and a dimensionless gas velocity U^* as follows:

$$d_p^* = d_p\left[\frac{\rho(\rho_p - \rho)g}{\mu^2}\right]^{1/3} \tag{2.38}$$

and

$$U^* = U\left[\frac{\rho^2}{\mu(\rho_p - \rho)g}\right]^{1/3} \tag{2.39}$$

Using the equation form suggested by Turton and Clark (1987), they presented the following useful approximation for the direct evaluation of the terminal velocity of particles:

$$U_t^* = \left[\frac{18}{(d_p^*)^2} + \frac{2.335 - 1.744\phi_s}{(d_p^*)^{0.5}}\right]^{-1} \qquad 0.5 < \phi_s < 1 \tag{2.40}$$

For spherical particles this expression reduces to:

$$U_t^* = \left[\frac{18}{(d_p^*)^2} + \frac{0.591}{(d_p^*)^{0.5}}\right]^{-1} \qquad \phi_s = 1 \tag{2.41}$$

To find the terminal velocity of single free falling particles, d_p^* and U_t^* are obtained from equations (2.38) and (2.40) or (2.41); then U_t may be determined using equation (2.39).

The ratio of U_t/U_{mf} strongly depends on particle size. Kunii and Levenspiel (1991) suggested the following values for spherical particles of one size and $\varepsilon_{mf} = 0.4$:

$$\frac{U_t}{U_{mf}} = 78 \qquad \text{For fine solids when } d_p^* < 1 \qquad (2.42)$$

$$\frac{U_t}{U_{mf}} = 9.2 \qquad \text{For large solids when } d_p^* > 100 \qquad (2.43)$$

2.10. Multicomponent Fluidized Beds

In recent years many applications of gas–solid fluidized bed technology have been developed in which more than one particulate species of a single size (or narrow size range) are present. As in all situations where particulate species of different density of wide size range are moving relative to each other, a dynamic equilibrium is set up between the mixing and segregation tendencies. In some fluidized bed processes, it is important that good mixing prevails; in others that segregation and thereby the separation of the different species be achieved; and in some cases both should be established in physically different parts of the equipment.

In binary systems, as with a single component, particle motion is caused by bubbles (Rowe et al., 1972b). However, for binary (and multicomponent) mixtures, the U_{mf} is a function of the two components and their relative proportions and varies from point to point within the bed, depending on the local composition. Thus there is a complex feedback relationship between the point U_{mf} and the superficial gas velocity.

Another complicating factor arises from measuring the minimum fluidization velocity. For example, the pressure drop versus gas flow rate relationship with increasing superficial velocity starting from the well–mixed condition is generally different from that obtained on subsequently reducing velocity. This is due to the segregation that may occur once the packed bed becomes fluidized, and that can continue during any subsequent changes in velocity until all fluidization has ceased. Thus the normal means of determining U_{mf} may no longer be applicable.

The segregating tendency of particles of different size or density in the fluidization of binary and/or multicomponent systems leads to a top–to–bottom variation in concentration. In particular, one component, the flotsam, tends to rise and the other, the jetsam, tends to sink (Rowe et al., 1972a). Such a tendency was also found in multicomponent beds (Nienow et al., 1978). When a binary mixture is fluidized, generally one species will have a lower U_{mf} than the other. The lower U_{mf} species will fluidize at velocity U_F (the fluid component) and the higher at U_P (the packed component) (Rowe et al., 1972a). If the mixture is fluidized at $U>>U_P$, and then U is reduced at a steady rate to zero (the defluidizing procedure), then, depending on the defluidizing procedure and the physical properties of the two components, the settled bed obtained will generally have one of the three mixing–segregation states indicated by Fig. 2.8(i).

For systems with only a small difference in size and of equal density, a good mixture may be obtained throughout the bed regardless of the defluidizing procedure (Fig. 2.8c). In this case a graph of ΔP against superficial gas velocity U (curve iic) provides a unique measure of minimum fluidization velocity U_M (as it does for each of the pure components U_F and U_P and as is also shown in Fig. 2.8).

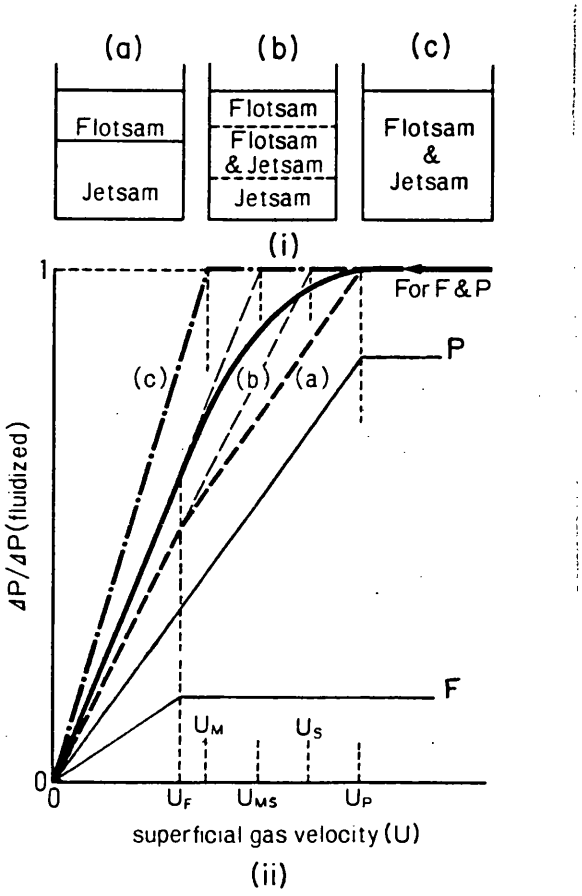

Fig. 2.8. Relationship between bed pressure drop and gas velocity; F: fluidized, P: packed (Nienow and Chiba, 1985).

At the other extreme, if one component is both considerably bigger and denser than the other, then the system might remain completely segregated independent of the defluidizing procedure (Fig. 2.8a). In this case ΔP plotted against U will again be unique and will be the sum of the contributions from the pure component (curve iia). However, in order to obtain a U_{mf} value, some special definition must be adopted, since at $U_F<U<U_P$ the upper part of the bed is well fluidized while the bottom is packed. A definition is one broadly equivalent to that for a pure component or for the completely mixed case; viz., the velocity at the intersection of the two extrapolated

linear portions of the plot corresponding to the regions where the whole bed is, first, fluidized ($U>U_P$) and, second, packed ($U<U_F$). This apparent minimum fluidization velocity is shown as U_S in Fig. 2.8.

Generally, the upper part of the bed is flotsam–rich, the lower jetsam–rich, and there is a mixed region in the middle (Fig. 2.8b). On going from U_P to U_F , a steadily decreasing amount of bed will be fluidized, but as long as at least some of it is, particle rearrangement can occur. If defluidization is slow and the species differ in density, Fig. 2.8b will tend towards Fig. 2.8a. If the species only differ in size and defluidization is rapid, Fig. 2.8b will tend towards Fig. 2.8c. In each case ΔP versus U will in general be as shown in Fig. 2.8(ii)b with U_{MS} being a function of the defluidization procedure.

2.11. Effects of Fines on Fluidization

Improving the fluidization behaviour of powders and fluidizing fine particles have been the subject of some investigations. As stated previously, fine particles normally have a cohesive behaviour and they are the most difficult to fluidize. Different means have been reported to reduce the problems involved in gas–solid fluidization:

1) Addition of fines to the host material.
2) Use of agitators in the bed to break up channels.
3) External vibration of the bed.

Addition of fines to the bed was reported (Geldart and Pope, 1983) to increase significantly the carryover of coarse particles and cause the carryover of even coarser particles which would have otherwise remained in the bed because their free fall velocity was higher than the gas velocity. According to Geldart and Pope (1983), the

amount of coarse found at a given level increased with gas velocity in both the absence and presence of fines, as expected, and the coarse hold–up decreased with height; however, the hold–up increased dramatically when fines were present and the larger the coarse, the smaller the effect of the fines even when the gas velocity was higher.

Zenz (1984) was probably the first to mention using ultrafine particles to improve the fluidization properties of powders (Reiling, 1992). He suggested adding 0.05 μm unagglomerated colloidal silica to observe *smoother* fluidization but did not carry out any experimental investigations.

Brooks and Fitzgerald (1985, 1986) found a type of fibrous carbon (TCM) which had a large bed expansion of over 100% and was free of bubbles in a gas fluidized bed which was similar to the behaviour of good quality liquid/solid fluidization. The carbon fibres were 0.1–0.3 μm in diameter and were normally expected to behave with major fluidization problems. According to Brooks (1991), at least some of TCM's desirable properties could be attributed to its electrical characteristics. Geldart reported (1973) that graphite coating of particles could be used to reduce problems associated with static electricity. This suggests that carbonaceous and therefore conducting property of TCM was likely to be an important factor in reducing interparticle forces and improving its fluidization behaviour. Additionally, very low density TCM was desirable for bubble free fluidization, since bubbles tend to be less stable in low density solids. A third feature of the TCM was its highly irregular particle shape, which seemed to allow the material to agglomerate to sizes which were more easily fluidized. The combination of density and shape was investigated by compacting TCM into smooth spherical particles which bubbled freely much like any other material of similar size and density when fluidized. As the granules broke up and the smooth surfaces disappeared, the material gradually returned to its normal non–bubbling state.

They also reported that TCM improved the fluidization of other Group A powders and permitted Group C cohesive powders to be fluidized. Mass concentrations of TCM in such mixtures were typically in the range of 20–80% depending on the properties of the cohesive powder and the desired fluidization quality. For instance, addition of 5% TCM to a Group A alumina, 60–300 μm in diameter, reduced bubbling and fluidization density in the bed and a bed of 50% of this material and kieselguhr behaved like TCM alone.

Dutta and Dullea studied (1990) the effects of the addition of Aluminium Oxide C (AOC) and Aerosil 200 (A200) on the cohesiveness and fluidization behaviour of a phosphate based nonporous cohesive powder which was a non–spherical Group C material (3.65 μm). Both additives were nonporous. AOC was fluffy with a diameter of 20 nm and was known to have a strong affinity for positive charge whereas A200 (high purity silica) had an amorphous structure (12 nm in diameter) as well as the tendency to develop a negative surface charge. They measured parameters such as Low Packed Bulk Density (BD), Tapped Density (TD) and Hausner Ratio (HR) at different additive concentrations. Hausner ratio is the ratio of the tapped density to the low packed bulk density and is greater than unity. A drop in HR shows a decrease in the cohesiveness of the powder.

They reported that BD increased with addition of ultrafines up to an AOC level of 0.35% and then decreased slowly. At its maximum point BD had an increase of 33% from the control sample which had no additive. The effect of AOC was less pronounced on the TD than the BD.

The HR and hence the powder cohesiveness decreased with AOC addition up to an AOC level of 0.35% which was considered to be the optimum concentration of AOC. The minimum HR corresponded to a 22% reduction with respect to the control sample. The concentration corresponding to the minimum HR was where the BD peaked which was a result of the stronger influence of additive on the BD rather than the TD. The same set of experiments were carried out for A200 and similar results were obtained. In this case the optimum concentration was 0.2%.

When fluidized, the blends containing 0.35% AOC or 0.2% A200 had maximum 90% expansion whereas the control sample had an expansion of 27%; very few channels were observed in the beds and the elutriation losses were lower than those for the sample with no additive. They believed that charge effects governed the operation of both additives. Their results indicated that the flow conditioning of A200 which had a negative charge, was superior to that of AOC which had an affinity for positive charge. According to them, SEM indicated no significant change in host surface coverage by additives between the initial and final bed samples; therefore the additive, in spite of its much smaller particle size, was not elutriated preferentially to the larger host material. They deduced that the force holding the additives to the host particles were stronger than the drag force in the fluid bed.

The point that there was an optimum additive concentration was also reported by others (York, 1975; Hollenbach et al., 1982). It is believed that at that point effective coverage of the particle surface is obtained and therefore additional coverage would not produce any significant effect. According to Hollenbach et al. (1982), bulk parameters (i.e., density and compressibility) were more sensitive indices to changes occurring in powders as compared to parameters determined in compacted specimens (i.e., yield in shear, internal friction). In other words, the magnitude of the latter changes was not

big enough to be revealed by a small number of experiments, especially where considerable variability (due to differences in size distribution for example) was an inherent characteristic of the system. The interaction between fines and the surface of the larger particles was not limited to particles of the same species. However, the existence of chemical or physical compatibility between the adhering particles is essential so that the system would not segregate.

The optimum concentration is not necessarily fixed for a given additive and it may well be a function of the host powder and additive physico–chemical properties. It may also be influenced by segregation of the additive particles in extremely dry host powders or by its uneven distribution in case of cohesive powders. At this critical concentration parameters such as density or Hausner ratio reach a stationary point and further addition of the additive may reverse the desirable effects.

Confirmation of the presence of the additives at the surface of the host particles is crucial to the analysis of the bulk behaviour. The reason is that the powder bed structure is strongly affected by interparticle forces, specially in the case of cohesive powders. It is, therefore, important to know whether the agent activity is through surface modification, that alters the interparticle friction and the capacity of the particles to form bridges or through reducing the bed porosity by being merely a filler of the interparticle space. Hollenbach et al. (1982) used sugar, 50–300 μm in diameter, as the host material with silicon oxide, sodium aluminium silicate, tricalcium phosphate and calcium stearate with a particle size of 0.5 μm as the additives. They observed a fairly uniform distribution of the additives at the surface of the host particles which suggested that the former mechanism was dominant. On the other hand, the observed increases in loose bulk density were generally dependent on the additive and the concentration. They deduced that the presence of the additive at the

host particle's surface physically separated the particle which resulted in reducing its attractive interparticle forces.

York (1975) prepared mixtures of fine silica with lactose and calcium hydrogen phosphate. He reported that by increasing additive concentration, flowability of the host material increased up to a limited concentration and there was no further improvement in the flow factor beyond that level.

Dutta and Dullea also reported (1991) that the external vibration of the bed would increase the bed expansion and reduce the elutriation. It also increased the bed pressure drop which was an indication of decreased channelling in the bed. In similar experiments, addition of saffil with a mean particle size of 3 μm to an inorganic fine (4.25 μm) decreased the BD and increased the Hausner ratio of the blend relative to the powder which reflected an increase in the cohesiveness of the material, due to the development of an enhanced structure caused by increased interparticle forces.

Geldart and Abrahamsen (1980) noted that the bed voidage increased with fluid density and viscosity while fines fraction and particle size and particle density decreased because a greater percentage of gas travelled into the emulsion phase. This was consistent with observations that an increase in operating temperature and pressure or fines content increased the fluidization quality. This was further substantiated by Yates and Newton (1986) who studied the catalytic dehydrogentation of butene–1. Conversion increased from 80% to 85% upon addition of 13% fines, and up to 92% conversion was obtained with 27% fines. They concluded that a higher concentration of fine particles caused more gas to flow through the emulsion phase. Rowe et al. (1978) reported that bubble shapes were changed and bubble rise velocity decreased when the fine content of beds of silicon carbide particles was increased.

Steeneken et al. (1986) used potato starch, 40 μm in diameter with a particle density of 1450 kg/m^3 containing 20% moisture as the host material and an amorphous silicon oxide, 18 nm, was the flow conditioner. They observed that addition of only a few parts per thousand of flow conditioner turned potato starch from a cohesive powder into a free–flowing one. Porosity and compressibility also decreased while bulk density increased significantly. Higher amounts of flow conditioners were less effective in reducing the porosity and compressibility which might be due to the fact that at such high levels of addition the very low packing density of the conditioner itself became noticeable. Potato starch with flow conditioner did not crackle, due to its very small compressibility.

They also reported powder properties were likely to be influenced by the size of the additive. At increasing particle size of the conditioner, a larger amount of it would be required to affect the flow properties of the powder. They believed that conditioner particles did not act like small ball bearings but rather diminished cohesion of starch powder by surface roughening.

Geldart and Wong (1987) reported that for Group A powders having a particle density less than about 1.4 g/cm^3 and a size range of 20–100 μm, the entrainment flux increased as the mean size was reduced. However, a size was eventually reached at which the entrainment flux ceased to increase with decreasing mean size and a reverse effect was observed upon further reduction in size. At the same point, the powder became cohesive and Group C behaviour was found as predicted.

They also showed that the addition of very fine particles, 5 μm in diameter, to a free–flowing powder produced a progressive reduction in entrainment rate at levels of

addition from 10 to 50%. This effect was attributed to the adherence of the fine particles to the larger ones, 90 μm in diameter. Group A type of behaviour changed to Group C behaviour above 30% addition.

Yang et al. (1985) observed that when talc, a Group C powder of 7 μm in diameter, was added to either a Group A or a Group B material, the fluidizing characteristics of either component were found to be improved by the presence of the other. In general, an intermediate composition, with optimum fluidizing characteristics surpassing that of either of the constituents was obtained. This result can be explained by a spacer role of the added particles whereas the results of Geldart suggested something more like a bridging role.

Geldart et al. (1979) used sand the host material and finer alumina with different concentrations and obtained the entrainment rate of the coarser particles. They reported that the fines were relatively unaffected by the coarse but the carryover of coarse was considerably enhanced by the fines. Presence of fines shifted the size distribution of the sand product towards the coarser end.

They attributed this effect to a momentum interchange mechanism between fines and coarse and postulated that denser, smaller particles having similar terminal velocities to the sand should be less affected by fines because they offer a small target area. They repeated the experiments with metal shot/alumina mixtures and reported the same trends however the shot seemed to be affected less by alumina.

An increase in the fines in the bed increased the amount and size of the coarse solids elutriated. Particles having terminal velocities larger than the superficial gas velocity were carried over in all cases where the powders had a wider size distribution or were

deliberately mixed together. The presence of fine particles enhanced the carry–over rate constant, but the finer particles were apparently unaffected by the coarse. It was also reported (Avedesian, 1977; Merrick and Highley, 1974) that particles having terminal velocities larger than the superficial gas velocity were found in the cyclone product even when the free–board was as high as 9 m.

Briens et al. (1992) fluidized polyethylene particles with a mean diameter of 400 μm in a 0.102 m i.d. carbon steel bed, using filtered dried air and injected negative and positive charges into the bed to completely neutralize all charges present on the bed particles. They reported that neutralization of particle charges, increased elutriation losses by about two orders of magnitude although it did not greatly affect the size distribution of the elutriated particles. Neutralization also made the fluidization much smoother, indicating that the electrostatic charges affected most of the bed particles.

They also confirmed that the smallest bed particles were not the most easily entrained. The particles smaller than 60 μm were not as easily entrained as 80 or 110 μm. This was observed regardless of fluidization period. In fact, particles smaller than 60 μm could not be selectively removed by elutriation. From a theoretical point of view, this is in sharp contrast to the assumption made by entrainment models (Zenz and Weil, 1958; Gugnoni and Zenz, 1980; Briens et al., 1988) that the smallest particles are more easily entrained.

Similar results were obtained for sand particles with a mean diameter of 65 μm and also cracking catalyst of 69 μm in a 0.61 m i.d. bed. Sand particles smaller than 30 μm and cracking catalyst smaller than 20 μm were more difficult to entrain. Changes in air relative humidity did not affect the bed expansion and/or the flux of particles

ejected from the bed surface; therefore the quality of fluidization of sand was not affected by electrostatic effects.

In experimental results reporting hydrodynamic properties of Group C particles in fluidized beds, agglomeration of particles has been observed (Morooka et al., 1988) resulting in good fluidization of hard–to–fluidize fine particles. It is hence inferred that the majority of fine particles in the bed, agglomerate into clusters which are easily fluidized and a small fraction of fine particles remain as fines free from the others. Also, it has been known that, when fine powder is mixed with large particles in a fluidized bed, the fine powder not only forms agglomerates (Kono and Tian, 1992; Kono et al., 1990) but also coats or attaches to the larger particles (Geldart and Wong, 1987; Kokkoris and Turton, 1991). It has also been prospected (Baeyens et al., 1992) that Group C fines added to Group A powder adhere to each other to form agglomerates having, effectively, a large size or adhere to large particles in the powder.

Geldart and Wong (1987) found that the addition of very fine Group C powders to a free–flowing Group A powder reduced the total entrainment rate and postulated that two mechanisms were involved: (a) for an A–type powder to which only a small amount of cohesive powder was added, the reduced entrainment could be due to the adhesion of small particles to the larger ones causing them to behave like the latter rather than acting independently; (b) for a mixture containing such a large amount of the cohesive additive that it behaved cohesively, bubble activity was much reduced and channelling increased, thus reducing entrainment.

Baeyens et al. (1992) added Group C powders to a number of Group A materials in proportions which ensured that they remained within Group A. They reported that the

elutriation rate constant, first increased with decreasing particle size, and then below a critical diameter it levelled off. It was attributed to the interparticle adhesion forces. Based on their experimental results, an empirical equation was presented to calculate the critical particle size at which interparticle forces start to dominate as:

$$d_{crit}\,\rho_p^{0.725} = 10{,}325 \qquad (2.44)$$

where d_{crit} is in microns and ρ_p is in kg/m^3.

Morooka et al. (1988) studied the fluidization of several powders and determined that some of the powders could be fluidized when gas velocity was in excess of their apparent minimum fluidization velocities, because Group C particles formed agglomerates during fluidization. Chaouki et al. (1985) and Pacek and Nienow (1990) also analyzed the self–agglomeration of Group C powders. Their results showed that some limited Group C fines could be sufficiently fluidized because of self–agglomeration, displaying a hydrodynamic behaviour similar to that of Group A powders. Kono and Tian (1992) made full use of self–agglomeration for densifying ultrafine powders in a fluidized bed.

Kono et al. (1986) reported that fluidization characteristics of fine powders, including their tensile strength and plastic deformation coefficients, could be changed by mixing Group A particles with Group C fines. Kono et al. (1987) observed agglomeration and segregation of Group C particles from the homogeneous emulsion phase of Group A and C mixtures when the mass fraction of Group C powder exceeded a certain saturation point. Kono et al. (1990) also reported the agglomeration of fine powders in gas–solid two–phase flow for A–C mixtures.

Mori et al. (1990, 1992) investigated vibro–fluidization of binary mixtures between Group C alumina and other alumina particles of various sizes covering Group C to Group A and measured elutriation rates of mixtures. They reported that the elutriation rate constant depended strongly on mixing ratios. They also found no segregation in the vibrated–bed of mixtures of Group C and Group A.

To investigate the effects of ultrafines on fluidization of Group A powders, Reiling (1992) used a number of Group C powders, different in shape, size and surface area. Measurement of powder cohesion using a Hosokawa Powder Tester showed that the cohesion increased with concentration of the ultrafines. The cohesion of various powder systems was found to depend on not only the ultrafine particle size, but also the surface properties like shape and type of ultrafine. Cohesion also increased with decreasing mean particle size of ultrafines added. Therefore, the concentration, particle size and shape of the additives had an important effect on the cohesion.

Group A/C cohesive powders exhibited larger emulsion porosity, delayed bubbling, up to 3 to 30 times higher U_{mb}/U_{mf} ratios, and over 200% bed expansion as a result of the addition of fines. The large bed expansions were also reflected in higher bed expansion index, n, larger powder deaeration times and larger emulsion phase porosities. Increasing bed expansion was due to a greater amount of gas flowing interstitially, which enhanced gas–solid contacting. These phenomena could only be the result of a greater percentage of the gas penetrating and travelling through the emulsion phase. Thus less gas was by–passing the bed in the form of bubbles which was advantageous in terms of enhancing the gas–solid contact.

Minimum fluidization velocity decreased with increasing ultrafine content which was attributed to a decrease in powder density. The lower the U_{mf}, the earlier the gas

could penetrate and begin to expand the bed. Incipient bubbling velocities increased with ultrafine concentration. It was inferred to particle networking and stabilization of the emulsion phase by interparticle forces. The higher the U_{mb}, the more the bed could expand before it began to bubble. The combination of the lower U_{mf}'s and the higher U_{mb}'s meant that more gas was flowing through the interstices of the particles resulting in larger bed heights at incipient bubbling and higher bed expansions. More cohesive powders had larger deaeration velocities which meant that the air could escape more quickly from the powder, allowing it to deaerate and settle faster.

The spontaneous agglomeration of ultrafine Group C particles and their effect on fluidization has been reported by researchers such as Meissner et al. (1964), Donsi and Massimilla (1973b), Chaouki et al. (1985), Hartley (1985), Morooka et al. (1988), Lauga et al. (1991). Meissner et al. (1964) concluded that fine particles of zinc oxide less than 0.25 μm agglomerated by spontaneous cohesion attributable to the action of van der Waals forces. High percentage void volumes (>90%) were reported for these zinc powders due to a cohesive structure. Coarse particles that show no interparticle forces always pack closely, 35 to 40% void volume. Donsi and Massimilla (1973b) developed a model for the role of van der Waals and capillary forces on the growth of cavities (bubbles) for particles in the range of 40 to 100 μm. Chaouki et al. (1985) studied the effect of van der Waals interparticle forces on agglomeration of fluidized Cu/Al_2O_3 aerogels, a class of Group C powders. They developed a comprehensive model to predict cluster size and hydrodynamic behaviour by making the assumption that van der Waals forces were acting between elementary grains. The clustering process is caused by bubble agitation and allows Group C powders to fluidize homogeneously rather than channel. Hartley et al. (1985) found that tensile strengths compared favourably with particle agglomeration based on van der Waals forces for submicron Ni, Si_3N_4, SiC, Al_2O_3 and TiO_2 powders in a small 3.5 cm glass column.

These submicron powders form agglomerates, in the order of 100–1000 μm when fluidized. They found that ultrafine powders could be smoothly fluidized by themselves if the gas velocity was large enough to disintegrate the particle structure. Lauga et al. (1991) improved the fluidizability of Group C Ni/SiO_2 aerogels by reducing interparticle forces.

Several authors (Matheson et al., 1949: Finnerty et al., 1969: Trawinski, 1953; Reiling, 1992) showed that addition of fines to fluidized beds lowered their viscosity. Low viscosity, low density beds favour destruction of bubbles and lead to smaller bubbles comparing to high viscosity beds. Smaller bubble sizes in turn imply an increase in the bed expansion since more gas travels through the bed interstitially. Hence, a plausible mechanism for smaller bubble size in fluidized beds is a lower emulsion phase viscosity.

2.12. Conclusions

On the basis of the above reports, it could be concluded that fine particles in a bed are in one of the three forms: elutriable freely moving fines, agglomerates of fines having fluidizable sizes, and fines attached to large particles. The presence of fines may affect the fluidization behaviour by changing parameters such as elutriation rate, minimum fluidization and bubbling velocities, bed density and viscosity. An optimum additive concentration appears to exist at which the flowability of the host powder improves significantly and further addition of fines may reverse the effects and/or yield no significant change. The existence of chemical or physical compatibility between host and fines is essential so that the system would not segregate.

There are some reports about the influence and the effects *fines* on fluidization. However, few researchers have investigated the effects of *ultrafines* on fluidization. Addition of some ultrafines have been reported to improve the fluidization quality but little systematic work has been carried out in this field. The reason for the large bed expansion, increase in fluidizability, reduced bubbling and entrainment and in general, particulate–like flow attributed to ultrafine particles have not been elucidated. While Geldart and Pope (1983) reported that addition of fines to the bed *increased* the carryover of coarse particles, Geldart and Wong (1987) as well as Dutta and Dullea (1990) mentioned a *decrease* in elutriation loss as a result of addition of ultrafines. There is a need, therefore, for some practical work and evidence of these effects which forms the basis of the experimental study to be presented and discussed in the following chapters.

Three different models were presented: the model of Mutsers and Rietema (1977a) considers only the interparticle forces in the bed while the original model of Foscolo and Gibilaro (1984) is based on the importance of hydrodynamic effects. This model was later modified (1985) by introducing interparticle forces and considering that these forces only influence the dynamics of the bed but some parameters of the model cannot be explicitly determined. The third approach, Reiling's model (1992), considers both interparticle forces and hydrodynamic effects. These models will be compared with experimental data in Chapter Four.

CHAPTER THREE

MATERIALS AND METHODS

This chapter describes different experiments which were carried out as well as the materials used and their properties.

The research project was divided into two sections: (i) systematic study of the properties of powders with and without ultrafines and (ii) fluidization. The former included measurements of particle size and size distribution, surface area, various densities, particle charge, powder viscosity, as well as pore size and pore size distribution of powders for several combinations of ultrafines and host materials.

The fluidization experiments consisted of measurements of minimum fluidization and minimum bubbling velocities and bed heights at minimum fluidization/ bubbling conditions. Bed collapse experiments were also carried out to investigate the expansion of the dense phase together with the expansion due to bubbles. The bed voidage was also determined and compared for various combinations of host materials and additives.

3.1. Materials

Two different Group A powders were used as the host materials for the experiments: Fluidized Cracking Catalyst (FCC) and silica. The FCC particles were spherical with a wide size distribution (Fig. 3.1) and a surface mean diameter of 56 μm and a particle

Fig. 3.1. Size distribution of FCC.

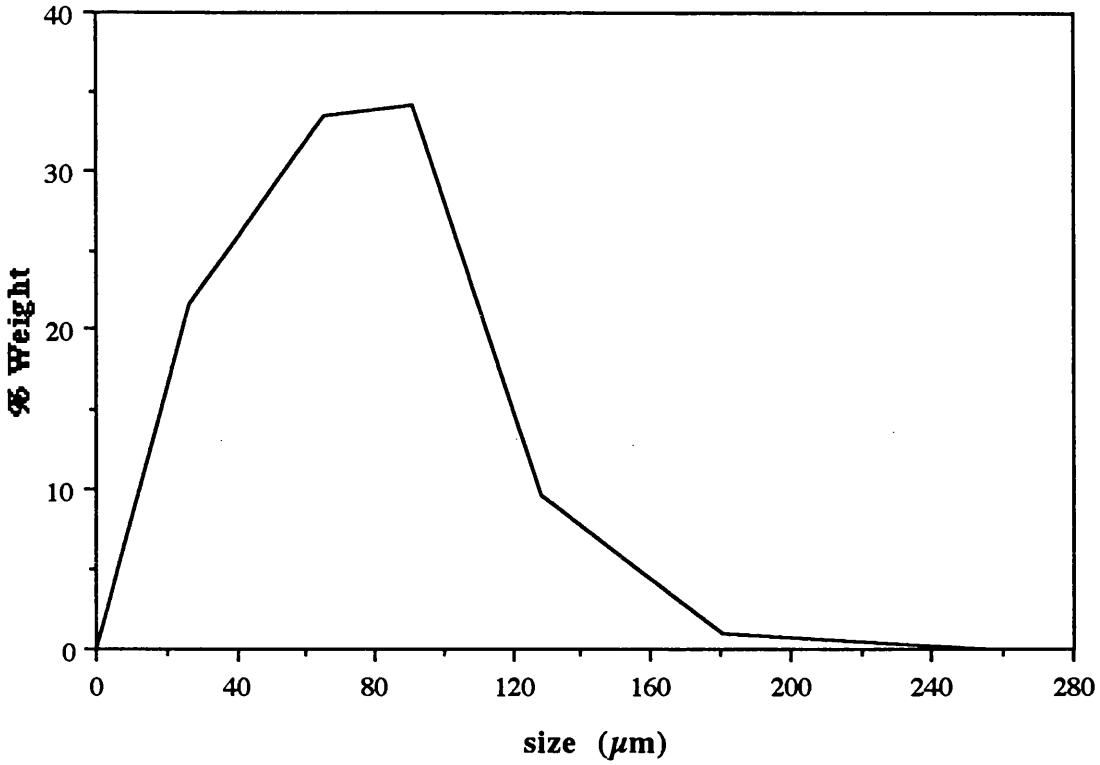

Fig. 3.2. Size distribution of silica.

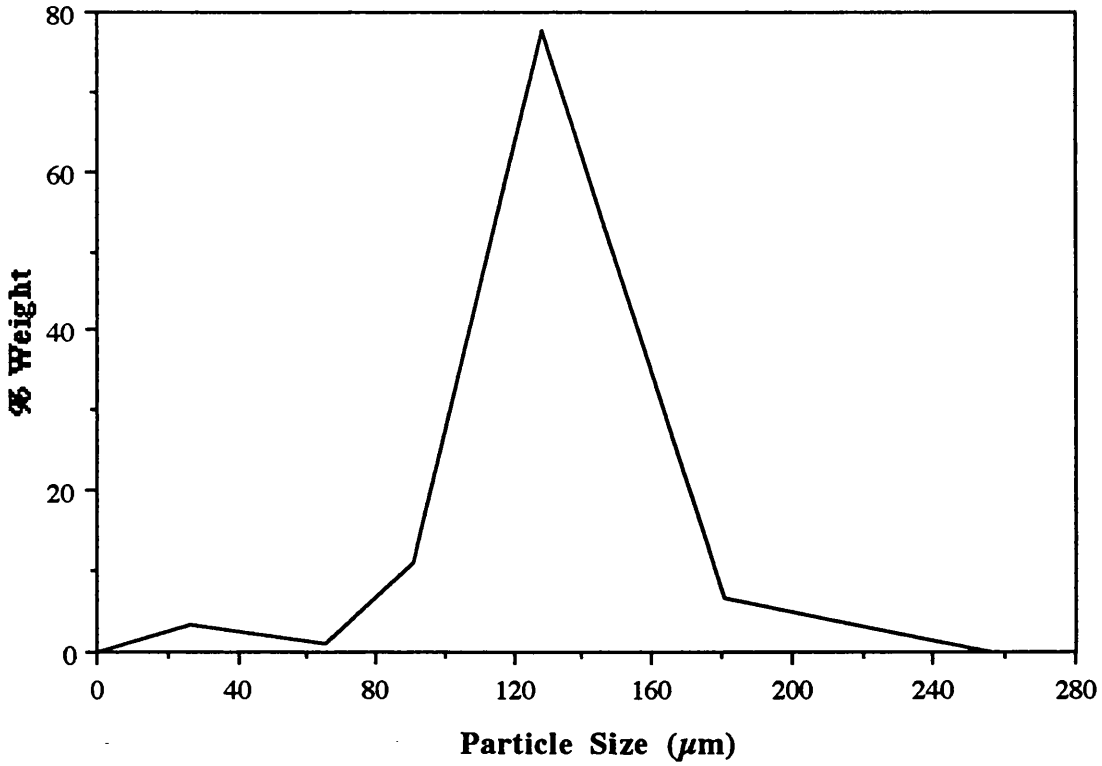

Fig. 3.3. Size distribution of kiesel–1.

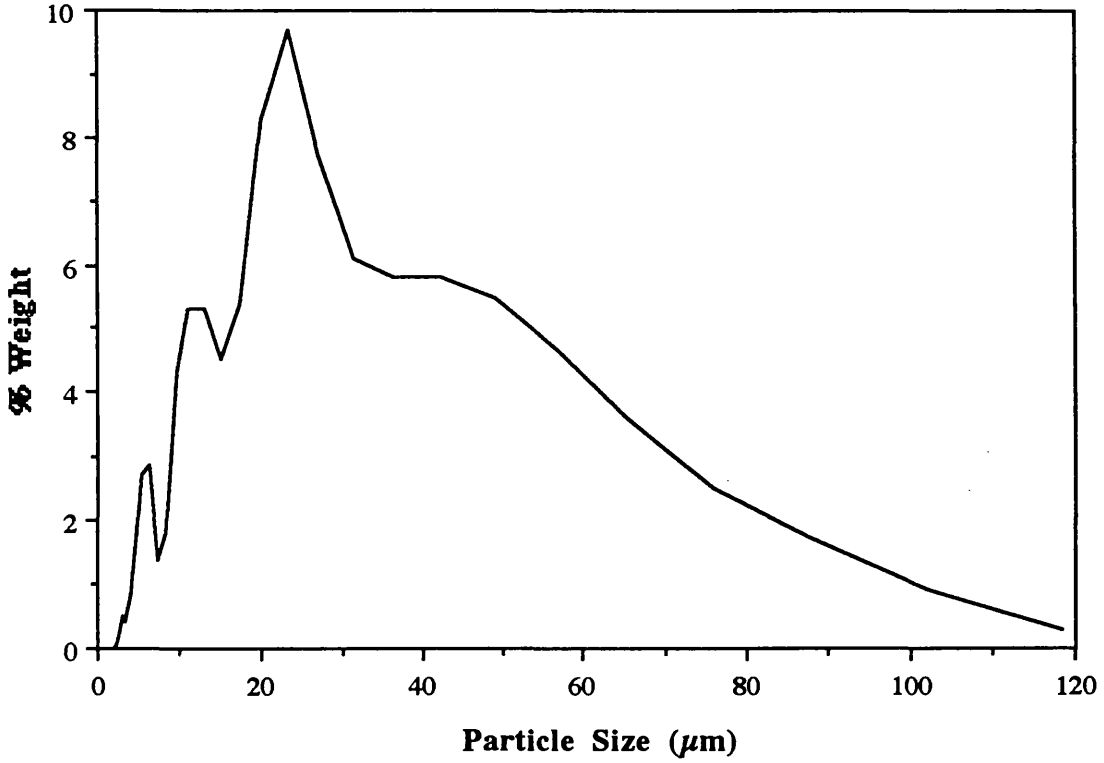

Fig. 3.4. Size distribution of kiesel–2.

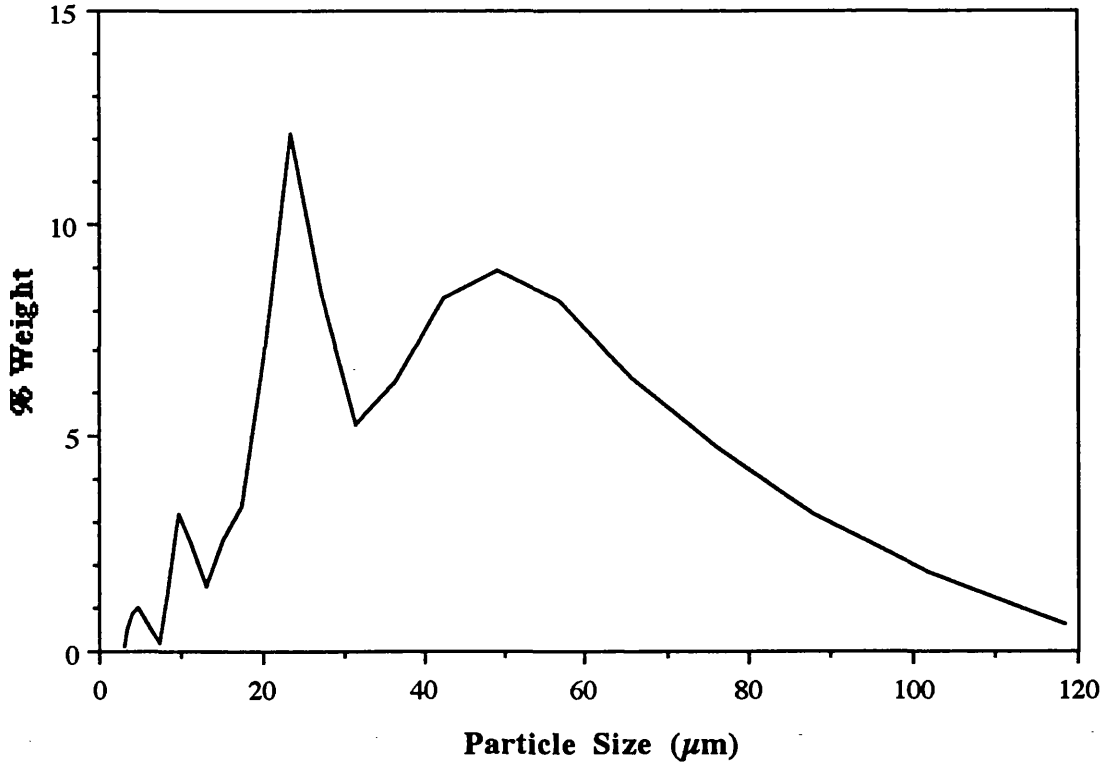

density of 1759 kg/m^3. The silica particles had a narrower size distribution (Fig. 3.2) and a mean size of 110 μm and their particle density was 718 kg/m^3. Physical properties of both of these materials were measured by the techniques that will be described in the following sections and are given in Table 3.1. Dissimilarity of the powders would afford a comparison between two materials with different particle size distribution, mean particle size, surface area and particle density.

In order to investigate the effect of ultrafines on Group C materials, two types of kieselguhr were used for the experiments: one with a mean particle size of 20 μm (Fig. 3.3) which was amorphous, porous and non-spherical (which will be referred to as kiesel–1). The bulk and skeletal density of this type were 202 and 2300 kg/m^3, respectively.

The other type of kieselguhr (kiesel–2) was 30 μm in diameter (Fig. 3.4) with particles more regular in shape and less porous. The bulk and skeletal density of this type were 289 and 2368 kg/m^3 respectively.

Table 3.1. Physical properties of FCC and Silica.

	FCC	Silica
Bulk Density (kg/m^3)	1168	402
Particle Density (kg/m^3)	1759	718
Skeletal Density (kg/m^3)	3120	2111
BET Surface Area (m^2/g)	162.8	351.7
Pore Volume, cc/g	0.252	0.9186
$\bar{d}_{sm}$ (μm)	56	110

The additives chosen were both hydrophil fumed silica with a primary particle size of about 120 Å according to the supplier (BDH Chemicals Ltd., Poole, England). Although the particles were very small, they agglomerated extensively due to their electrostatic charges and high surface area of 200 m^2/g (according to supplier). One type of fumed silica (which will be referred to as S1 fumed silica in the thesis) had a skeletal density of 3998 kg/m^3 and this value was 2700 kg/m^3 for the other type (M5 CAB–O–SIL). They both had a bulk density of 70 kg/m^3.

3.2. Equipments and Methods

3.2.1. Observation of Powders by SEM

Scanning Electron Microscopy (SEM) was used to study particle shape and size as well as their surface morphology specially in mixtures. In SEM a fine beam of electrons of medium energy (5–50 keV) is caused to scan across a series of parallel tracks. These electrons interact with the sample, producing secondary electron emission, back–scattered electrons, light and X–rays. Each of these signals can be detected and displayed on the screen of a cathode ray tube like a television picture. Examinations are generally made on photographic records of the screen. The SEM is considerably faster and gives more three dimensional details then transmission electron microscopy (TEM).

Samples as large as 25 mm × 25 mm can be accommodated and parts viewed at magnifications varying from 20 to 100,000× at resolutions of 15–20 nm as compared to 0.3–0.5 nm for the TEM (Allen, 1990). Because of its great depth of focus, the SEM can provide considerable information about the form of a particle and its surface morphology. Its depth of focus is nearly 300 times of the optical microscope.

Sample powders were dusted on an aluminium stub which had already been covered with a thin layer of adhesive. With an Emitech K550 gold sputter, a thin gold coating was formed onto the particles to dissipate charge caused by the electron beam of the microscope. The stubs were then placed in the specimen holder ensuring that the top of the stubs were level with the surface of the holder. The samples were then placed in the vacuum chamber of the SEM and the chamber vented. This was signified once the current meter light was ignited. The voltage of the electron beam was then entered and the filament current control rotated clockwise (usually 70–80 μA) until two peak deflections of the trace were observed. After one or two other minor adjustments, the surface of the sample was viewed at various magnifications and appropriate photomicrographs taken.

It should be noted that the SEM will only provide good images if the sample conducts electricity. The gold coating must be thick enough to ensure conductivity, but not so thick as to obscure the surface features. Also, some materials are easily damaged by very high coating currents. This was avoided by lowering the coating currents and lengthening the deposition times.

Electron micrographs in Section 4.1 show FCC, Silica and kieselguhr particles with and without additives at various magnifications. Higher magnifications show the surfaces of the particles in more details. They will be discussed in more detail in Section 4.1.

3.2.2. Sample Preparation

The powders were dried at 120 °C overnight for all the tests. Mixtures were prepared by weighing out the appropriate amount of ultrafines and host material. The total mixture was then blended using an impeller with two blades which were coated with rubber to avoid particle breakage during blending. Mixing time was normally five minutes, when an evenly dispersed and homogeneously mixed powder was obtained. The mixing would be continued when any agglomerate was observed by naked eye. In some experiments drying temperature and mixing time were increased to 150 °C and 40 minutes respectively but no significant changes were observed in the final results. The blending was carried out at ambient temperature, pressure and humidity. Samples were left in sealed containers for a few days before use.

SEM pictures were taken from the host materials before and after blending in the same manner as the mixtures were produced. No difference in particle size distribution was detected; therefore the mixing procedure did not alter the size distribution of the host materials.

M5 CAB–O–SIL was added to FCC, silica and kiesel–2 while S1 fumed silica was added to kiesel–1. Samples of silica and/or FCC were prepared in concentrations of 1, 2.5, 5, 10 and 15% weight ratio of ultrafines to the total weight of the additive and the host material. Samples of kieselguhr and ultrafines were in concentrations of 1, 2, 3, 4 and 5% wt.

3.2.3. Particle Size Measurements

SEM pictures provide a good indication of particle shape and size. However, some other methods were also used for particle size measurements depending on the particle size of the material in order to quantify their size distribution. Each technique will be described below :

3.2.3.1. Sieving

Sieving which is the easiest, cheapest and probably the oldest method for powder sizing, is applicable for liquid suspensions (wet analysis) as well as for analysis of dry powders. In this technique, a number of sieves with different standard meshes are nested one on top of another in a descending order with the largest aperture size sieve on the top. The stack forms a cylinder which normally sits on a pan called receiver. Agitation results in an increase in sieving efficiency.

The sieve apertures are classified as coarse (4 to 100 mm), medium (0.2 to 4 mm) and fine (less than 0.2 mm), which are mainly woven wire or punched plate sieves. Fine sieves below 0.04 mm or microsieves, however, are manufactured electrolytically from perforated metal foils. The weight of the sample depends on the density of test particles; a powder mass of 20 to 60 g of fine particles and 60 to 150 g of coarse ones are recommended for a sieve of 20 cm diameter. Sieve size is based on the median average of the particle sizes on the central sieve.

The appropriate sieving time is on the basis of different recommendations. BS1796 (1952) suggests that the sieving classification should be continued until less than 2% of the particles pass through in any 5 minutes of sieving process. In general 20 minutes

sieve classification time is sufficient for a successful dry analysis. Fine particles are likely to be aggregated during the process and the effect of this problem can be reduced by vibration.

The main problems associated with sieving are blinding and damage to the apertures due to vibration. Also, different particle shapes and surface patterns may result in analytical errors due to specific geometries or cohesive forces, respectively. Prolonged test runs is also a disadvantage specifically as an on–line particle size analyzer.

Particle size of FCC was measured by a nest of 20 cm Tyler sieves in the range of 300–53 μm using a shaker. 150 g of the powder was sieved for 25 minutes and the weight of the powder in different sieves and the receiver was measured. The powder was then sieved for a further 5 minutes and collected sample on each sieve was weighed again. There was little difference between the two sieve analysis (less than 2%). Therefore 30 minutes was found to be the optimum time for sieving. Mean particle size of the sample, d_{sm}, was then determined by equation (2.8).

In order to measure the size of silica particles, 100 g of the powder was used with the same nest of sieves and shaker; sieving time was 30 minutes.

3.2.3.2. Malvern

SEM pictures showed that particle size of kieselguhr was below 53 μm, the smallest sieve available. Therefore, sieving was not the appropriate method to determine the particle size distribution. In this case a Malvern 3600E sizer was used which was interfaced with a personal computer to data acqusition. Malvern 3600E system consists of a complete laser particle sizer optimized for the measurement of powders dispersed in

liquids. The operation of the Malvern is based on the light interaction. When particles are suspended in a transparent fluid with a refractive index different from that of particles, they cause an interruption to the light beam passing through the fluid. The light deviated by each particle at a given angle, caused by reflection, diffraction and/or refraction, is collected and then related to the size of particles.

A very small amount of sample was dispersed in distiled water in the cell of the Malvern. The stirrer was switched on and the data were collected for each sample. This device measures the particle size in the range of 1–118 μm. Since the powders had to be dispersed in a liquid, measurement of the particle size of the mixtures was not practical by this technique.

3.2.3.3. Elzone

Small size of ultrafines made most particle sizing techniques inappropriate, therefore particle size of M5 CAB–O–SIL and S1 fumed silica was measured by an Elzone 80XY particle sizing instrument attached to an IBM personal computer for the rapid acquisition and analysis of data. The Elzone device operates using the electrical sensing zone method. This device measures the effective diameter of a particle as it traverses an electrical field set up across a small orifice (8–2000 μm in diameter). Passage of a particle through the field increases the electrical field resistance. The magnitude of these changes may be related to the particle diameter, and counted to yield a complete particle size distribution. Sodium acetate was used as the buffer to disperse particles. A high level of dilution was required in order to reduce the coincidence level (which is an indication of the error) on measurements to below 1.0%. The Elzone device operates using the electrical sensing zone method. An 18 μm orifice tube was used for measurements, giving a detectable size span of 0.651 to 13.2 μm at the settings used.

Particle size of both ultrafines was found to be 0.71 μm which suggests a degree of agglomeration during sample preparation and measurement. The total error for the determination of the mean particle sizes was about 5 %.

3.2.4. Surface Area and Porosity

An Omnisorp 100 (Fig. 3.5) was used to determine the total pore volume and the surface area of samples. Omnisorp 100 is a gas adsorption instrument which uses nitrogen as the adsorbate and is based on BET theory (after Brunauer, Emmett and Teller, 1938). Gas adsorption technique basically involves determination of the gas necessary to form a monolayer on the surface to be measured (Lowell and Sheilds, 1984). The number of the molecules required to form this layer may be evaluated, and since the area occupied by each molecule is known (or may be estimated), the surface area of the material may be calculated. The more energetic sites are covered first as the pressure is increased but it does not imply that no adsorption occurs on sites of less potential. Rather, it implies that the average residence time of a physically adsorbed molecule is longer on the higher–energy sites. Accordingly, as the adsorbate pressure increases the surface becomes progressively coated and the probability that a gas molecule will strike and be adsorbed on a previously bound molecule increases. Clearly then, prior to complete surface coverage, the formation of second and higher adsorbed layers will commence. In reality, there exists no pressure at which the surface is covered with exactly a completed physically adsorbed monolayer. The effectiveness of the BET theory is that it enables an experimental determination of the number of molecules required to form a monolayer, despite the fact that exactly one monomolecular layer is never actually formed.

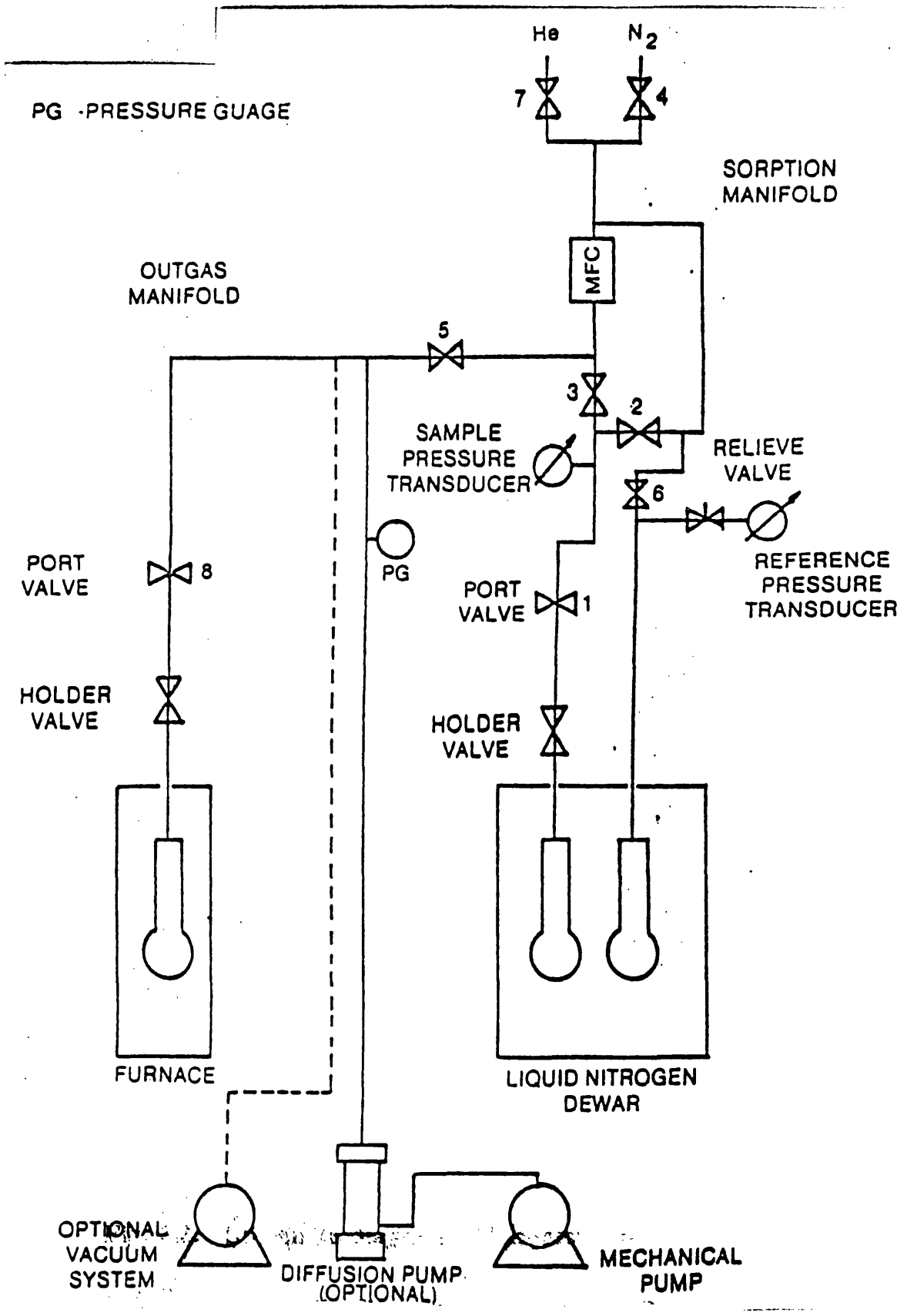

Fig. 3.5. Schematic diagram of Omnisorp 100.

Each sample was thoroughly dried before the test. A sample holder was weighed; a small amount of sample was added to the sample holder and re–weighed. The diffusion pump was switched on. The tap arrangement was fitted to the top of the sample tube holder. The tap on the sample attachment was closed. The blank tube (dummy) was removed from the left hand port of the Omnisorp and the sample/tap arrangement was fitted in its place. The furnace temperature was set at the required level (250°C for silica and 300° C for FCC blends). The vacuum button (valve 8) was pressed.

The pressure gauge on the instrument would show an increase in pressure as the neck of the sample tube was degassed. When the pressure returned to 10^{-2} torr, the tap on the sample tube was slowly opened. The tap was gently turned until a slight resistance was felt. When the tap was turned, the pressure gauge would register a rise in pressure. Care was taken that the pressure would not rise above 10^{-1} torr for more than 30 seconds otherwise overheating and damage to the diffusion pump oil would result. Additionally, because the sample tube was at atmospheric pressure when attached, opening the tap rapidly, the sample would be sucked up the tube into the Omnisorp. Once the tap was fully open, the sample was left in the left hand port to degas. When comparisons between samples are to be made, it is important to leave them for the same length of time. Silica blends were left for 5 hours while this period was 3 hours for FCC mixtures. To insulate the furnace, a small wad of glass wool or cotton was pushed into the top of the furnace, around the stem of the sample tube.

The system was interfaced with a personal computer for automatic data logging. When switched on, the computer would automatically load the Omnisorp software in and the sample information (e.g. sample ID and weight) were entered in a file. Approximately 30 minutes before the sample was due to be removed from the furnace, the liquid

nitrogen bath was filled by opening the liquid valve on the dewar. The nitrogen level was automatically controlled by a sensing device clipped to the inside of the glass dewar.

When the dagassing period was complete, the tap on the sample tube attachment was closed and by depressing valve 8, it was isolated from the vacuum manifold. The sample holder was removed from the left hand port and allowed to cool down at room temperature. The furnace was switched off and the blank tube was replaced in the port. The cooled sample tube was wrapped in a wick. The sealing tube from the right hand port of the Omnisorp was removed and the sample tube was carefully and slowly submerged into the liquid nitrogen bath and then inserted into the joint. The diffusion pump was turned off. The reference holder was pumped down and some nitrogen was allowed to penetrate into it. The sample holder valve was opened and the expanded foam cover was placed on top of the liquid nitrogen bath. The experiment would start by typing RUN in the computer and the instrument was left to do the test mainly overnight.

When the experiment was complete, the tap on the dewar was closed and the nitrogen control valve depressed. The sample was removed from the nitrogen bath and replaced by a dummy. It was allowed to warm up to room temperature so that the wick could be removed and the sample re–weighed. The new weight was entered and the required data were taken from the computer. The sample holder was washed, cleaned and left to dry at room temperature.

The skeletal density, pore area, pore size and its distribution were also measured using a Micromeritics Autopore II 9220 Mercury Porosimeter (Fig. 3.6) which was interfaced with a personal computer for automatic data acquisition. Mercury porosimetry provides a convenient method for measuring the density of powders. This technique gives the skeletal density of those powders which do not possess pores or voids smaller than

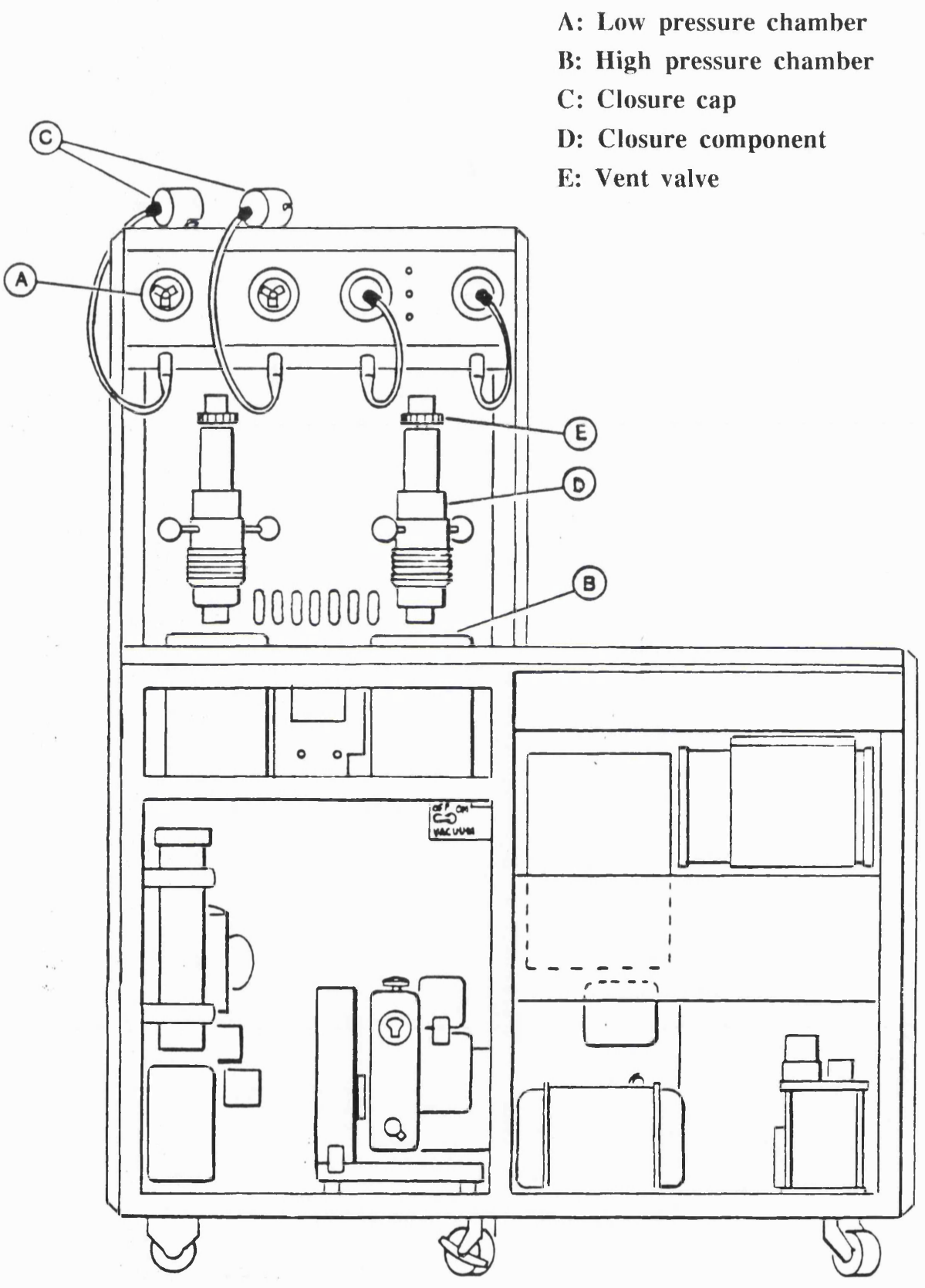

Fig. 3.6. Schematic diagram of mercury porosimeter.

those into which intrusion occurs at the highest pressure attainable in the porosimeter and provides apparent densities for those powders that have pores smaller than those corresponding to the highest pressure.

The volume of the sample, including pores smaller than 7.26 μm is first determined at ambient pressure (1 atm). This is accomplished by weighing the cell filled with mercury and then the cell containing sample filled with mercury. After converting the weights of mercury to the corresponding volumes, using the density table, the sample volume can be determined as the difference between the two mercury volumes. The volume of the sample and thus the density, including pores smaller than 18 Å, is calculated as the difference between the sample volume and the volume of mercury intruded at 60,000 psia.

The mercury porosimeter, vacuum pump and computer were all switched on. An appropriate amount of sample was put into a sample holder (penetrometer) which had already been weighed. The penetrometer containing the sample was weighed again in order to find the weight of the sample. It was then sealed using an adhesive and put in the low pressure chamber. Up to four penetrometers could be placed in the porosimeter at the same time as there were four low pressure run chambers. All the ports were tightened and after defining the run condition for each sample, including the sample weight and the density of mercury at ambient condition, the low pressure run was started. The operation was automatic: the sample was initially vacuumed down to 100 μm Hg, filled with mercury and pumped up to atmospheric pressure again. When the low pressure run was IDLE, the run was complete. The penetrometers were taken out of the chambers and weighed again. They were then placed in the high pressure chambers (only two chambers were available) and the ports were tightened very slowly but tightly. After entering the sample information, the high pressure run was started. The pressure

gradually increased up to 60,000 psia in the system and the penetrometers were filled with mercury at equilibrium. It then returned to the atmospheric pressure; when the high pressure run was IDLE, the run was complete. The required data were obtained by the computer. The penetrometers were taken out of the instrument. The used mercury was collected in a bottle and the penetrometers were washed and cleaned with an appropriate detergent. Using an ultrasonic bath would aid cleansing. They were rinsed off and left to dry at room temperature.

3.2.5. Bulk Density (BD)

A perspex cylinder of 7.04 cm internal diameter and 4 cm in height was used to determine the bulk density of the samples. Eight transparent scales were stuck on the cell at equal distances to provide direct height measurement. Samples were freely poured into the cell and the height was measured at different points. Knowing the sample weight and calculating the bulk volume, the bulk density of each sample was determined. Each test was carried out three times and the average was taken into consideration.

3.2.6. Skeletal Density (SD)

Skeletal density is the ratio of the mass to the volume occupied by that mass. Therefore, contributions to the volume made by pores or internal voids are neglected when measuring the skeletal density. If the powder has no porosity, the skeletal density can be measured by displacement of any fluid in which the solid remains inert. However, usually the solid particles contain pores, cracks or cervices which will not be completely penetrated by a displaced liquid. In these instances, a gas can be used as the displaced fluid.

A Micromeritics AccuPyc 1330 helium pycnometer was used to measure the skeletal density as well as the porosimeter already referred to in section 3.2.4. Pycnometers operate on the principle of gas displacement. Helium is the most frequently used gas because the inertness and the small size of the helium atom enables it to penetrate even to the smallest pores (Lowell and Shields, 1984). Once the sample volume and mass have been determined, the skeletal density is readily calculated. Measurement of the skeletal density provides a method to investigate whether the additives fill the pores of the host.

Up to about 75% of the cell was filled with the sample and its weight was measured. The cell was placed into the pycnometer chamber and the lid was closed tightly. Sample weight was entered into the program. The analysis start with purging the chamber. A purge was used strictly for sample clean up and air and moisture removal from the chamber's inside. After bringing all volumes to ambient pressure, the sample cell was pressurized to 20 psig and then returned to a lower pressure and the powder (solid) volume was determined using physical laws. Knowing the mass of the sample and its volume, the skeletal density may be evaluated. The instrument was set up to carry out each test 40 times and the average values were taken.

3.2.7. Particle Density

Particle Density was determined using the skeletal density and the pore volume of the samples in the following manner: Let the particle mass, skeletal density and its pore volume per unit mass be M, ρ_s and V_p respectively. The solid volume would then be M/ρ_s and the volume of the particle $M(V_p + \frac{1}{\rho_s})$. Therefore the particle density can be obtained as:

$$\rho_p = \frac{\text{Particle Mass}}{\text{Particle Volume}} = \frac{\rho_s}{\rho_s V_p + 1} \qquad (3.1)$$

3.2.8. Particle Charge

The usual method for measuring the charge on powders is to collect a powder sample in a Faraday Cup connected to an electrometer. This method is based on the theory suggested by Stephen Gray (1729) that charge resides only on the outer surface of the conductors (Duffin, 1990). A charged material, completely within the cup, produces a deflection which does not depend on the exact position of the material and remains even when the sample touches the inside of the cup.

A Keithley 610CR electrometer was connected to a shielded vessel (Fig. 3.7). The vessel was then discharged to ground using a metal rod. The sample was added to the inner cell through a funnel without touching the set-up. As soon as the sample entered the cup, a deflection was detected in the electrometer. When the reading was too small, more sample was added to the cell. The charge was measured and its type (i.e. negative or positive) was noted. The inner cell was then taken out and weighed; the powder charge–to–mass ratio was determined. The values, however, did not have an absolute meaning as some spurious deflection always would exist in the system which was the limit of accuracy in the measurements. The measurements did characterize the state of electrostatics of the material in its unaerated condition, such that the higher the measured charge, the higher the true sample charge. This method provided a qualitative indication of the magnitude of the charge on the particles but did not give the charge actually present. Since these measurements were used only comparatively, the approach was considered suitable for the purpose of this study.

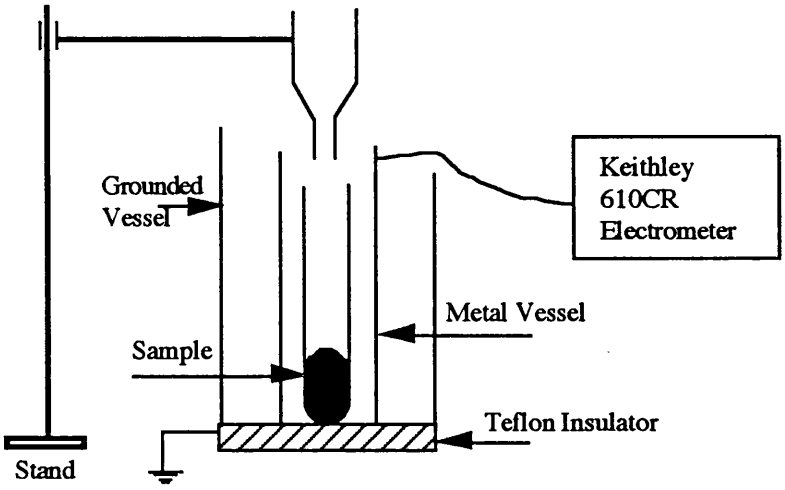

Fig. 3.7. Schematic representation of the experimental apparatus for particle charge measurement.

3.2.9. Viscosity Measurement

As presence of large amounts of ultrafines might change the physical properties of the continuous phase, the viscosity of CAB–O–SIL was measured by a modified concentric cylinder. Viscometers generally measure either the resistance to flow or the drag or torque produced by movement of an element through the fluid. By means of a cylinder that rotates at a known speed with respect to a stationary outer concentric cylinder, the rate of change of velocity, du/dy, is determined. By measurement of the torque on the inner cylinder, the shear stress can be computed. The ratio of shear stress, τ, to rate of change of velocity, du/dy, expresses the viscosity according to Newton's law of viscosity (Streeter and Wylie, 1985):

$$\tau = \mu \frac{du}{dy} \qquad (3.2)$$

Newton's law of viscosity does not predict the shear stress in all fluids. Fluids are classified as Newtonian or non–Newtonian, depending upon the relationship between shear stress and shear rate. In Newtonian fluids the relation is linear (Welty et al., 1984), as shown in Fig. 3.8. In non–Newtonian fluids, the shear stress depends on the rate of shear. While fluids deform continuously under the action of shear stress, plastics will sustain a shear stress before deformation occurs. The *ideal plastic* has a linear stress–strain relationship for stresses greater than the yield stress. Thixotropic substances such as printer's ink have a resistance to deformation that depends upon deformation rate and time.

The viscosity of a material is a measure of its resistance to deformation rate. Tar and molasses are examples of highly viscous fluids; air and water, which are the subject of engineering interest, are examples of fluids with relatively low viscosities.

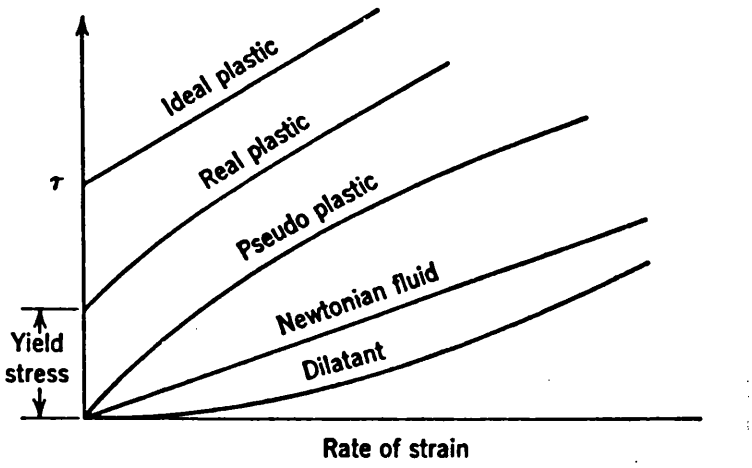

Fig. 3.8. Stress–strain relationship for Newtonian and non–Newtonian fluids (Welty et al., 1984).

Applying equation (3.2) to a concentric cylinder will yield (Streeter and Wylie, 1985):

$$\frac{T}{2\pi r_1^2 L} = \mu \frac{2\pi r_2 N}{60b} \qquad (3.3)$$

where T is the torque, r_1 and r_2 the radii of the inner and outer cylinders, L height of the material in the viscometer, N speed of rotation in rpm, b the clearance between the cylinders and μ is the viscosity. Therefore when shear stress is plotted against the rate of shear, the slope of the line is the viscosity.

A schematic diagram of the apparatus used is shown in Fig. 3.9. The diameter of the outer cylinder was 10.2 cm while the inner cylinder was 6.5 cm in diameter, closed at both ends with a rod passing through its axis. The rod was inserted into an opening in the outer cylinder which was tightly fixed to a solid base. The rod was connected to a Heidolph RZR 2101 electronic motor with digital display of speed and torque. The error

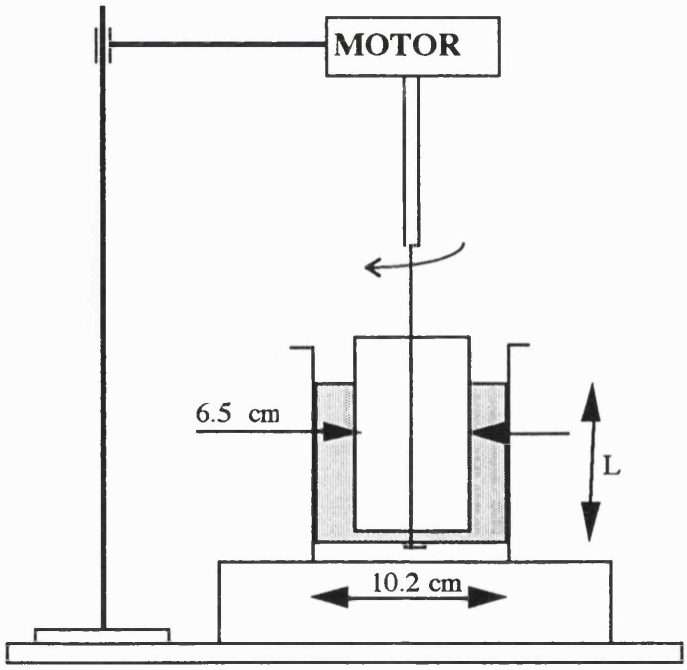

Fig. 3.9. Schematic diagram of the viscometer.

in speed and torque measurements were ±3% and ±5% respectively according to the supplier (Lab–Plant Ltd., Cliffe End Firs, Longwood Road, Huddersfield, West Yorkshire).

Some powder was put in the gap between the cylinder and the height was measured. The motor was switched on and at different speeds, the torque was measured. The experiments were carried out by increasing and also decreasing speeds and the differences were noted. Shear stress was calculated and plotted versus rate of shear and the slope of the line was taken as the viscosity of the material.

3.2.10. Fluidization Experiments

The apparatus used for fluidization experiments consisted of two glass beds of 5 and 10 cm in diameter and 1 m in height to facilitate flow visualization (Fig. 3.10). Gas flow rate was measured by a set of calibrated rotameters in the range of 0–160 l/min. A transparent scale was stuck on each rig to provide direct measurement of bed height. Pressure drop across each bed was measured by a manometer. In order to reduce the entrainment during fluidization, a glass disengagement section was considered. The dust which left the bed was collected by passing the output of the rigs through a water–scrubber, a 70 cm column packed with 1/2" raschig rings. Two fixed beds of silica gel of 5.5 cm in diameter and 70 cm long were used to dry the incoming air to the rigs.

Fluidization experiments were carried out at ambient pressure and temperature using a sintered distributor plate. Each test was carried out three times (unless otherwise stated) and an average was taken from the results. When the bed surface fluctuated due to bubbling, both minimum and maximum bed expansions were considered and a mean value was used to plot the expansion curves. The bed expansion was determined as:

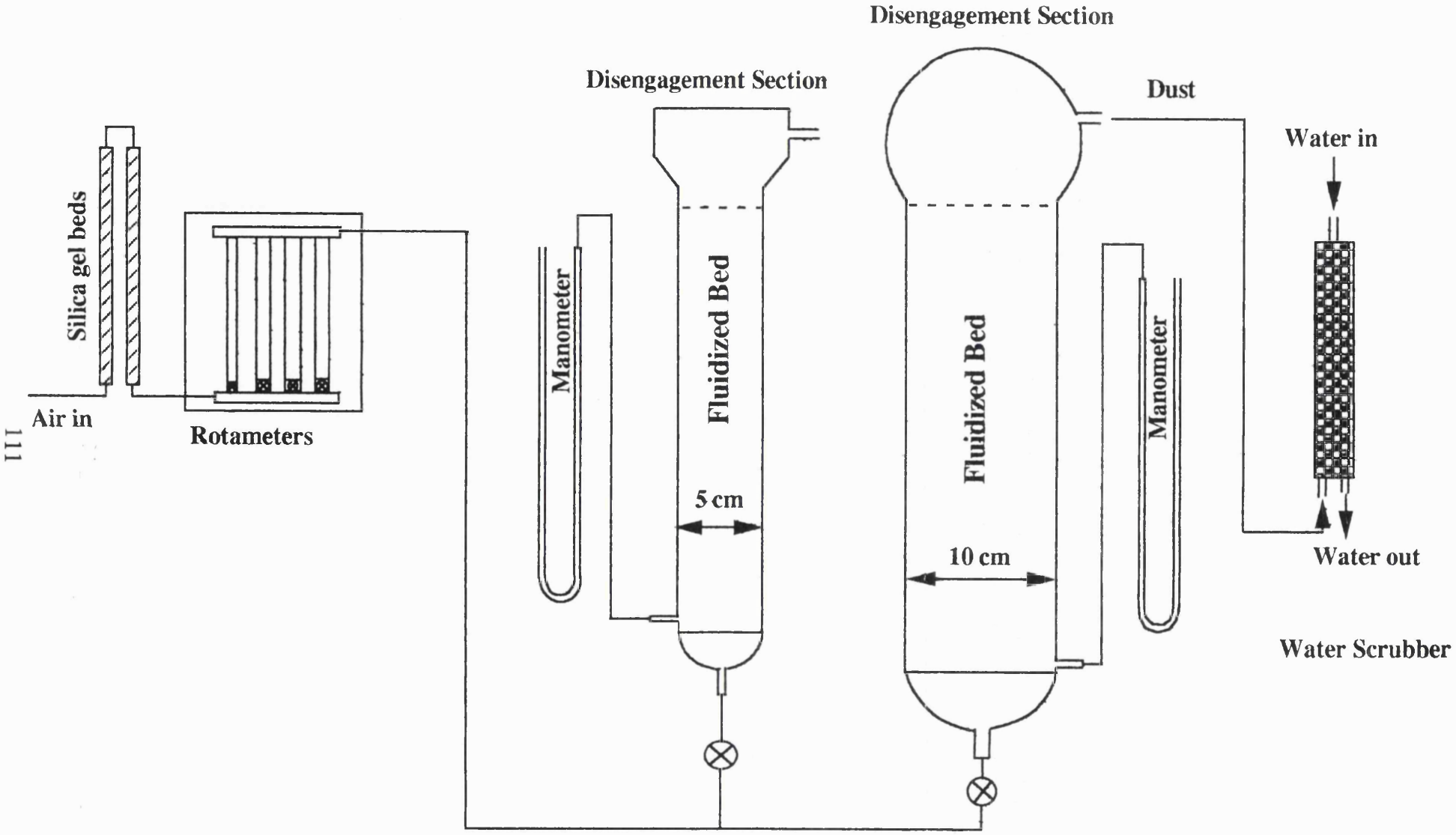

Fig. 3.10.Schematic diagram of the fluidized beds.

$$\text{Bed expansion} = \frac{H_{mb} - H_{mf}}{H_{mf}} \times 100 \qquad (3.4)$$

where H_{mf} and H_{mb} are the bed heights at minimum fluidization and minimum bubbling conditions, respectively.

Bed voidage was calculated using the following equation:

$$\varepsilon = 1 - \frac{M}{\rho_p A H} \qquad (3.5)$$

where M is the bed weight, ρ_p the particle density of the host material, A the bed cross–sectional area and H the corresponding bed height. The bed voidage of the loose packed bed can also be found by:

$$\varepsilon = 1 - \frac{\rho_b}{\rho_p} \qquad (3.6)$$

where ρ_b is the bulk density of the powder.

The bed material was weighed before and after each experiment to determine any losses due to elutriation.

3.2.11. Bed Collapse Experiments

The occurrence of a homogeneous bed expansion seems to be of little practical importance as it usually occurs at very low gas velocities. In fact it is a very important phenomenon. The dense phase usually remains at a higher porosity than ε_{mf} (van Swaaij, 1985). This can be easily checked by the so–called bed collapse experiment (Rietema, 1967). Fig. 3.11 demonstrates the principle: After the flow rate interruption, the gas bubbles escape rapidly from the bed and the expansion due to the gas bubbles

can be easily separated from the dense phase expansion. It is clear that the permeability of the dense phase can also be much higher than at incipient fluidization. The dense phase expansion is in fact the basis of the A–B boundary in Geldart classification. Type B solids do not show this homogeneous expansion.

A thin walled aluminium bed of 10×10 cm and 1 m in height fitted with a uniformly permeable porous plate distributor and connected to a solenoid valve was used for bed collapse experiments (Fig. 3.12). The air flow rate was set to slightly above U_{mb} (as will be explained in section 4.4.1). The air supply was suddenly terminated by closing the inlet valve on the windbox and evacuating the windbox by opening a separate valve simultaneously. The latter step makes the deaeration velocity independent of windbox volume or grid pressure drop (Abrahamsen and Geldart, 1980). The bed height was then recorded as a function of time by filming the entire process using X–ray

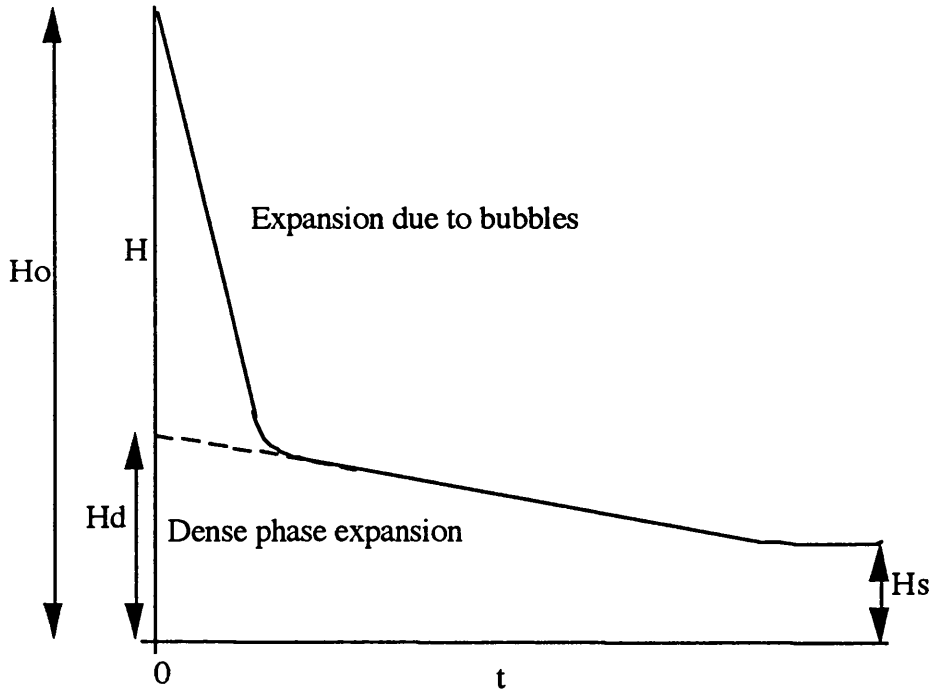

Fig. 3.11. Typical bed collapse curve; gas flow is suddenly interrupted at t = 0.

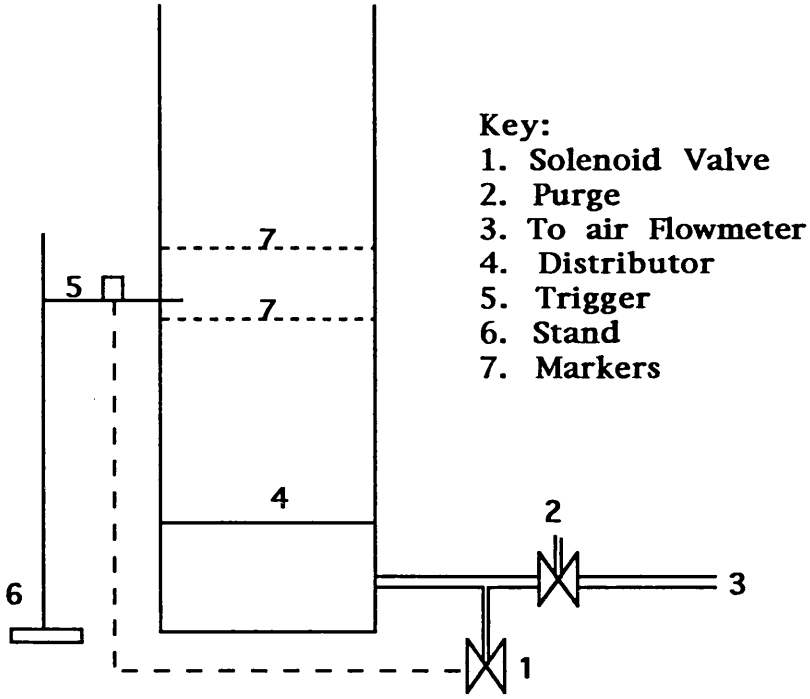

Fig. 3.12. Schematic diagram of the bed collapse set-up (Not to scale).

visualization technique and a JVC video cassette recorder BR–S600E. The trigger would show when the experiment was initiated and/or the air supply was cut off (i.e. t = 0) on the video. The frame number was also displayed on the tape. 25 frames were taken per second; therefore the interval between any two subsequent frames was 0.04 s. Two copper rods, 5 cm apart, were stuck on the bed as a reference for calculations and analysing the data. The bottom marker was 18 cm from the distributor.

The film was then replayed and at various intervals the tape paused; employing Optimas package and calibrating the height using the references (copper rods), the bed height and frame number (and therefore time elapsed) were recorded. Each test was repeated twice and an average was taken from the results.

Dense phase expansion and the expansion due to bubbles were calculated as:

$$\text{Dense phase expansion} = \frac{H_d - H_s}{H_s} \times 100 \qquad (3.7)$$

$$\text{Expansion due to bubbles} = \frac{H_o - H_d}{H_d} \times 100 \qquad (3.8)$$

where H_d is the bed height corresponding to the dense phase and H_s and H_o are the settled and initial bed heights respectively.

CHAPTER FOUR

RESULTS AND DISCUSSIONS

The results of the experiments described in the previous chapter are presented and discussed here. This chapter is divided to four sections: Measurements relating to physical properties of the powders will be described first as they are later used in determination of parameters such as particle density, viscosity and density of the continuous phase. Fluidization and bed collapse experiments will be presented next in detail in separate sections followed by a comparison of results to various stability models predicting transition from particulate to aggregate fluidization. The results are discussed at the end of each section.

4.1. Morphology of Powders

SEM pictures taken from CAB–O–SIL and FCC, silica and kieselguhr with and without additives are shown in Figs. 4.1.1 to 4.1.34. Fig. 4.1.1, 4.1.2 and 4.1.12 show that ultrafine particles (CAB–O–SIL and S1 fumed silica) agglomerated extensively. The size of the agglomerates were in the range of 20–70 μm. FCC particles were spherical (Fig. 4.1.3) and a few irregularly shaped particles along with broken ones could be observed. This is caused by particle attrition and occurs due to the particles impacting each other. Silica samples were fresh and therefore there were less attrited and broken particles in silica (Fig. 4.1.15) comparing to FCC.

It was found that there was an upper limit to the amount of Group C ultrafines that could be added to a Group A catalyst. The maximum concentration is termed the *saturation* or *solubility* limit of the powder blend. Above this limit, the ultrafine particles segregated from the bulk mixture and formed spherical agglomerates which are known as *floccules* in powder industry. Floccules are primary particles held together by temporary association due to van der Waals forces. These floccules can breakup under shear and reform at rest. The formation of floccules may be studied by comparing different SEM pictures. While no agglomerates could be observed up to 1% wt CAB–O–SIL (Figs 4.1.5 and 4.1.17), agglomerates began to form at or above 2.5% wt additives (Figs. 4.1.7 and 4.1.19). These were specially noticeable at 5% wt and above (Figs. 4.1.9 to 4.1.12 and Figs. 4.1.20 to 4.1.22). The size of the agglomerate appeared to be independent of the additive concentration once they were formed, mainly in the range of 1–30 μm.

Observation of lots of segregated ultrafines in Fig. 4.1.7, FCC with 2.5% wt CAB–O–SIL showed that the host particles were saturated while less agglomerates were observed in the same concentration of ultrafines with silica (Fig. 4.1.19). This is due to large surface area of silica (372.41 m^2/g) comparing to FCC (94.92 m^2/g) which will be mentioned in the next section.

No segregation was observed in the mixtures of additives and kieselguhr (Figs. 4.1.25 to 4.1.28 and Figs. 4.1.30 to 4.1.34) therefore the host material was not saturated with ultrafines even at 5% wt concentration; although kieselguhr particles were 20–30 μm in diameter, much smaller than silica (110 μm) or FCC (56 μm). Kieselguhr particles were more irregular than FCC and silica, therefore they probably had more *interstitial* sites

despite their smaller particle size. Further investigation is required to study the important factors in agglomeration and/or segregation of the additives from the powder blends.

Several notable observations can be made from the SEM micrographs. The agglomerates in the blends (Figs. 4.1.5 to 4.1.13 and Figs. 4.1.17 to 4.1.22) were markedly smaller than those of the neat additives (Fig. 4.1.1). The agglomerate sizes in the blends were between that of the primary particles (i.e., 120 Å) and agglomerates that form in the pure ultrafine powders (30–100 μm). This may be attributed to the dispersion forces during mixing.

There was a fairly uniform distribution of the additives at the surface of the host material which suggested that ultrafines acted as bridges and did not merely fill the interparticle voids. There was not a significant change in the host surface coverage by additives between initial and final bed samples (Figs. 4.1.11 and 4.1.12) which showed that the force holding the additives to the host particles was stronger than the drag force applied by the fluid bed.

Another visual observation was that at low loadings, the Group C ultrafine particles appeared to prefer to adhere to and evenly coat the outer surfaces of the Group A host particles (Figs. 4.1.5 to 4.1.8 and Figs. 4.1.17 to 4.1.20). The ultrafines interspersed themselves randomly on the surface of the host material. It appeared that there was a maximum number of ultrafine particles that could fill the interstitial sites and coat the larger ones. As the ultrafines content increased, the additives interacted with one another and formed agglomerates or secondary particles larger than their primary diameter. Eventually, the ultrafines form solid–solid bridges among themselves, giving rise to a cross–linked type particle network.

Fig. 4.1.1. CAB–O–SIL (× 100).

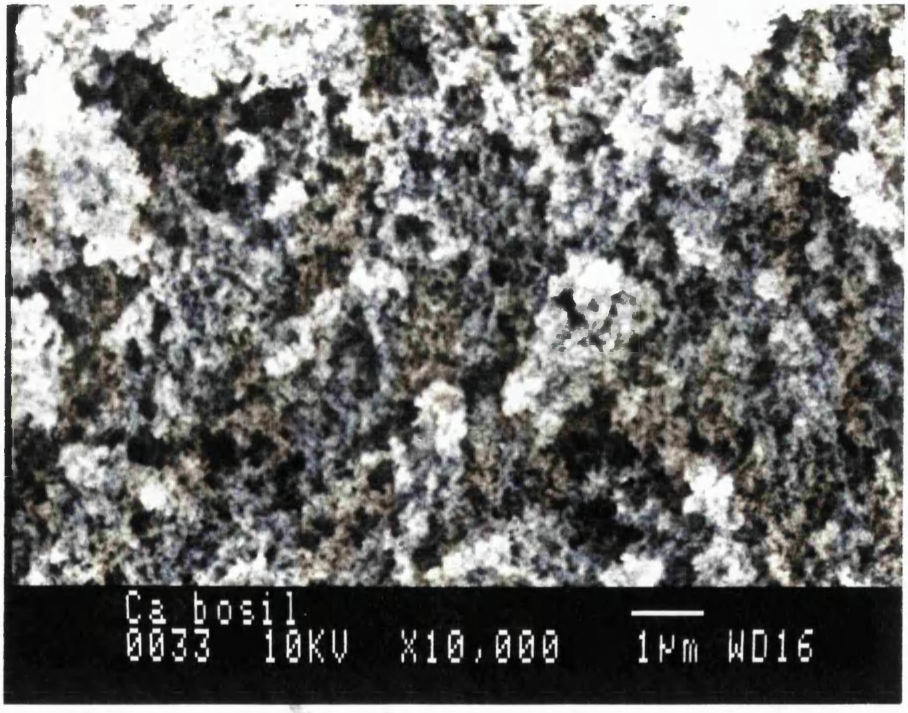

Fig. 4.1.2. CAB–O–SIL (× 10,000).

Fig. 4.1.3. FCC with no additive (× 100).

Fig. 4.1.4. FCC with no additive (× 3000).

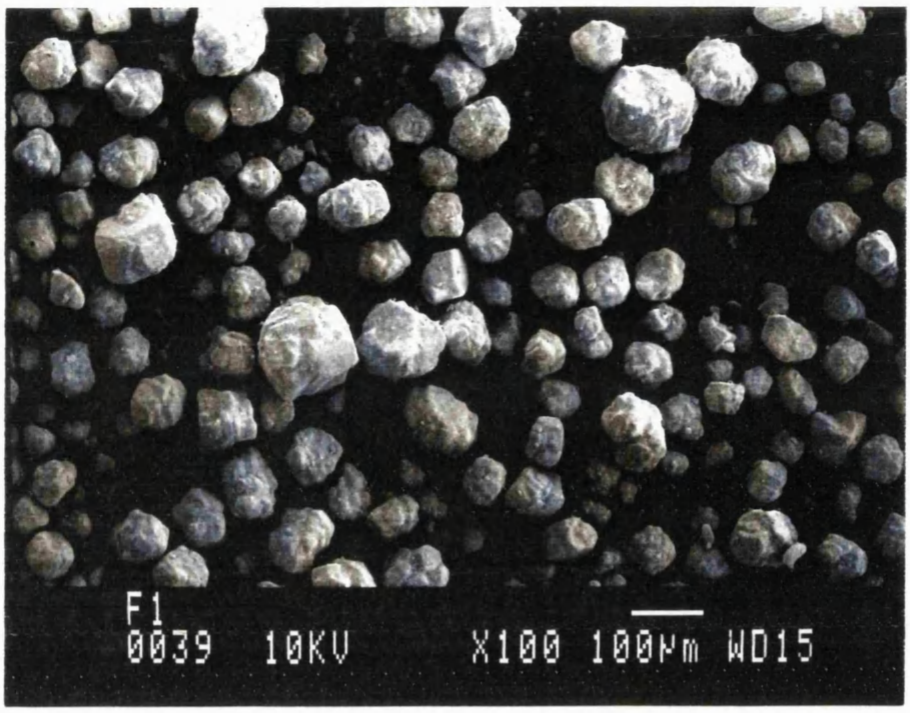

Fig. 4.1.5. FCC with 1% CAB-O-SIL (× 100).

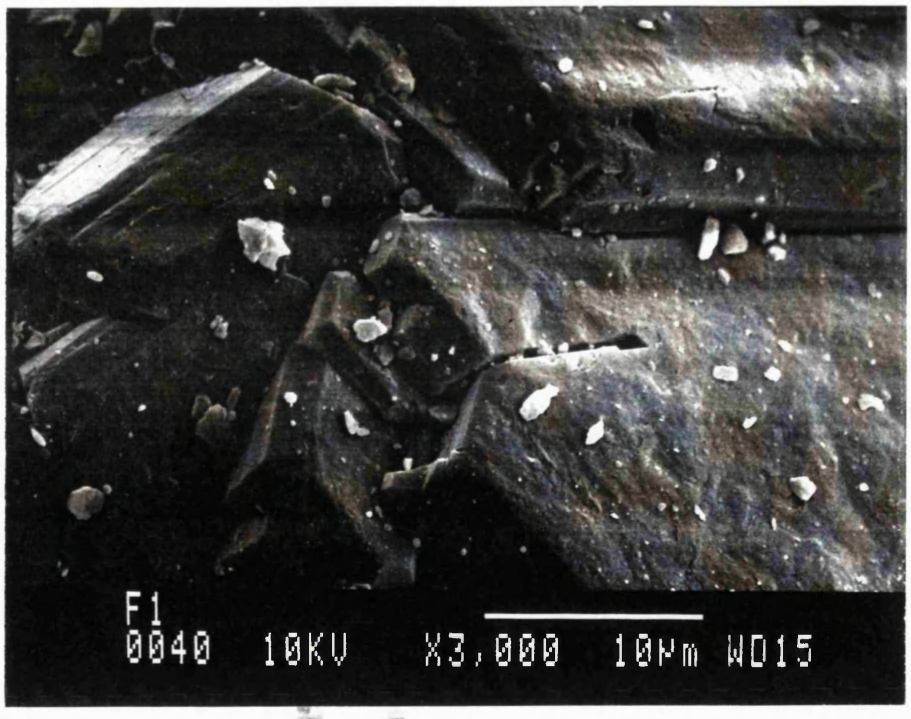

Fig. 4.1.6. FCC with 1% CAB-O-SIL (× 3000).

Fig. 4.1.7. FCC with 2.5% CAB–O–SIL (× 100).

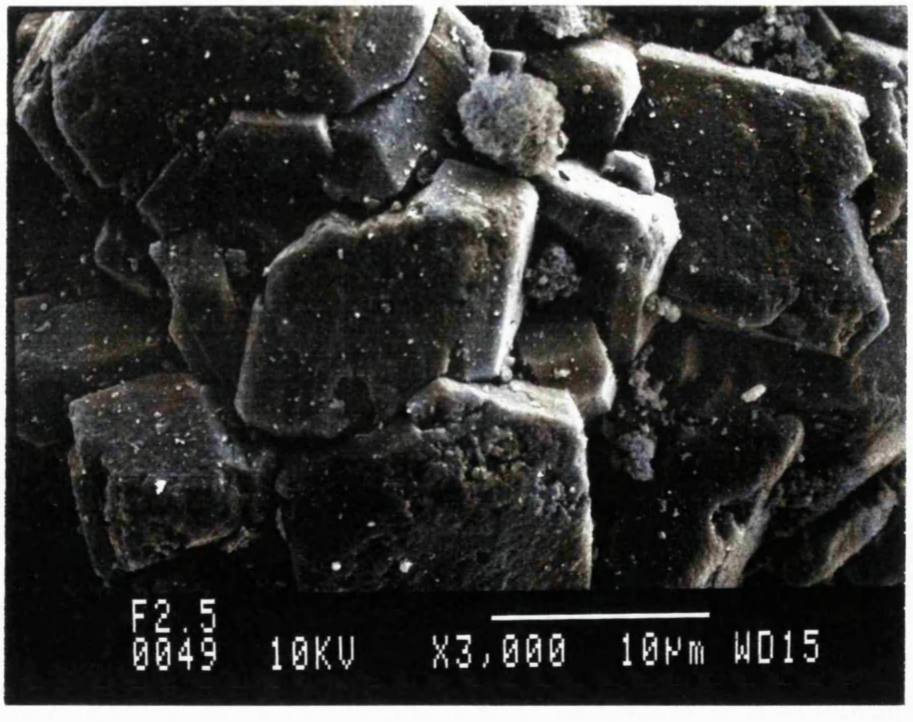

Fig. 4.1.8. FCC with 2.5% CAB–O–SIL (× 3000).

Fig. 4.1.9. FCC with 5% CAB-O-SIL (× 100).

Fig. 4.1.10. FCC with 10% CAB-O-SIL (× 100).

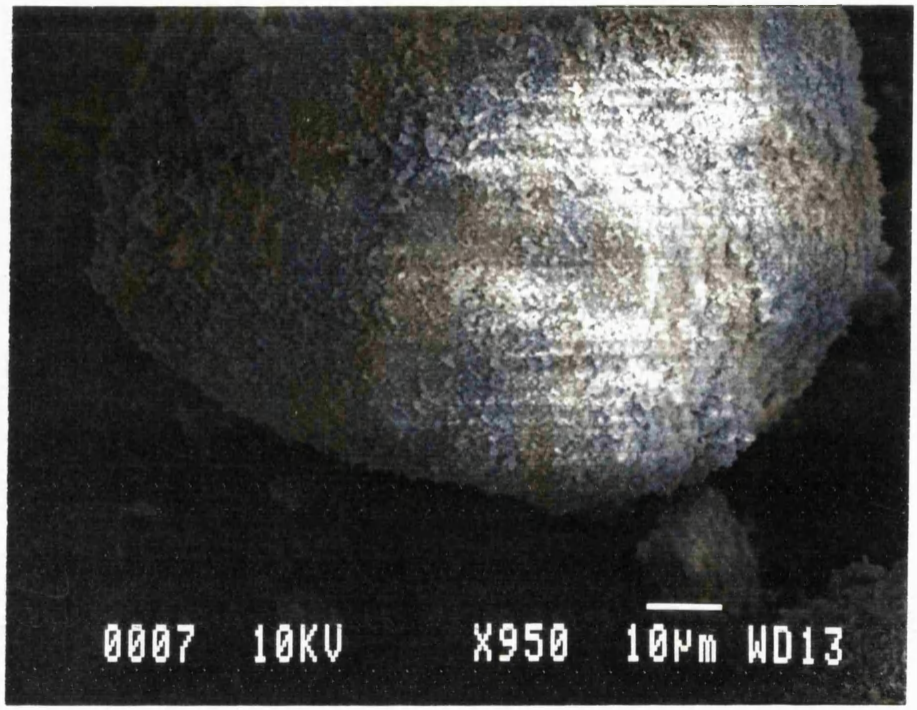

Fig. 4.1.11. FCC with 5% CAB–O–SIL before fluidization (× 950).

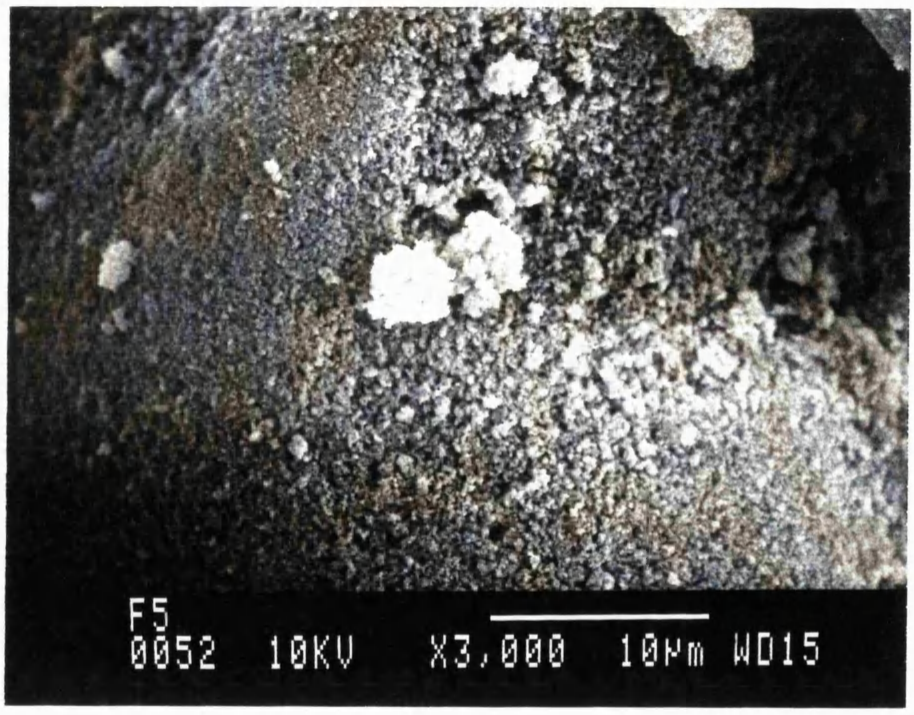

Fig. 4.1.12. FCC with 5% CAB–O–SIL after fluidization (× 3000).

Fig. 4.1.13. FCC with 15% CAB–O–SIL (× 100).

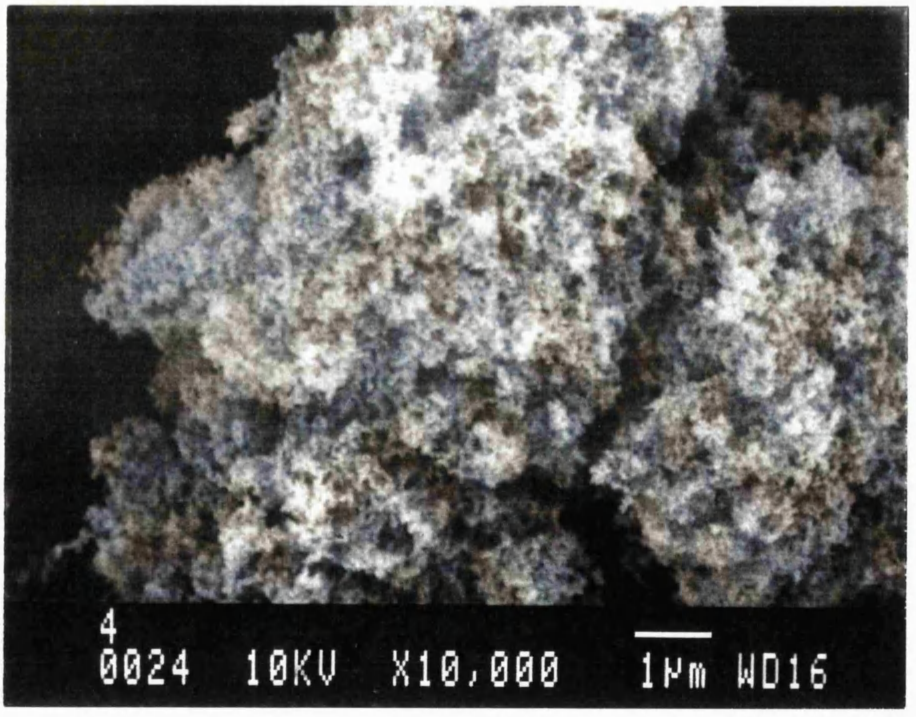

Fig. 4.1.14. S1 fumed silica (× 10,000).

Fig. 4.1.15. Silica with no additive (× 100).

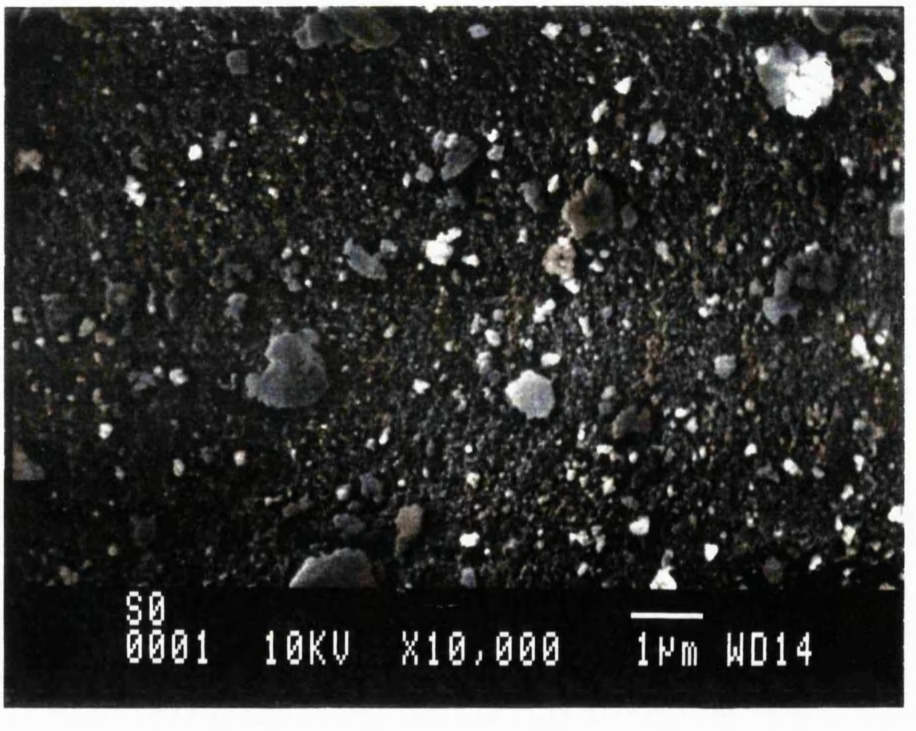

Fig. 4.1.16. Silica with no additive (× 10,000).

Fig. 4.1.17. Silica with 1% CAB–O–SIL (× 100).

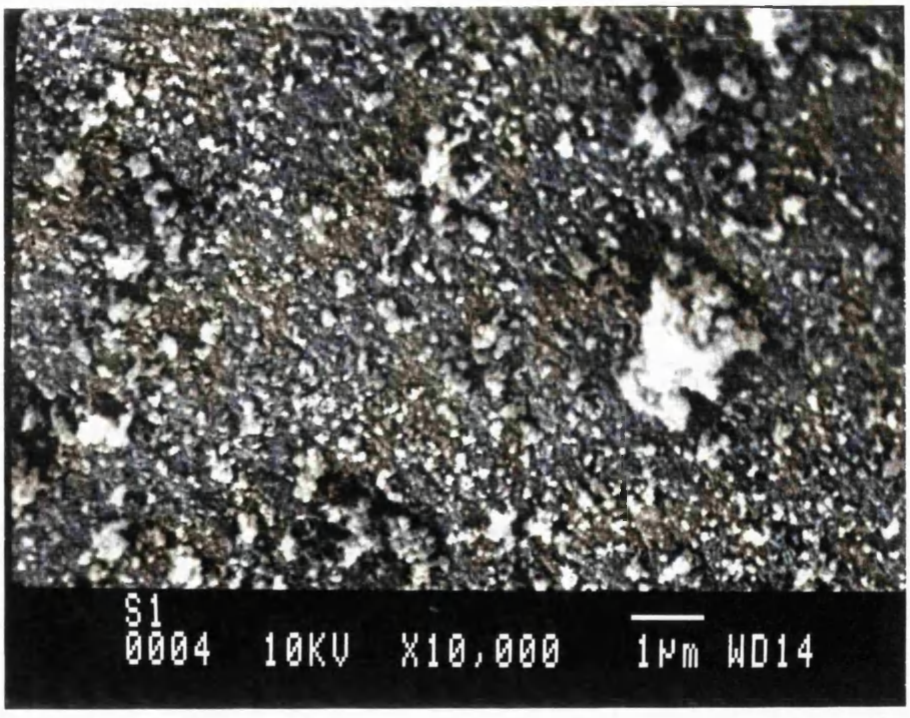

Fig. 4.1.18. Silica with 1% CAB–O–SIL(× 10,000).

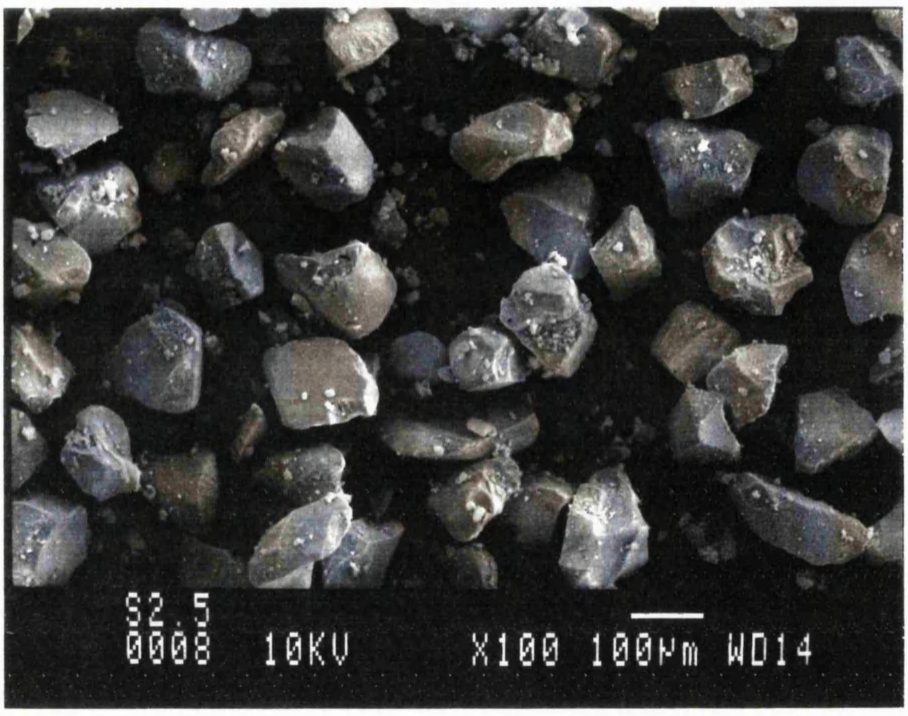

Fig. 4.1.19. Silica with 2.5% CAB-O-SIL (× 100).

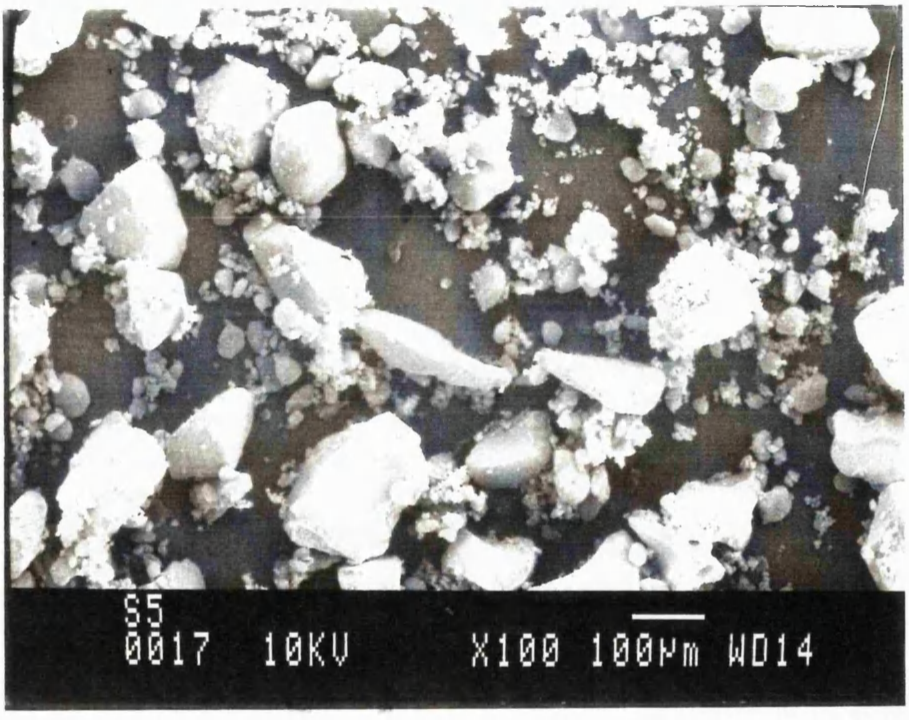

Fig. 4.1.20. Silica with 5% CAB-O-SIL (× 100).

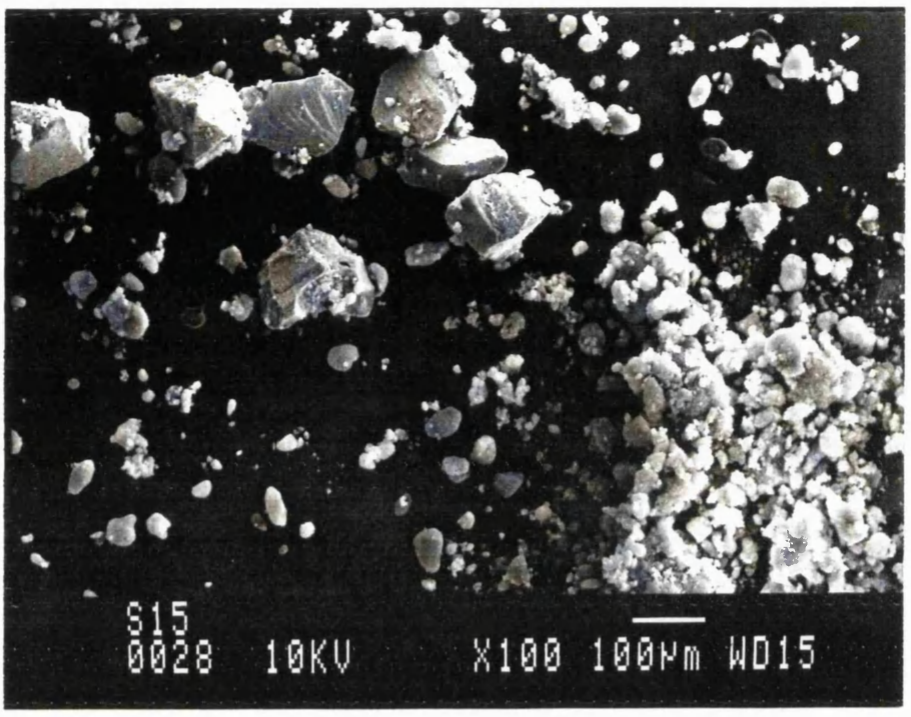

Fig. 4.1.21. Silica with 15% CAB-O-SIL (× 100).

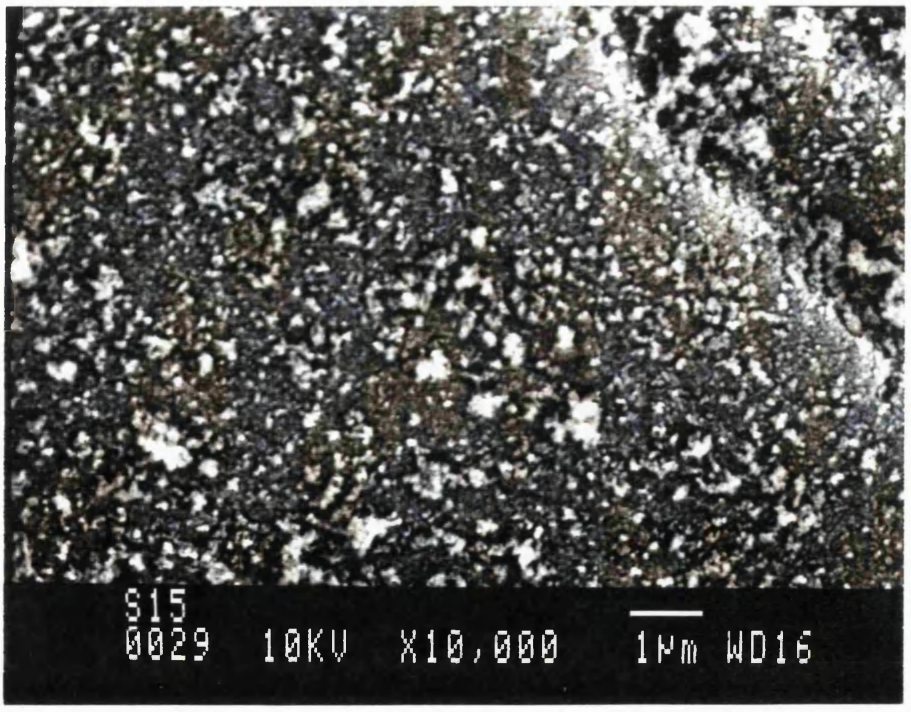

Fig. 4.1.22. Silica with 15% CAB-O-SIL (× 10,000).

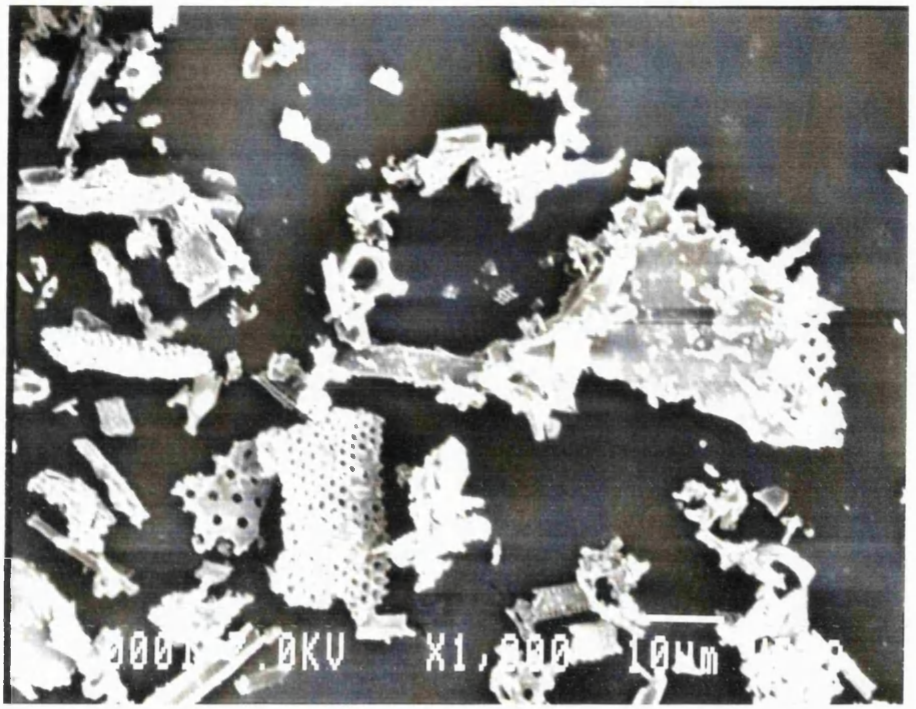

Fig. 4.1.23. Kiesel–1 with no additive (× 1000).

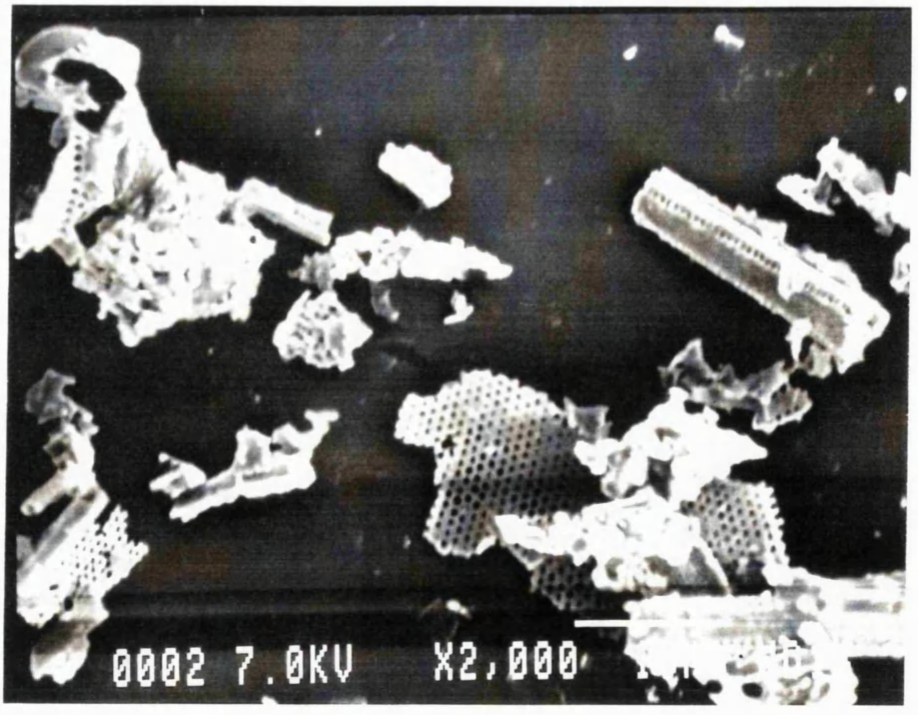

Fig. 4.1.24. Kiesel–1 with no additive (× 2000).

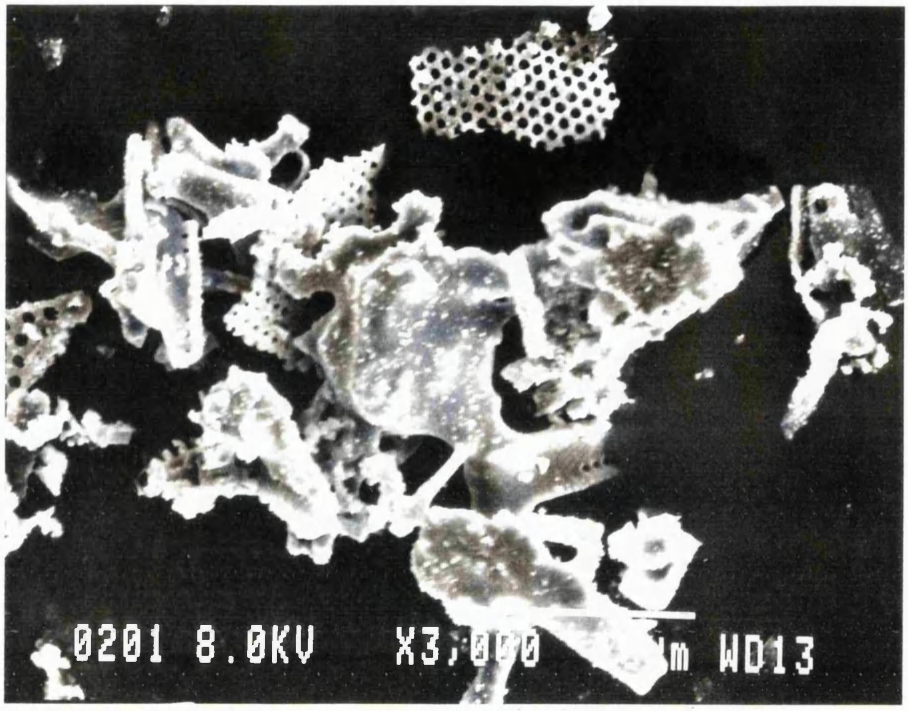

Fig. 4.1.25. Kiesel–1 with 1% S1 fumed silica (× 3000).

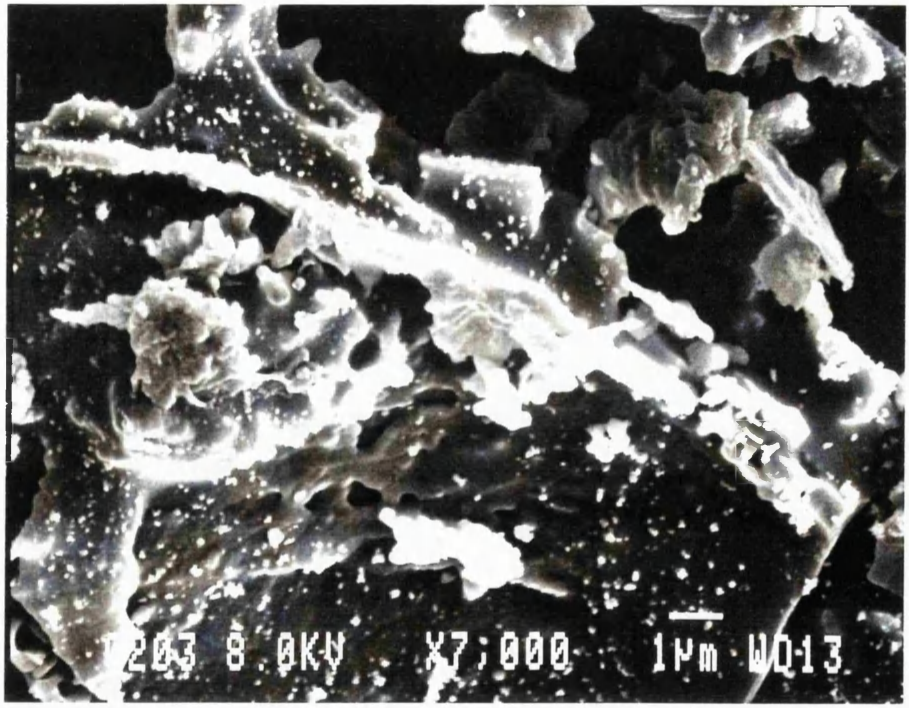

Fig. 4.1.26. Kiesel–1 with 1% S1 fumed silica (× 7000).

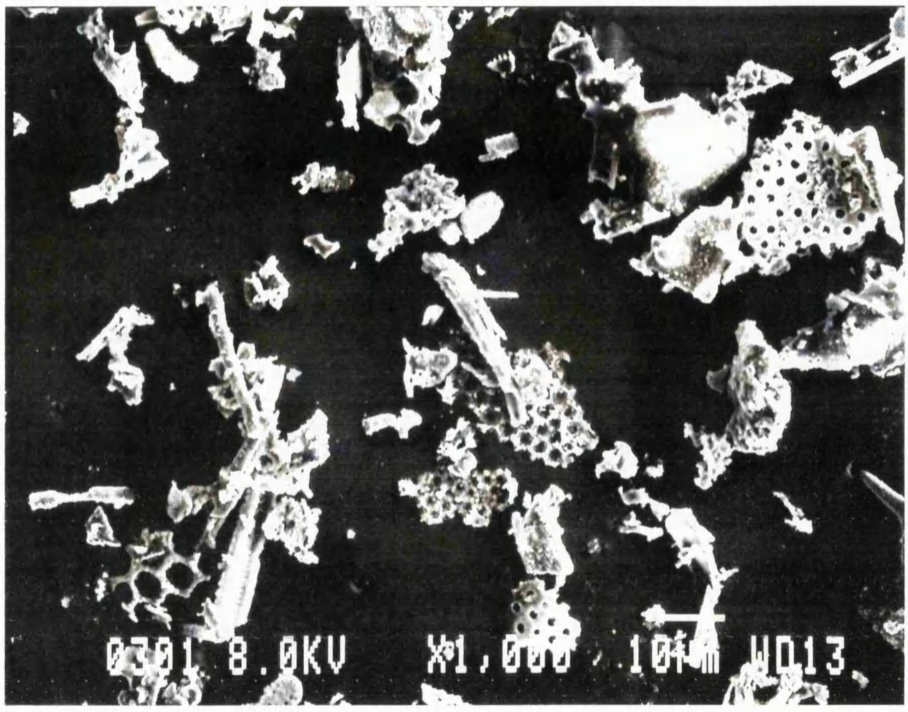

Fig. 4.1.27. Kiesel–1 with 3% S1 fumed silica (× 1000).

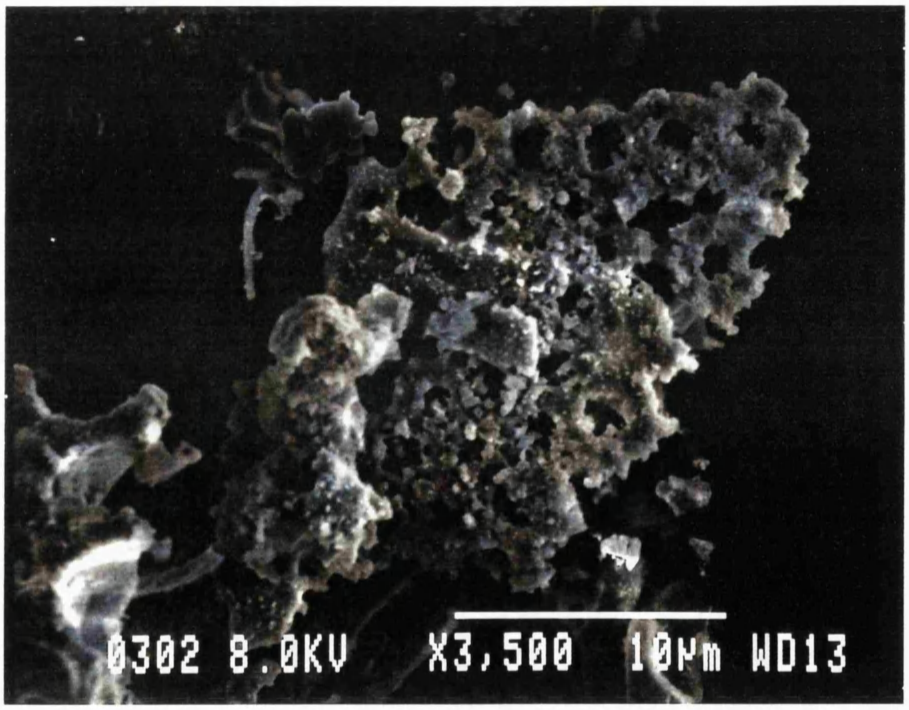

Fig. 4.1.28. Kiesel–1 with 3% S1 fumed silica (× 3500).

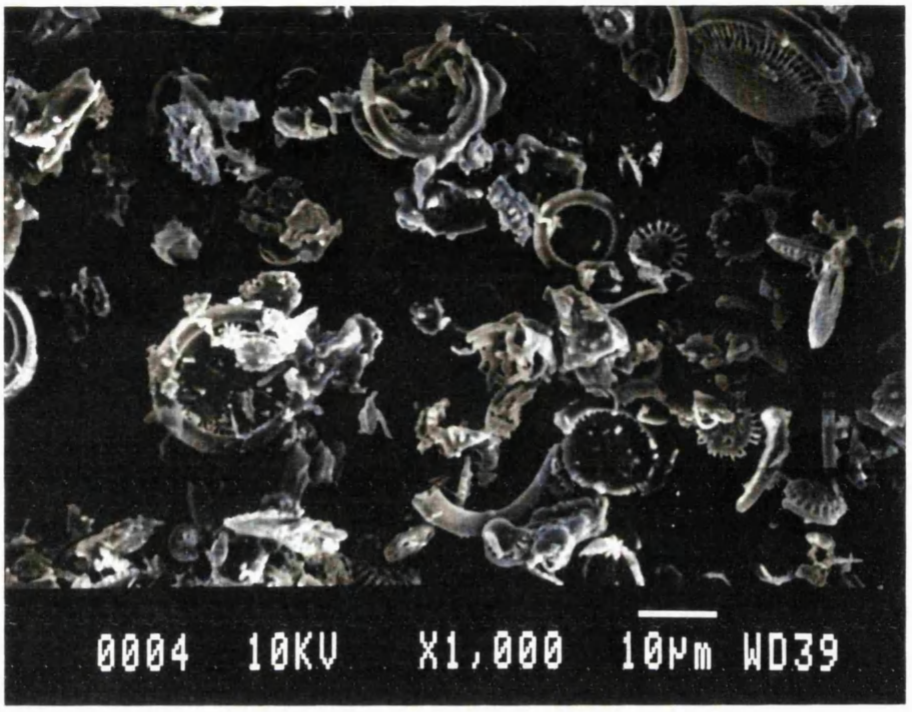

Fig. 4.1.29. Kiesel–2 with no additive (× 1000).

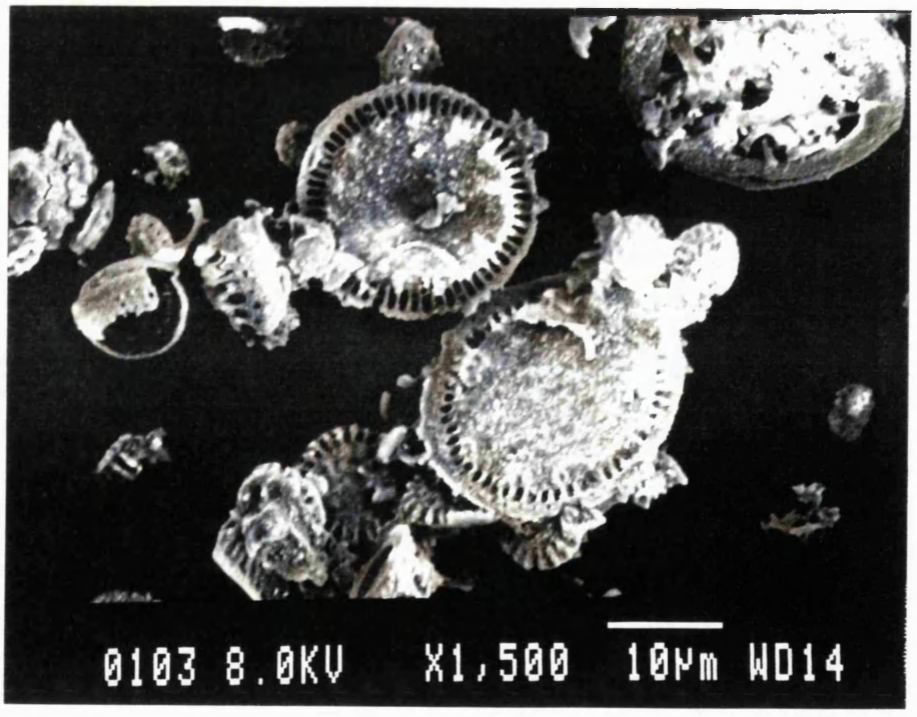

Fig. 4.1.30. Kiesel–2 with 1% CAB–O–SIL (× 1500).

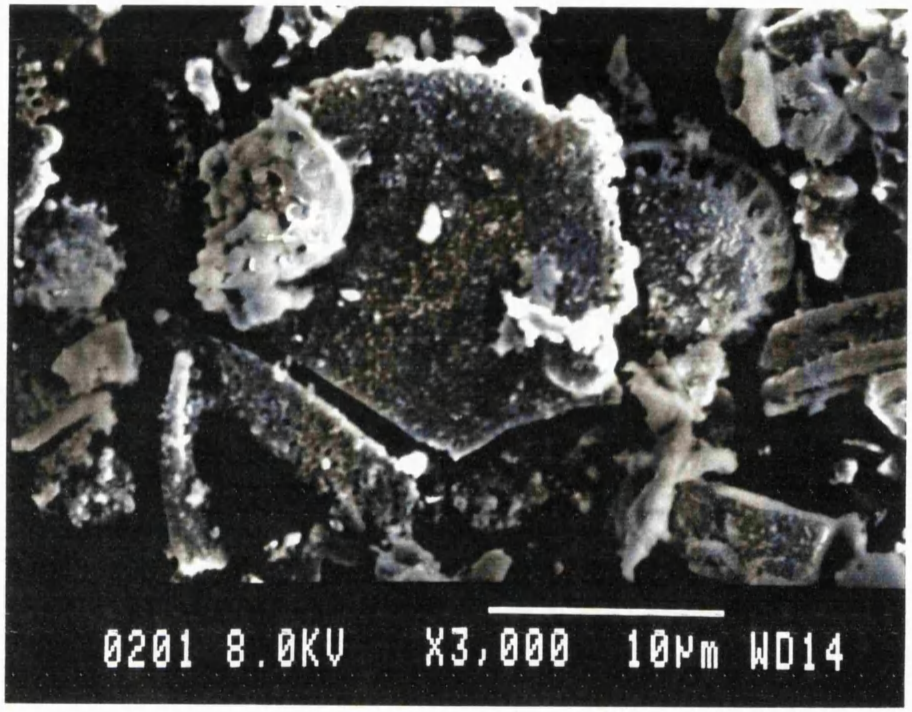

Fig. 4.1.31. Kiesel–2 with 2% CAB–O–SIL (× 3000).

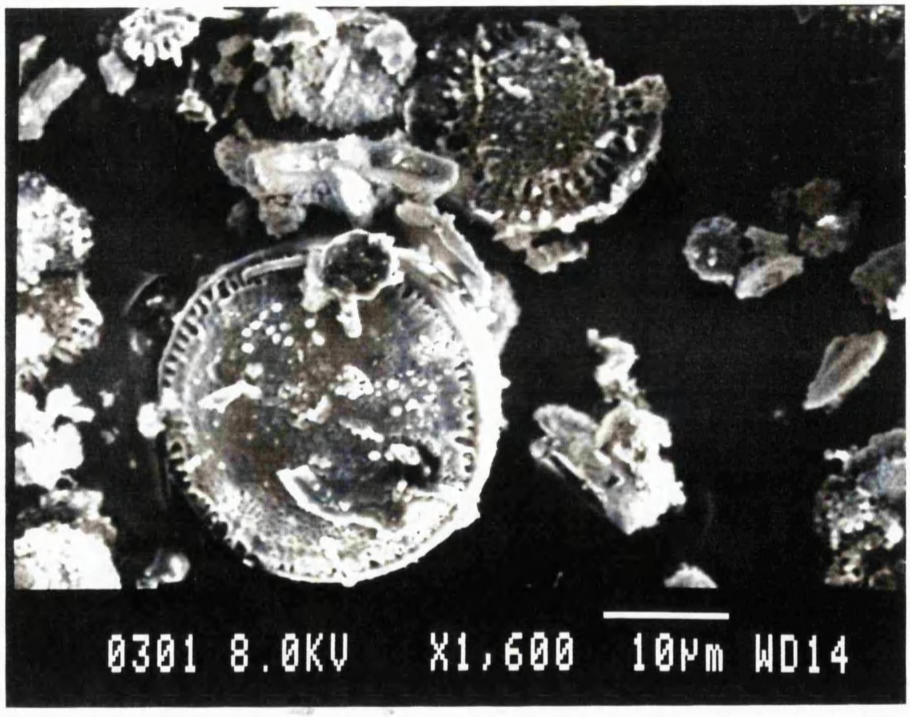

Fig. 4.1.32. Kiesel–2 with 3% CAB–O–SIL (× 1600).

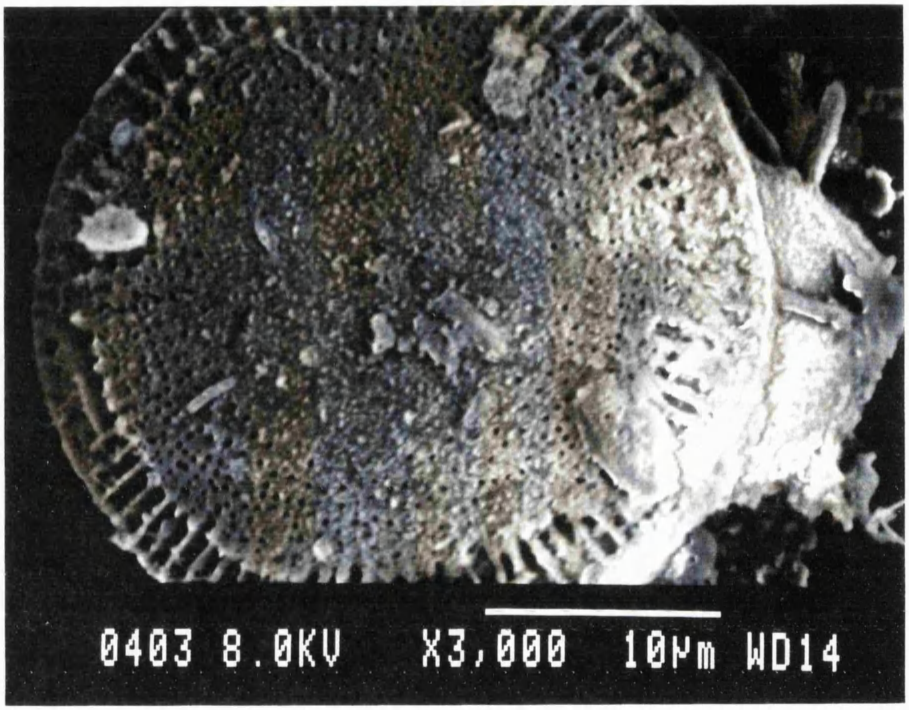

Fig. 4.1.33. Kiesel–2 with 4% CAB–O–SIL (× 3000).

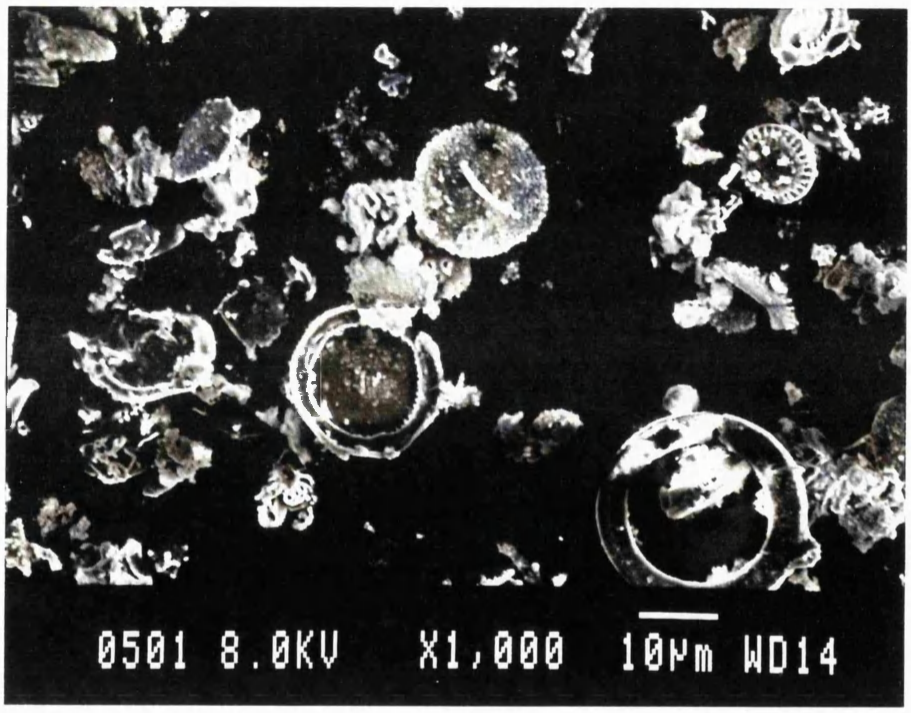

Fig. 4.1.34. Kiesel–2 with 5% CAB–O–SIL (× 1000).

4.2. Measurement of Physical Properties

In this section various physical properties of mixtures of FCC, silica and kieselguhr with different additive concentration are investigated; which include bulk density, skeletal density, surface area, pore volume, pore area and pore diameter of the powder blends as well as electrostatic charge and viscosity of ultrafines. These data help distinguish the Group C particles in terms of their ability to impart cohesion to Group A powders. The physical properties of various powder systems were found to depend mainly on concentration of additives but also on surface properties and particle shape of both ultrafines and the host material. Each of these properties is discussed in more detail below and Tables 4.2.1 to 4.2.4 summarize them. It should be mentioned that neither kieselguhr nor the ultrafines responded well to Omnisorp and/or Porosimeter; therefore the study of their structure (i.e.; surface area, pore diameter, pore volume, etc.) was not possible.

4.2.1. Porosity and Surface Area

The pore volume of FCC and silica were found to be 0.252 and 0.919 cc/g, respectively. Addition of ultrafines increased the total pore volume of the blends (Figs. 4.2.1 and 4.2.2). The pore volume of FCC mixtures constantly increased with ultrafines. When 15% CAB–O–SIL was present in the blend, the pore volume was 0.375 cc/g; an increment of 50%. The pore radii were below 200 Å for all samples, mainly in the range of 10–30 Å. It should be noted that the values shown in Tables 4.2.1 and 4.2.2 were the average between the *host particles covered with ultrafines* and the *segregated additive agglomerates*. The presence of unattached ultrafine particles would obviously increase the pore volume and pore area of the blends. But even at 1% concentration when the

Fig. 4.2.1. Effect of CAB-O-SIL on the total pore volume of FCC.

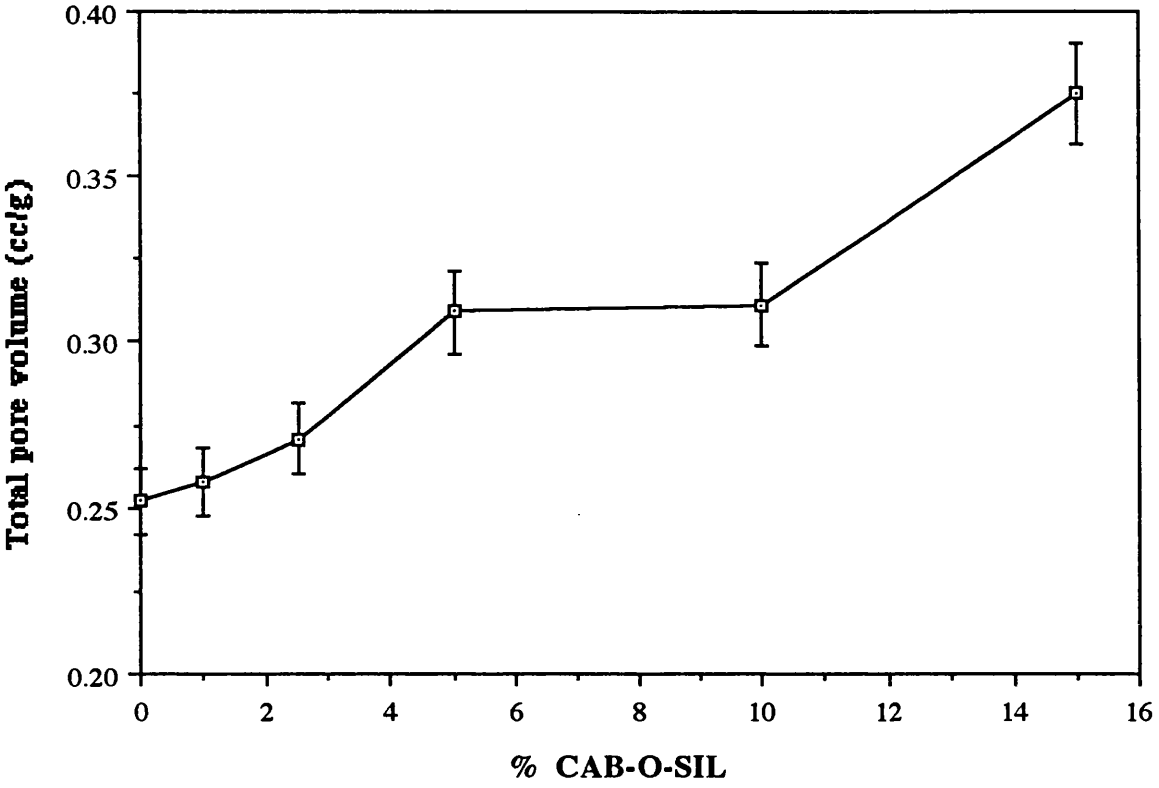

Fig. 4.2.2. Effect of CAB-O-SIL on the pore volume of Silica.

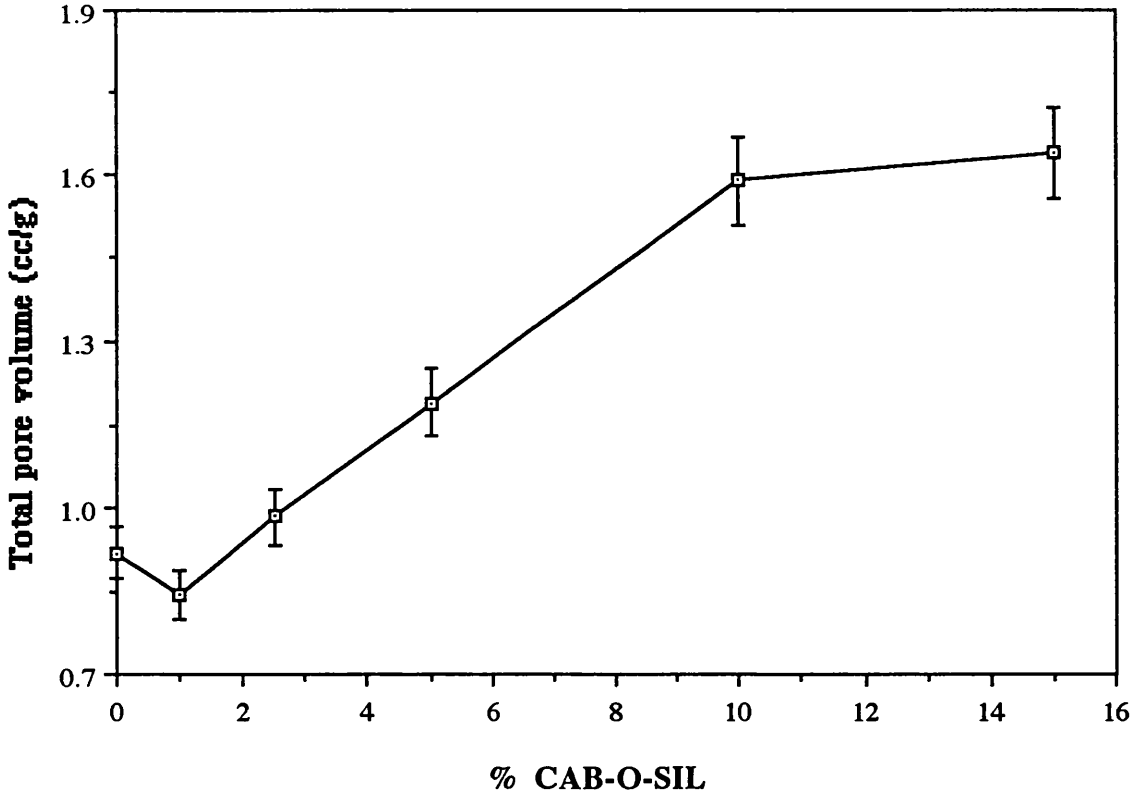

Table 4.2.1. Effect of the addition of CAB–O–SIL on physical properties of FCC.

CAB–O–SIL (wt %)	CAB–O–SIL (vol %)	Bulk Density (kg/m^3)	Skeletal Density (kg/m^3) (pycnometer)	(kg/m^3) (porosimeter)	Total Pore Volume (cc/g)	BET Surface Area (m^2/g)	Total Pore Area (m^2/g)
0	0	1168	3120	2581	0.252	162.8	125.08
1	13.7	1028	3102	1462	0.258	176.1	94.04
2.5	28.7	701	3104	1624	0.271	146.0	84.06
5	45.3	578	3047	1907	0.309	129.3	111.38
10	63.6	333	2983	1902	0.311	122.0	130.86
15	73.5	257	2970	1610	0.375	140.6	163.19

Table 4.2.2. Effect of the addition of CAB–O–SIL on physical properties of silica.

CAB–O–SIL (wt%)	CAB–O–SIL (vol%)	Bulk Density (kg/m^3)	Skeletal Density (kg/m^3) (pycnometer)	(kg/m^3) (porosimeter)	Total Pore Volume (cc/g)	BET Surface Area (m^2/g)	Total Pore Area (m^2/g)
0	0	402	2111	1436	0.9186	351.7	596.43
1	5.5	362	2123	1482	0.8444	295.3	590.43
2.5	13	326	2128	1517	0.9825	355.0	588.69
5	23	293	2130	1210	1.1880	415.7	516.86
10	39	245	2141	1074	1.5897	337.1	392.11
15	50	212	2239	1419	1.6392	328.4	600.17

Table 4.2.3. Effect of the addition of S1 fumed silica on physical properties and fluidization of kiesel–1.

S1 Fumed silica (wt %)	Bulk Density (kg/m^3)	Skeletal Density (kg/m^3)	U_{mf} (cm/s)	COMMENTS
0	197	2300	–	Could not be fluidized
1	221	2317	1.7	–
2	240	2326	1.4	–
3	239	2325	–	Not reproducible
4	227	2348	1.9	More scatter comparing to the others
5	219	2372	1.5	–

Table 4.2.4. Effect of the addition of CAB–O–SIL on physical properties and fluidization of kiesel–2.

CAB–O–SIL (wt %)	Bulk Density (kg/m^3)	Skeletal Density (kg/m^3)	U_{mf} (cm/s)	COMMENTS
0	289	2368	–	Could not be fluidized
1	336	2394	0.25	
2	328	2397	0.60	
3	306	2409	–	Channeling
4	282	2457	–	Channeling
5	280	2438	0.44	

host was mainly covered with CAB–O–SIL and hardly any unattached agglomerates were detected, the pore volume did not decrease which confirmed that the additives did not fill the pores of the host.

There was a slight decrease in the pore volume of silica when 1% CAB–O–SIL was added but the change was within the limit of accuracy of measurements and could not be related to filling of pores. In general, a similar trend was observed in pore volume of FCC and silica samples. The increase in porosity was in good agreement with the decrease in the bulk density and also the increase in the settled bed voidage to be discussed in sections 4.2.2. and 4.4.

The BET surface area of FCC was 162.8 m^2/g and as 1% CAB–O–SIL was added, the surface area of the mixture increased slightly (Fig. 4.2.3). The increment was within the limit of accuracy of measurements but it could also be an indication of more surface imperfections and a fluffy structure by the coverage of host particles. Addition of 1% ultrafines, decreased the BET surface area of silica from 351.7 to 295.3 m^2/g (Fig. 4.2.4) which showed that the host particles were smoother but it then increased again. Since the BET values at higher additive concentrations corresponded to the average between the covered host particles and the ultrafine aggregates, no general conclusion about the coverage of the primary particles could be drawn for these blends.

Pore area of FCC and silica were 125.08 and 596.43 m^2/g, respectively and as the ultrafines were added, pore area of mixtures decreased. The effect of ultrafines on the surface and pore area of the powder blends, in general, was not as significant as their porosity. Specially for silica no considerable change was detected.

Fig. 4.2.3. Effect of CAB-O-SIL on the BET surface area of FCC.

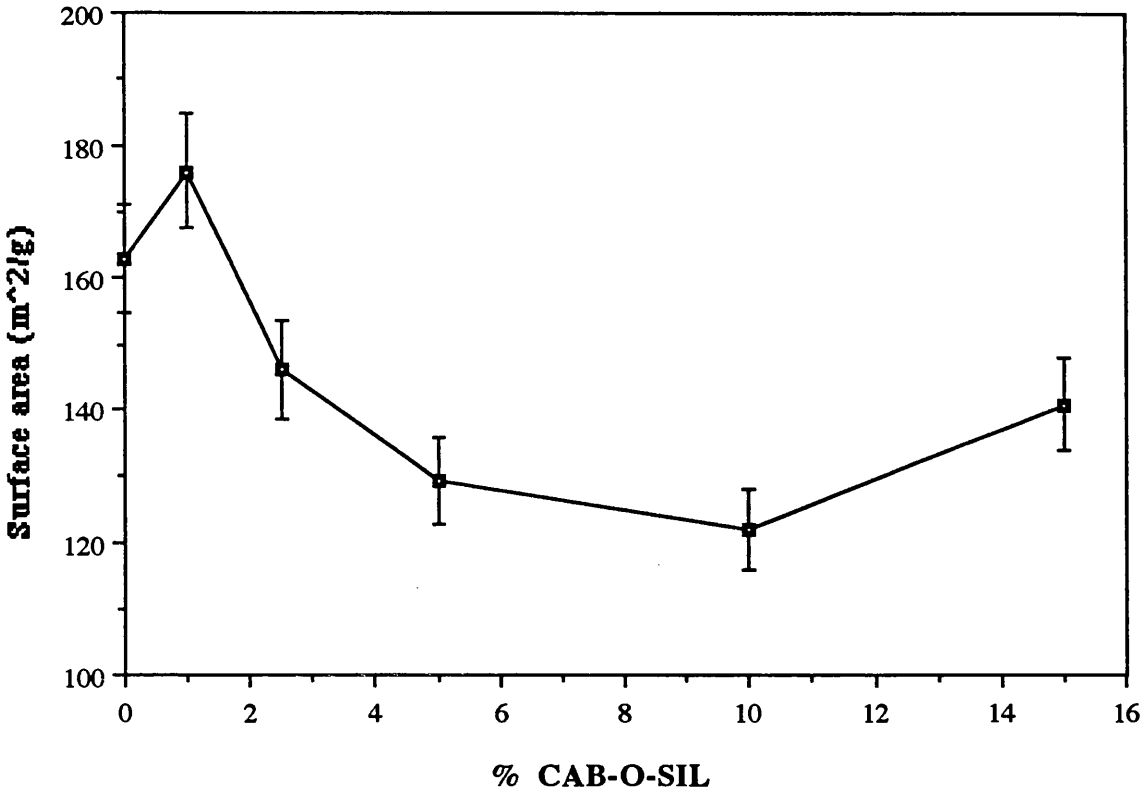

Fig. 4.2.4. Effect of CAB-O-SIL on the BET surface area of Silica.

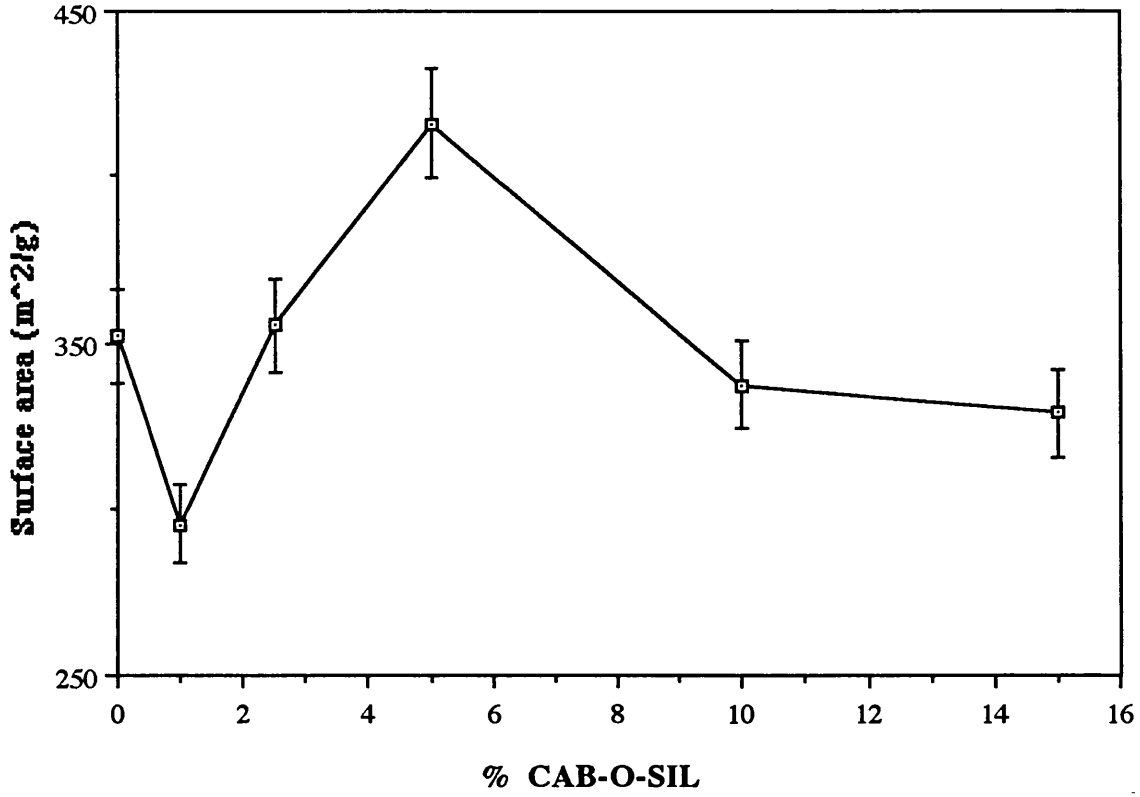

4.2.2. Bulk Density (BD)

There was a dramatic lowering of the bulk density of FCC mixtures with an increase in the ultrafine loading (Fig. 4.2.5). The bulk density of FCC was 1168 kg/m^3 which was reduced to 257 kg/m^3 by adding 15% CAB–O–SIL to the powder. (Note that the bulk density of CAB–O–SIL was 70 kg/m^3). The bulk density of silica was 402 kg/m^3 which reduced to 212 kg/m^3 (Fig. 4.2.6) when 15% CAB–O–SIL was present in the blend. Reduction of BD suggested that ultrafines did not merely fill the interparticle voids despite their very small particle size. Rather they formed a particular network which resulted in a more porous structure.

For kieselguhr mixtures, however, the bulk density increased when low concentrations of ultrafines were added (Figs. 4.2.7 and 4.2.8). The BD of kiesel–1 was 197 kg/m^3 which increased to 240 kg/m^3 when 2–3% wt S1 fumed silica was added and then decreased again to 219 kg/m^3 for the 5% mixture which was still higher than for the neat host material. The BD of kiesel–2 was 289 kg/m^3 which increased to 336 kg/m^3 for the 1% blend and then decreased. For the sample containing 5% CAB–O–SIL, the bulk density was 280 kg/m^3, less than the corresponding value for the kiesel–2 by itself. The maxima observed in the bulk densities of the powder blends was significant considering that the BD of the additives (70 kg/m^3) was much lower than kieselguhr and could be due to highly irregular shape of kieselguhr particles which provided more interstitial sites for ultrafines to be attached. As more ultrafines were added to the host, the BD started to decrease. It should be noted that these changes were observed *below* the saturation limit of the kieselguhr particles. A similar trend might be obtained for silica and/or FCC mixtures of less than 1% additive; prior to segregation of ultrafines but it requires further investigation.

Fig. 4.2.5. Effect of CAB-O-SIL on the Bulk density of FCC.

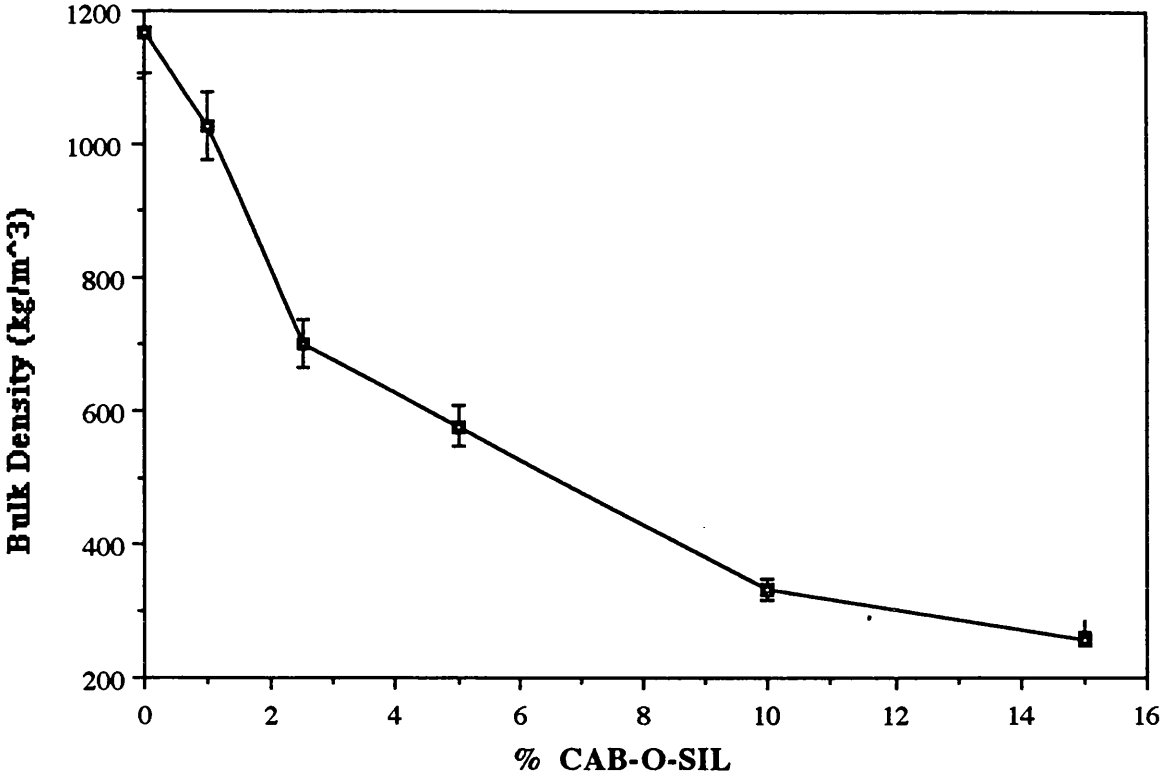

Fig. 4.2.6. Effect of CAB–O–SIL on the bulk density of silica.

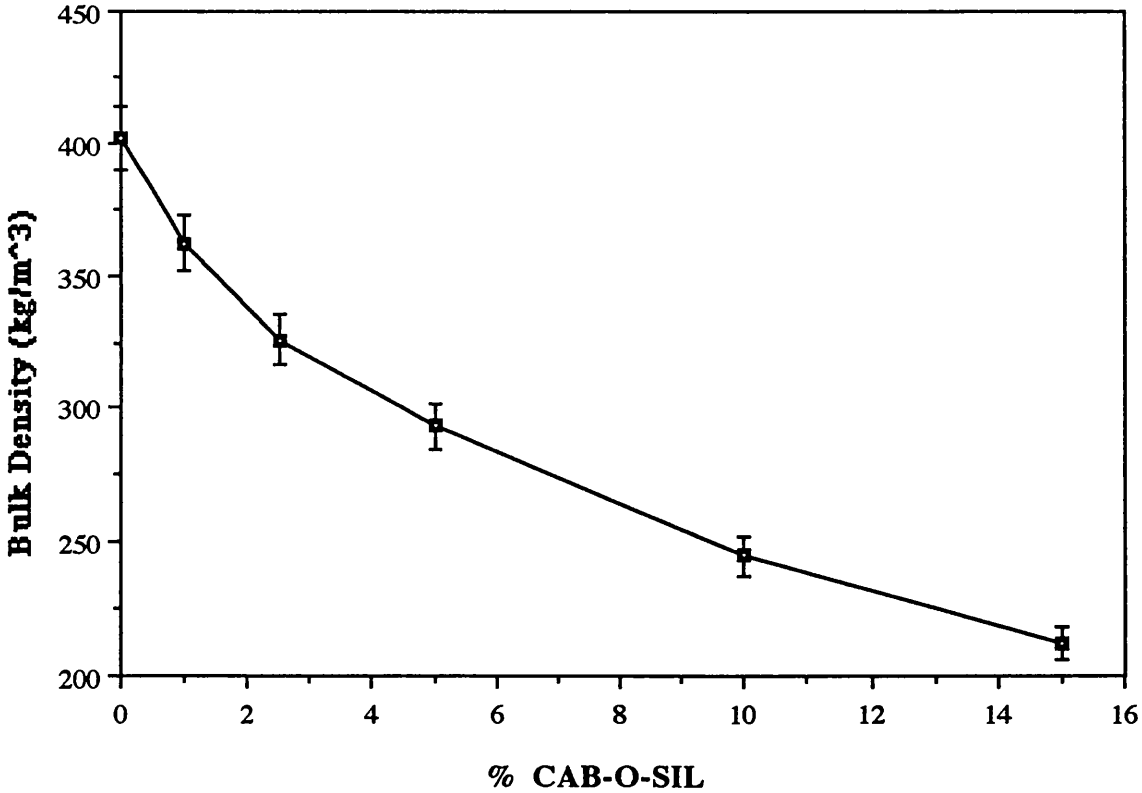

Fig. 4.2.7. Effect of S1 fumed silica on the bulk density of kiesel–1.

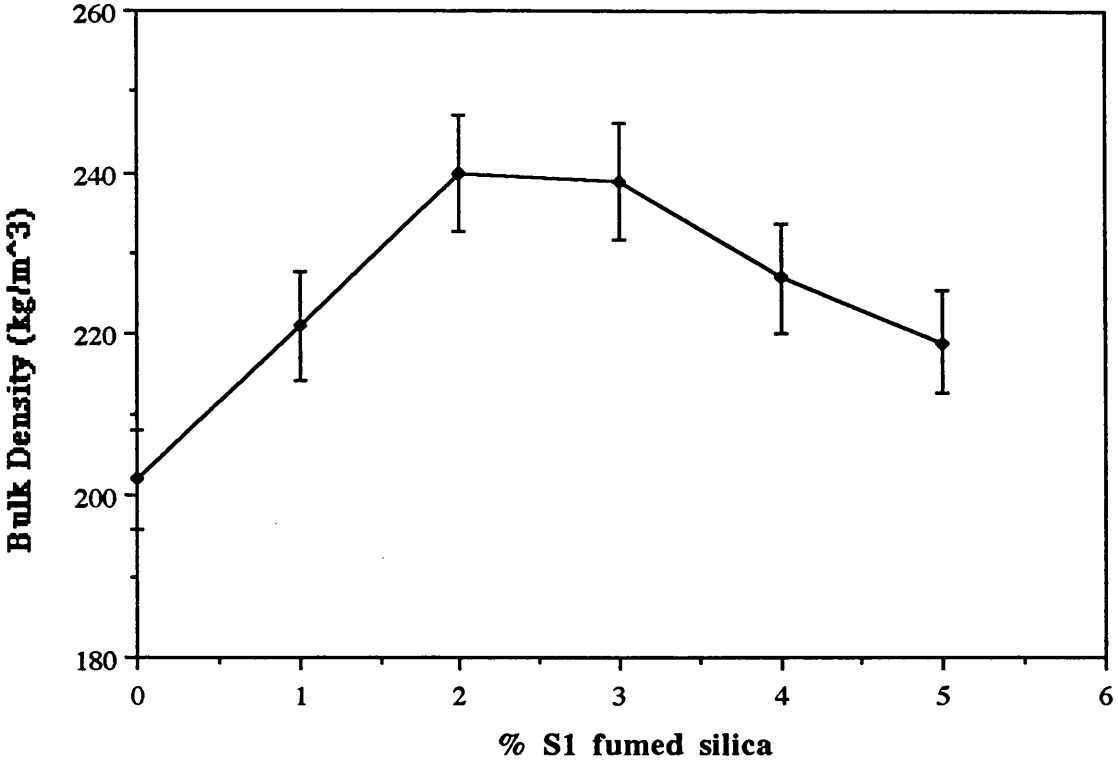

Fig. 4.2.8. Effect of CAB-O-SIL on the bulk density of kiesel–2.

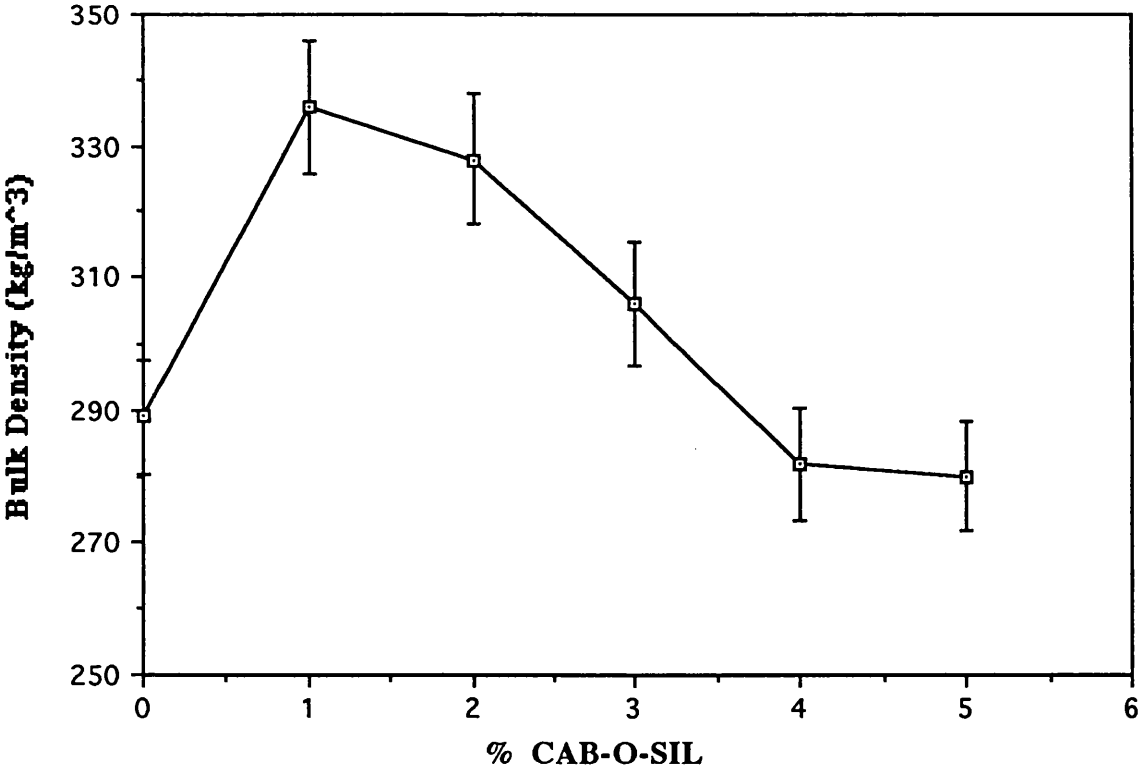

4.2.3. Skeletal Density (SD)

Skeletal densities of FCC and CAB–O–SIL were found to be 3135 and 2700 kg/m^3, respectively. An increase in the skeletal density, providing that the SD of the additives is lower than the host material, confirms that the additives fill the pores of the coarser particles. When ultrafines were added to FCC, the skeletal density of the *mixture* decreased (Fig. 4.2.9) which showed that the additives did not fill the pores of the host and was in agreement with the decrease in bulk density. Skeletal densities found at higher concentrations were basically *mean* values of SD of covered host material and segregated ultrafines so no general conclusion may be drawn from them.

The skeletal density of silica was 2111 kg/m^3 and presence of additives increased the SD of the mixtures (Fig. 4.2.10). For S1 fumed silica and kiesel–1, the skeletal densities were found to be 3998 and 2300 kg/m^3, respectively, and the SD of the powder blend increased with additive concentration (Fig. 4.2.11). Addition of CAB–O–SIL to kiesel–2 increased the skeletal density from 2368 kg/m^3 for the neat sample to 2438 kg/m^3 for the 5% mixture (Fig. 4.2.12) which was similar to the previous case. Since the SD of the ultrafines were larger than kieselguhr and/or silica, the increase in the skeletal density with additive concentration was not unexpected.

The values obtained by pycnometer were all significantly larger than the ones provided by porosimeter. This is attributed to the much smaller size of helium molecules used in the pycnometer comparing to mercury employed in porosimeter which enables it to penetrate into micropores more extensively. Porosimetry showed a sharp decrease in skeletal density for samples containing 1% CAB–O–SIL which could be due to the

Fig. 4.2.9. Effect of CAB-O-SIL on the skeletal density of FCC.

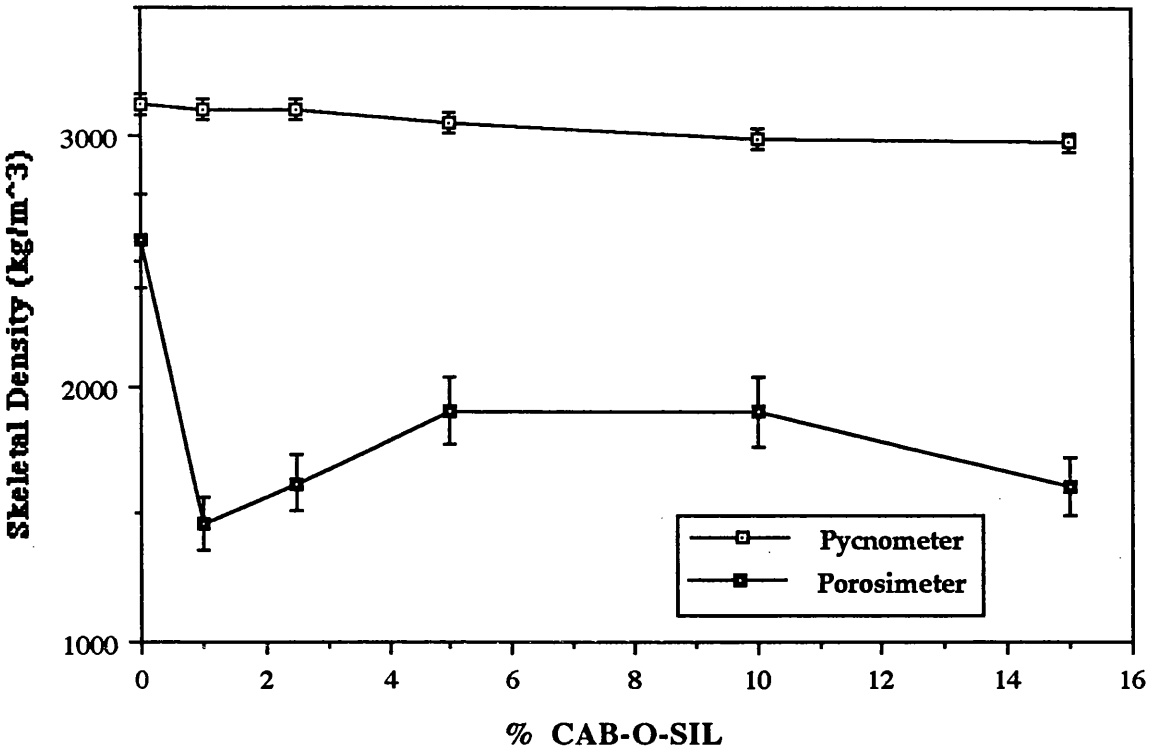

Fig. 4.2.10. Effect of CAB–O–SIL on the skeletal density of silica.

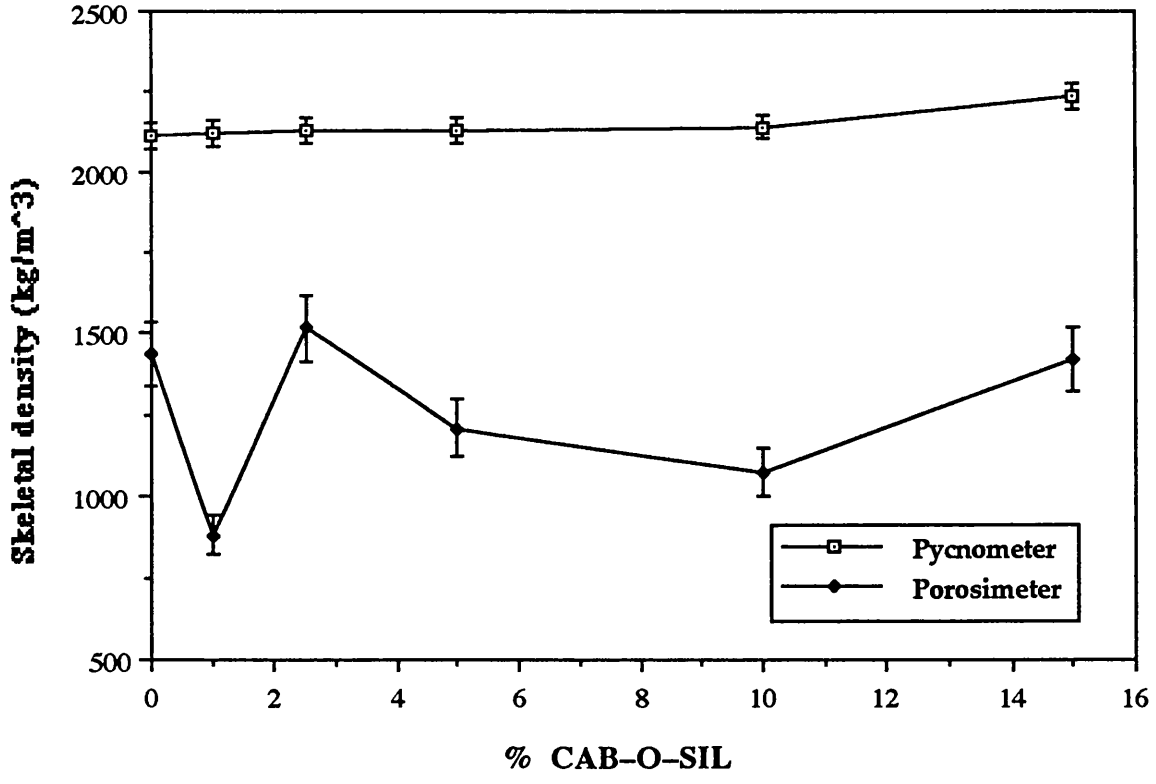

Fig. 4.2.11. Effect of S1 fumed silica on the skeletal density of kiesel–1.

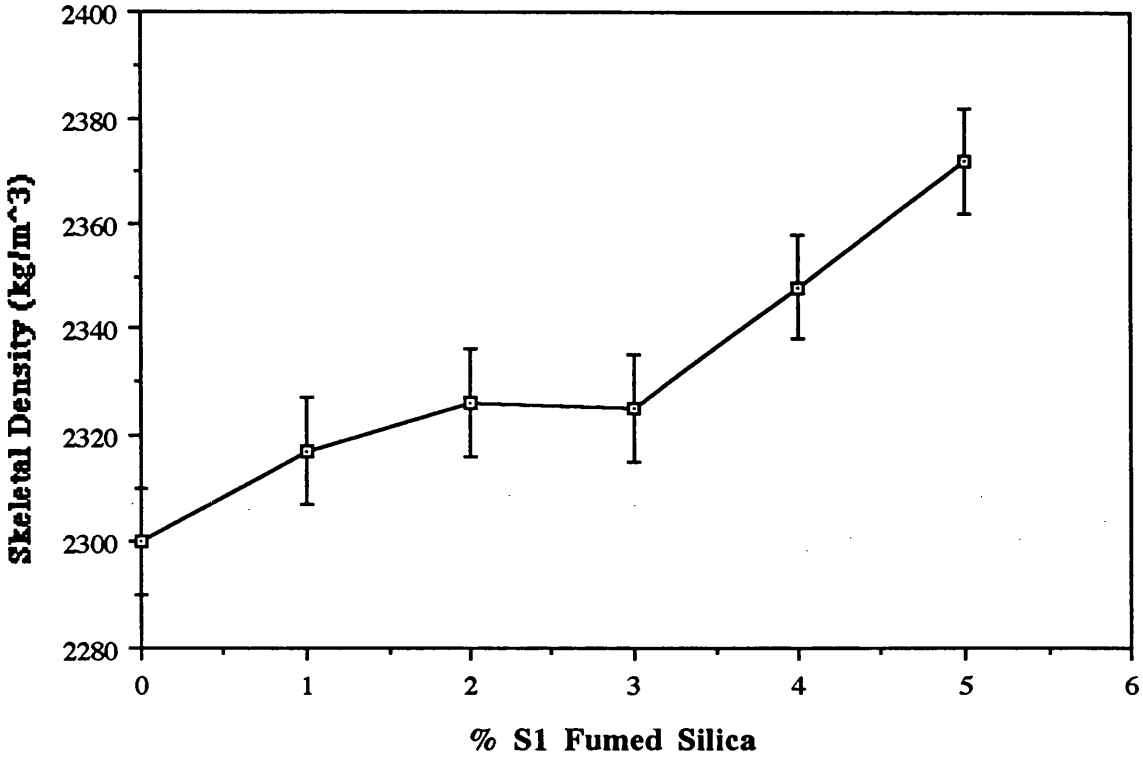

Fig. 4.2.12. Effect of CAB-O-SIL on the skeletal density of kiesel–2.

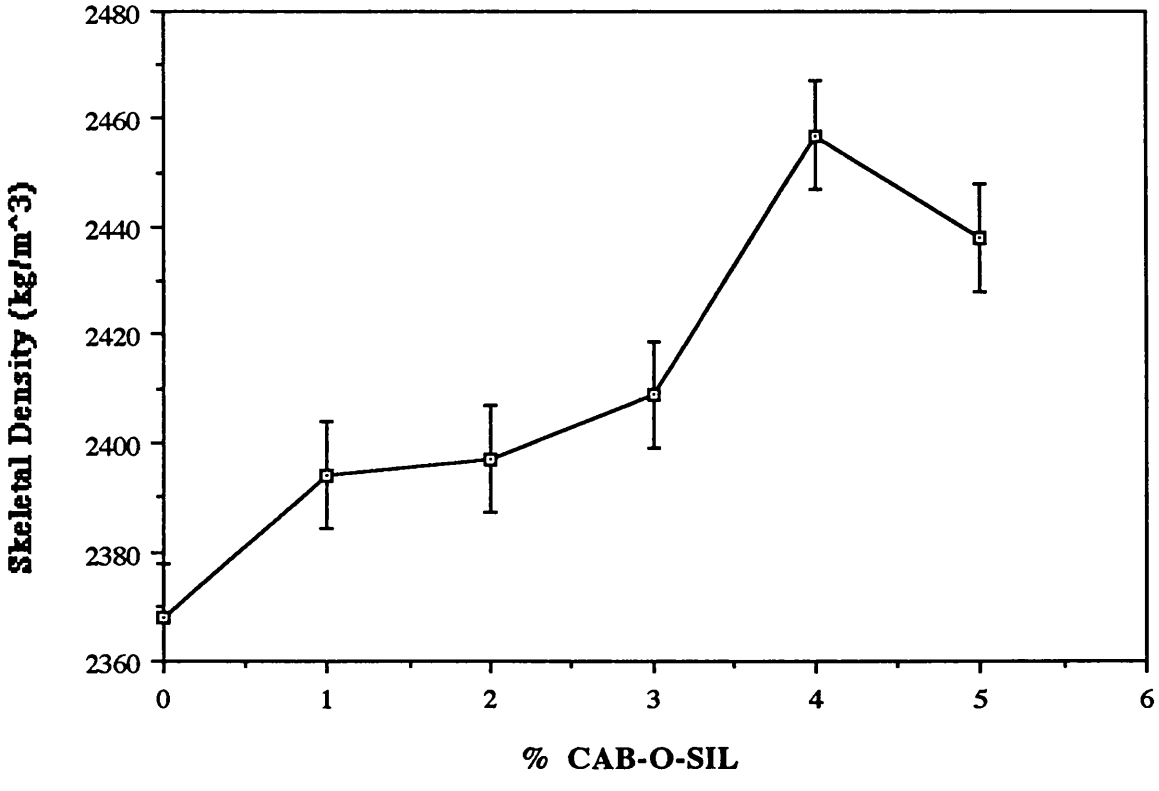

coverage of the host material by additives and preventing the intrusion of mercury into pores.

4.2.4. Particle Density

The skeletal density of FCC obtained from the pycnometer was (3120 kg/m^3) and the pore volume measured by the Omnisrp was 0.252 cc/g (2.52×10^{-4} m^3/kg). Using equation (3.1), the particle density of FCC was found to be 1759 kg/m^3. The skeletal density and pore volume of silica were 2111 kg/m^3 and 9.816 m^3/kg, respectively, which corresponded to a particle density of 718 kg/m^3.

4.2.5. Particle Charge

It was found that 1.79×10^{-9} C/g negative charge was on CAB–O–SIL particles. The charge was about 1.19×10^{-9} for S1 fumed silica. The presence of electrostatic charge on the particles was not unexpected, since the powder tended to stick extensively to any container and spatula during handling. As particles were dried at 120 °C overnight and they were very light (BD = 70 kg/m^3), they could easily be charged during handling due to contact electrification as they rubbed against each other. Electrical discharge of a powder mainly depends on its insulating properties and the humidity of environment. No significant charge was detected on mixtures of FCC and silica with CAB–O–SIL as presence of coarser particles reduced the friction between the ultrafine particles which was the main cause of formation of electrostatic charge on neat CAB–O–SIL particles.

4.2.6. Viscosity of CAB–O–SIL

Viscosity of CAB–O–SIL was measured using the concentric cylinder device described in section 3.2.9. Each test was repeated three times and shear stress data were plotted against shear rate values (Fig. 4.2.13). A linear relationship was found between the shear stress and the shear rate which is the characteristic of an ideal plastic (see Fig. 3.8). As the powder was very light, during the test some powder left the viscometer. Therefore, there was some scatter in the intercepts of the lines (yield stress) but the slopes which would determine the viscosity of the powder were in good agreement and the viscosity was found to be 0.166 Pa.s. This value will be used in section 4.5 to determine the viscosity of the continuous phase.

Fig. 4.2.13. Determination of the viscosity of CAB–O–SIL.

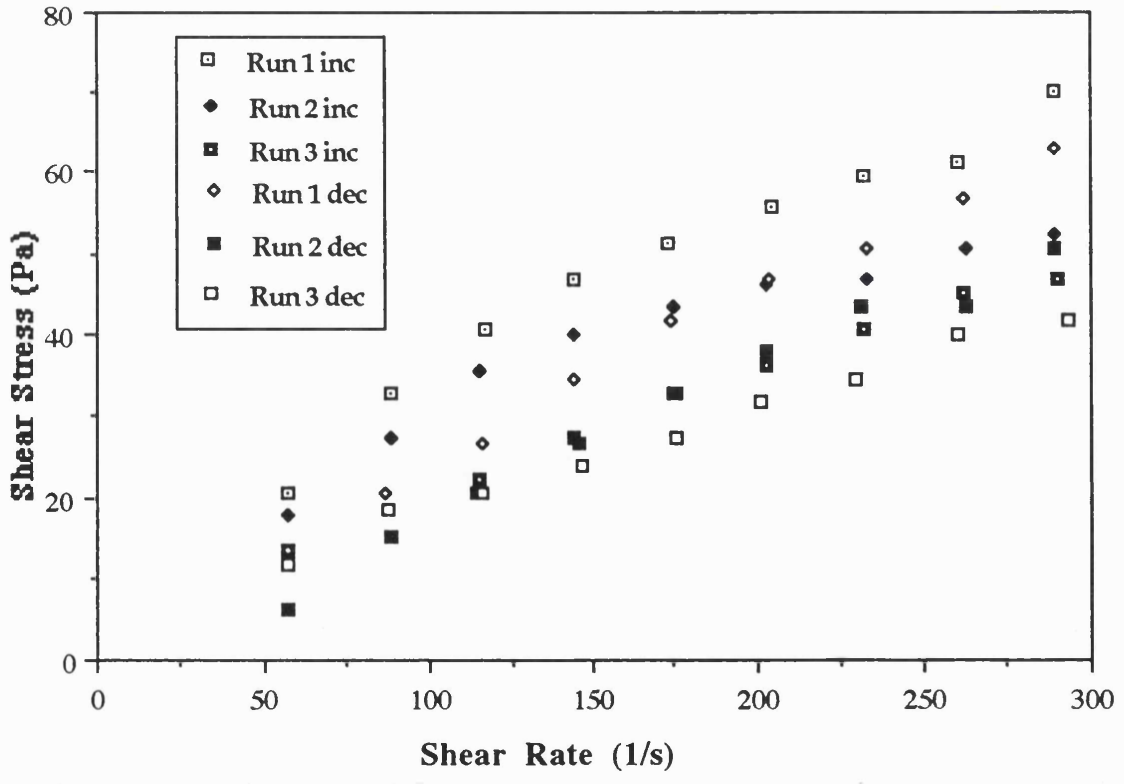

4.2.7. Discussions

Reduction in the bulk density of FCC and silica mixtures by addition of CAB–O–SIL showed that the ultrafines did not merely fill the interparticle voids. Rather they formed a particular network which results in a looser bed structure. In the case of kieselguhr, bulk density initially increased and a maxima was observed and it then decreased. The increase in the BD was due to the mesh–type particles of kieselguhr which would easily accommodate the ultrafines within the bed. This trend was similar to observations of Dutta and Dullea (1990) for a Group C powder with AOC and A200 (see section 2.11). In their system the BD peaked at concentrations as low as 0.35% and 0.2%. The consequent decrease in bulk density confirmed the formation of a more porous structure. It should be noted that this change in bulk density of kieselguhr was observed *below* the saturation limit of the host particles and it is likely that a similar trend could be observed in FCC and silica blends below 1% additive concentration, where ultrafines still act by covering the host.

Segregated ultrafines were observed at concentrations as low as 2.5% in FCC and silica in kieselguhr blends but even at 5% additive concentration, no agglomerates of ultrafines were detected. It suggested that particle shape of the host particles was an important factor in saturation limit. Irregularity of kieselguhr particles provided more interstitial sites for additives, therefore surface area of the host increased and more ultrafines could be attached to the host particles.

The change in the bulk density depended on the particle shape of the host material and ultrafines. The maxima in bulk density for kiesel–1 mixtures corresponded to 3% S1 fumed silica while the bulk density of kiesel–2 mixtures peaked at 1% CAB–O–SIL

concentration. The change was due to more irregular shape of kiesel–1 particles comparing to kiesel–2.

Ultrafines could easily develop a negative charge by contact electrification. Therefore they tended to part and disperse evenly in mixtures but their contact during processes such as fluidization cannot be avoided. This could affect the fluidization of the material.

4.3. Fluidization

In order to find the velocity at incipient fluidization and bubbling, fluidization experiments were mostly carried out in the 10 cm bed. The air flow rate was gradually increased to about $3U_{mb}$ and then reduced to zero. Pressure drop and bed height were plotted against air velocity and minimum fluidization velocity was found using the data obtained during defluidization. U_{mb} was determined as the last point at which bubbles could be observed in the bed when superficial air velocity was reduced. The results of all the fluidization experiments will be discussed here.

4.3.1. Effect of Bed Diameter

In order to compare the behaviour of the material in beds of different diameters, some glass ballotini in the range of 150–180 μm and particle density of 2920 kg/m^3 (Group B) was fluidized and the minimum fluidization velocities were determined in both beds (Figs 4.3.1 and 4.3.2). The experimental values of U_{mf} were 7.3 and 4.9 cm/s in the 5 and 10 cm rigs, respectively, which showed that as the bed diameter increased in this range, the U_{mf} decreased. The results were in agreement with the observations of Ormiston et al. (1965) and Rowe and Everett (1972) regarding the effect of bed thickness and/or diameter on the fluidization behaviour although none of the existing correlations used for U_{mf} prediction considers the bed diameter as an important and/or effective factor.

Assuming the voidage at minimum fluidization to be $\varepsilon_{mf} = 0.4$ and taking the sphericity of glass particles as 1, the U_{mf} predicted by the Carman–Kozeny Equation (2.4) was 2.7 cm/s. The modified Ergun Equation (2.5) estimated U_{mf} to be 2.8 cm/s which agreed

Fig. 4.3.1. Fluidization of Ballotini in the 10 cm bed.

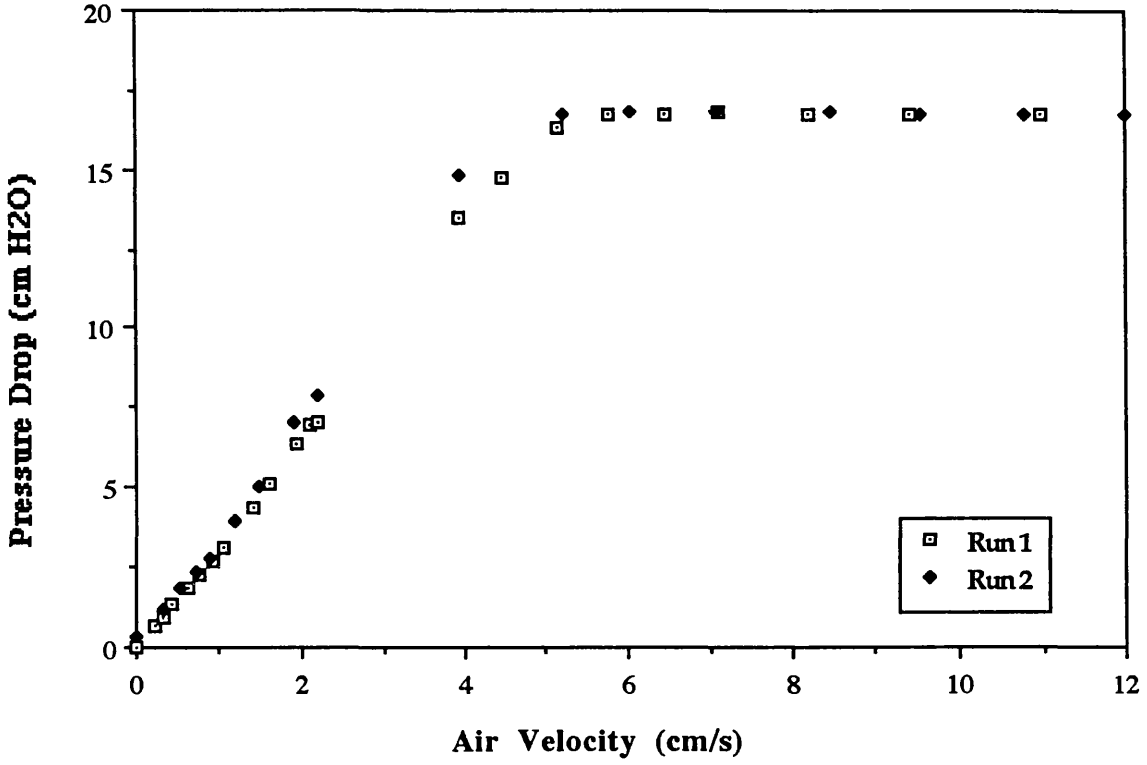

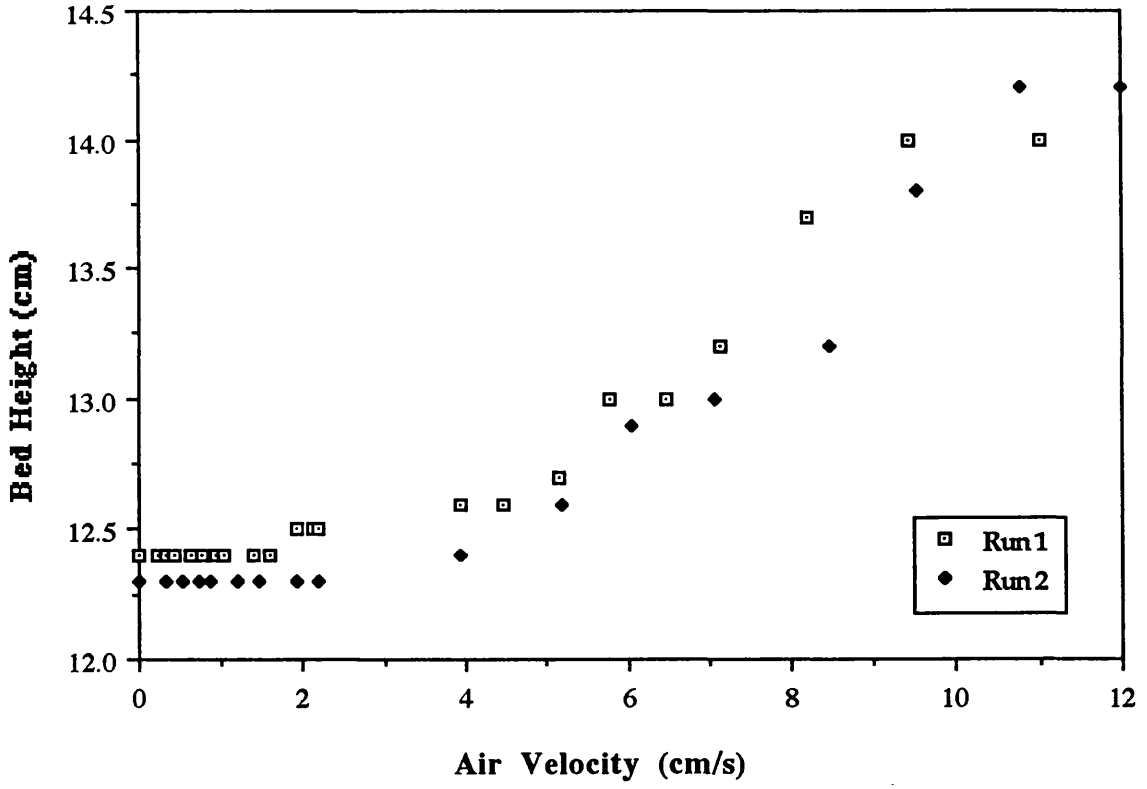

Fig. 4.3.2. Fluidization of glass ballotini in the 5 cm bed.

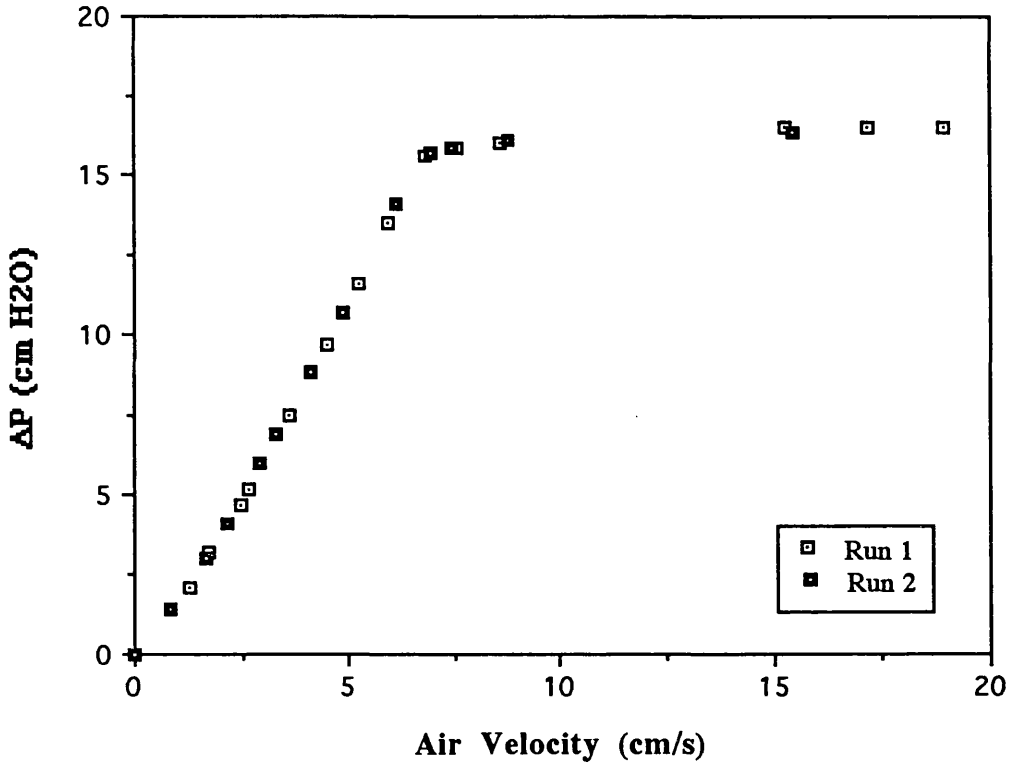

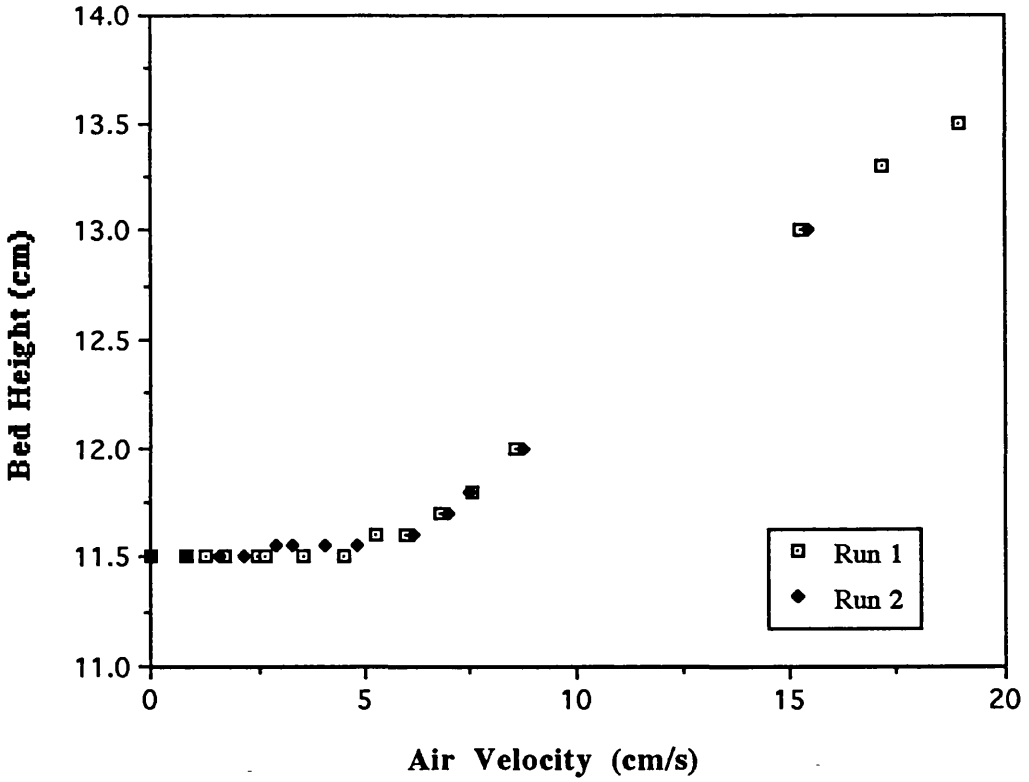

with the prediction of the Carman–Kozeny equation. However, these predicted values were much lower than the experimental ones (7.3 and 4.9 cm/s) indicating that the beds were probably too small. Considering a linear relationship between bed diameter and U_{mf} in this range (see Fig. 2.2), and extrapolating the line to U_{mf} = 2.8 cm/s, corresponded to a bed diameter of 14.4 cm. Therefore, in beds of smaller than 14.4 cm, the U_{mf} would be a function of bed diameter which was in good agreement with the value reported by Rowe and Everett (1972) for 210 μm alumina ; i.e. 15 cm.

4.3.2. Fluidization of Ultrafines

CAB–O–SIL fluidized by itself divided into two layers during the experiment: the top layer fluidized quite normally but the bottom layer remained still and formed agglomerates which were larger adjacent to the distributor and gradually became smaller towards the top layer. At higher flow rates, a part of the still layer fluidized but the pressure drop in the bed was negligible. In general the bed did not show normal behaviour, as expected from a Group C powder, therefore U_{mf} could not be determined in this case. S1 fumed silica had a similar behaviour when fluidized by itself.

4.3.3. Fluidization of FCC

FCC fluidized normally in the 10 cm bed and the U_{mf} was experimentally found to be 0.43 cm/s (Fig. 4.3.3) and its U_{mb} was determined as 0.95 cm/s. The bed expansion between incipient fluidization and incipient bubbling was determined by equation (3.4):

$$\text{Bed expansion} = \frac{H_{mb} - H_{mf}}{H_{mf}} \times 100 \qquad (3.4)$$

12% bed expansion was observed for FCC when fluidized by itself. The effect of addition of CAB–O–SIL was then investigated on the fluidization behaviour of FCC (Figs. 4.3.3–4.3.8). The results are summarized in Table 4.3.1.

Fig. 4.3.9 shows that as the concentration of CAB–O–SIL increased, the U_{mb} increased but the U_{mf} decreased; however the effect of additives was found to be more pronounced on U_{mb} than U_{mf}. As a result, the bed expansion increased significantly (Fig. 4.3.10). The 15% mixture had a bed expansion of 51% which was quite remarkable comparing to FCC without any additive. In general, fluidization of FCC was much smoother in the presence of ultrafines. The decrease in U_{mf} could be due to the decrease in the particle density of the host material, as it is covered with ultrafines. Addition of ultrafines led to a sharp decrease in the bulk density as already referred to in section 4.2.2, therefore the bed became more porous and capable of holding the gas within itself and consequently U_{mb} increased.

The elutriation loss was found to decrease from 1% for FCC to about 0.2% for samples containing 2.5–10% additive as shown in Table 4.3.1 which suggested that ultrafines were not easily elutriated from the bed despite their very small particle size. The decrease in elutriation disproved the belief (Zenz and Weil, 1958; Gugnoni and Zenz, 1980; Briens et al., 1988) that finer particles normally leave the bed in early stages of fluidization. There was not a significant change in the host coverage by additives before and after fluidization as already mentioned in section 4.1, therefore ultrafines were not elutriated preferentially to the larger host material which suggested that the force which held the particles together was larger than the drag force applied to them during fluidization.

Fig. 4.3.3. Fluidization of FCC.

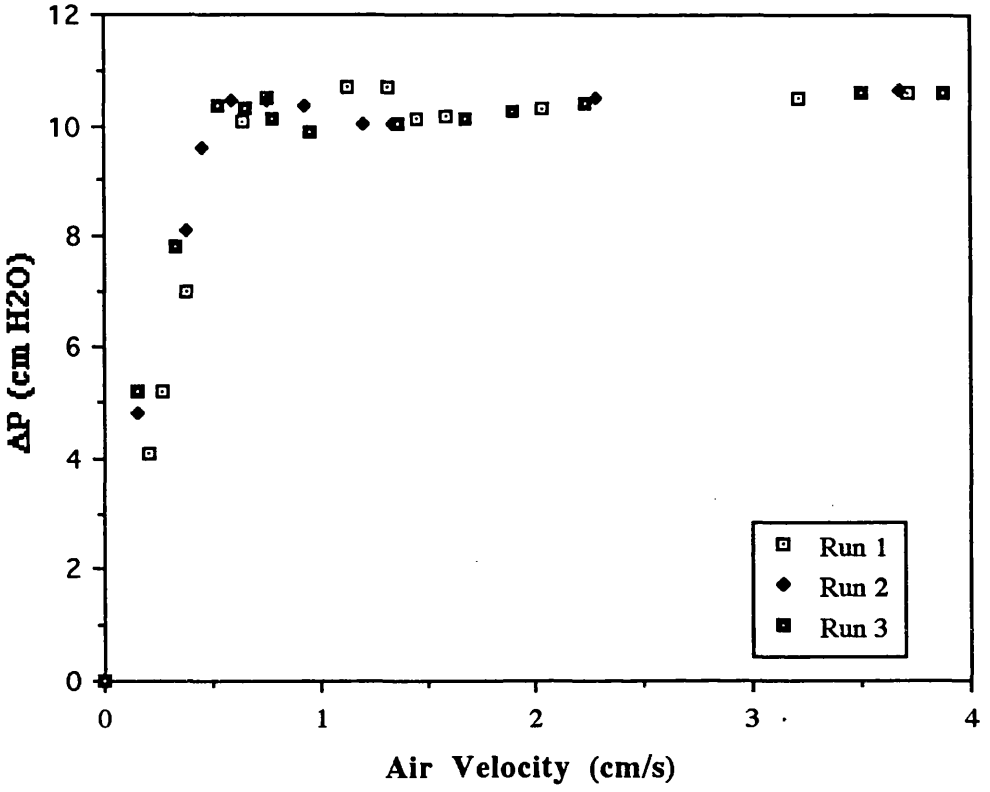

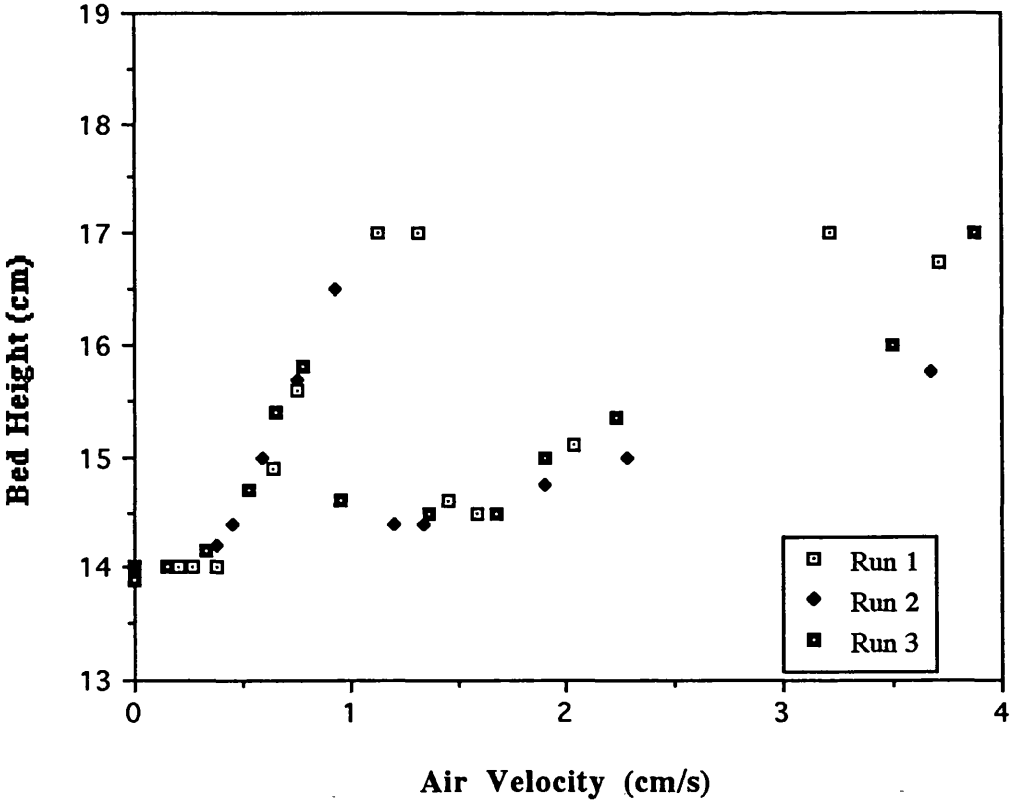

Fig. 4.3.4. Fluidization of FCC with 1% CAB–O-SIL.

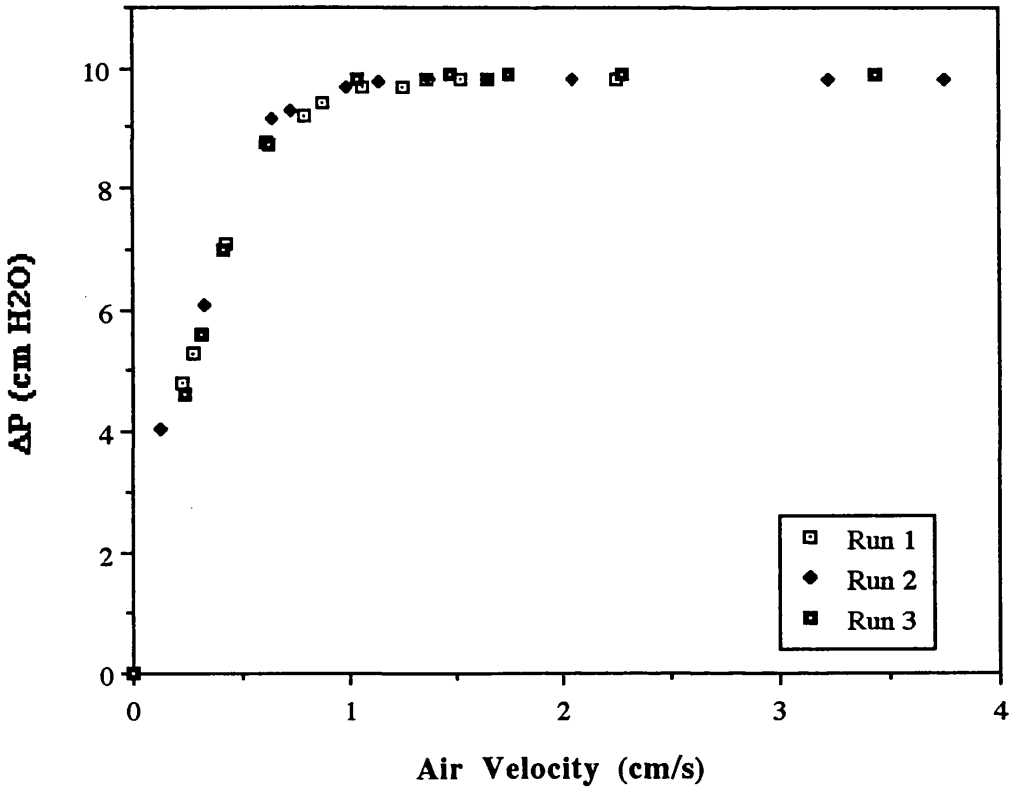

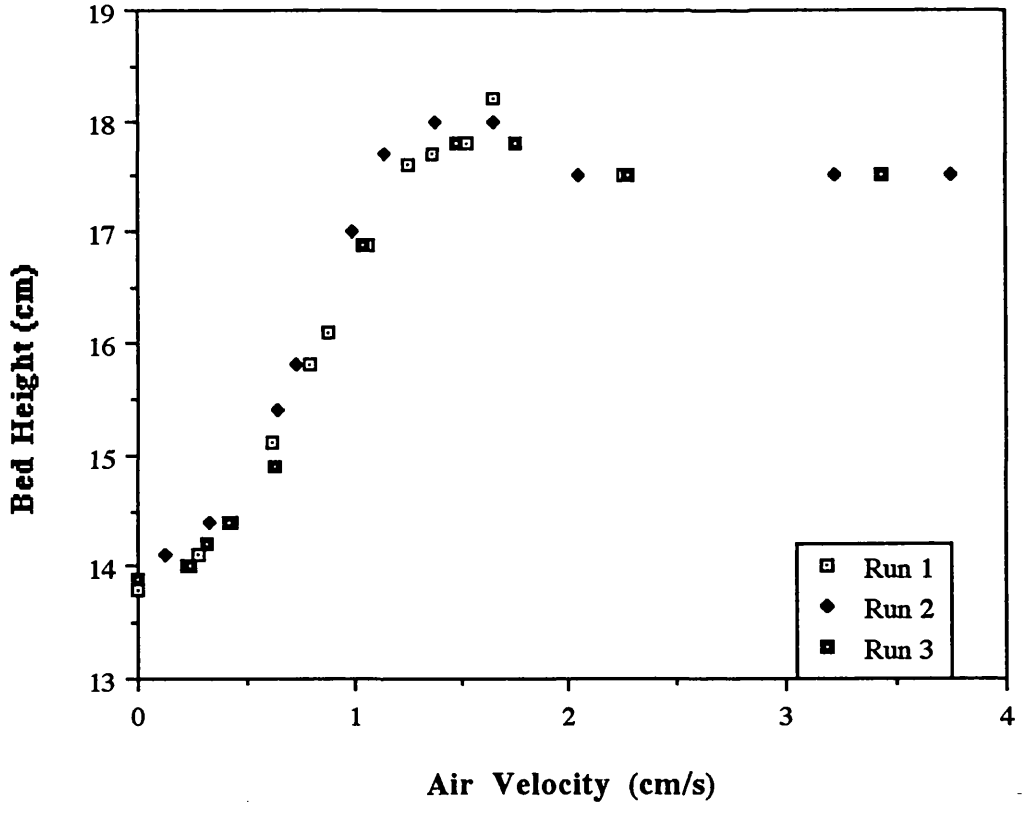

Fig. 4.3.5. Fluidization of FCC with 2.5% CAB-O-SIL.

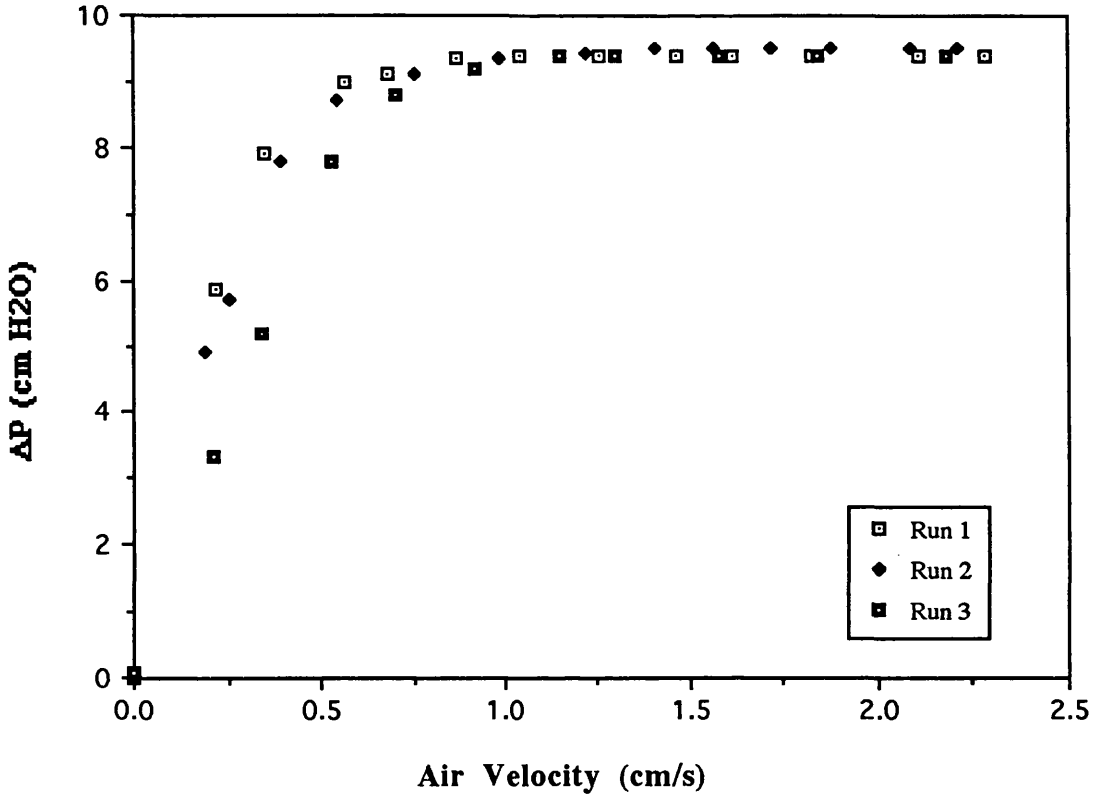

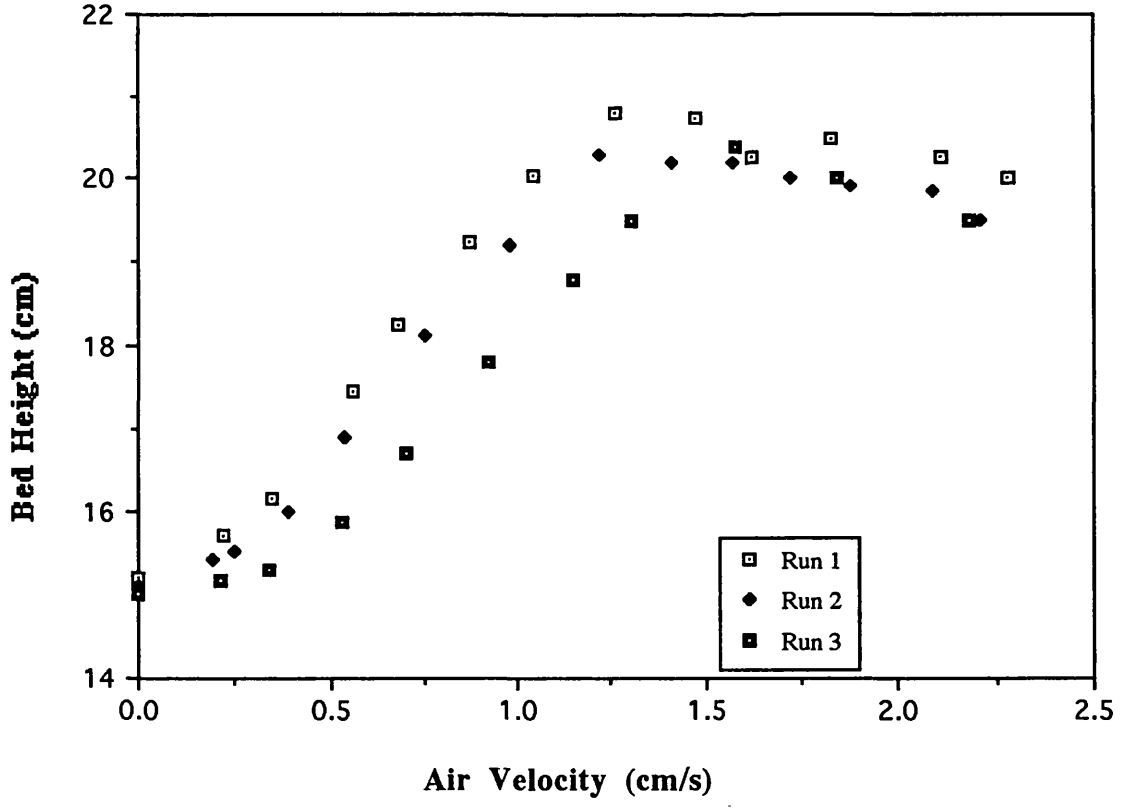

Fig. 4.3.6. Fluidization of FCC with 5% CAB-O-SIL.

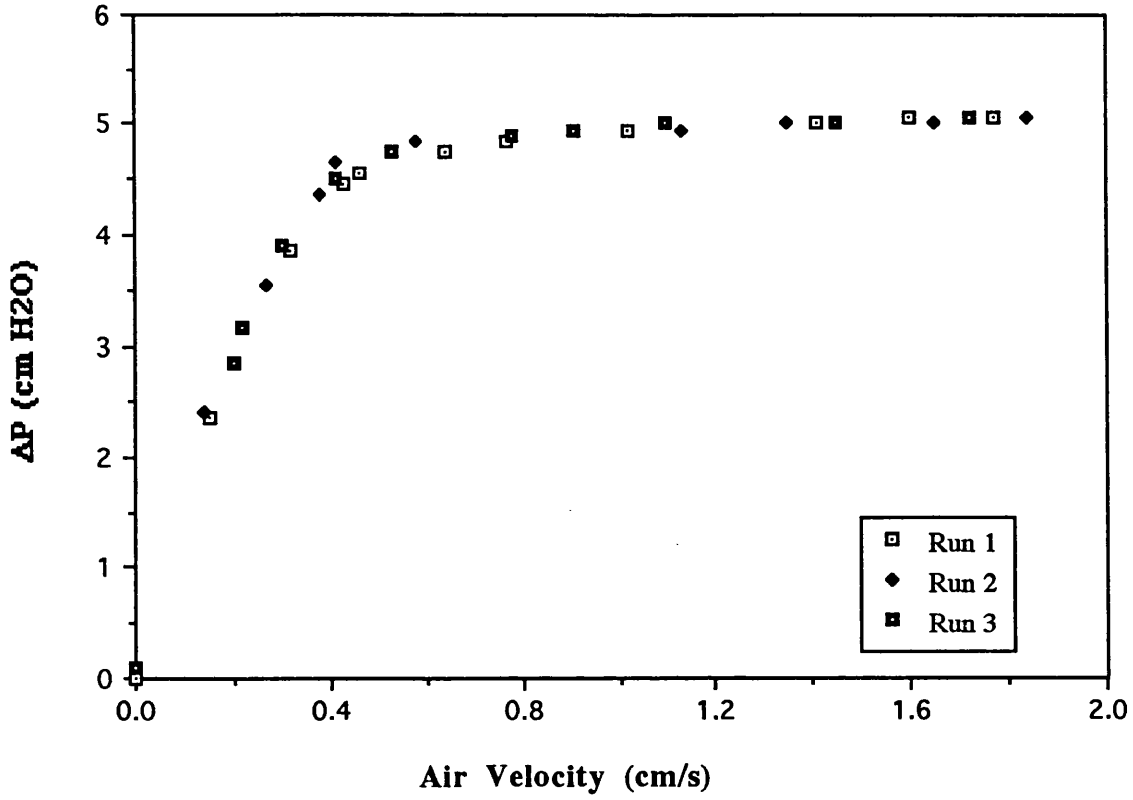

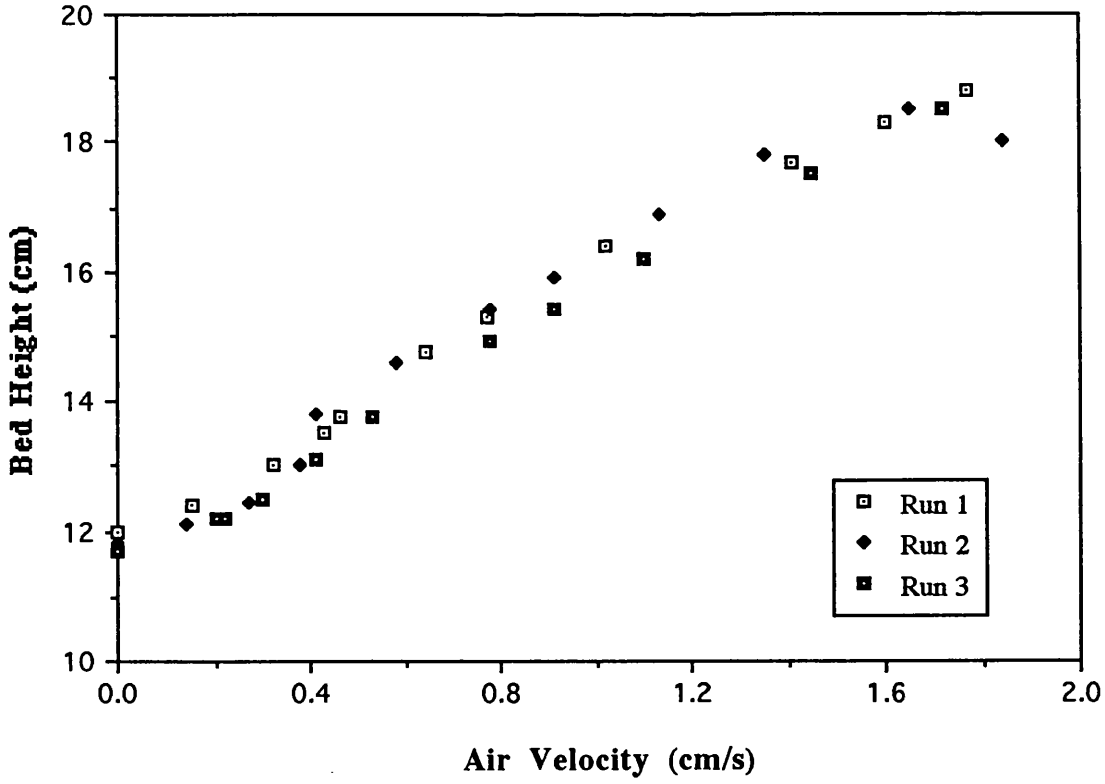

Fig. 4.3.7. Fluidization of FCC with 10% CAB-O-SIL.

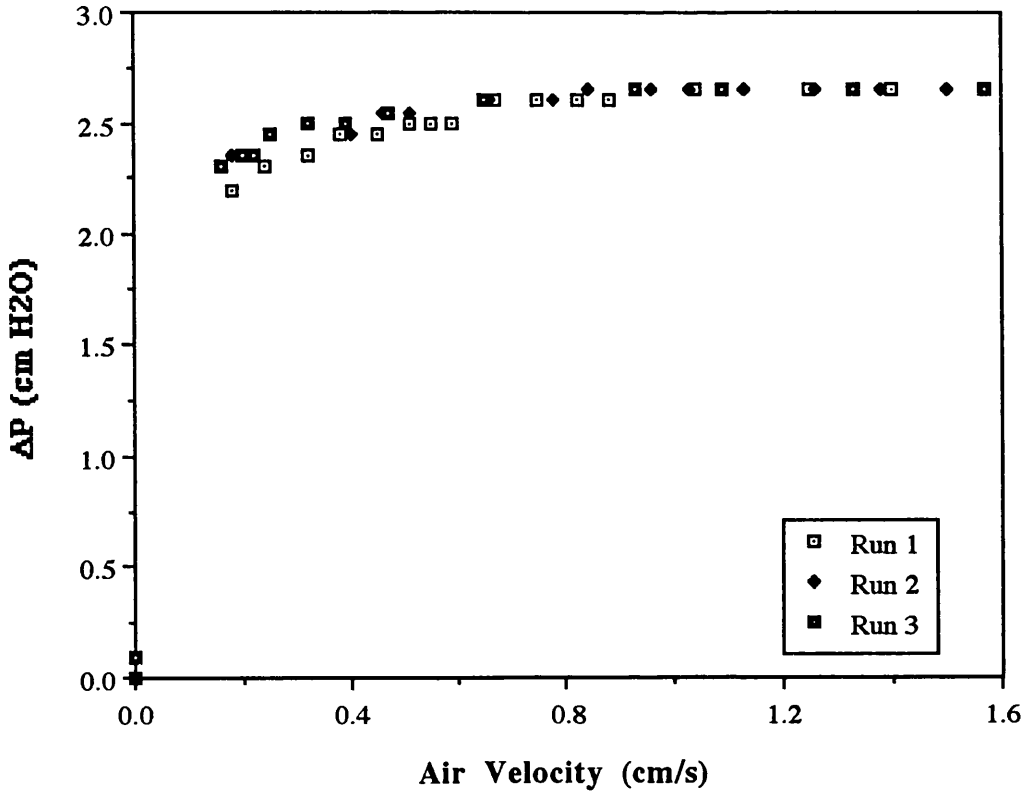

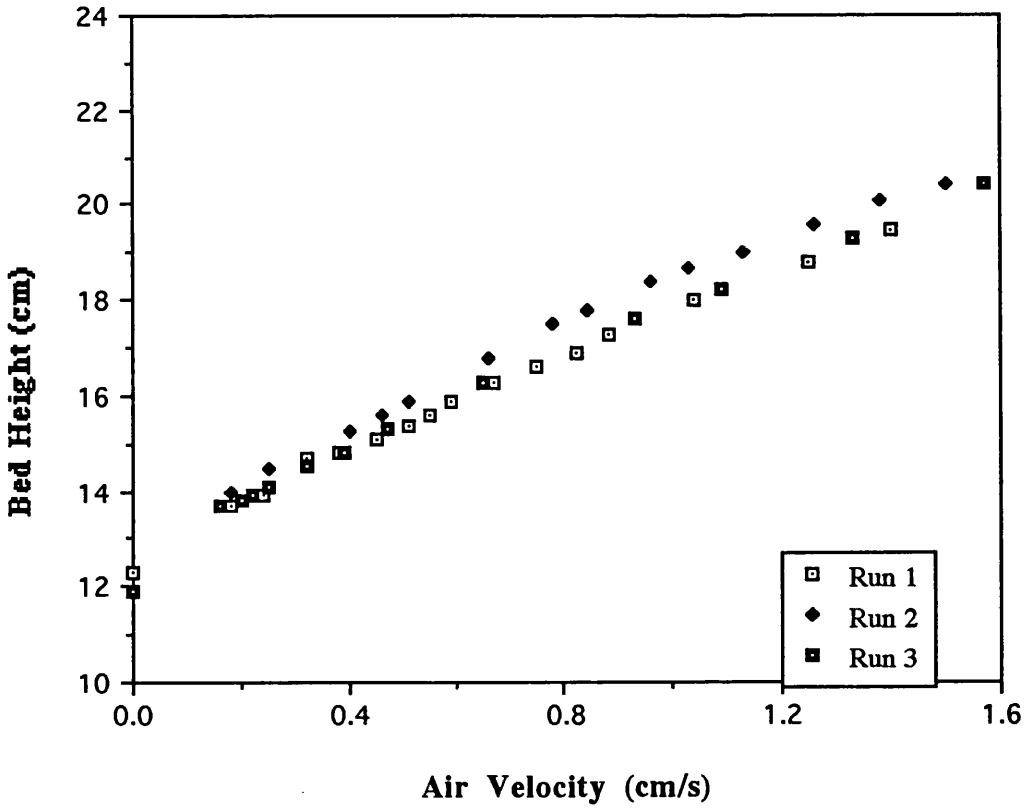

Fig. 4.3.8. Fluidization of FCC with 15% CAB-O-SIL.

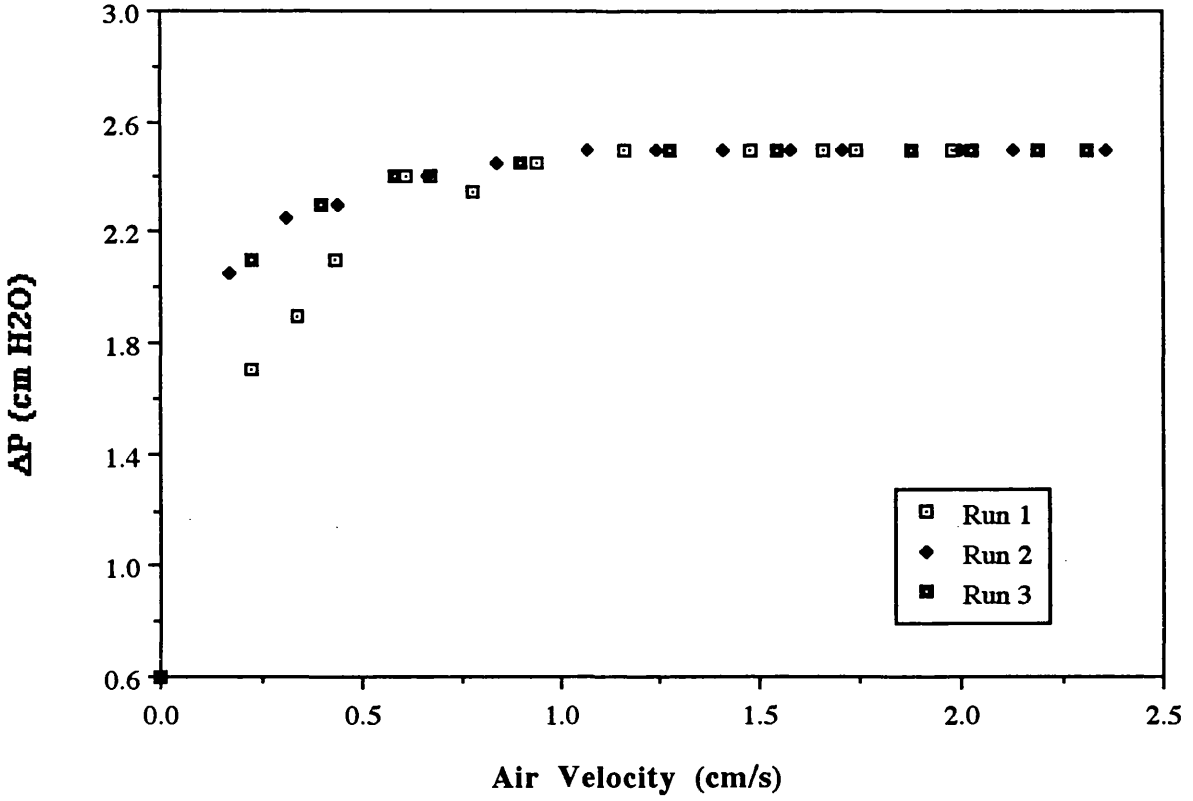

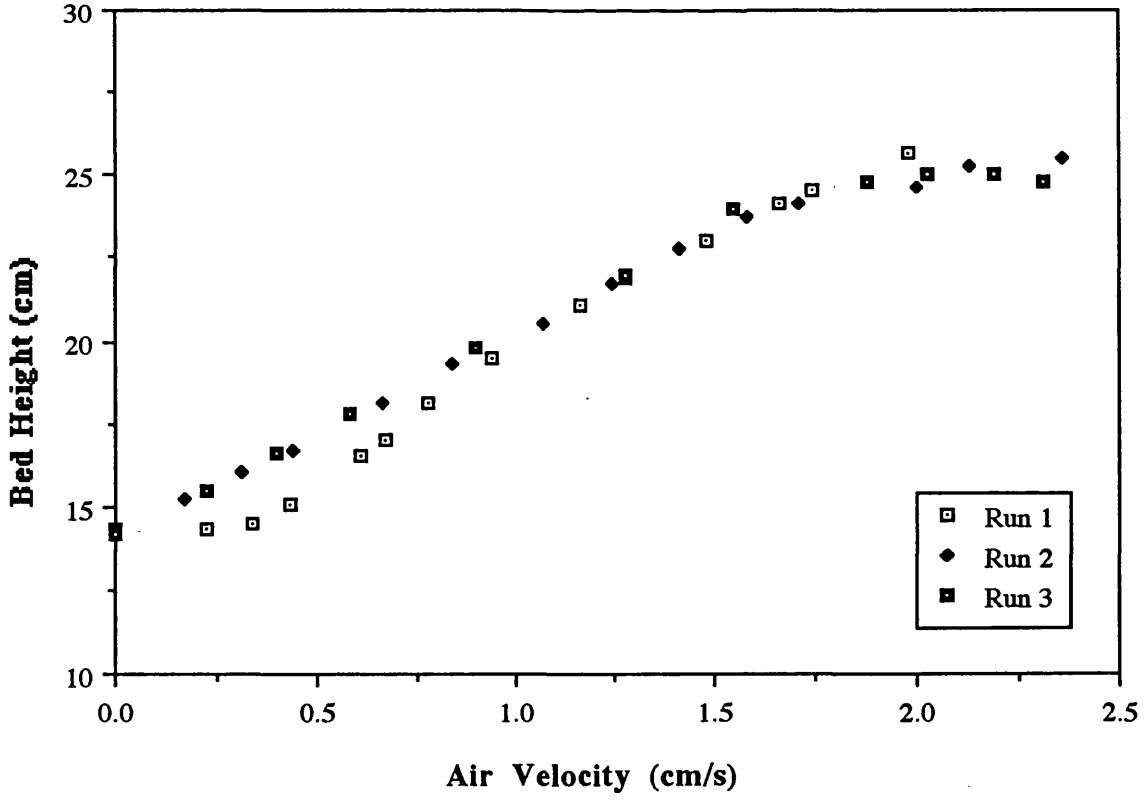

Table 4.3.1. Effect of the addition of CAB–O–SIL on fluidization behaviour of FCC.

CAB–O–SIL (wt%)	Bed weight (g)	ε_{lp}	U_{mf} (cm/s)	H_{mf} (cm)	ε_{mf}	U_{mb} (cm/s)	H_{mb} (cm)	ε_{mb}	Bed Expansion (%)	Elutriation loss (%)
0	1000	0.336	0.43	14.7	0.5075	0.95	16.5	0.561	12	1.0
1	900	0.416	0.5	14.7	0.5568	0.95	16.7	0.610	14	0.5
2.5	850	0.601	0.45	16	0.6155	1.24	20	0.692	25	0.15
5	500	0.671	0.31	12.5	0.7105	1.2	17.8	0.797	42	0.2
10	300	0.811	0.2	13.8	0.8426	1.8	20.1	0.892	46	0.26
15	240	0.854	0.21	15.3	0.8865	1.55	23.1	0.925	51	0.4

Voidage of the loose packed bed increased from 0.336 for FCC to 0.854 for the 15% mixture (Fig. 4.3.11) as shown in Table 4.3.1 which was due to a more porous and looser structure in the bed. Bed voidage of FCC at incipient fluidization was found to be 0.508 using equation (3.5) which increased to 0.888 for the sample containing 15% CAB–O–SIL. Although there was a considerable change in ε_{mf}, it was mainly due to the increase in the loose packed voidage. The ε_{mb} increased from 0.561 to 0.925. Obviously, ε_{mb} was always greater than ε_{mf} since $U_{mb}>U_{mf}$.

The ratio of the experimental pressure drop across the bed, ΔP, to the ideal pressure drop, M.g/A, has been related to the cohesion of the bed (Geldart et al., 1984). This ratio; i.e. $\Delta P.A/(M.g)$, which is sometimes referred to as the normalized bed pressure drop, decreases with an increase in the cohesion of the bed. Ideal, experimental and normalized pressure drop of FCC mixtures are shown in Table 4.3.2 and Fig. 4.3.12 shows that addition of CAB–O–SIL reduced the normalized pressure drop across the bed and therefore increased the cohesion. The cohesion was imparted to Group A material by ultrafines.

It should be mentioned that the bulk density of FCC was much higher than CAB–O–SIL (1168 kg/m^3 comparing to 70 kg/m^3); i.e. a mixture of 15% CAB–O–SIL by weight actually contained nearly 74% additive by volume. Hence samples with higher concentrations of additives were not considered in the experiments.

Fig. 4.3.9. Effect of CAB–O–SIL addition on Umf and/or Umb of FCC.

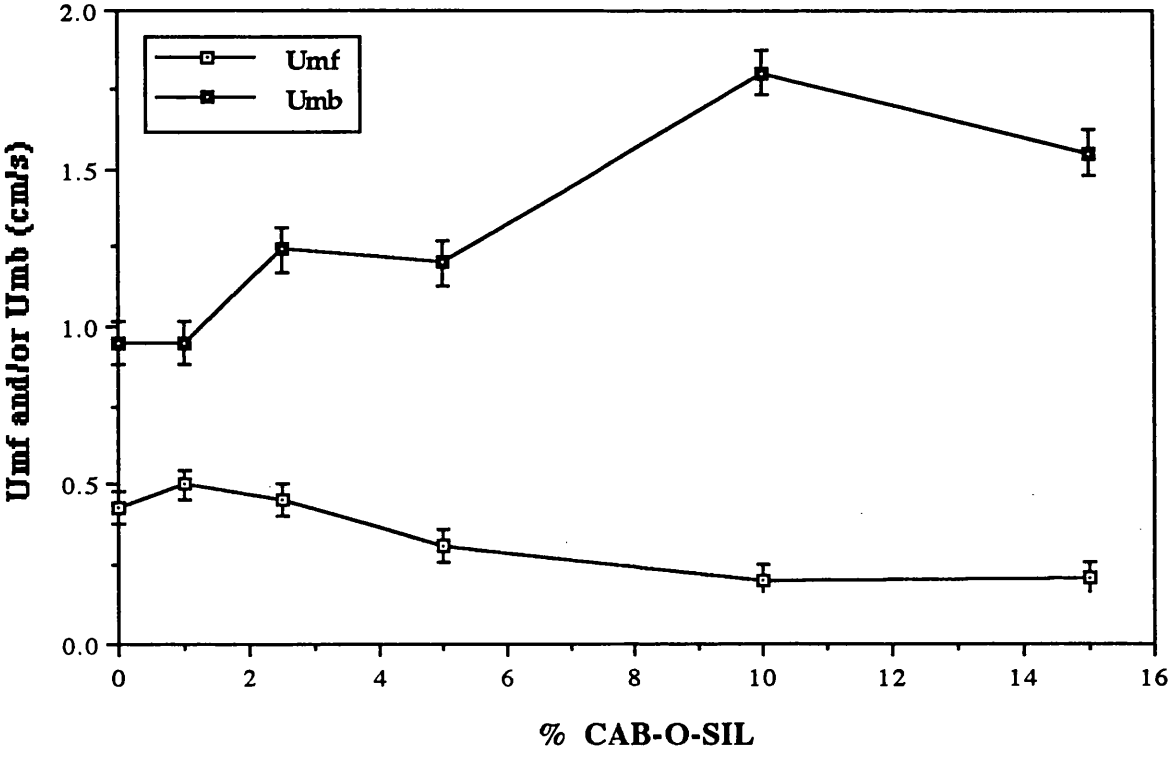

Fig. 4.3.10. Effect of CAB-O-SIL on the expansion of FCC.

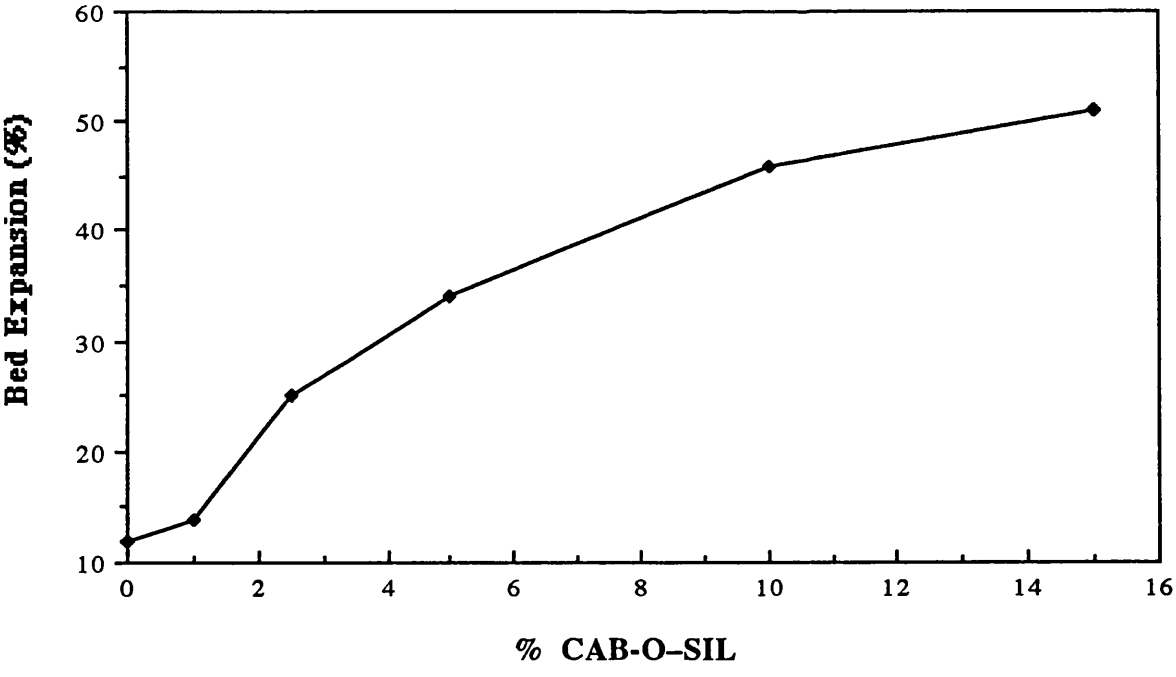

Fig. 4.3.11. Effect of CAB–O–SIL on the bed voidage of FCC.

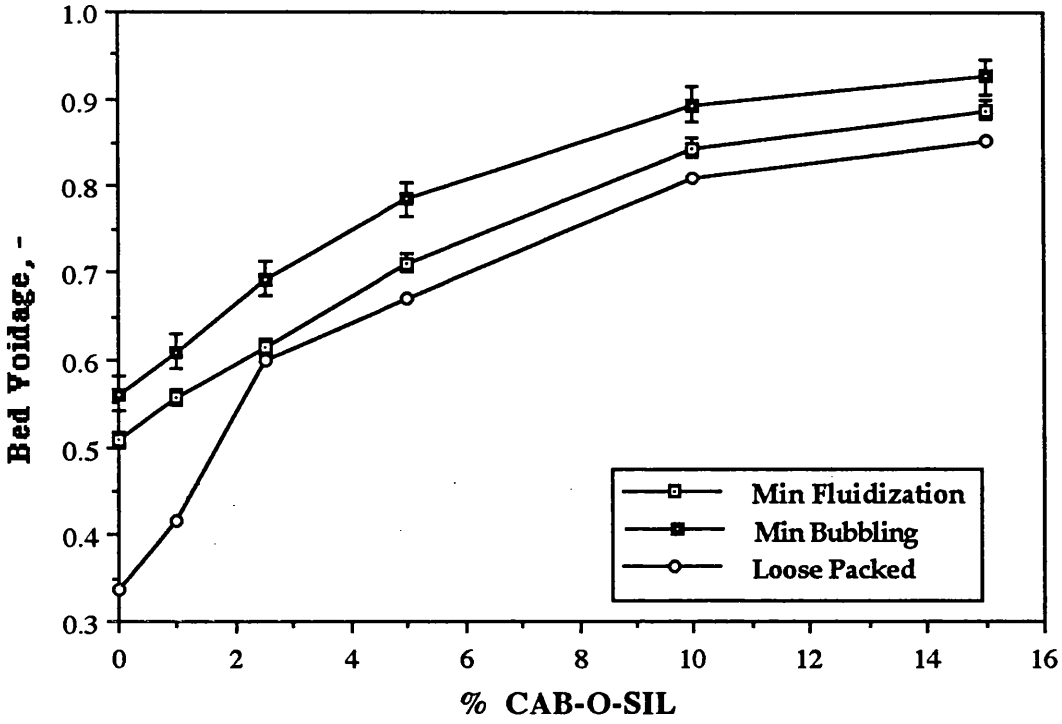

Fig. 4.3.12. Effect of CAB-O-SIL on the normalized pressure drop of FCC mixtures.

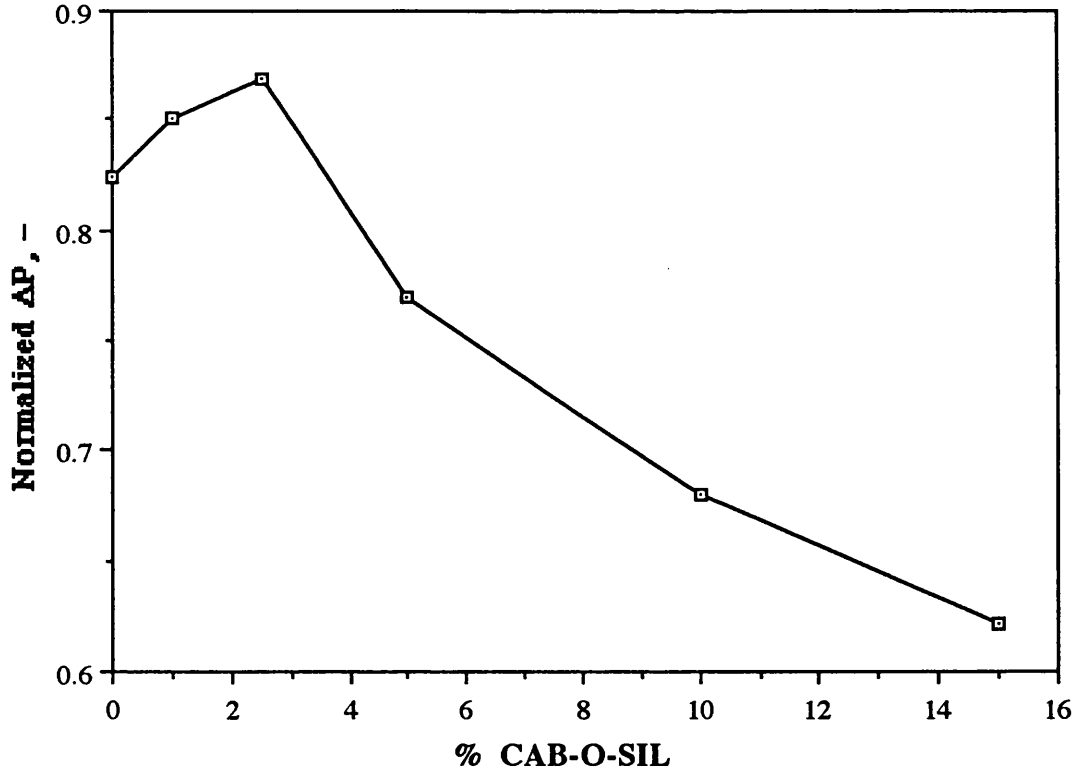

Table 4.3.2. Effect of CAB–O–SIL on the normalized poressure drop of FCC mixtures.

CAB–O–SIL (wt%)	Ideal ΔP, Pa	Experimental ΔP, cm H2O	Experimental ΔP, Pa	Normalized ΔP
0	1249.048	10.5	1029.63	0.824
1	1124.143	9.75	956.09	0.851
2.5	1061.691	9.4	921.76	0.868
5	624.524	4.9	480.49	0.769
10	374.714	2.6	254.96	0.680
15	299.772	1.9	186.31	0.622

4.3.4. Fluidization of Silica

Silica showed a normal behaviour when fluidized by itself in the 10 cm bed and had a U_{mf} of 0.66 cm/s (Fig. 4.3.13); the U_{mb} was found to be 1.15 cm/s which corresponded to 9.5% bed expansion. Silica was then fluidized with different concentrations of CAB–O–SIL (Figs. 4.3.14–4.3.18); the results are summarized in Table 4.3.3.

The U_{mf} slightly decreased with the concentration of CAB–O–SIL in the bed (Fig. 4.3.19), however, the effect was again more noticeable on the U_{mb} which increased significantly. The bed expansion, therefore, increased up to 56% for the 15% mixture (Fig. 4.3.20) which was considerably more than for silica without any ultrafines. In general, the fluidization of silica was smoother in the presence of the ultrafines. The elutriation loss was found to decrease from 1.8% for silica to nearly zero for samples containing above 2.5% CAB–O–SIL.

The voidage of the loose packed bed increased from 0.440 for silica to 0.705 when 15% wt CAB–O–SIL was present in the blend (Fig. 4.3.21). The ε_{mf} of silica was found to be 0.557 which increased to 0.799 and when 15% CAB–O–SIL was added to the host material the ε_{mb} increased from 0.595 to 0.871. The behaviour was quite similar to FCC already mentioned in section 4.3.3 and the increase in the bed voidage was in agreement with the drop in bulk density of the mixtures. The voidage was a strong function of concentration of ultrafines as shown in Figs. 4.3.11 and 4.3.21 and additives appeared to be more effective on the voidage of FCC than silica. Bed expansions could be related to the porosity of the emulsion phase or the amount of gas dispersed in the solid phase. The increasing porosity of the emulsion phase reflected an

Fig. 4.3.13. Fluidization of silica.

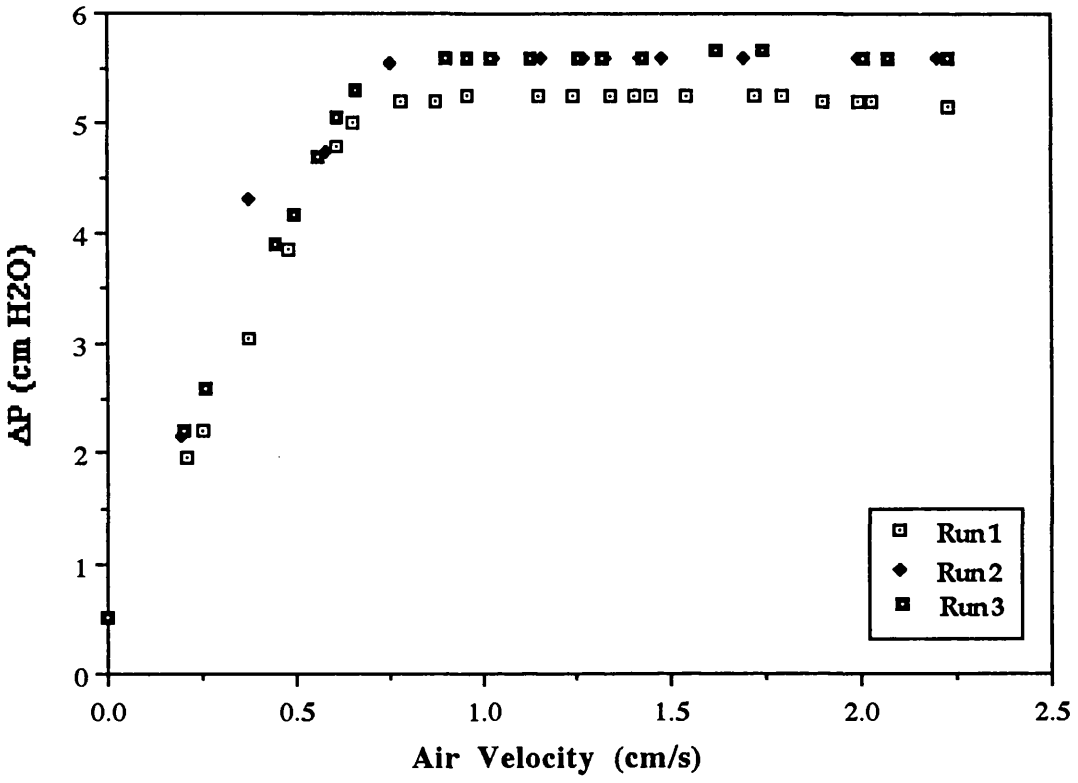

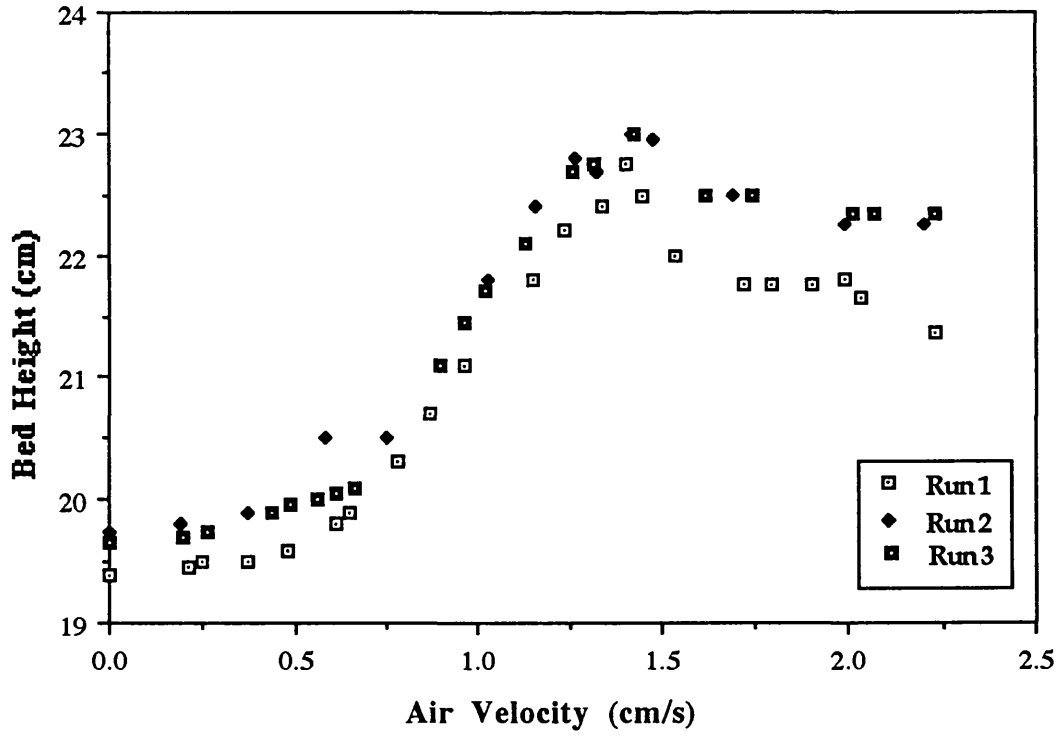

Fig. 4.3.14. Fluidization of silica with 1% CAB-O-SIL.

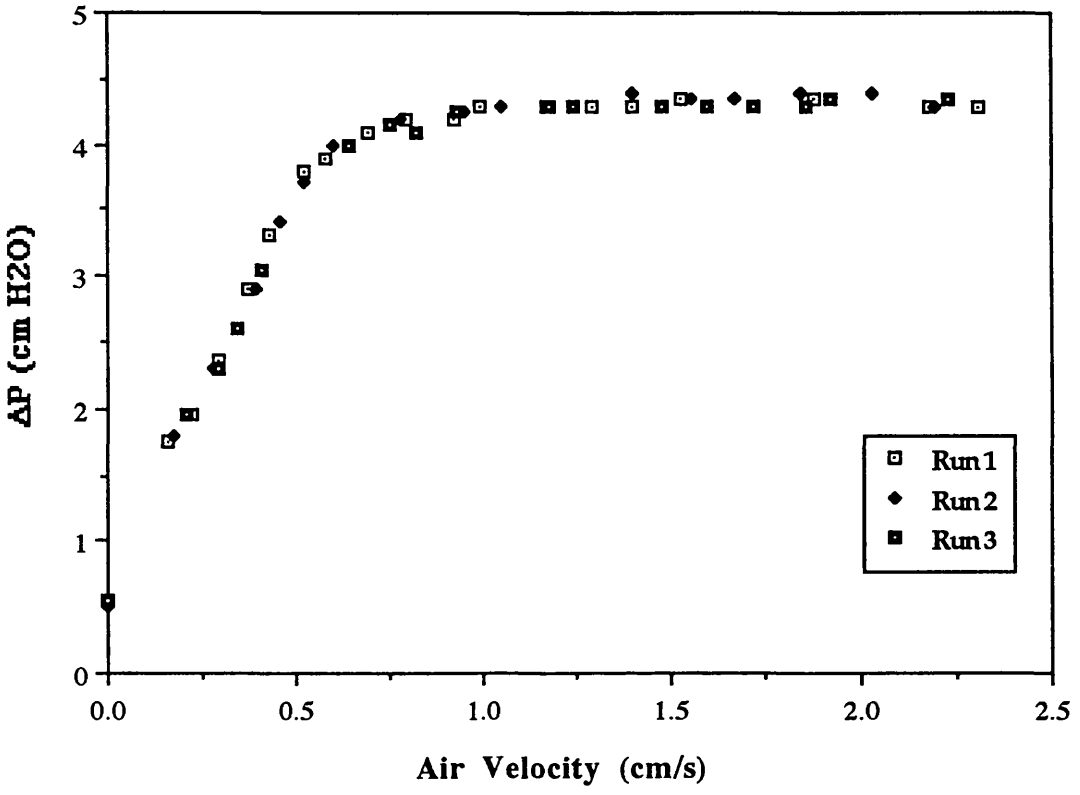

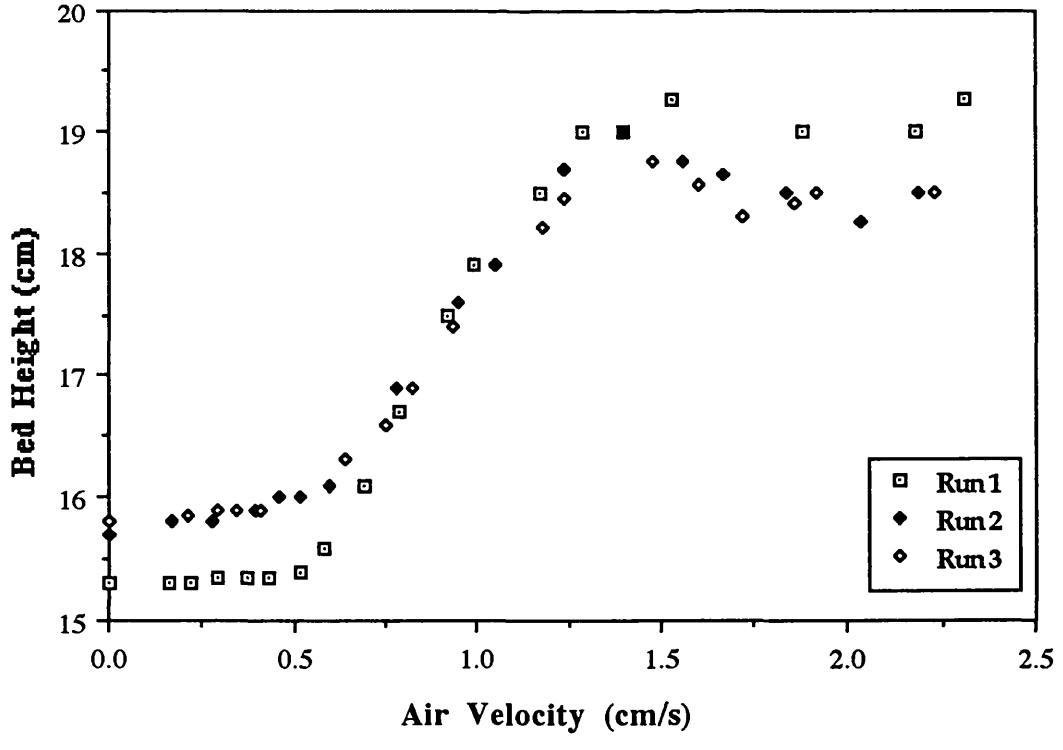

Fig. 4.3.15. Fluidization of silica with 2.5% CAB-O-SIL.

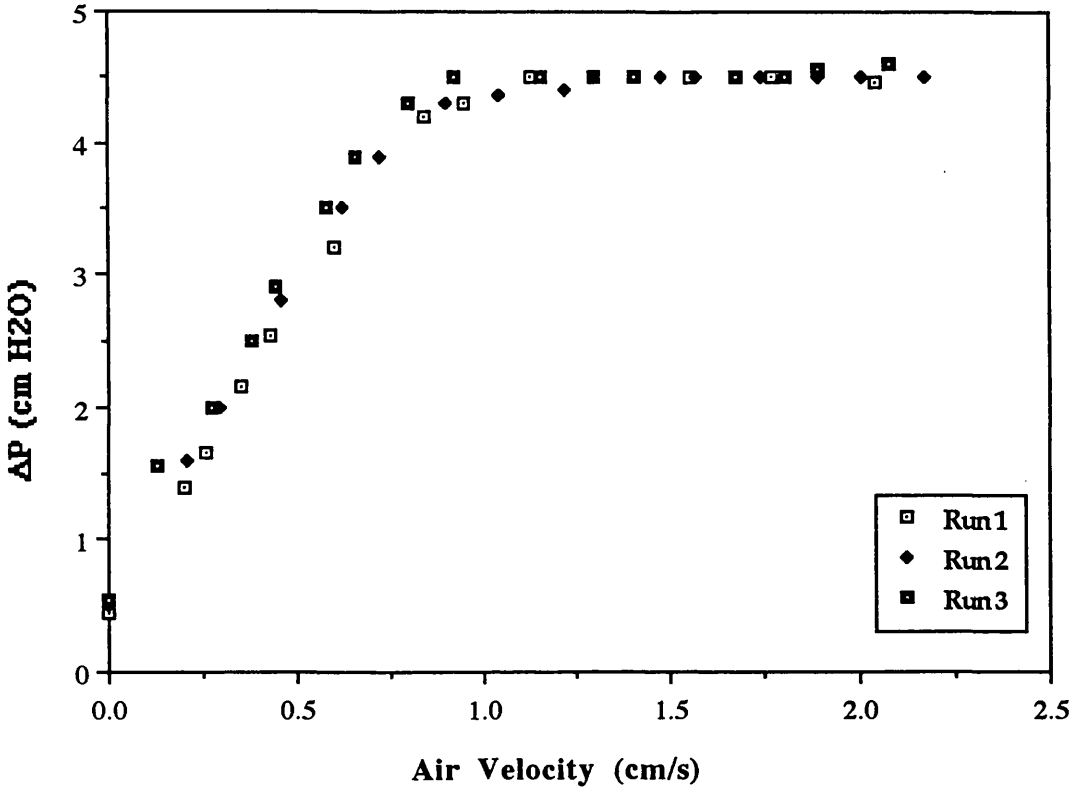

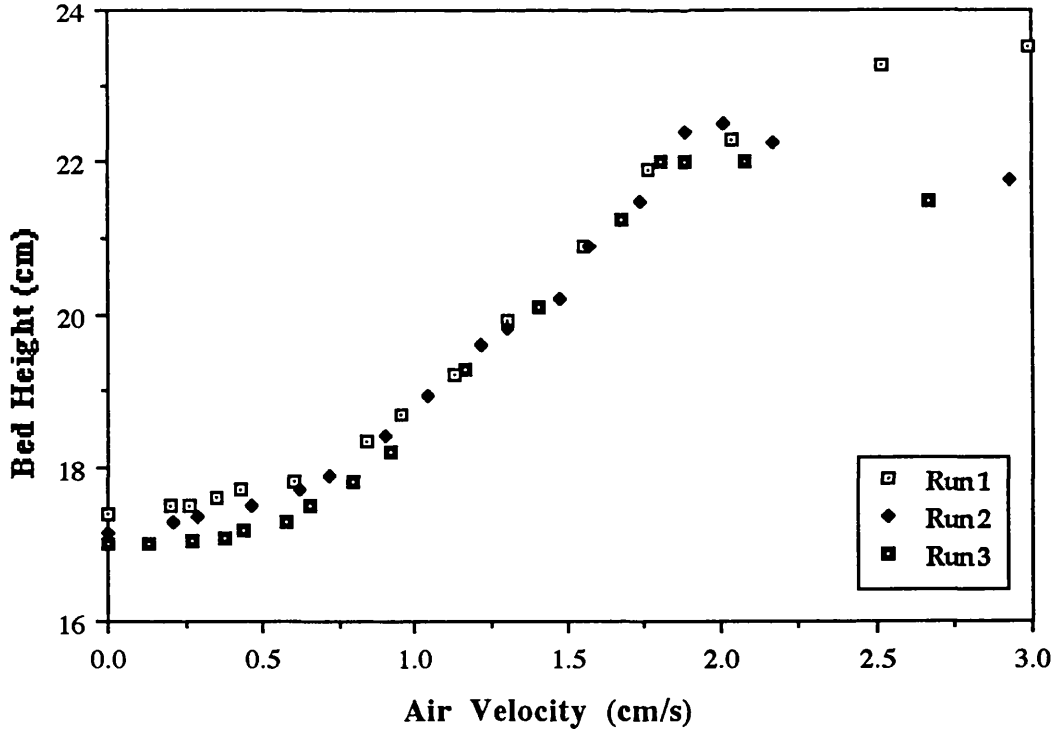

Fig. 4.3.16. Fluidization of silica with 5% CAB-O-SIL.

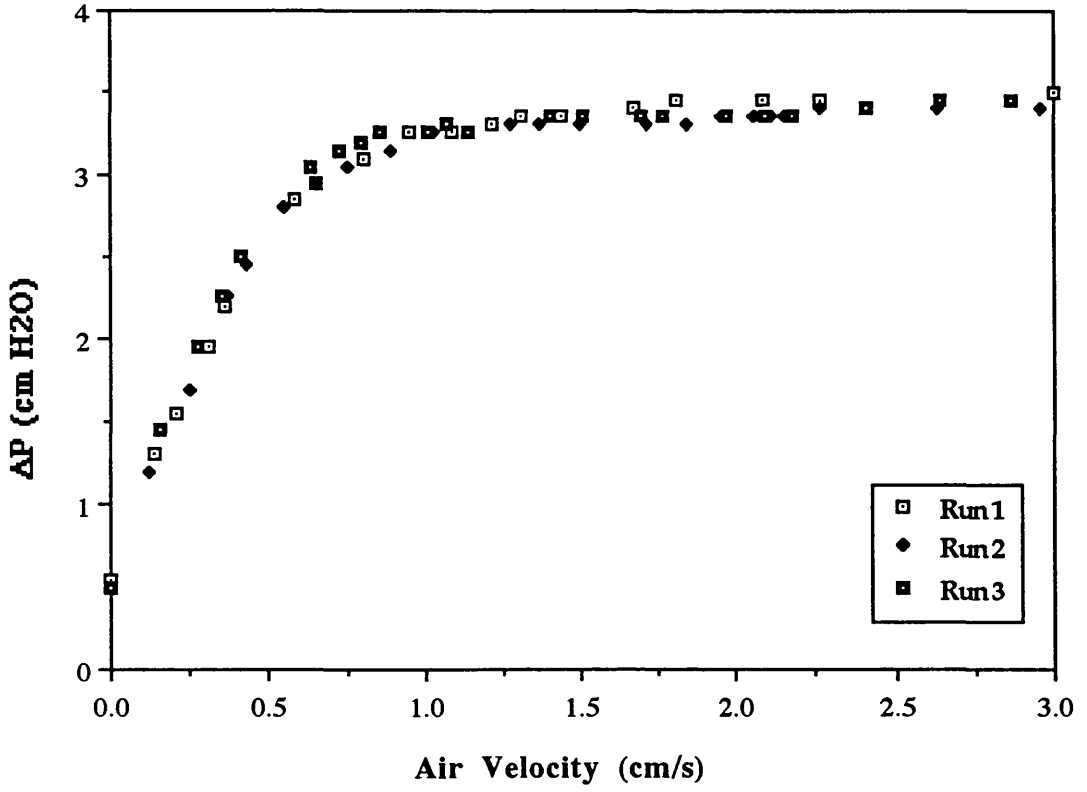

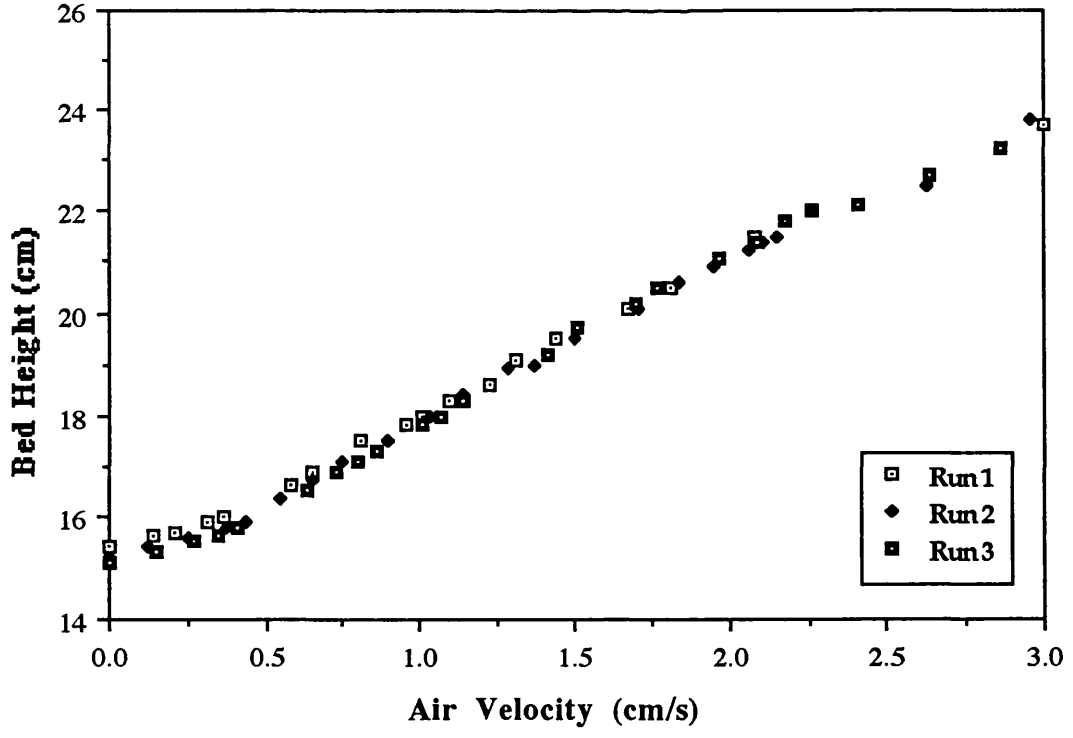

Fig. 4.3.17. Fluidization of silica with 10% CAB-O-SIL.

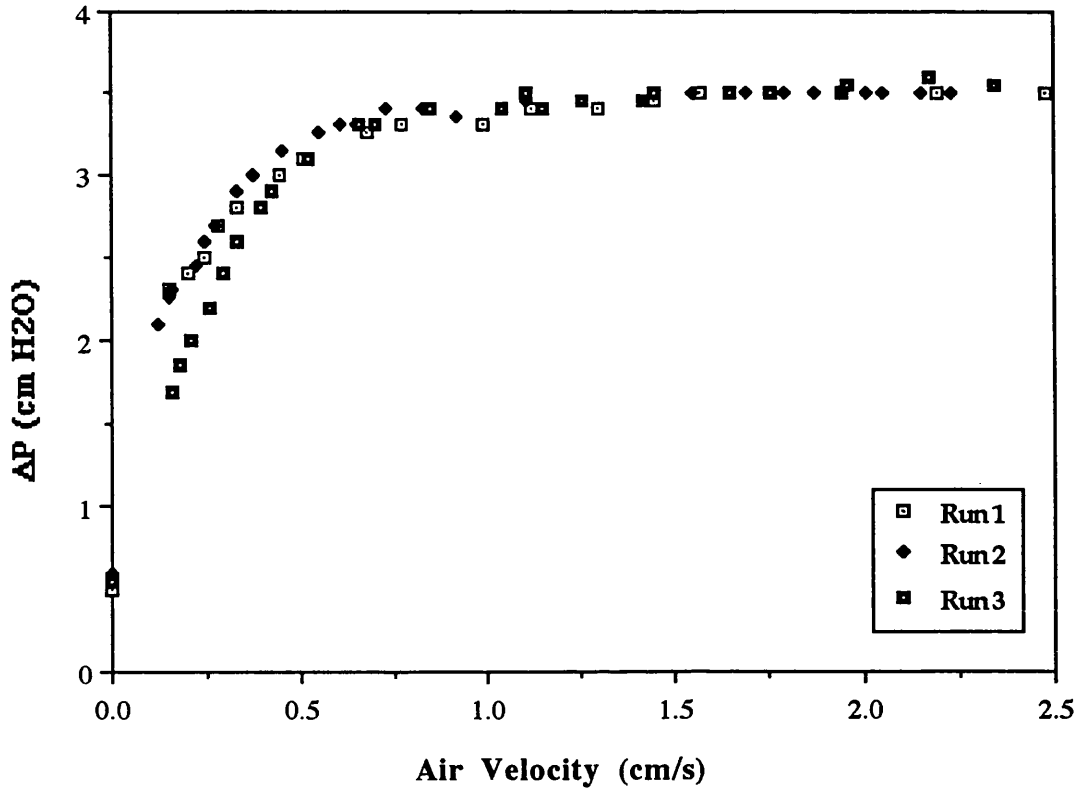

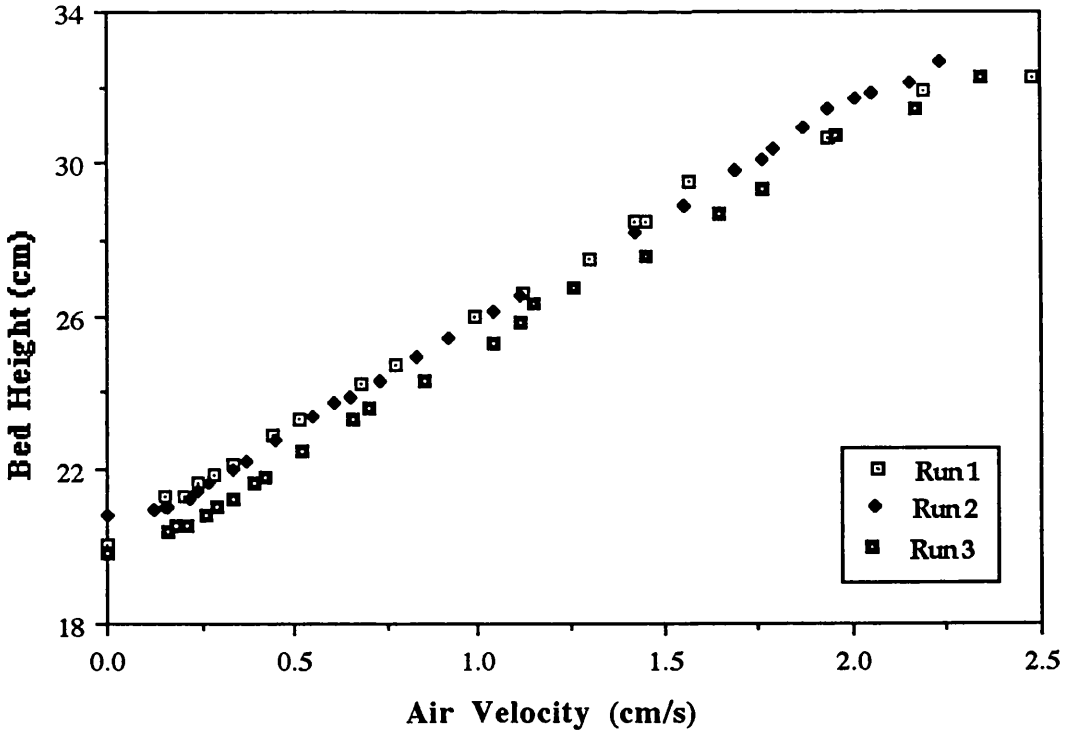

Fig. 4.3.18. Fluidization of silica with 15% CAB-O-SIL.

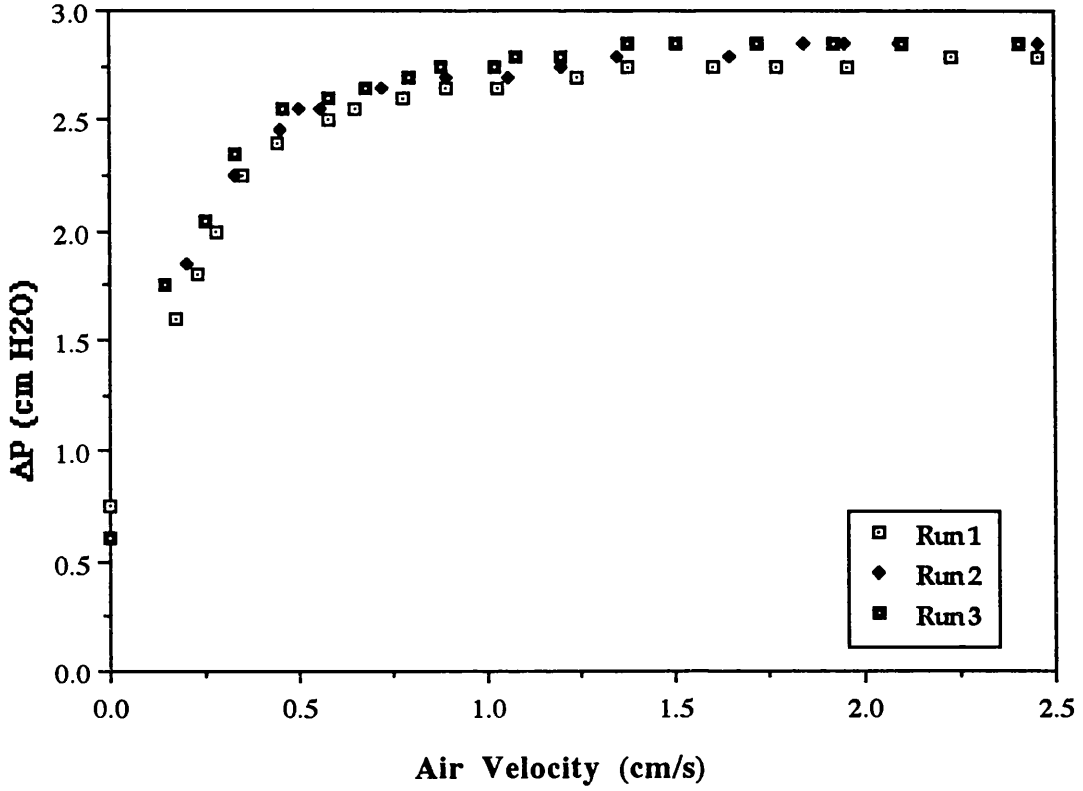

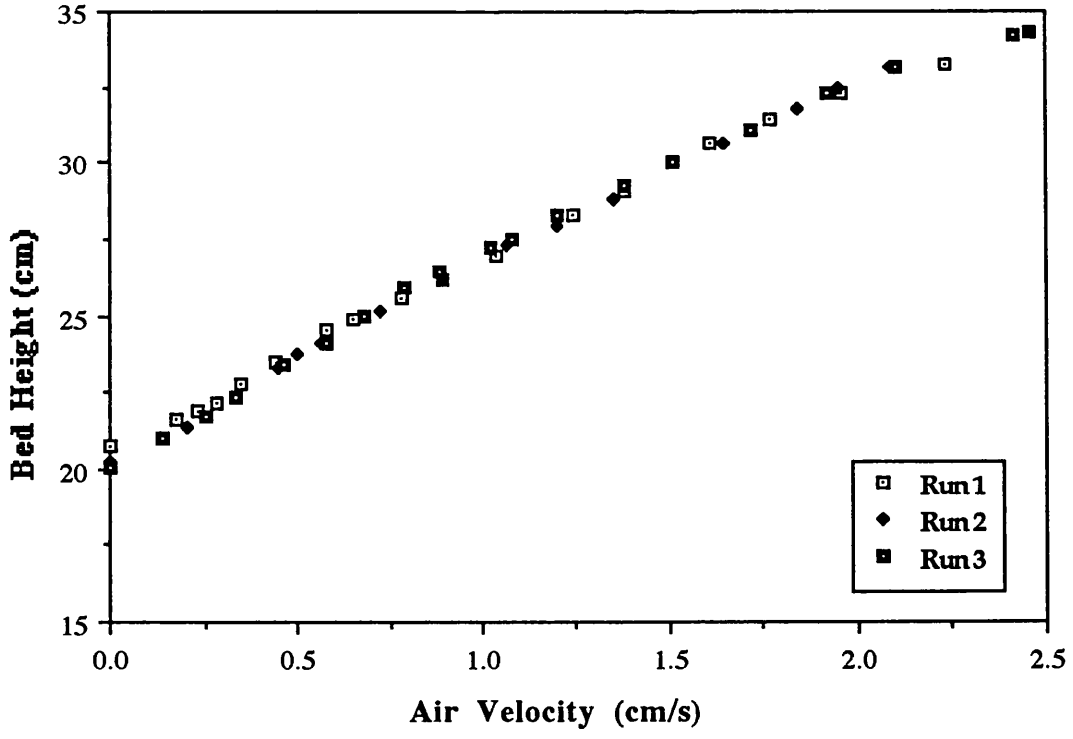

Table 4.3.3. Effect of addition of CAB–O–SIL on fluidization of Silica.

CAB–O–SIL (wt%)	Bed weight (g)	ε_{lp}	U_{mf} (cm/s)	H_{mf} (cm)	ε_{mf}	U_{mb} (cm/s)	H_{mb} (cm)	ε_{mb}	Bed Expansion (%)	Elutriation loss (%)
0	500	0.440	0.66	20.0	0.5567	1.15	21.9	0.5951	9.5	1.8
1	404	0.496	0.61	16.0	0.5527	0.95	17.6	0.5934	10	0.91
2.5	401	0.546	0.79	18.0	0.6047	1.4	20.1	0.646	12	0.38
5	300	0.592	0.58	16.5	0.6776	2.6	22.5	0.7636	36	≈ 0
10	300	0.659	0.25	21.5	0.7526	1.95	30.9	0.8278	44	≈ 0
15	250	0.705	0.27	22.05	0.7989	2.6	34.4	0.8711	56	≈ 0

Fig. 4.3.19. Effect of CAB-O-SIL on Umf and Umb of Silica.

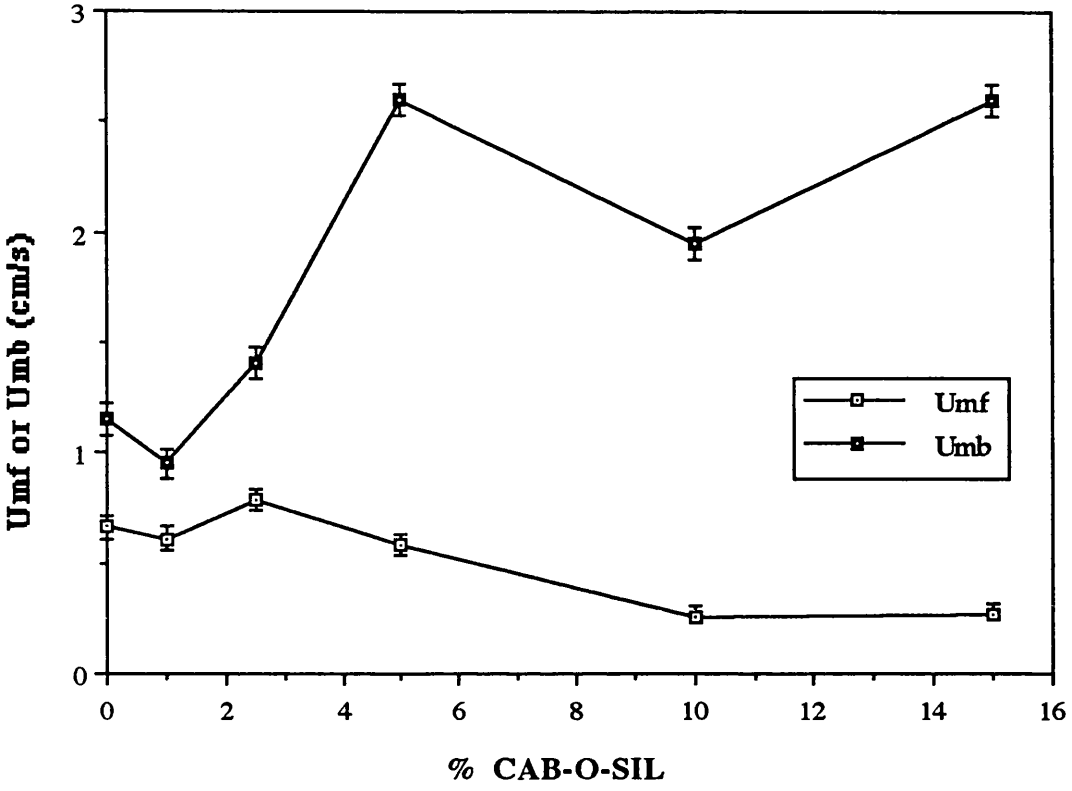

Fig. 4.3.20. Effect of CAB-O-SIL on the bed expansion of silica.

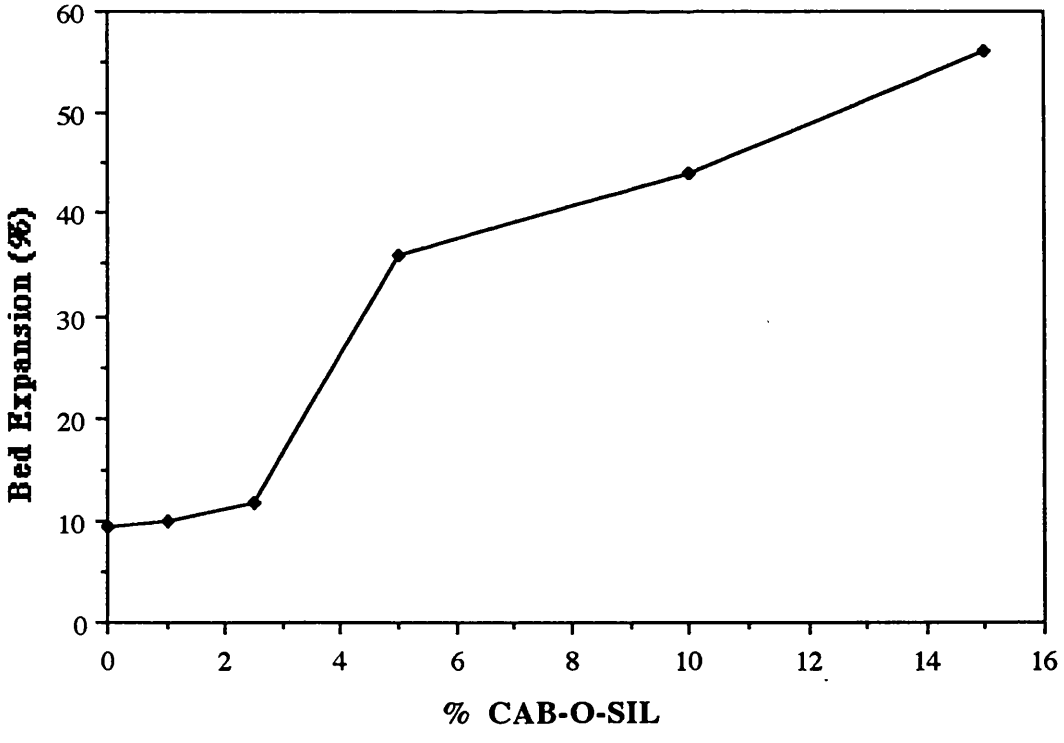

Fig. 4.3.21. Effect of CAB-O-SIL on the bed voidage of silica.

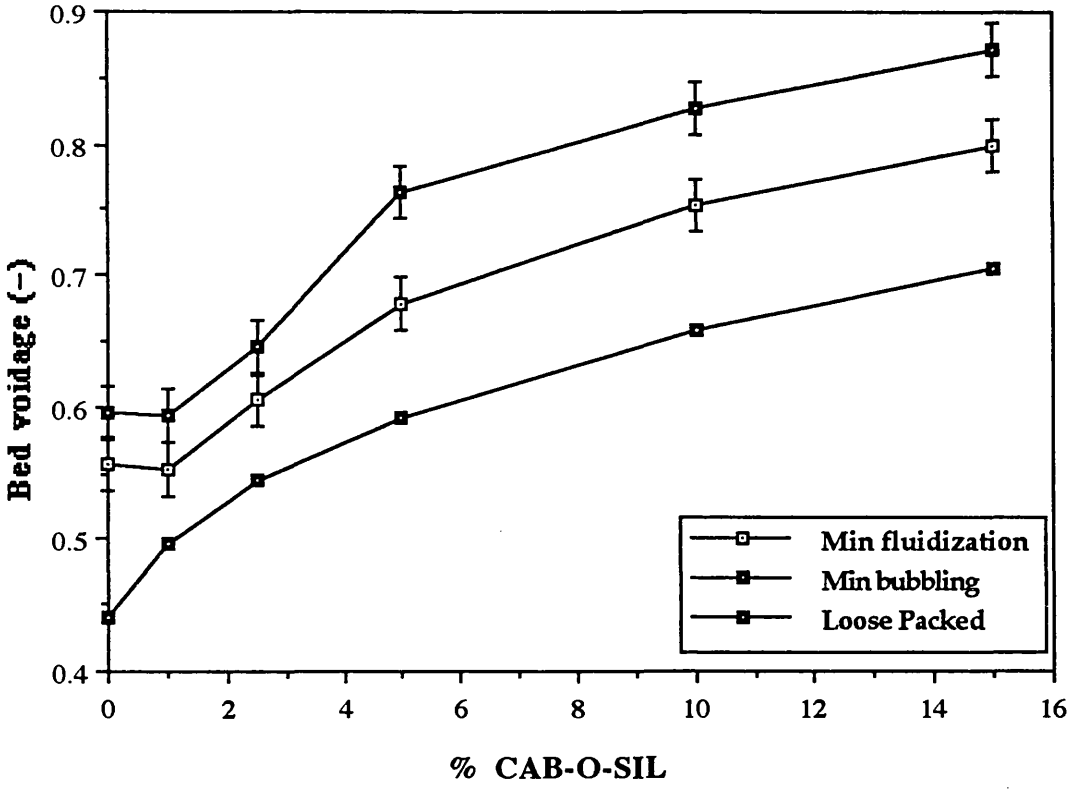

Fig. 4.3.22. Effect of CAB-O-SIL on the normalized pressure drop of silica.

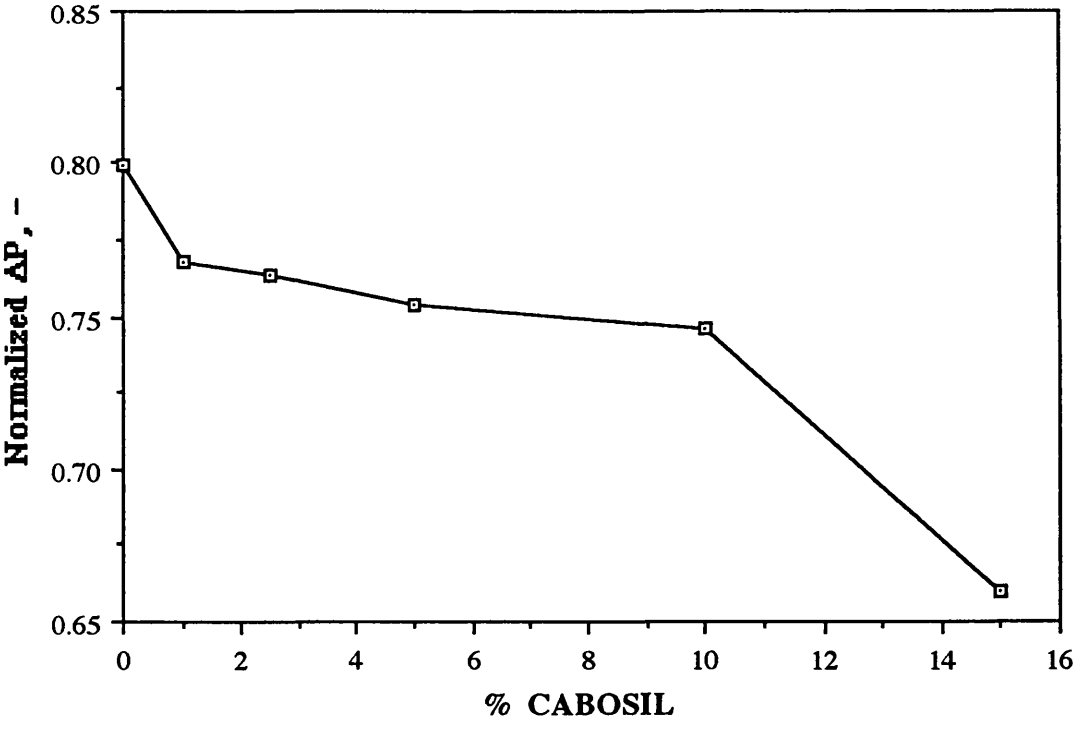

Table 4.3.4. Effect of CAB–O–SIL on the normalized poressure drop of silica mixtures.

CAB–O–SIL (wt%)	Ideal ΔP, Pa	Experimental ΔP, cm H2O	Experimental ΔP, Pa	Normalized ΔP
0	624.524	5.09	499.125	0.799
1	504.615	3.95	387.337	0.768
2.5	500.868	3.90	382.434	0.764
5	374.714	2.88	282.413	0.754
10	374.714	2.85	279.471	0.746
15	312.262	2.10	205.926	0.660

increase in the bed expansion due to the addition of ultrafines. An increase in bed expansion implied that more gas was present in the emulsion phase and resulted in improved gas/solid contact.

Ideal, experimental and normalized pressure drop of silica mixtures are given in Table 4.3.4 and Fig. 4.3.22 shows that addition of CAB–O–SIL to the bed, again decreased the normalized pressure drop which was an indication of increase in the cohesion of the bed.

4.3.5. Fluidization of Kiesel–1

Kiesel–1, with a mean particle size of 20 μm, did not fluidize well by itself, as expected from a Group C material. The powder lifted as a plug initially and then broke up completely and fell to the bottom of the bed. There was significant channelling in the bed and the elutriation loss was considerable. It was not possible to measure the height of the bed during the experiment since the powder tended to stick to the walls of the bed due to its cohesion. Consequently, the minimum fluidization velocity and/or bed expansion could not be determined.

Kiesel–1 was then fluidized with up to 5% hydrophil fumed silica in the 5 and 10 cm beds. It should be mentioned that the fluidization behaviour of the mixtures appeared to depend on the age of the blend. Fresh samples lifted as a plug and there was a lot of channelling without any significant pressure drop in the bed. But after a week, increasing the gas flow rate would result in an increase in the bed pressure drop. Considering that there was some unbalanced negative charges on fumed silica particles, the above mentioned change in the fluidization behaviour of the mixtures, could be the

result of formation and/or an increase in the existing electrostatic charges during mixing which would gradually leak during storage.

The characteristic curves of the fluidization experiments are shown in Figs. 4.3.23–4.3.32. It could be seen that the behaviour of the mixtures was dependent on the bed diameter as explained in section 4.3.1. While the fluidization of the 5% mixture involved severe channelling in the smaller rig (Fig. 4.3.27), the experiment was carried out with less problem in the bigger bed (Fig. 4.3.32) and a quite consistent value of 1.5 cm/s was obtained for the minimum fluidization velocity.* In general, the fluidization in the 5 cm bed involved more channelling and there was more scatter in the corresponding curves; therefore a consistent value for U_{mf} could not be obtained. The results of the fluidization in the 10 cm bed are summarized in Table 4.2.3.

During the experiments, the powder tended to stick to the walls of the bed and presented severe fluidization problems associated with Group C powders. Tapping the bed would result in an increase in the bed height and pressure drop which must be the result of filling or rearrangement of channels in the bed which allowed the gas to pass the bed more uniformly. It was normally difficult to see the top surface of the bed and therefore determine the minimum bubbling velocity visually. Although the characteristic curves showed a significant increase in the bed height with gas flow rate (up to three times the initial bed height) during the experiments, the expansion between U_{mf} and U_{mb} could not be obtained. Further experiments may be carried out using X–ray facilities to study the bed behaviour in more detail.

* This value seems to be very high and could be the result of the large scatter in the data points.

Fig. 4.3.23. Fluidization of kiesel–1 with 1% S1 fumed silica in the 5 cm bed.

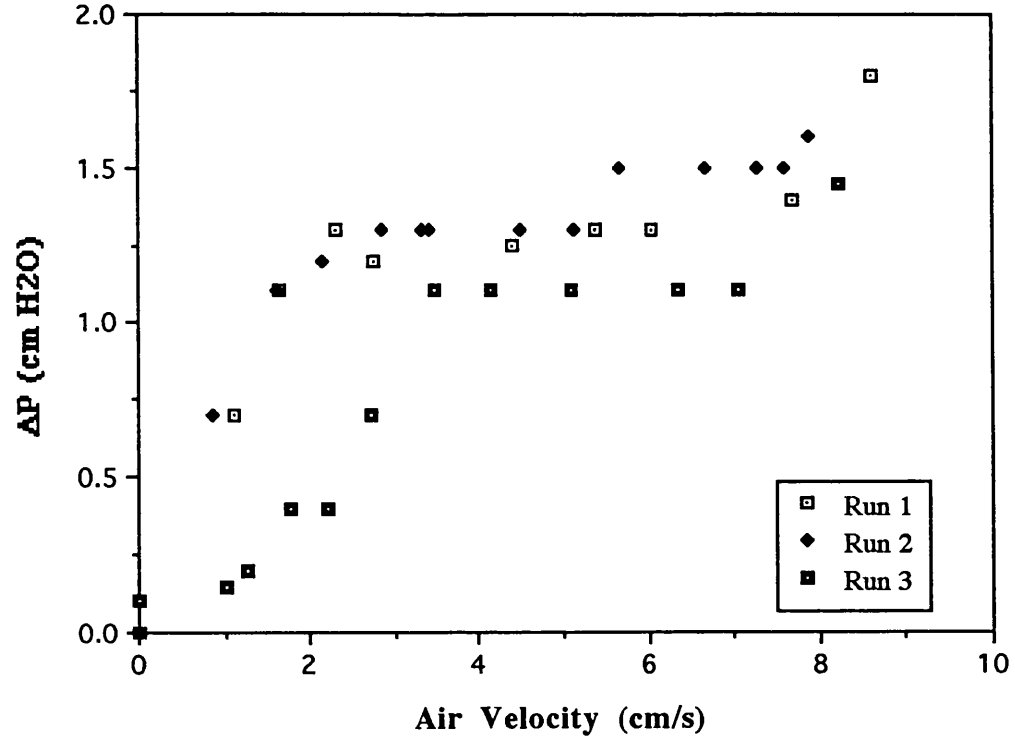

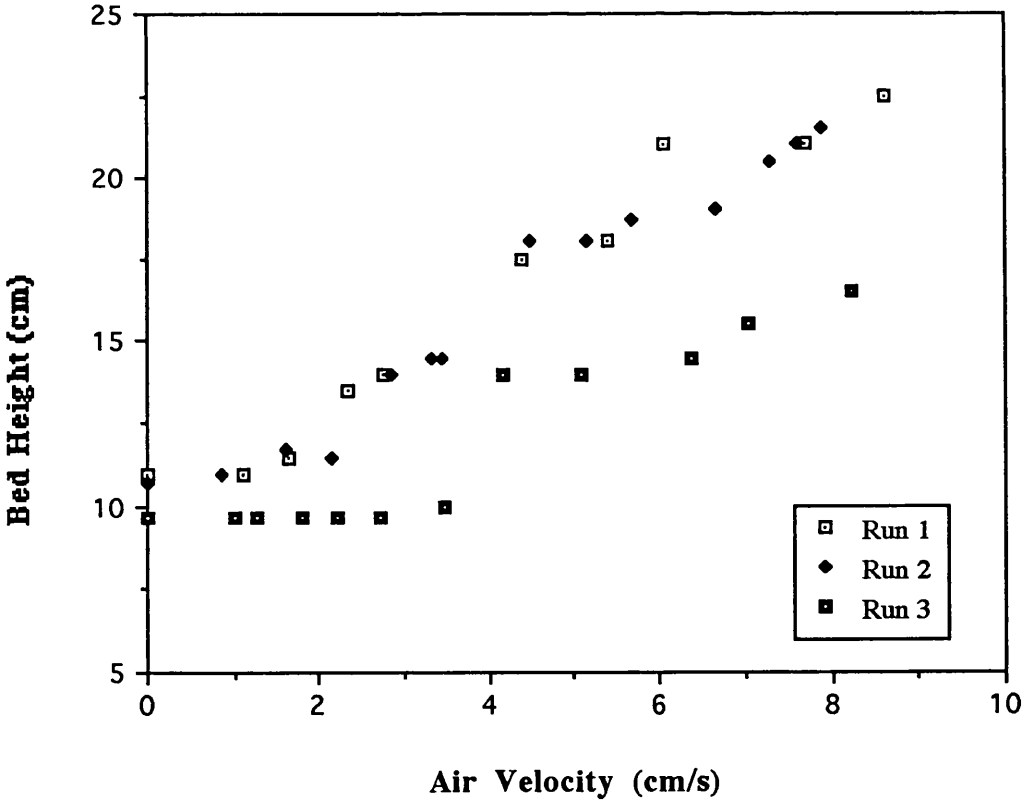

Fig. 4.3.24. Fluidization of kiesel–1 with 2% S1 fumed silica in the 5 cm bed.

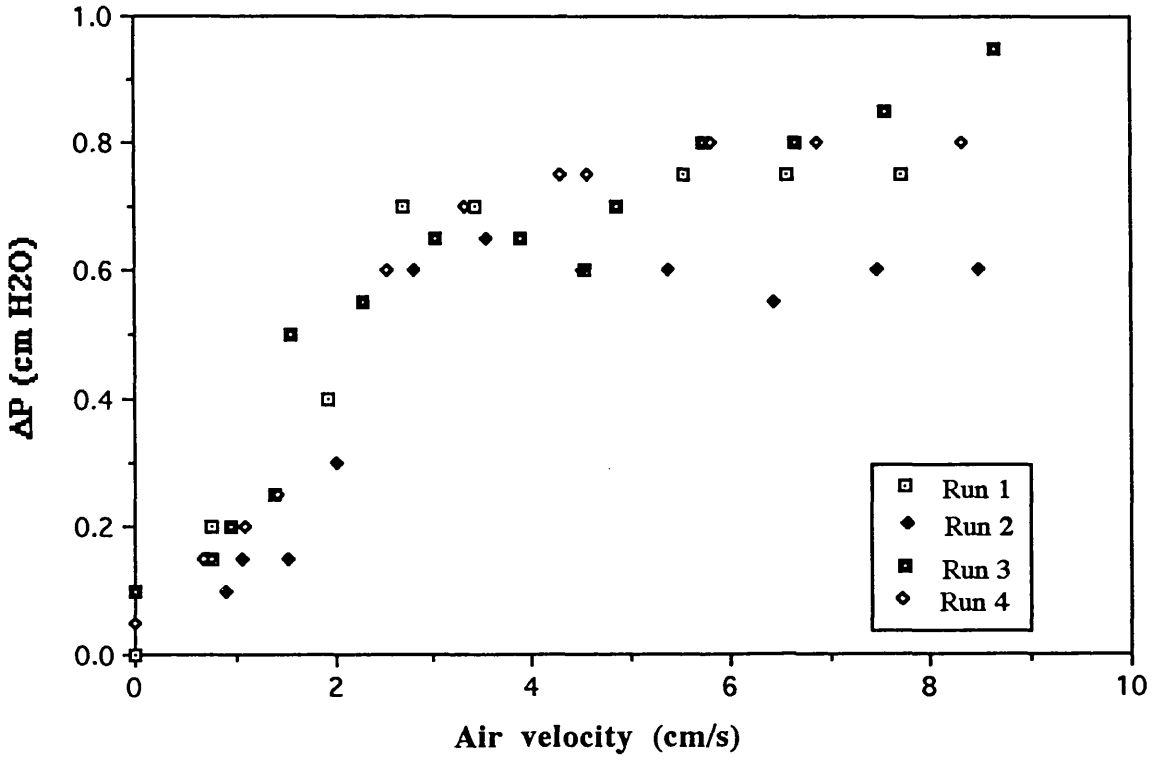

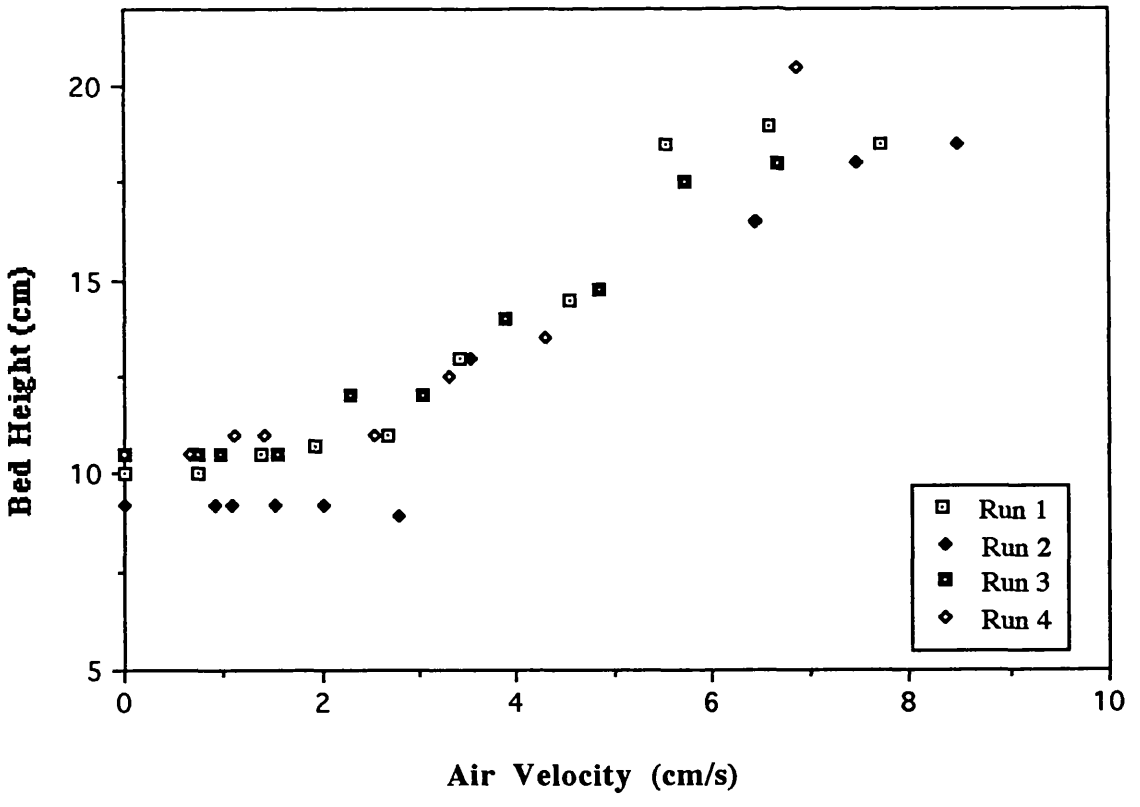

Fig. 4.3.25. Fluidization of kiesel–1 with 3% S1 fumed silica in the 5 cm bed.

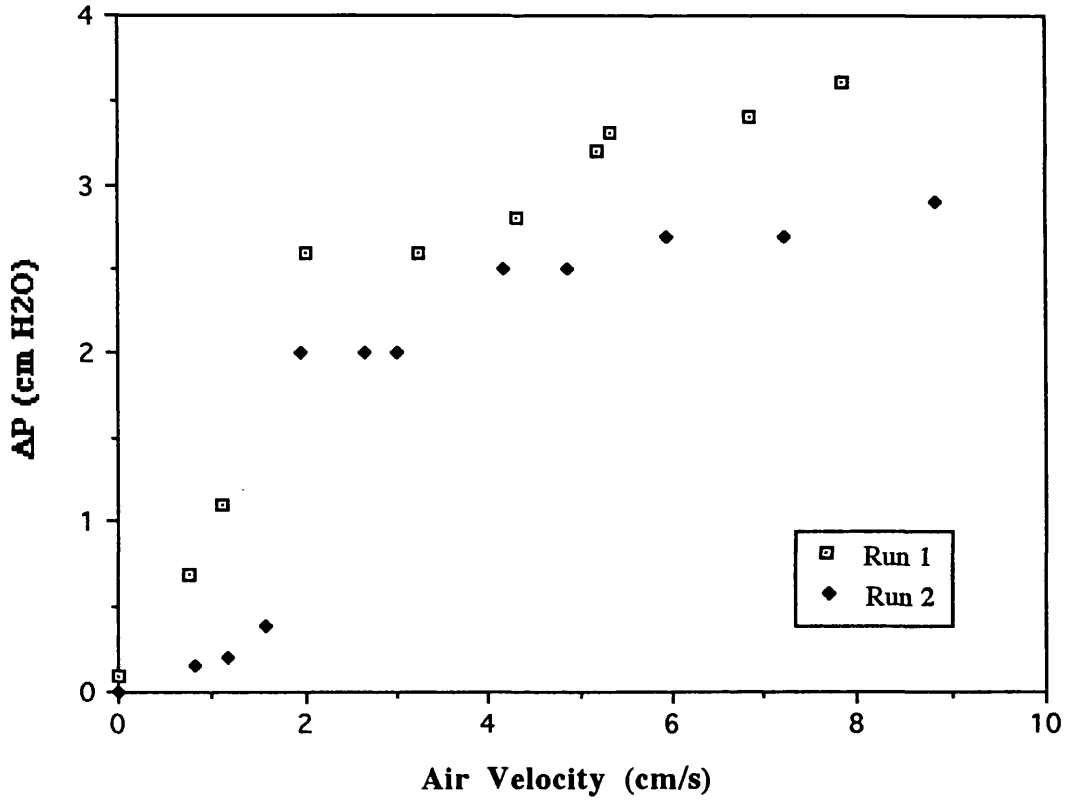

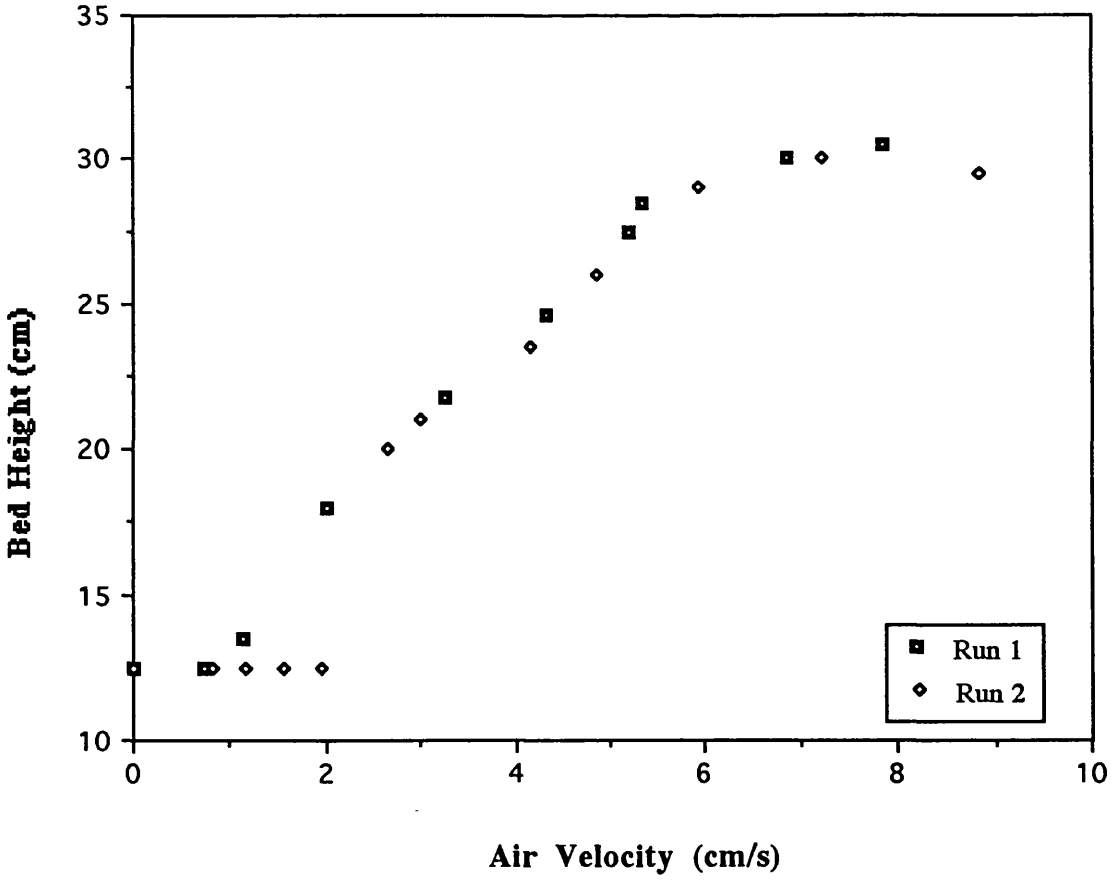

Fig. 4.3.26. Fluidization of kiesel–1 with 4% S1 fumed silica in the 5 cm bed.

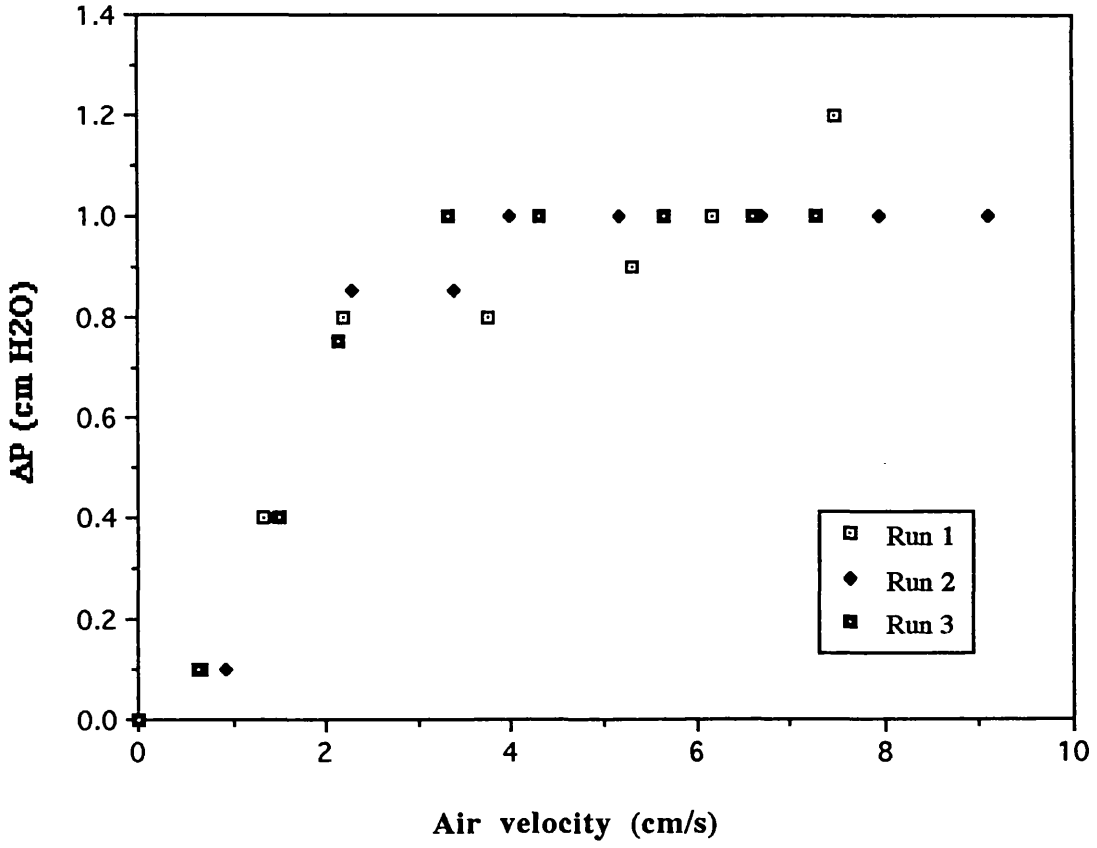

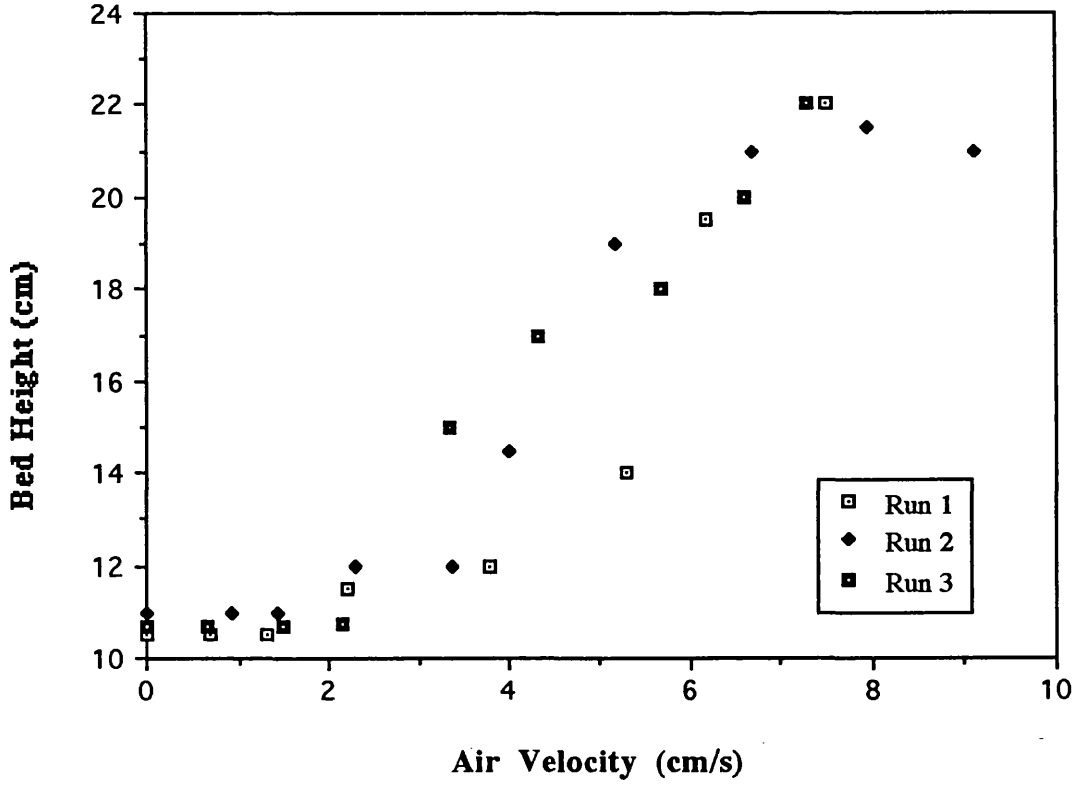

Fig. 4.3.27. Fluidization of kiesel–1 with 5% S1 fumed silica in the 5 cm bed.

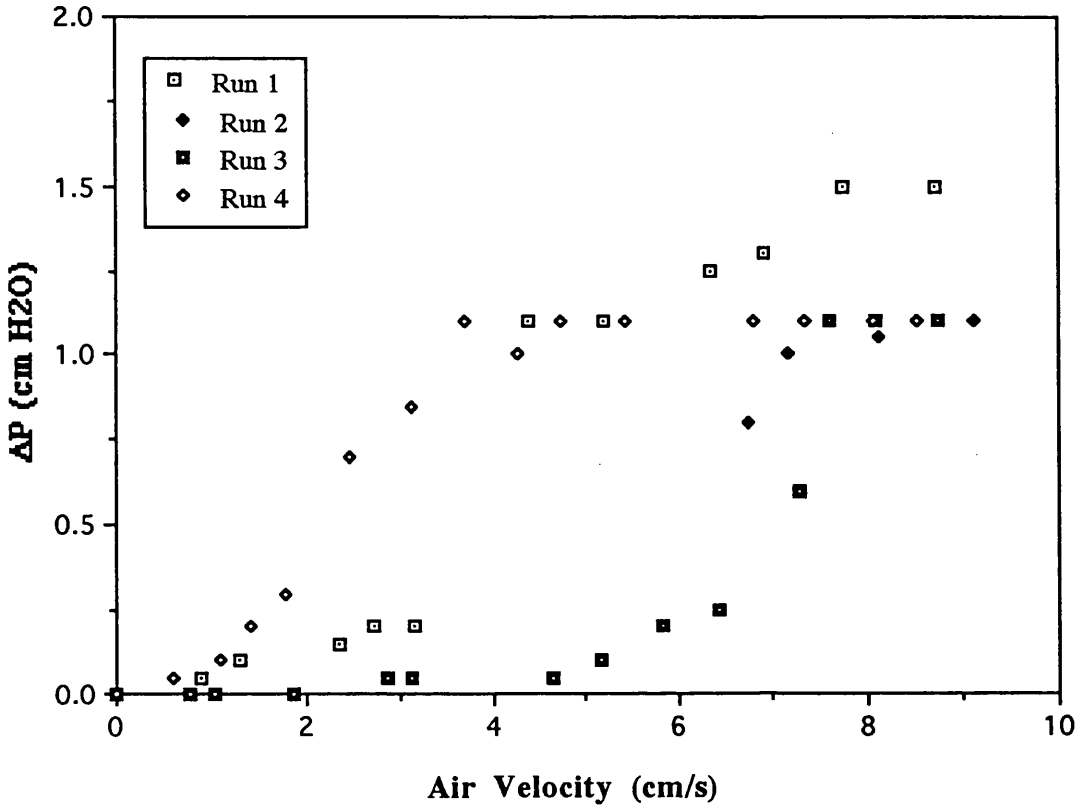

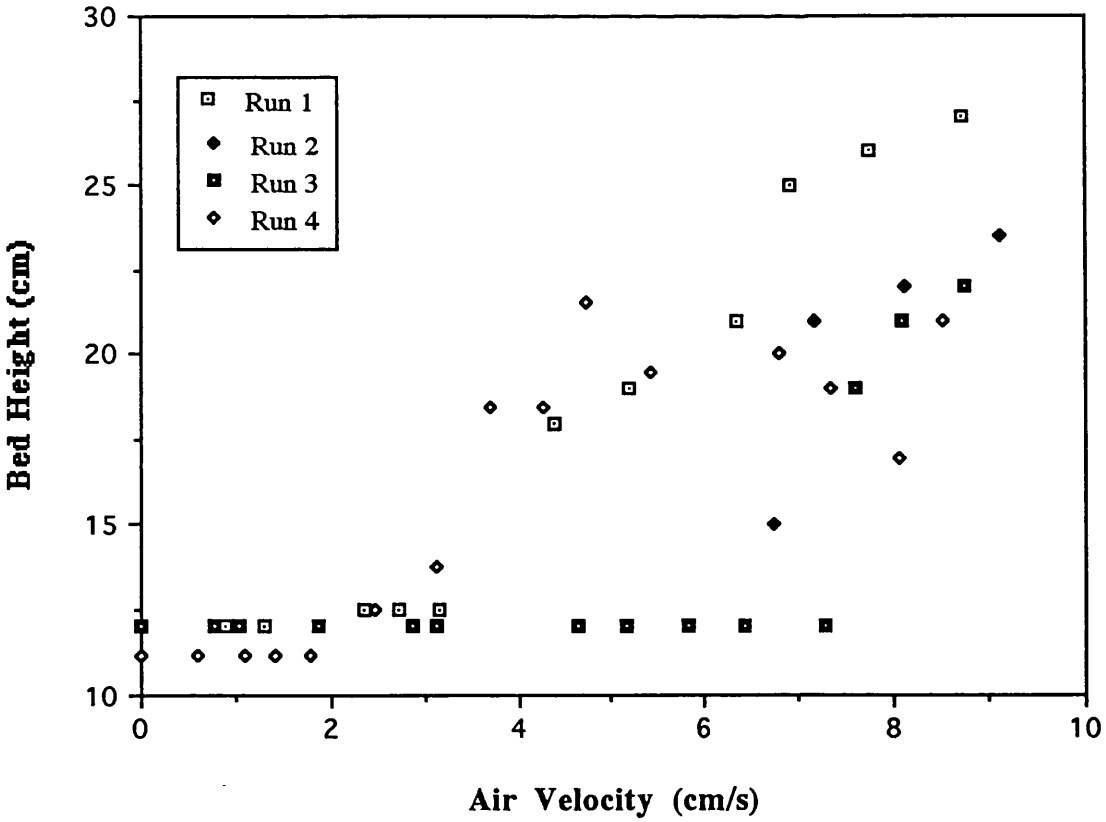

Fig. 4.3.28. Fluidization of kiesel–1 with 1% S1 fumed silica in the 10 cm bed.

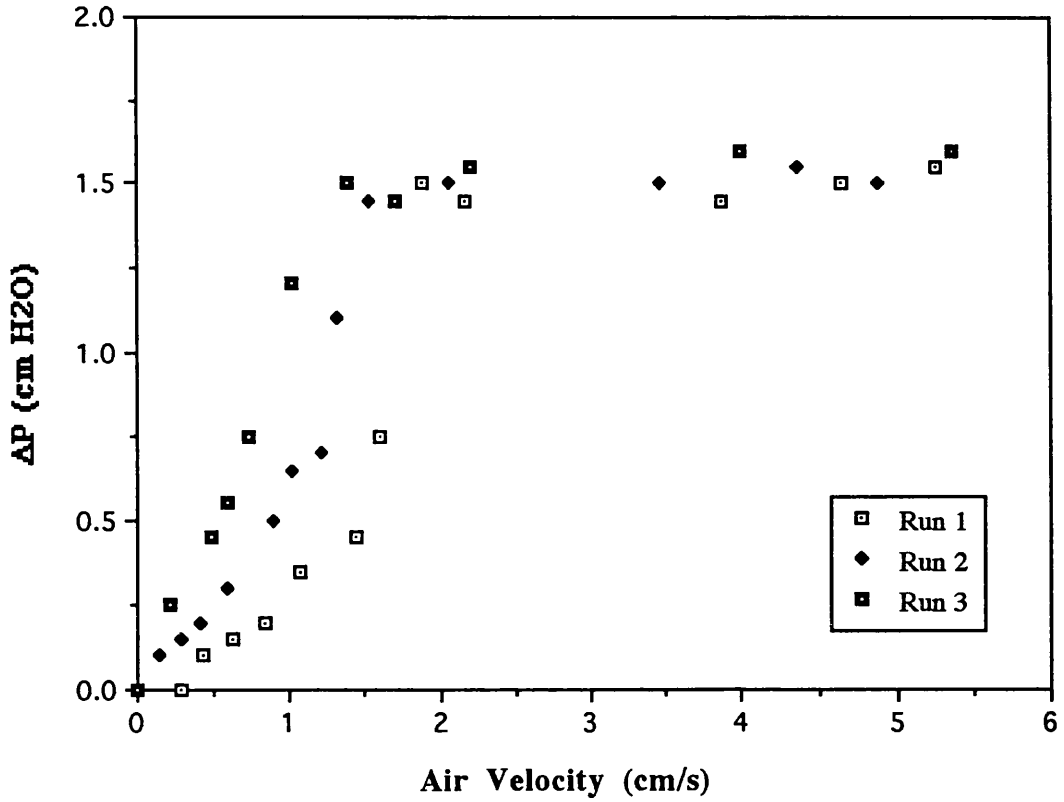

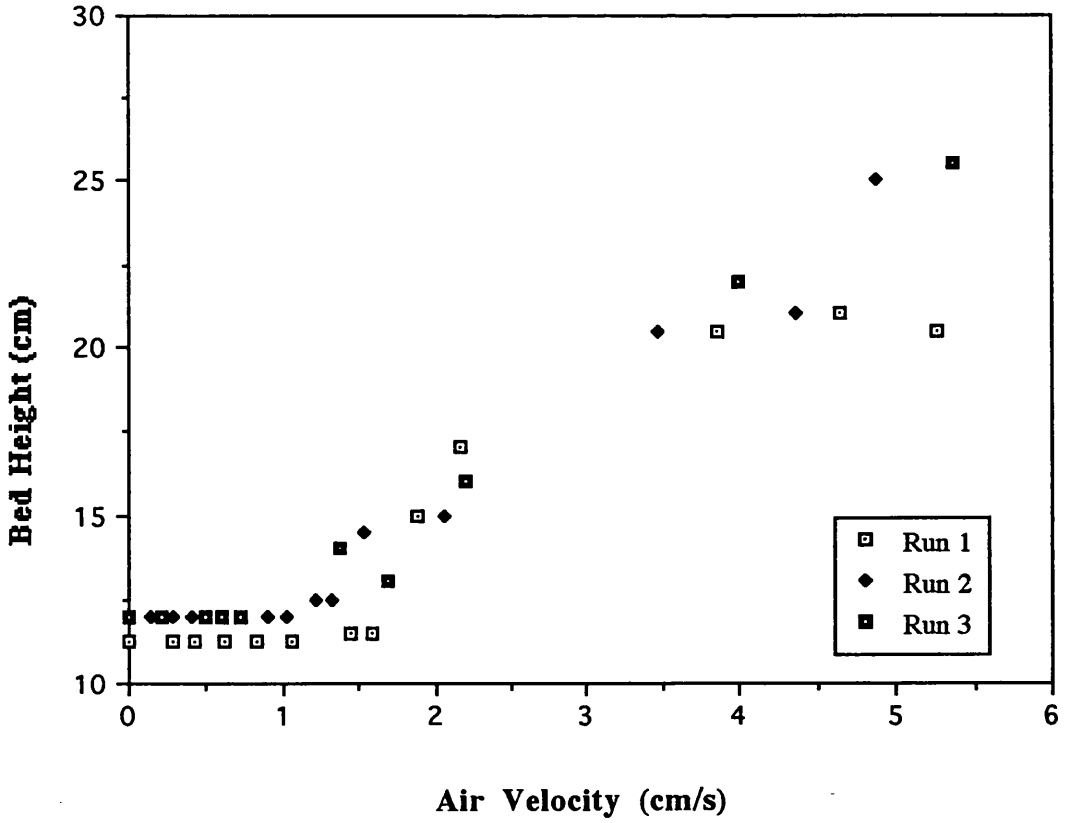

Fig. 4.3.29. Fluidization of kiesel–1 with 2% S1 fumed silica in the 10 cm bed.

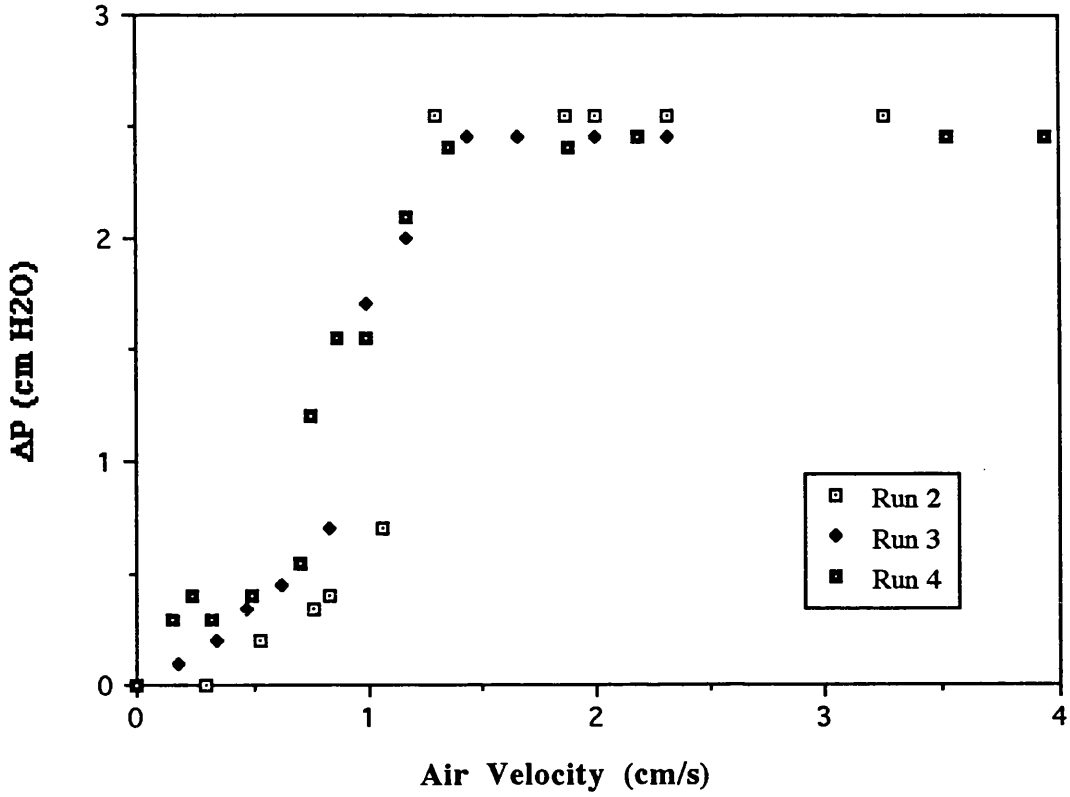

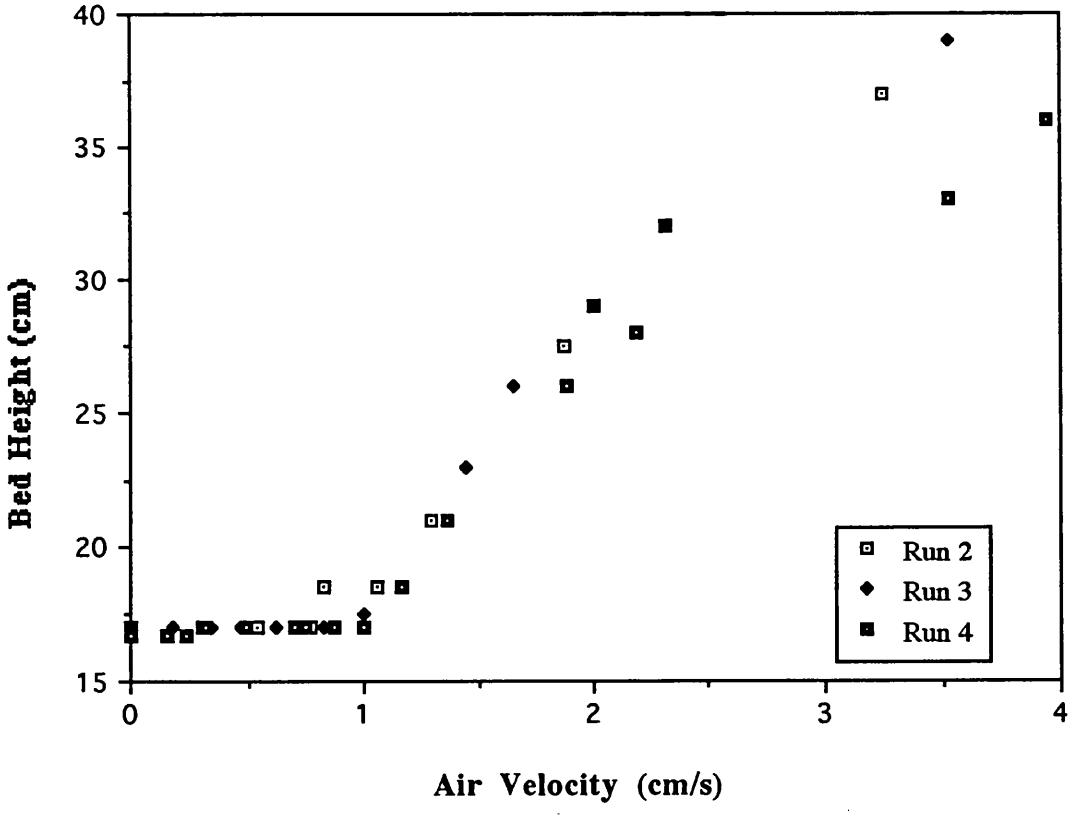

Fig. 4.3.30. Fluidization of kiesel–1 with 3% S1 fumed silica in the 10 cm bed.

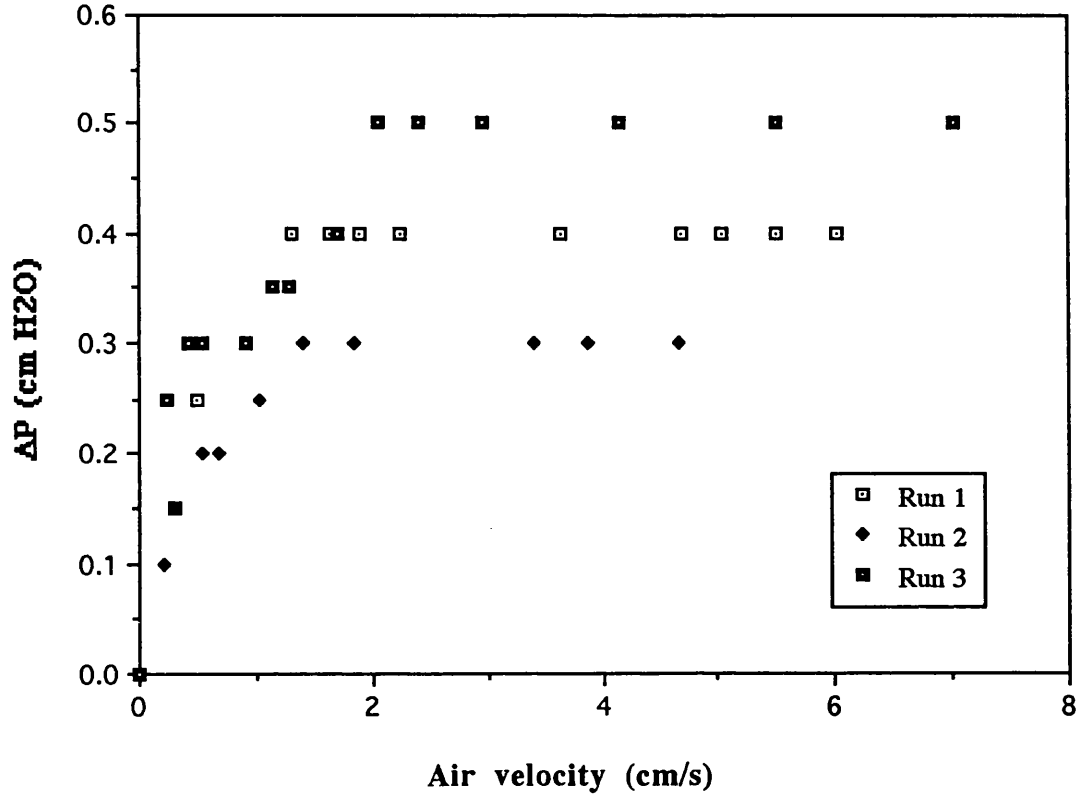

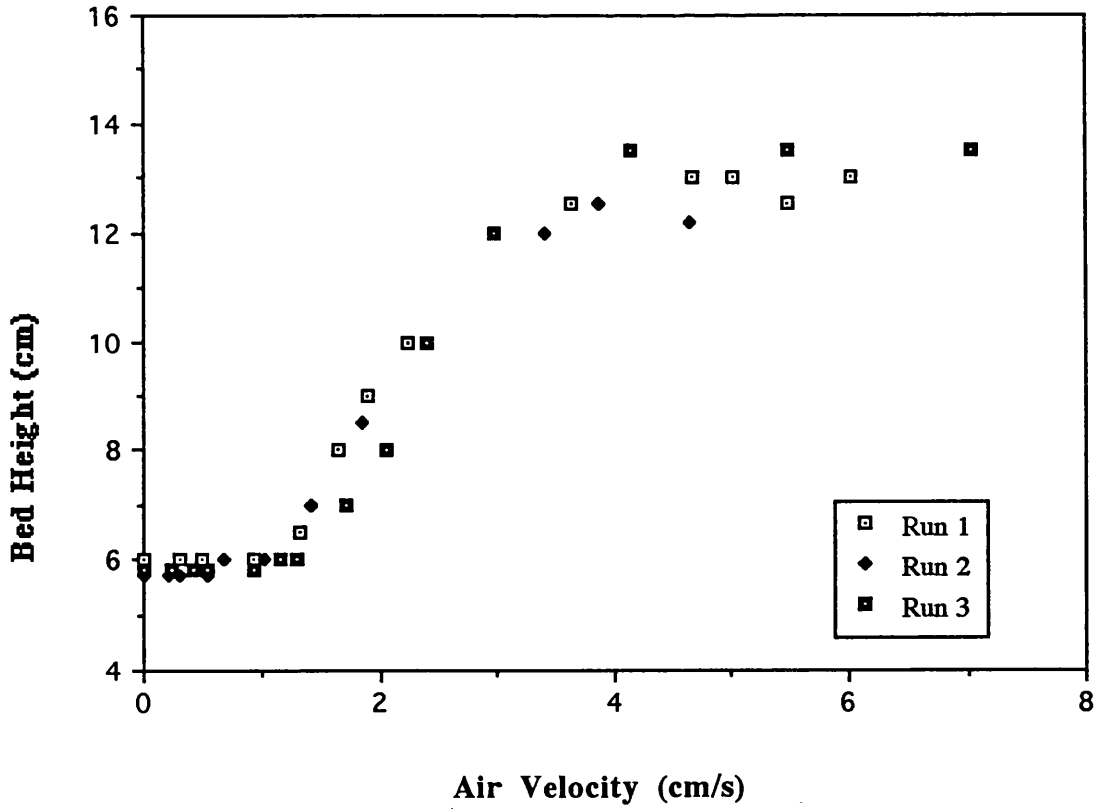

Fig. 4.3.31. Fluidization of kiesel–1 with 4% S1 fumed silica in the 10 cm rig.

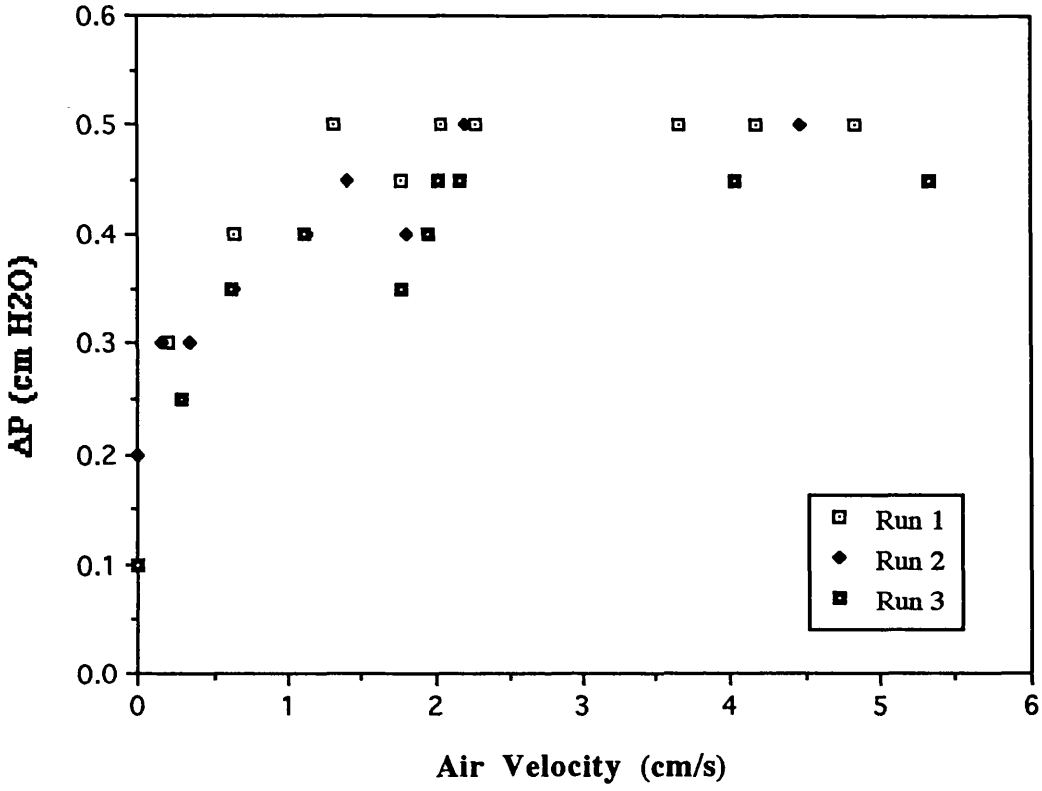

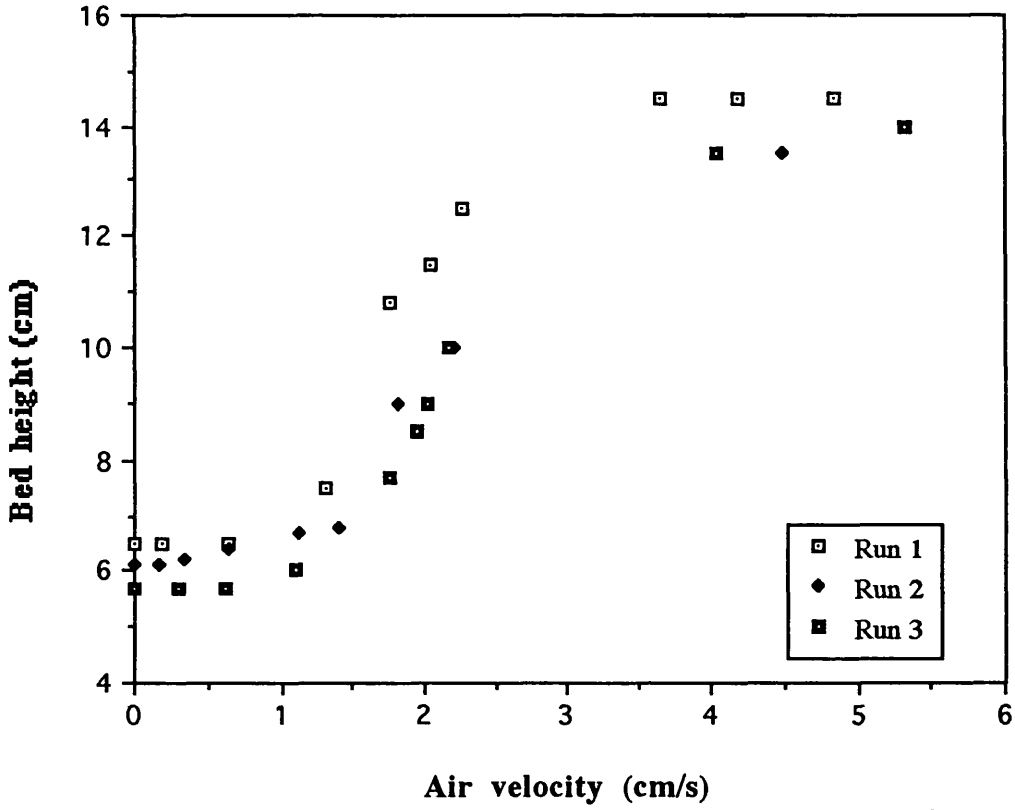

Fig. 4.3.32. Fluidization of kiesel-1 with 5% S1 fumed silica in the 10 cm bed.

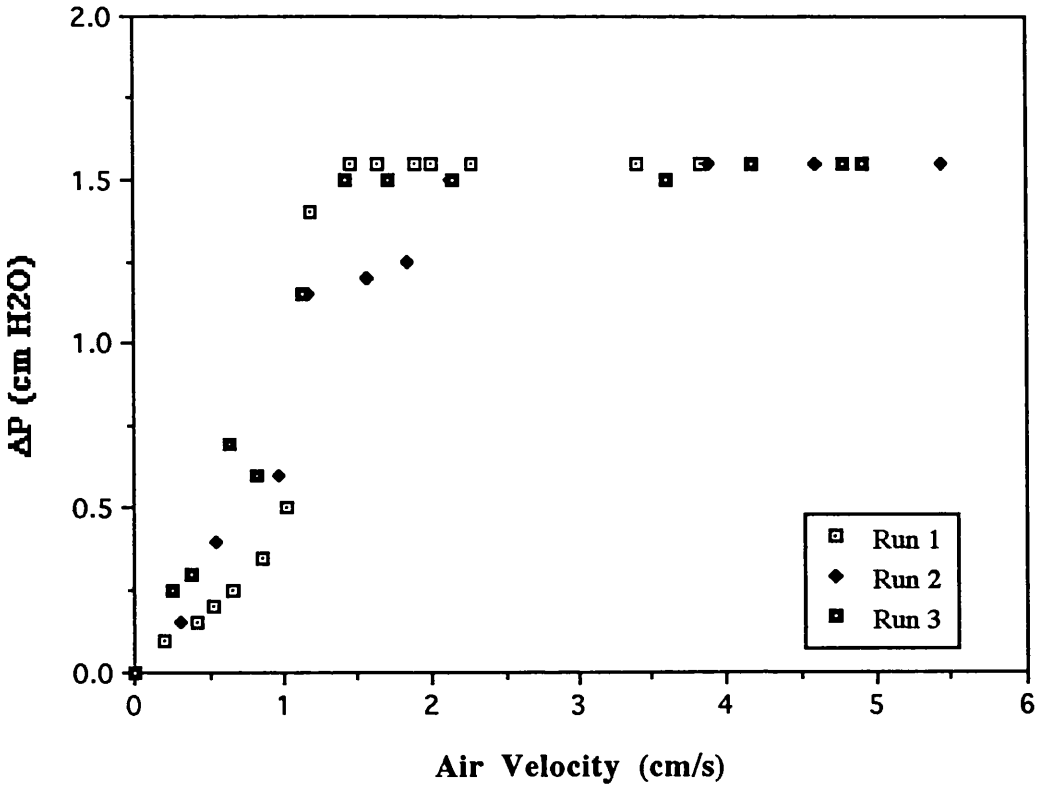

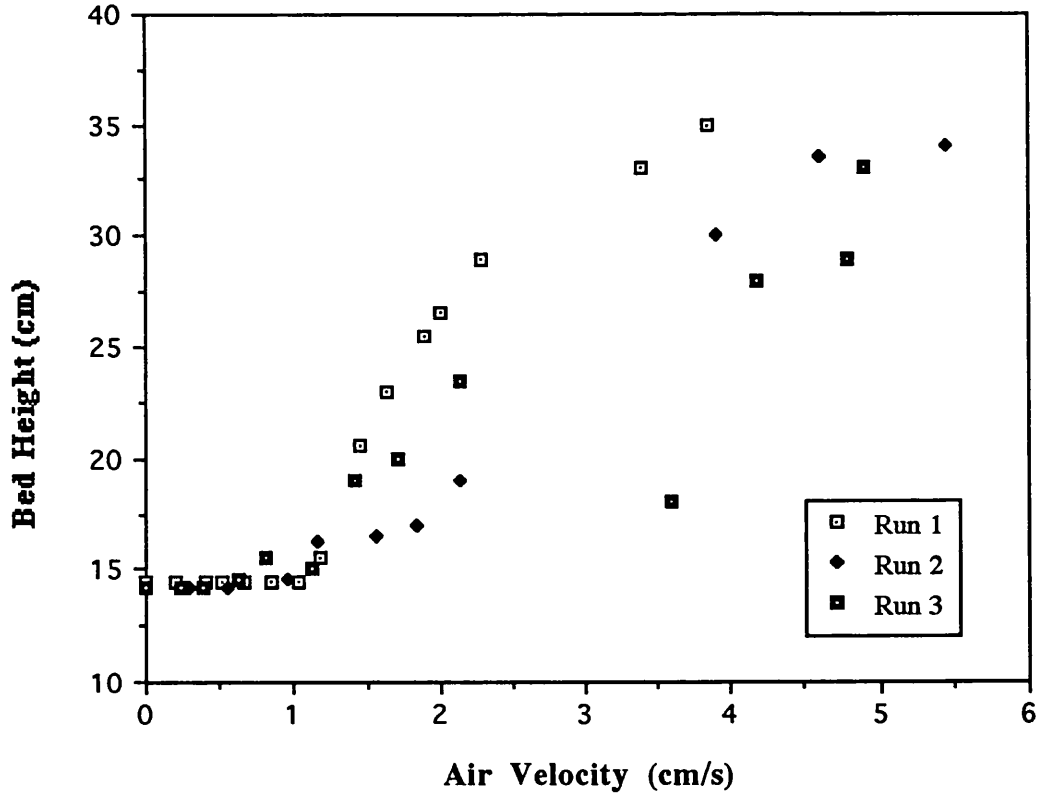

4.3.6. Fluidization of Kiesel–2

The fluidization of Kiesel–2, with a mean particle size of 30 μm, involved major channelling as expected for a Group C material which was similar to the kiesel–1. The results of the fluidization of kiesel–2 with up to 5% CAB–O–SIL in the 10 cm bed are shown in Figs. 4.3.33–4.3.37 and are summarized in Table 4.2.4. The experiments were highly reproducible for the 1% mixture (Fig. 4.3.33) and the U_{mf} was determined as 0.25 cm/s. Bubbling started near U_{mf} therefore the bed expansion between minimum fluidization and minimum bubbling velocities was negligible. The fluidization of the 2% sample involved some channelling (Fig. 4.3.34) but the U_{mf} was obtained as 0.6 cm/s. The experiment involved major channelling for the 3 and 4% mixtures (Figs. 4.3.35 and 4.3.36) while the 5% sample fluidized quite well (Fig. 4.3.37). The bed expanded very smoothly and the minimum fluidization velocity was found to be 0.44 cm/s. Bubbling began at 2.1 cm/s and the bed expansion between U_{mf} and U_{mb} was about 80% which was remarkable considering that neither kieselguhr nor CAB–O–SIL could individually be fluidized.

Comparing Tables 4.2.3 and 4.2.4 shows that there was a major difference between the fluidization behaviour of kiesel–1/S1 fumed silica and kiesel–2/CAB–O–SIL. Considering that both additives were hydrophil fumed silica with the same surface area and the host materials were kieselguhr, the dissimilarity in the systems must be due to different physical properties such as particle shape and density of the host material and ultrafines which provided an alternate particle network.

Fig. 4.3.33. Fluidization of kiesel-2 with 1% CAB-O-SIL in the 10 cm rig.

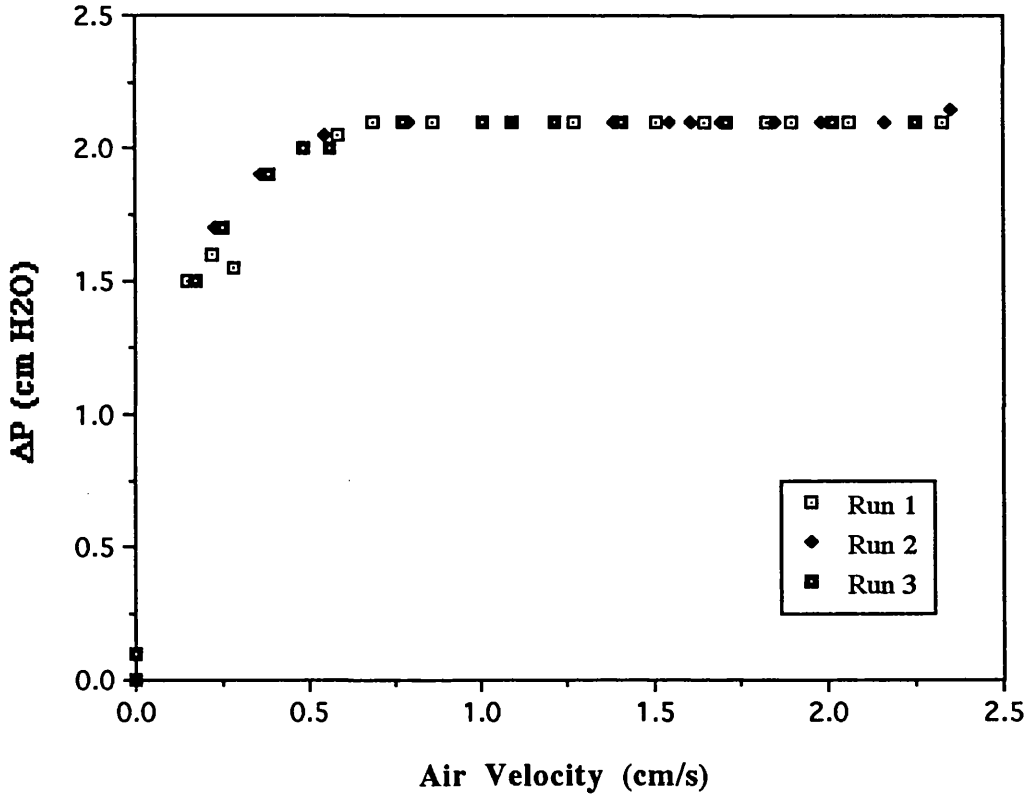

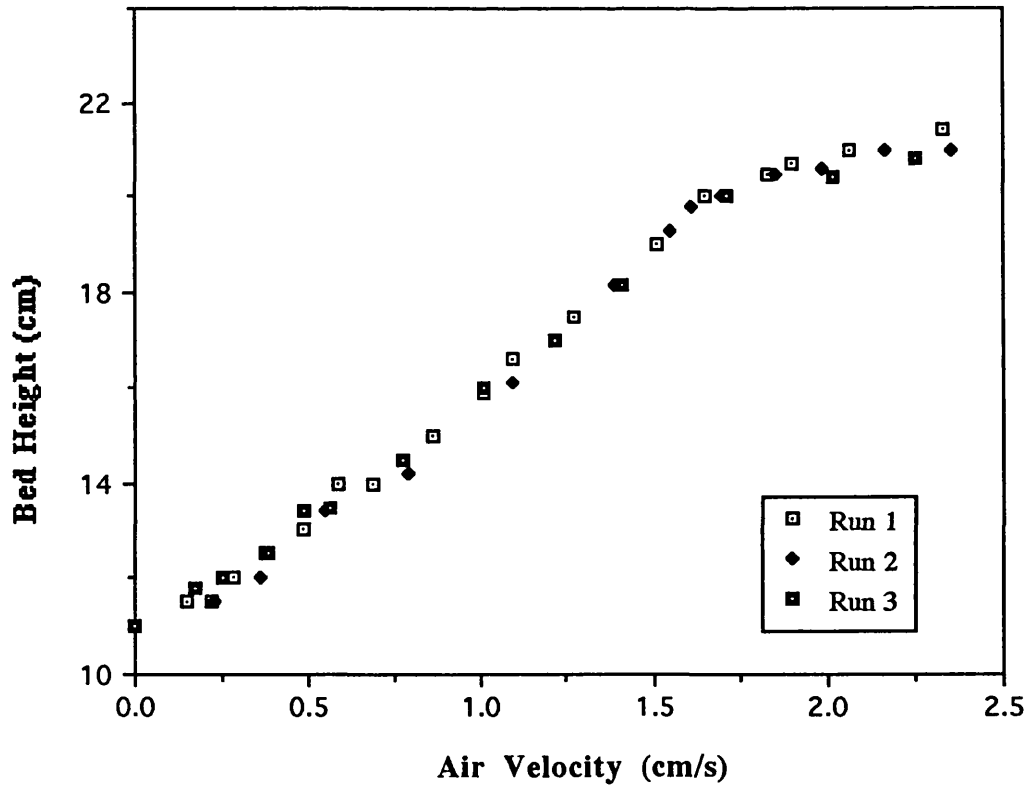

Fig. 4.3.34. Fluidization of kiesel–2 with 2% CAB-O-SIL in the 10 cm rig.

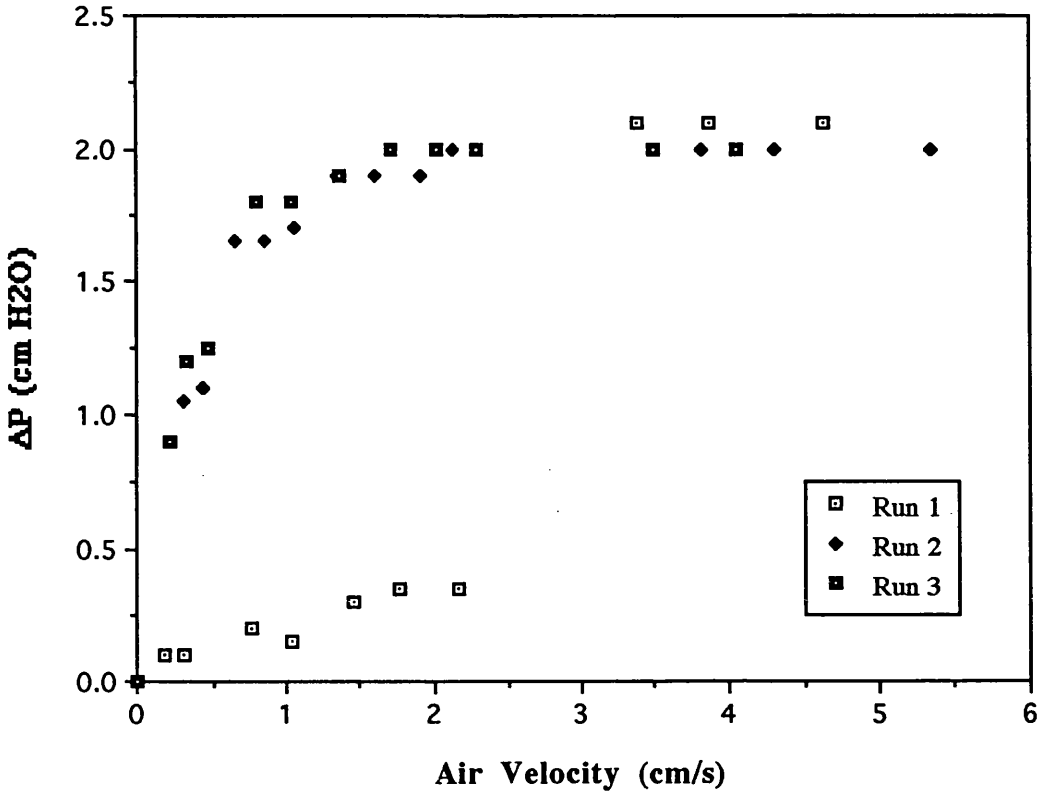

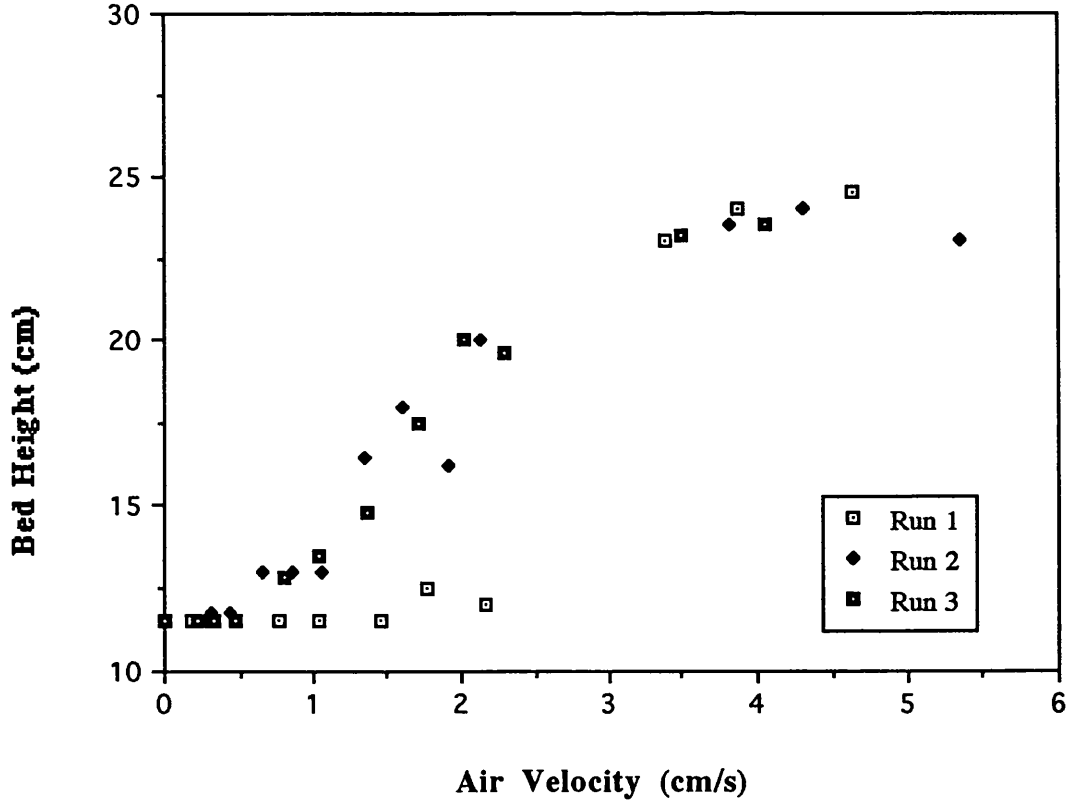

Fig. 4.3.35. Fluidization of kiesel–2 with 3% CAB-O-SIL in the 10 cm rig.

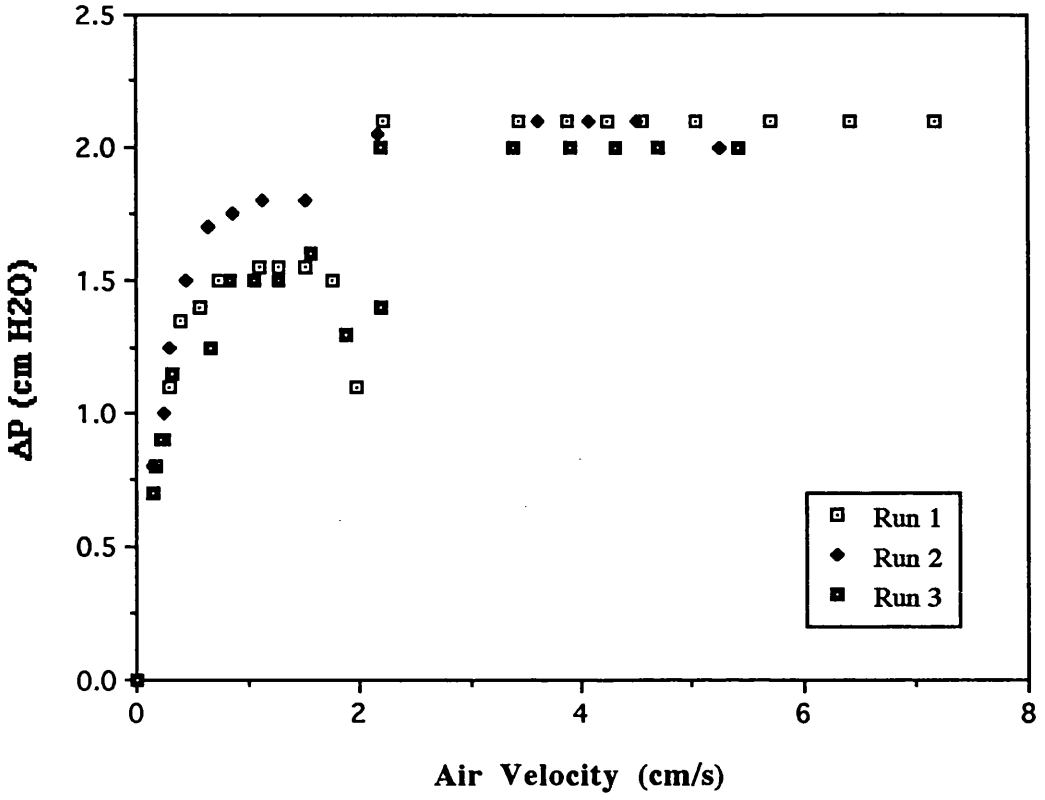

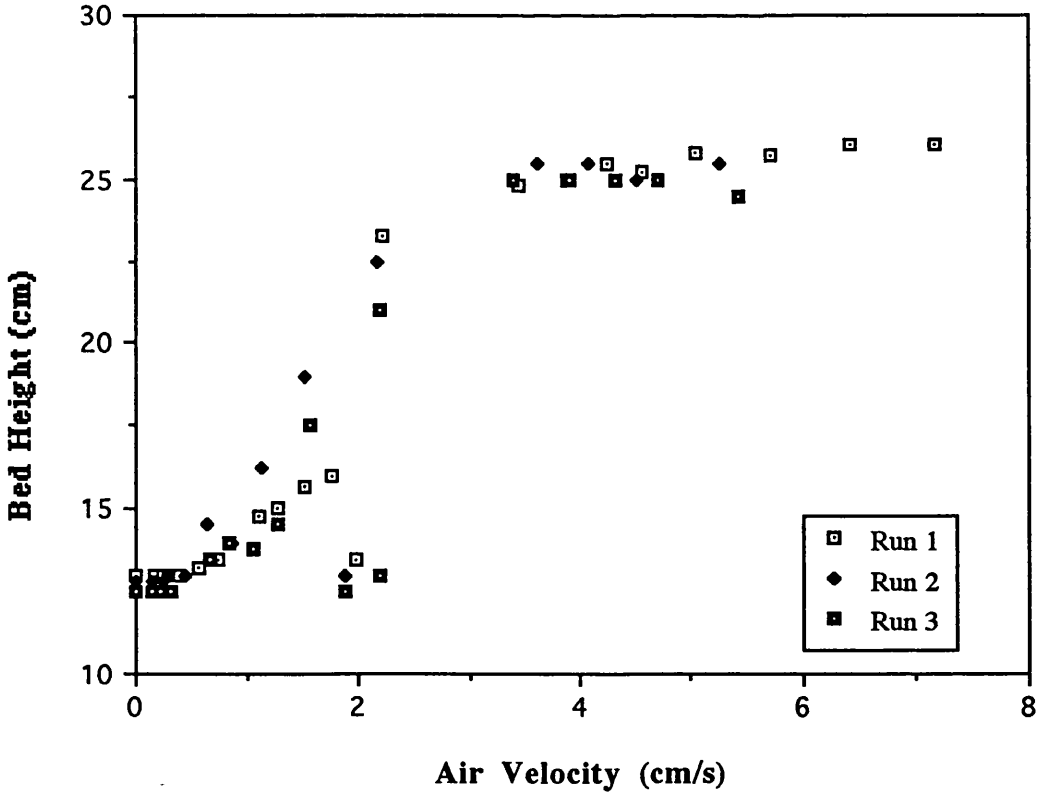

Fig. 4.3.36. Fluidization of kiesel–2 with 4% CAB-O-SIL in the 10 cm rig.

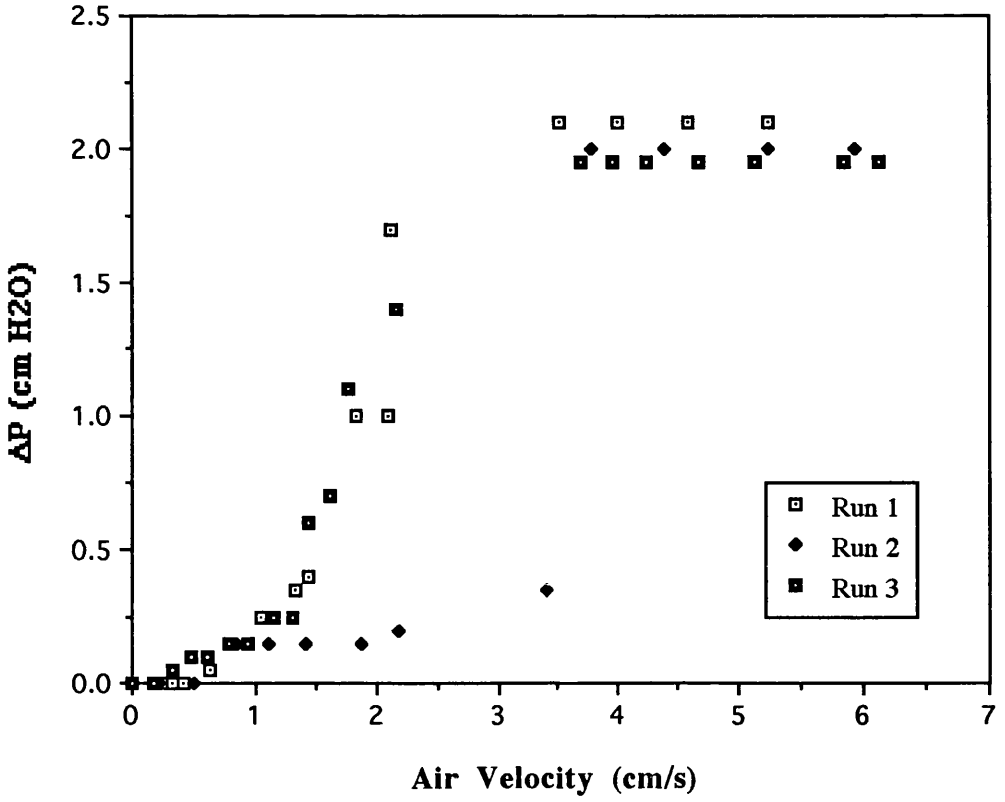

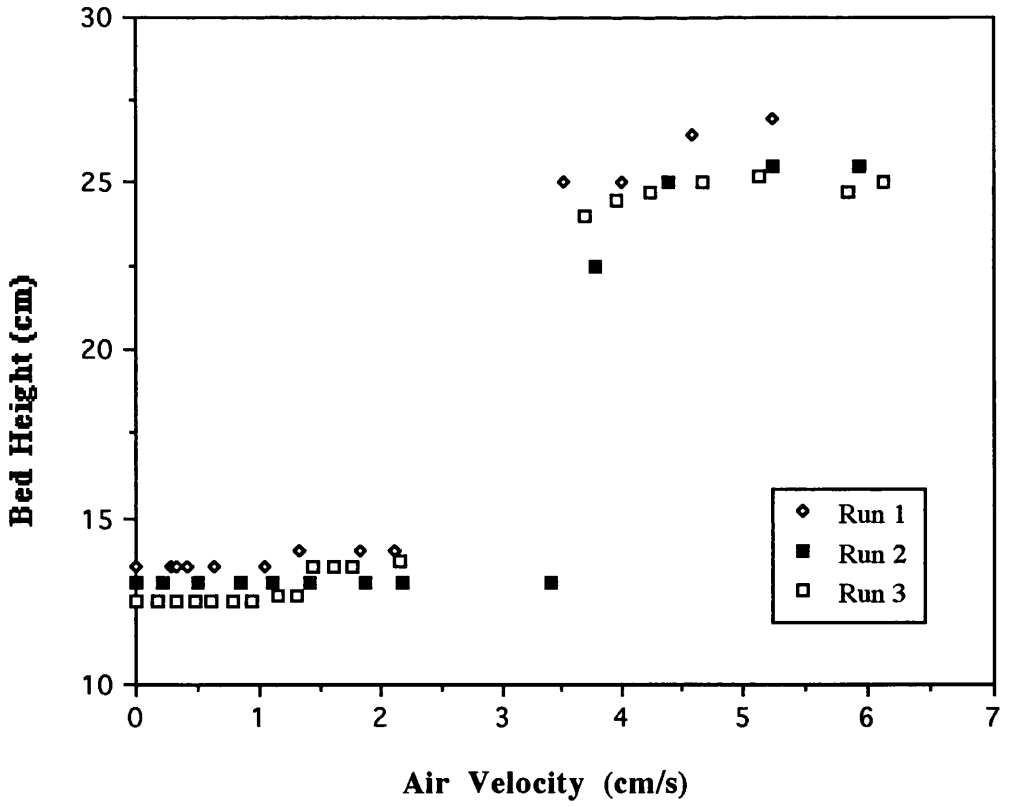

Fig 4.3.37. Fluidization of kiesel–2 with 5% CAB-O-SIL in the 10 cm rig.

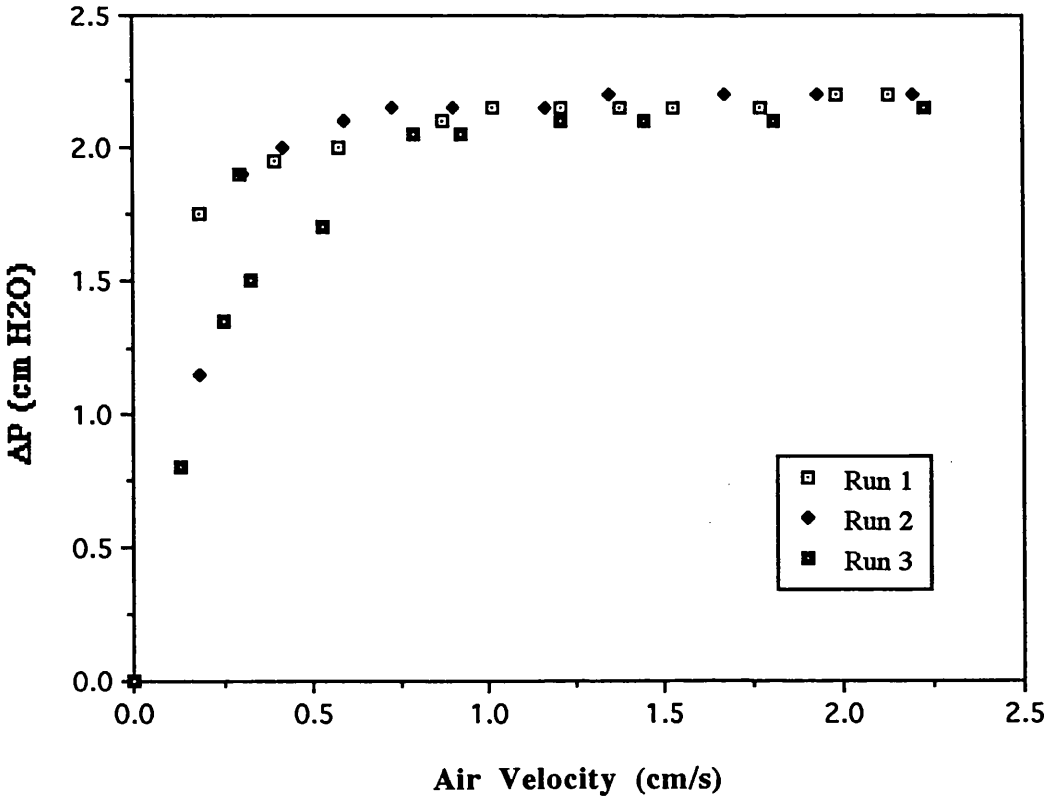

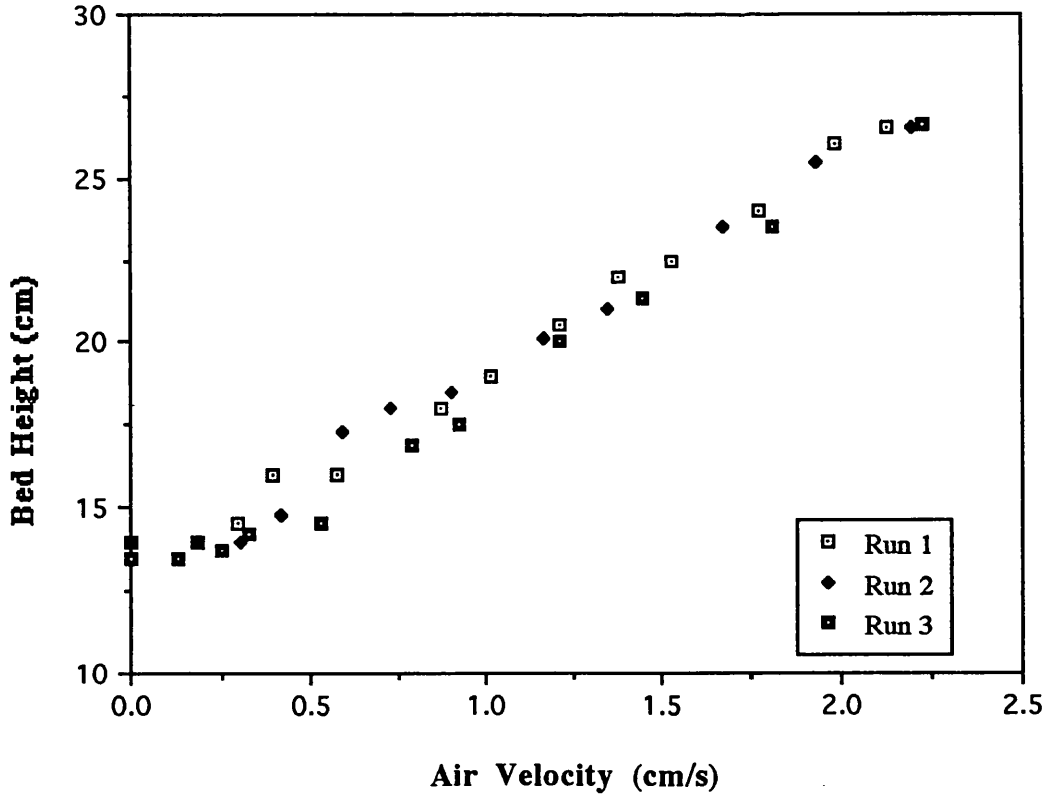

4.3.7. Discussions

The minimum fluidization velocity of FCC and silica blends decreased with addition of CAB–O–SIL to the bed. This was attributed to a decrease in the particle density of the host material as they were covered with additives. Addition of ultrafines resulted in the formation of a more porous bed structure which was more capable of holding the gas within itself and increased the U_{mb}. It should be noted that U_{mb} was always bigger than U_{mf}. Thus, a feature that is characteristic of Group A powders still remains even when they are mixed with a Group C powder.

Martin (1983) defined *delayed* bubbling as the amount of gas that travels through the interstices of the particles in excess of incipient fluidization. The degree of delayed bubbling depends on the powder cohesion and strength of interparticle forces. Therefore quantities such as U_{mb}–U_{mf} and the ratio of incipient bubbling to incipient fluidization U_{mb}/U_{mf} are important factors which should be considered in any complete study of fluidization. Since U_{mb} increased and U_{mf} decreased with addition of ultrafines, there was an increase in the excess interstitial gas flow (Figs. 4.3.38 and 4.3.39) which allowed the bed to expand further prior to the onset of bubbling and gave rise to the large bed expansions. This is extremely advantageous in achieving better gas–solid contact.

Considering that U_{mf} decreases with the bed diameter up to a limit (Rowe and Everett, 1972), the effect is more pronounced in larger columns providing that U_{mb} does not change with the bed size. Figs 4.3.38 and 4.3.39 show that CAB–O–SIL increased U_{mb}/U_{mf} by a factor of about 9 for FCC and silica blends. Therefore 9 times as much gas could pass through the emulsion phase before the onset of bubbling.

Normalized pressure drop increased in the bed which was an indication of an increase in the bed cohesion. This was not unexpected since ultrafines were cohesive Group C particles which would impart cohesion to the blend. However, as the concentration of ultrafines increases in the bed, a critical limit would be reached where the blend becomes too cohesive to show favourable fluidization behaviour. Geldart and Wong (1987) reported that addition of a Group C powder improved the entrainment rate of a Group A but above 30% addition the blend showed Group C behaviour . This confirms the existence of an optimum limit where effective coverage of the host material is reached and further addition of ultrafines could reverse the desirable effects.

Experiments carried out on ballotini in beds of 5 and 10 cm showed that the U_{mf} was a function of bed diameter in that range. This effect was also observed in fluidization of kiesel–1 blends. Fluidization of kiesel–1 with 5% S1 fumed silica in the 5 cm bed involved major channelling, however, the experiment was carried out normally and U_{mf} could be determined.

Kieselguhr with different shapes demonstrated dissimilar fluidization behaviour which suggested that particle shape of the host material was an important factor as it would affect the network formed by ultrafines and host particles.

The maximum flow rate for all the experiments was $3U_{mb}$. Minimum bubbling velocity increased with ultrafine concentration. Therefore the maximum gas flow rate increased with mass fraction of CAB–O–SIL. Yet the elutriation loss decreased in the bed which was supported by increase in cohesion and the formation of a particular bed structure which kept the particles together and resisted their departure from the bed.

Fig. 4.3.38. Effect of CAB-O-SIL on delayed bubbling of FCC.

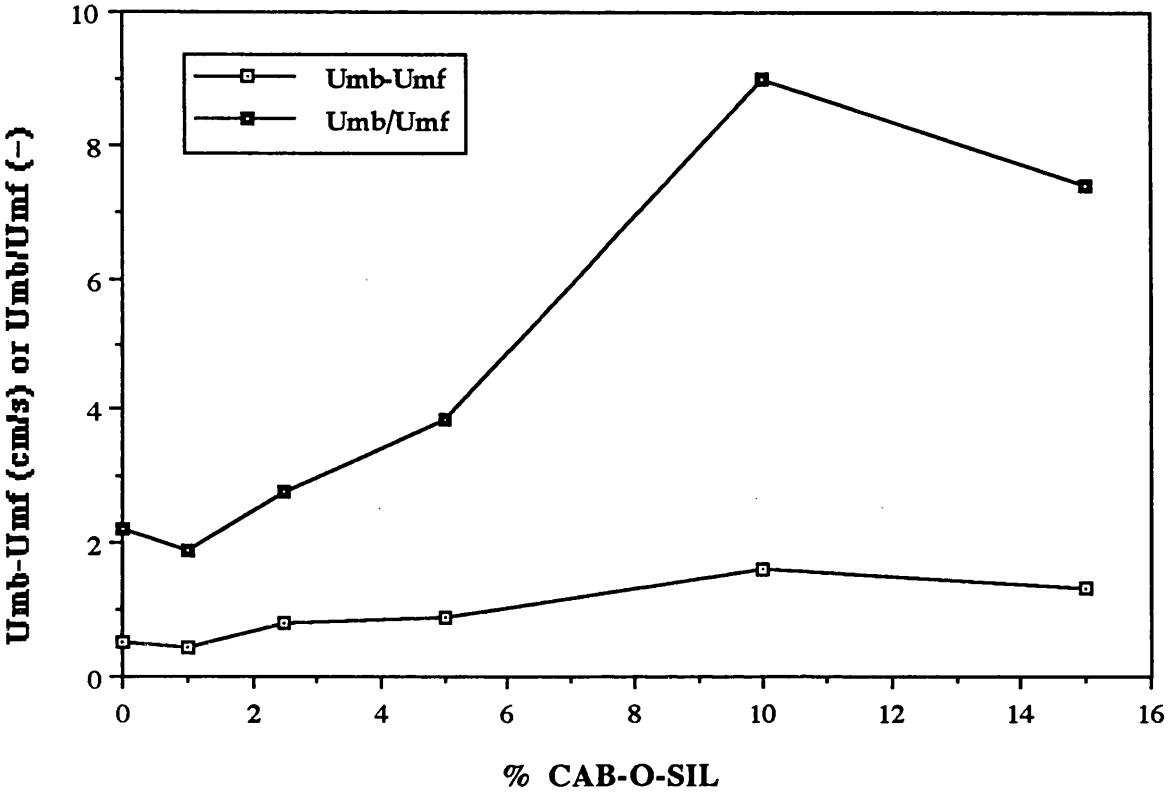

Fig. 4.3.39. Effect of CAB-O-SIL on delayed bubbling of silica.

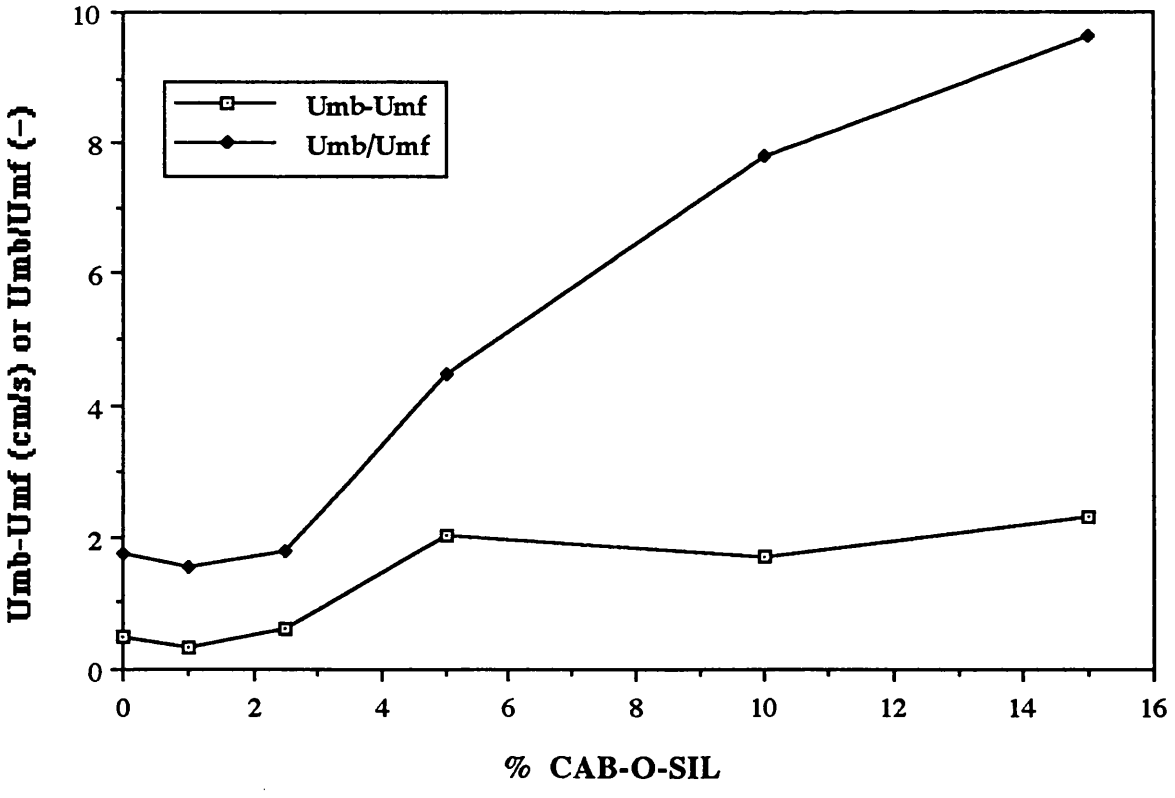

4.4. Bed Collapse Experiments

Bed collapse experiments were carried out to determine the voidage and expansion of the dense phase and separate it from the expansion due to bubbles. As mentioned earlier in section 3.2.11, the air flow rate in bed collapse experiments should normally be set slightly above the minimum bubbling velocity. Since the U_{mb} was a function of additive concentration, bed collapse experiments were mainly carried out at $1.5 \times U_{mb}$ for all the samples. To investigate the effect of flow rate, however, the test was carried out at different gas velocities for FCC with 2.5% CAB–O–SIL; it will be discussed in section 4.4.1.

4.4.1. Bed Collapse of FCC

Figs. 4.4.1–4.4.6 show the results of the bed collapse experiments of FCC with up to 15% CAB–O–SIL which are summarized in Table 4.4.1. It can be observed that the reproducibility of the data was very good and in particular the scatter in samples containing more additives was very little. This was in agreement with the smoother fluidization behaviour already mentioned (section 4.3.3).

The bed heights decreased very fast in the first second then decreased rather linearly until it was within a few millimetres of the static bed height. The rapid initial decrease was due to the escape of bubbles which moved through the bed at a velocity higher than the the emulsion phase gas. The deaeration velocity was then taken as the slope of the linear part of the bed collapse curve. Extrapolating this line back to t = 0, gave the true height of the emulsion phase without the gas bubbles (H_d). This height was used to determine the voidage of the dense phase.

Fig. 4.4.1. Bed collapse of FCC.

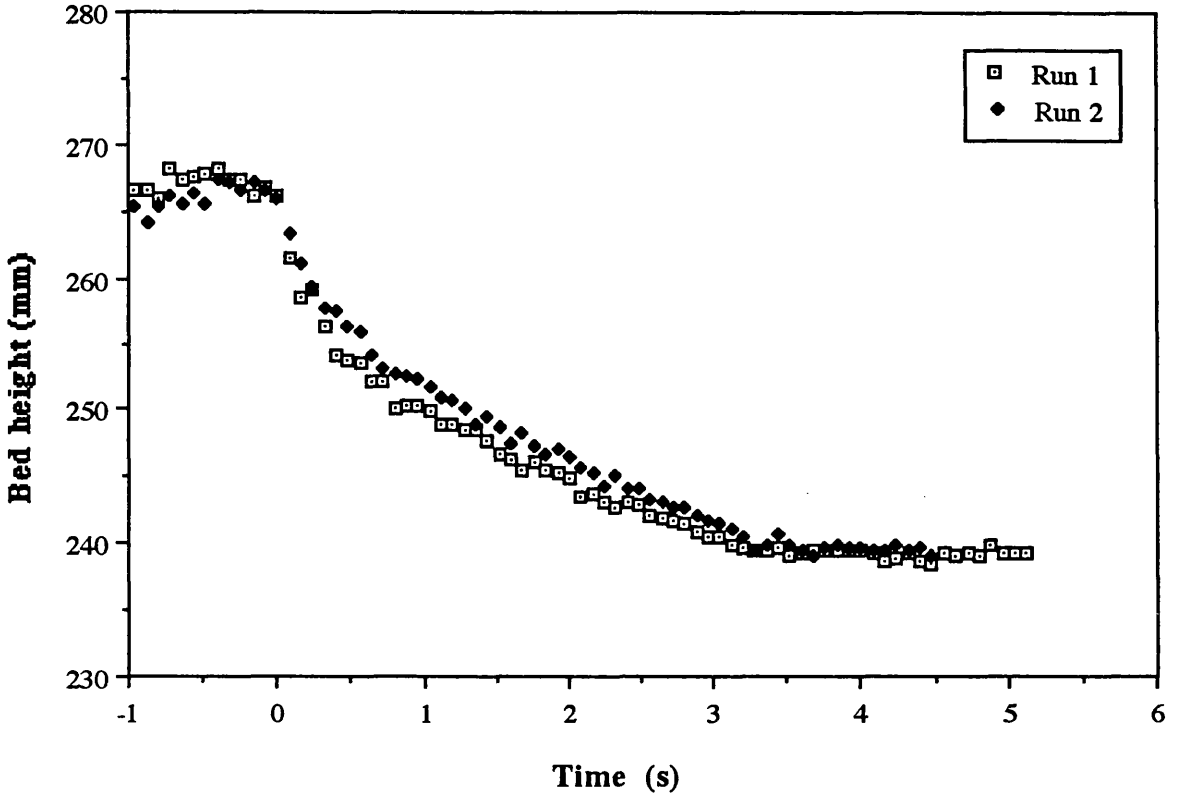

Fig. 4.4.2. Bed collapse of FCC with 1% CAB-O-SIL.

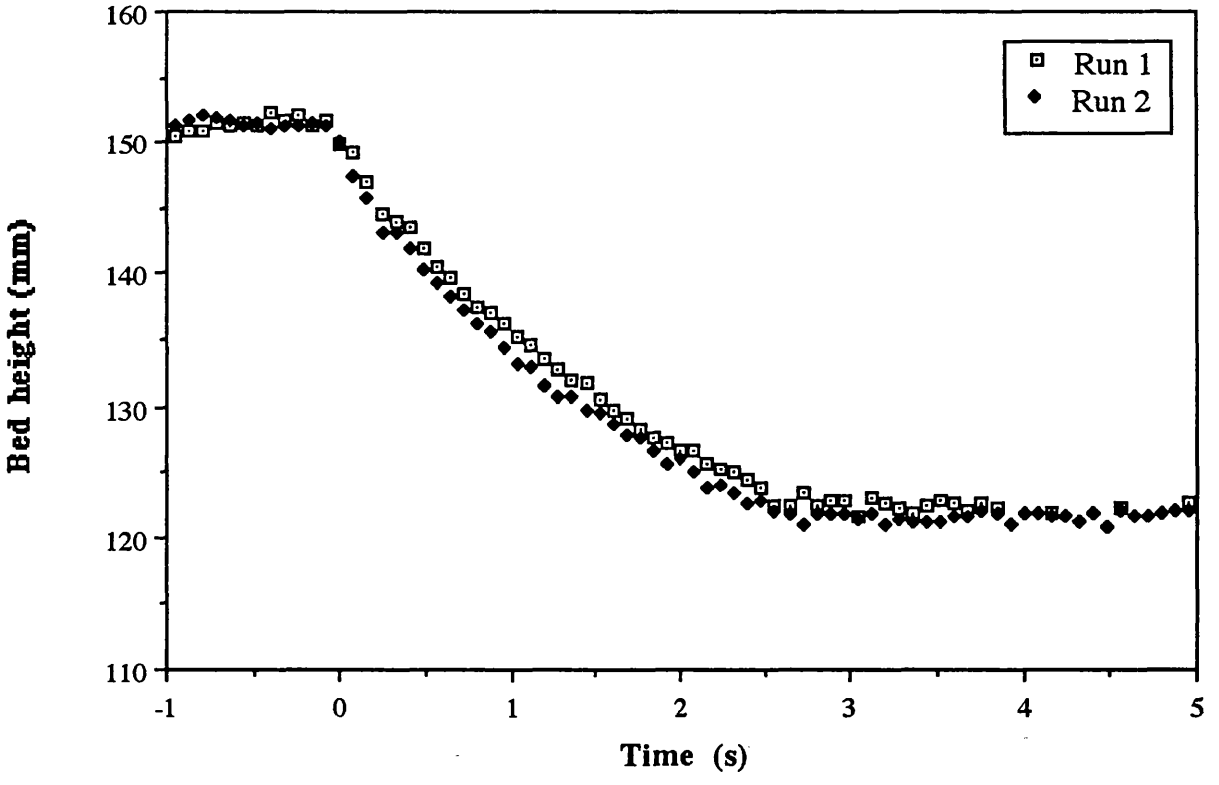

Fig. 4.4.3. Bed collapse of FCC with 2.5% CAB-O-SIL.

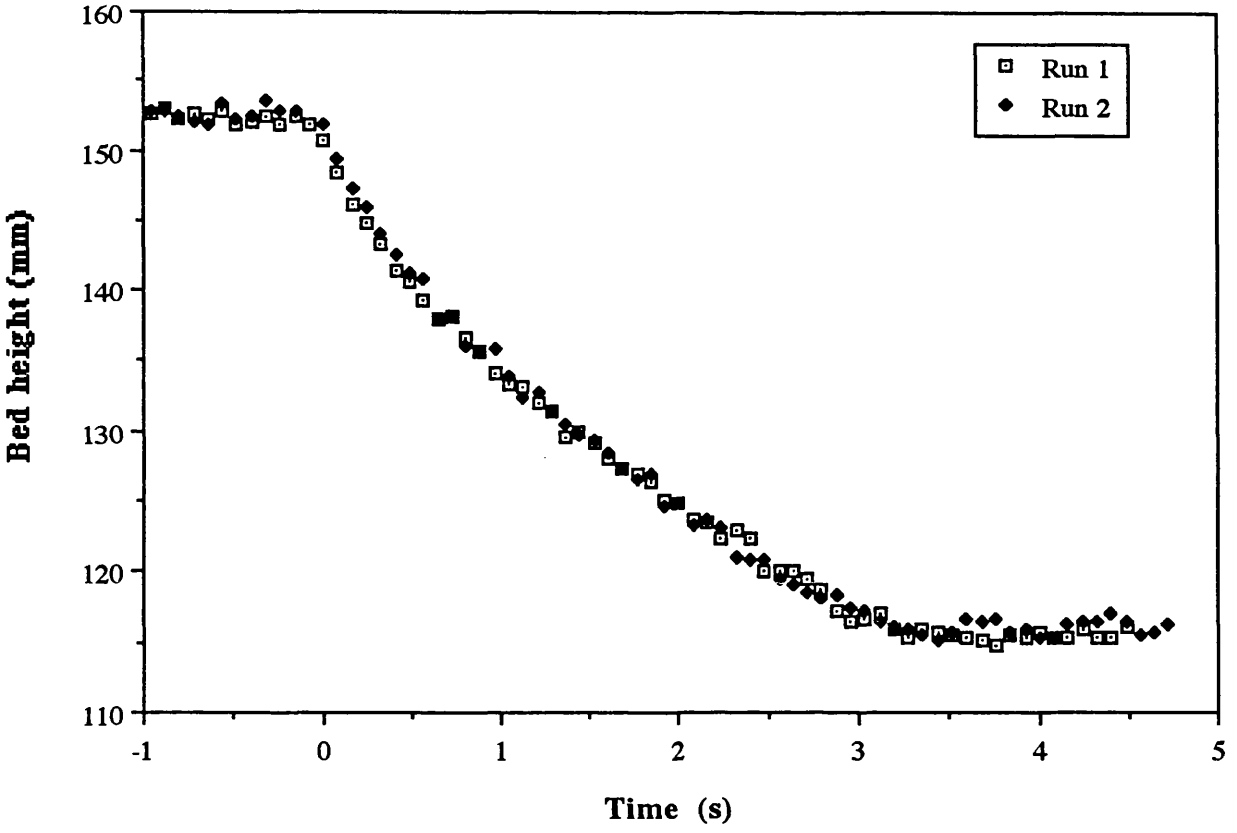

Fig. 4.4.4. Bed collapse of FCC with 5% CAB-O-SIL.

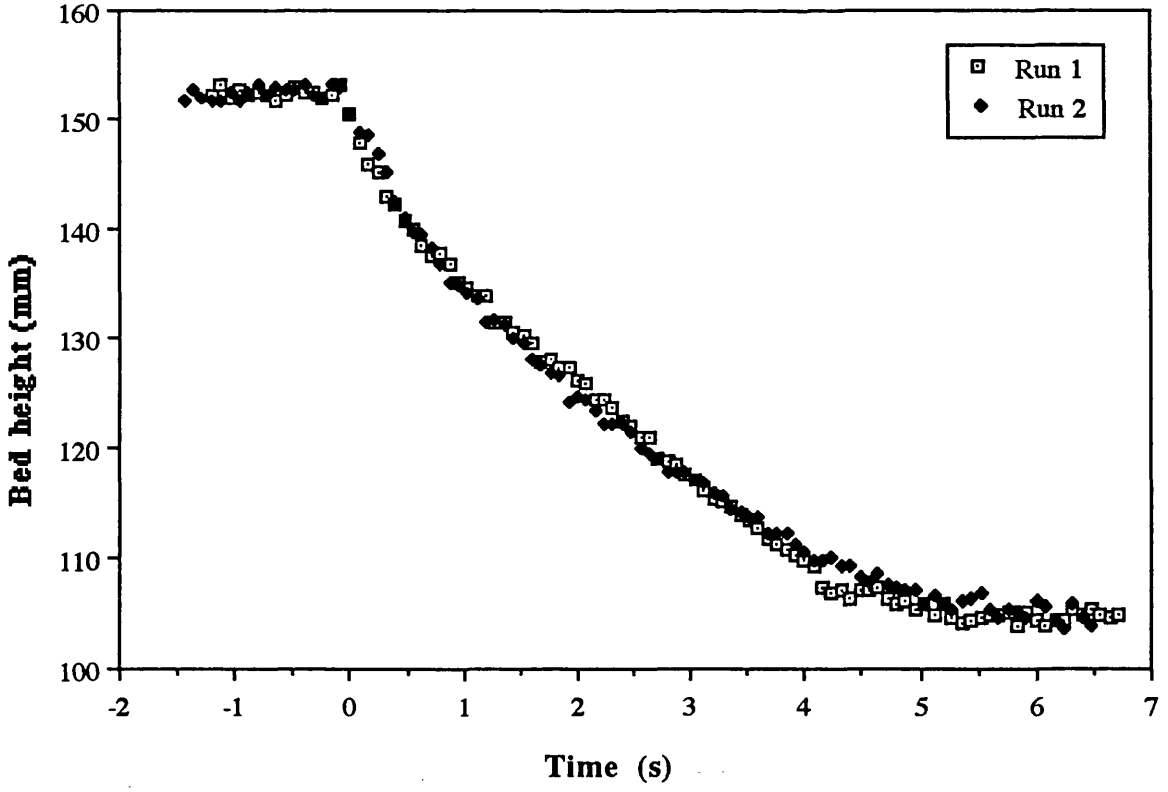

Fig. 4.4.5. Bed collapse of FCC with 10% CAB–O–SIL.

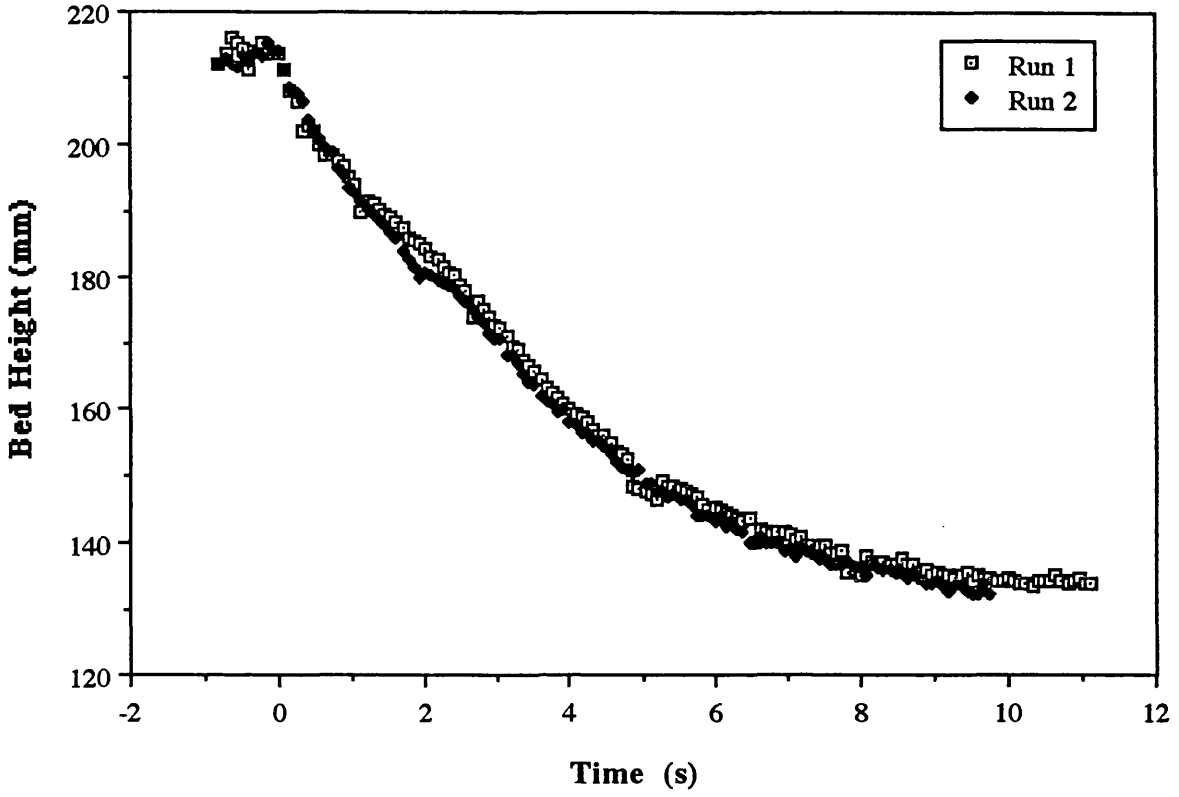

Fig. 4.4.6. Bed collapse of FCC with 15% CAB–O-SIL.

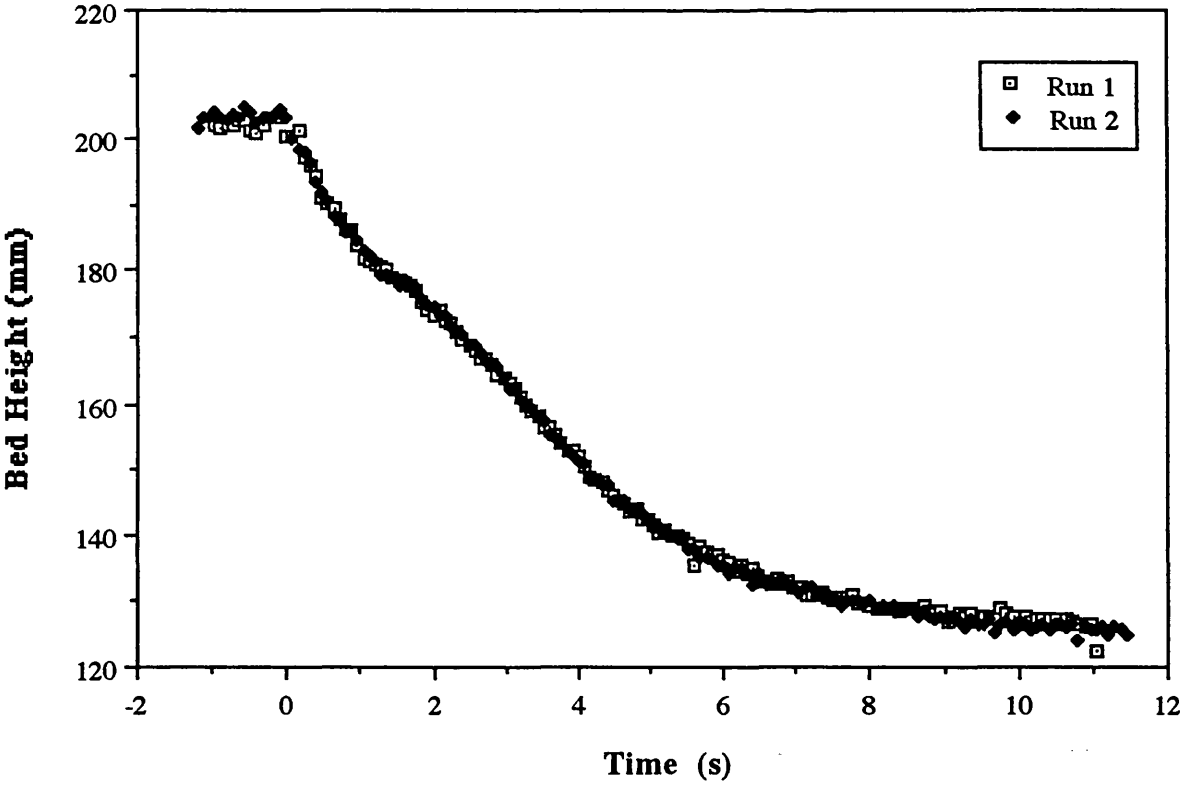

Table 4.4.1. Calculation of bed expansion and voidages of FCC with different concentrations of CAB–O–SIL.

CAB–O–SIL (wt%)	H_o (mm)	H_d (mm)	H_s (mm)	M (g)	Dense phase Expansion (%)	Expansion due to bubbles (%)	ε_s	ε_d
0	266.45	256.40	239.22	3080	7.18	3.92	0.27	0.32
1	151.39	144.80	121.39	1088	19.29	4.55	0.49	0.57
2.5	152.48	143.59	115.55	900	24.27	6.19	0.56	0.64
5	152.40	142.51	104.80	590	35.98	6.94	0.68	0.77
10	213.44	204.83	130.33	440	57.16	4.20	0.81	0.88
15	202.84	194.63	122.95	290	58.30	4.22	0.87	0.92

Dense phase expansion and the expansion due to bubbles were calculated using equations (3.7) and (3.8):

$$\text{Dense phase expansion} = \frac{H_d - H_s}{H_s} \times 100 \qquad (3.7)$$

$$\text{Expansion due to bubbles} = \frac{H_o - H_d}{H_d} \times 100 \qquad (3.8)$$

The dense phase expansion of FCC without any additive was 7.2% and addition of ultrafines increased the dense phase expansion up to 58% for the blend containing 15% CAB–O–SIL (Fig. 4.4.7). The effect of CAB–O–SIL was more significant on the dense phase expansion as shown while the change in the expansion due to bubbles was less noticeable. Addition of more than 10% CAB–O–SIL did not affect the results considerably.

The bed voidage of the emulsion phase and the settled bed were calculated using H_d and the height of the settled bed, H_s, together with equation (3.5). Settled bed voidage, ε_s, of FCC was 0.27 (Fig. 4.4.8) and when 15% CAB–O–SIL was added to the sample, ε_s increased to 0.87. The voidage of the emulsion phase, ε_d, was 0.32 for FCC which increased to 0.92 . The increase in bed voidage with additive concentration was due to a looser bed structure as already mentioned (see section 4.3.3) and it was analogous to the decrease in the bulk density of the mixtures already discussed.

To investigate the effect of gas flow rate, the test was repeated on FCC with 2.5% CAB–O–SIL at different gas velocities (Fig. 4.4.9). Different expansions and bed voidages

were determined as given in Table 4.4.2 and plotted in Figs. 4.4.10 and 4.4.11. Expansion due to bubbles at U_{mb} was 4.8% which increased to 9.9% at $3\times U_{mb}$, as expected; whereas there was not a significant change in the dense phase expansion in the region $1-2\times U_{mb}$ and it slightly dropped at $3\times U_{mb}$. Bed voidage of the settled bed and the dense phase were also fairly constant and were not dependent on the gas flow rate in this range.

Fig. 4.4.7. Effect of CAB-O-SIL on different expansions of FCC.

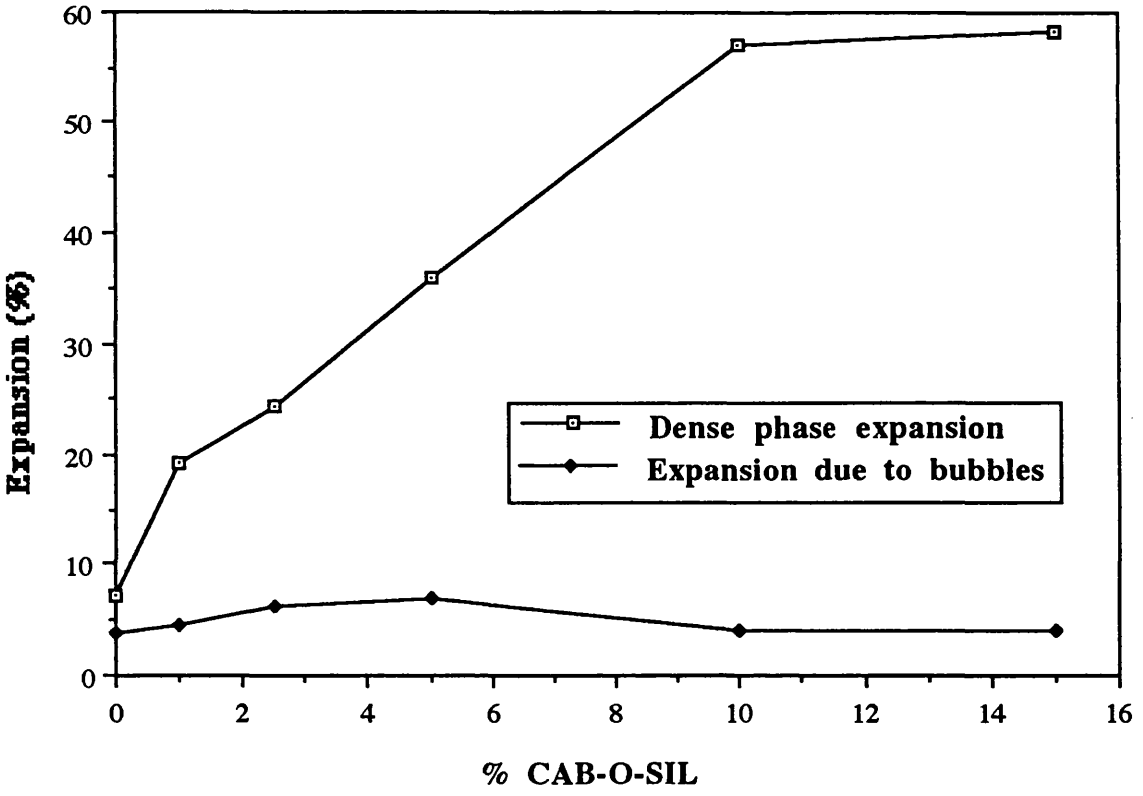

Fig. 4.4.8. Effect of CAB-O-SIL on the bed voidage of FCC.

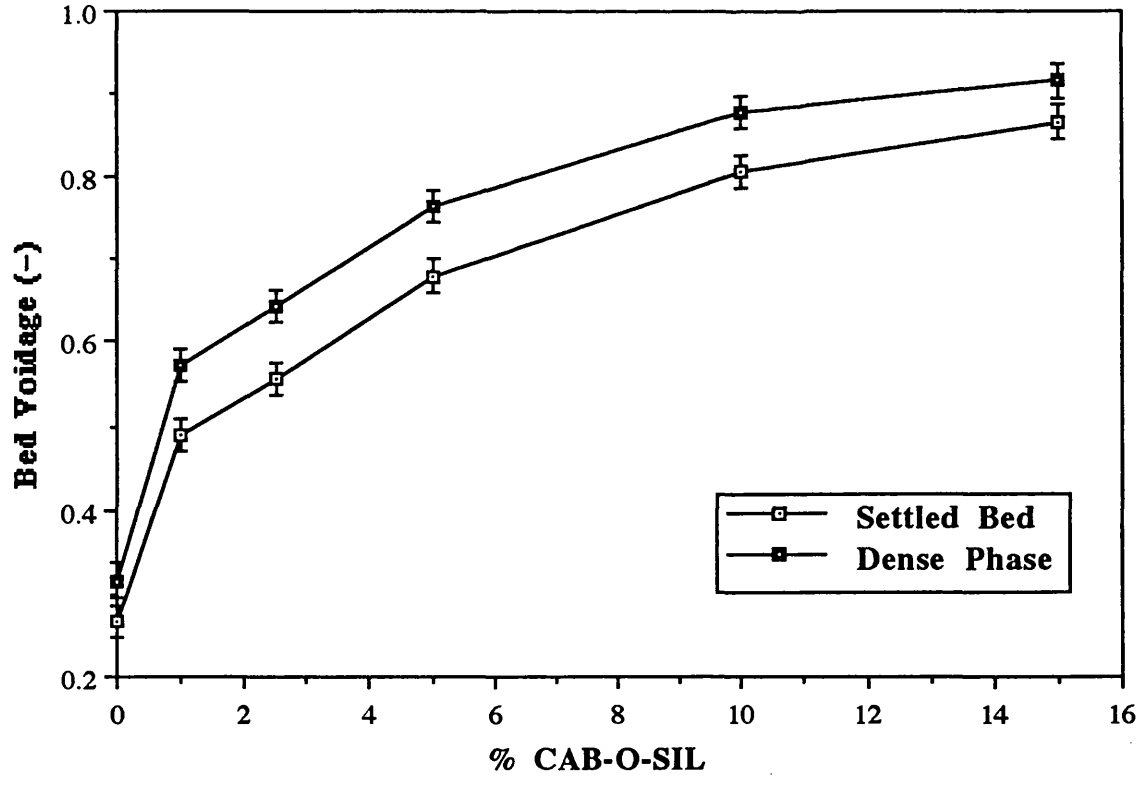

Fig. 4.4.9. Effect of initial flow rate on the bed collapse of FCC with 2.5% CAB-O-SIL.

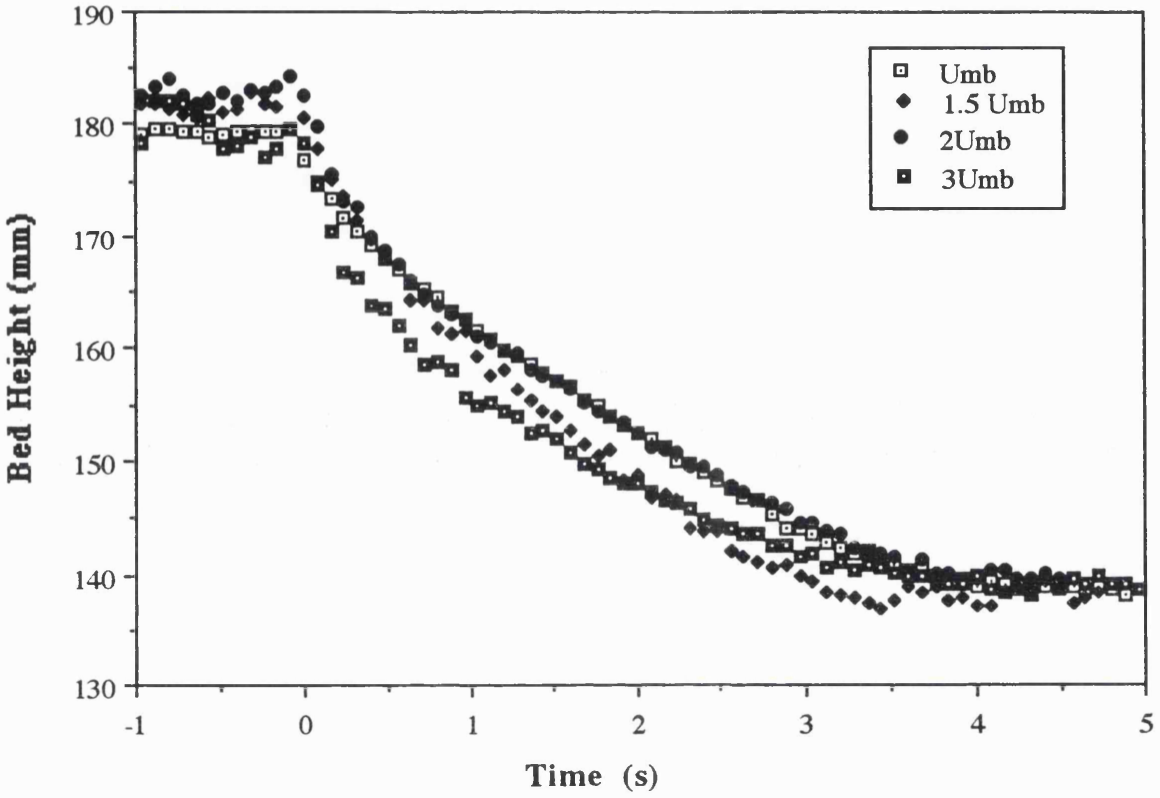

Fig. 4.4.10. Effect of air flow rate on bed expansion FCC with 2.5% CAB-O-SIL.

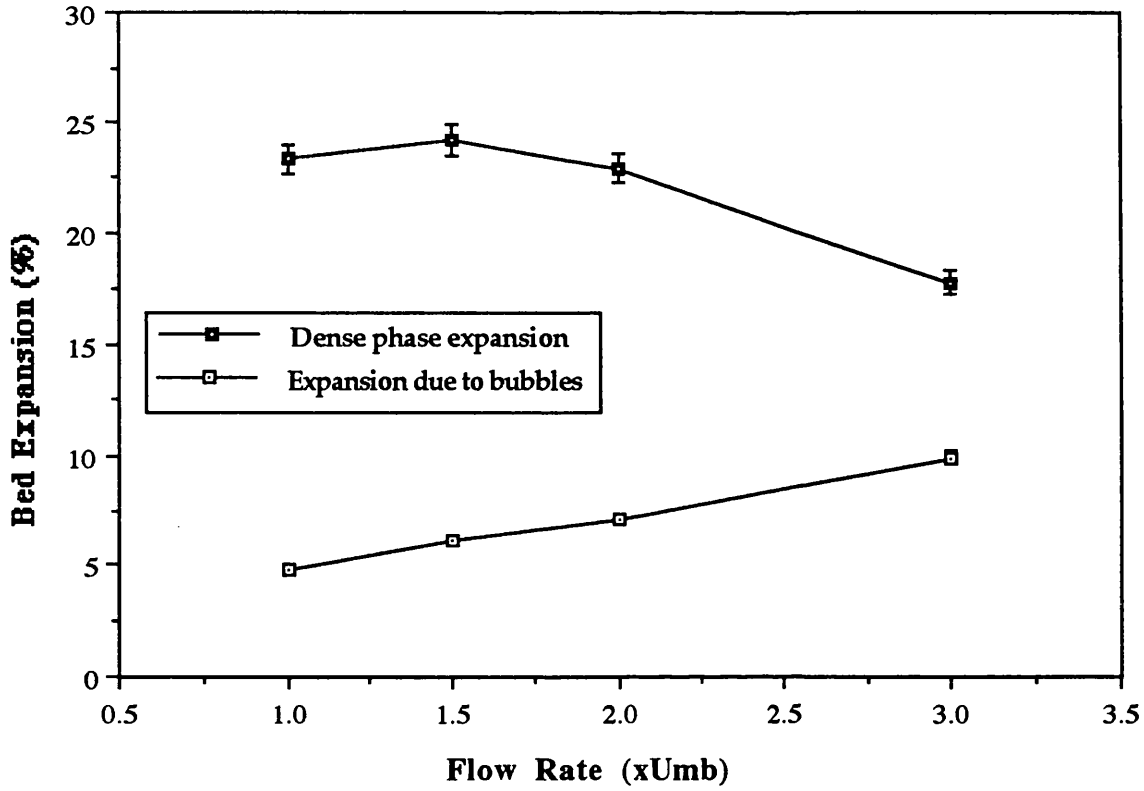

Fig. 4.4.11. Effect of air flow rate on bed voidage of FCC with 2.5% CAB-O-SIL.

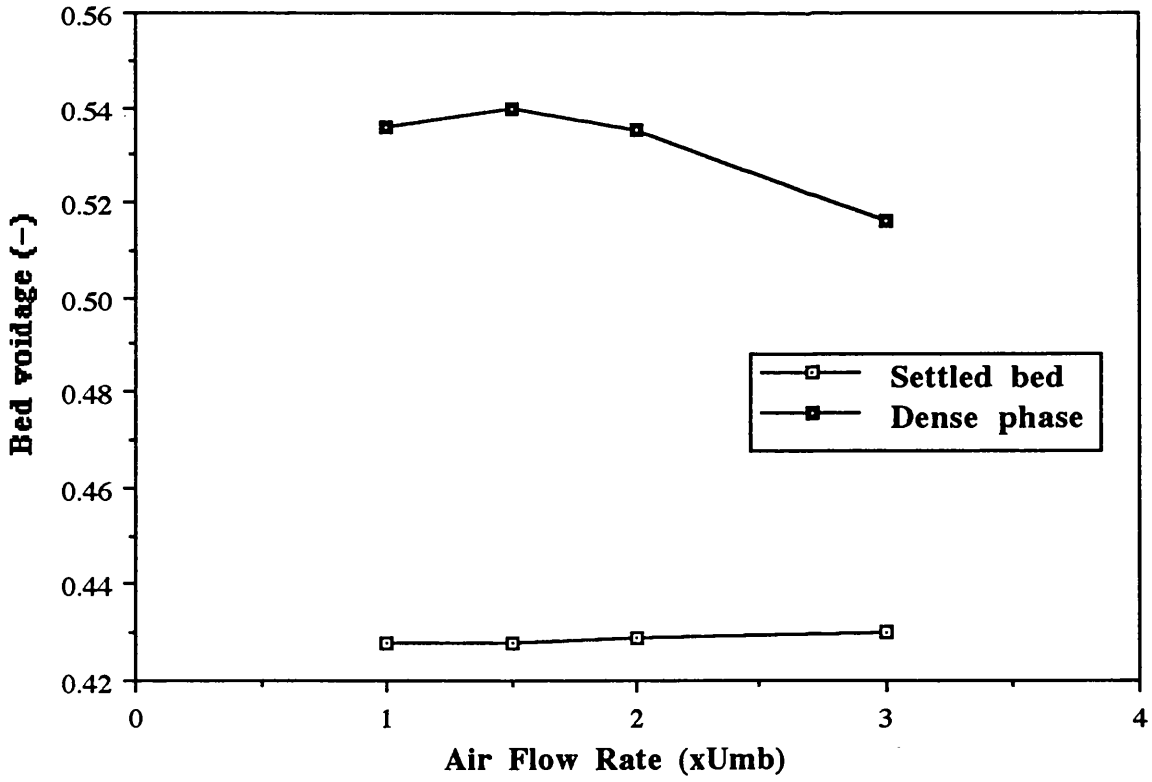

Table 4.4.2. Calculation of bed expansion and voidages for FCC with 2.5% CAB-O-SIL at different flow rates.

Gas Flow rate	H_o (mm)	H_d (mm)	H_s (mm)	Dense phase Expansion (%)	Expansion due to bubbles (%)	ε_s	ε_d
$1\times U_{mb}$	179.27	171.068	138.72	23.32	4.80	0.56	0.64
$1.5\times U_{mb}$	182.98	172.31	138.66	24.27	6.19	0.56	0.64
$2\times U_{mb}$	182.79	170.67	138.82	22.94	7.10	0.56	0.64
$3\times U_{mb}$	180.01	163.79	139.08	17.76	9.90	0.56	0.63

4.4.2. Bed Collapse of Silica

Bed collapse curves of silica with up to 15% CAB–O–SIL are shown in Figs. 4.4.12–4.4.17. The data was quite reproducible and there was little scatter in them. Dense phase expansion and the expansion due to bubbles were then determined as shown in Table 4.4.3. Dense phase expansion of silica was 8.6% (Fig. 4.4.18) which increased to about 50% for the 15% CAB–O–SIL blend while the expansion due to bubbles increased from 5% to 10%. Therefore, the effect of CAB–O–SIL was again much more significant on the dense expansion while the increase in the expansion due to bubbles was less noticeable. Addition of more than 10% CAB–O–SIL hardly improved the results.

Voidage of the settled bed of silica was 0.45 (Fig. 4.4.19) and addition of 15% CAB–O–SIL increased the ε_s to 0.76 which was due to the looser bed structure. The voidage of the dense phase, ε_d, of silica was 0.492 which increased to 0.84 for the 15% blend. The change in the dense phase voidage was significant but it was again mainly due the increase in ε_s. These results were analogous to FCC.

Fig. 4.4.12. Bed collapse of silica.

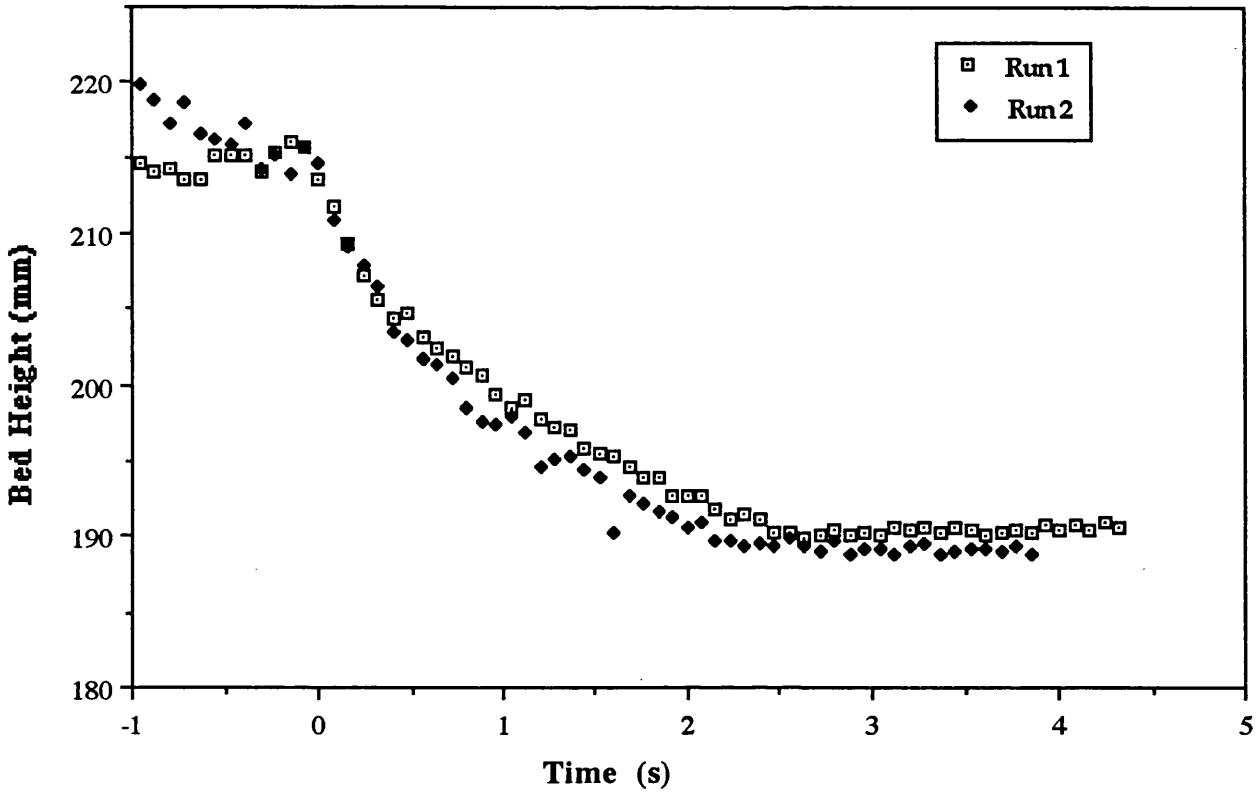

Fig. 4.4.13. Bed collapse of silica with 1% CAB-O-SIL.

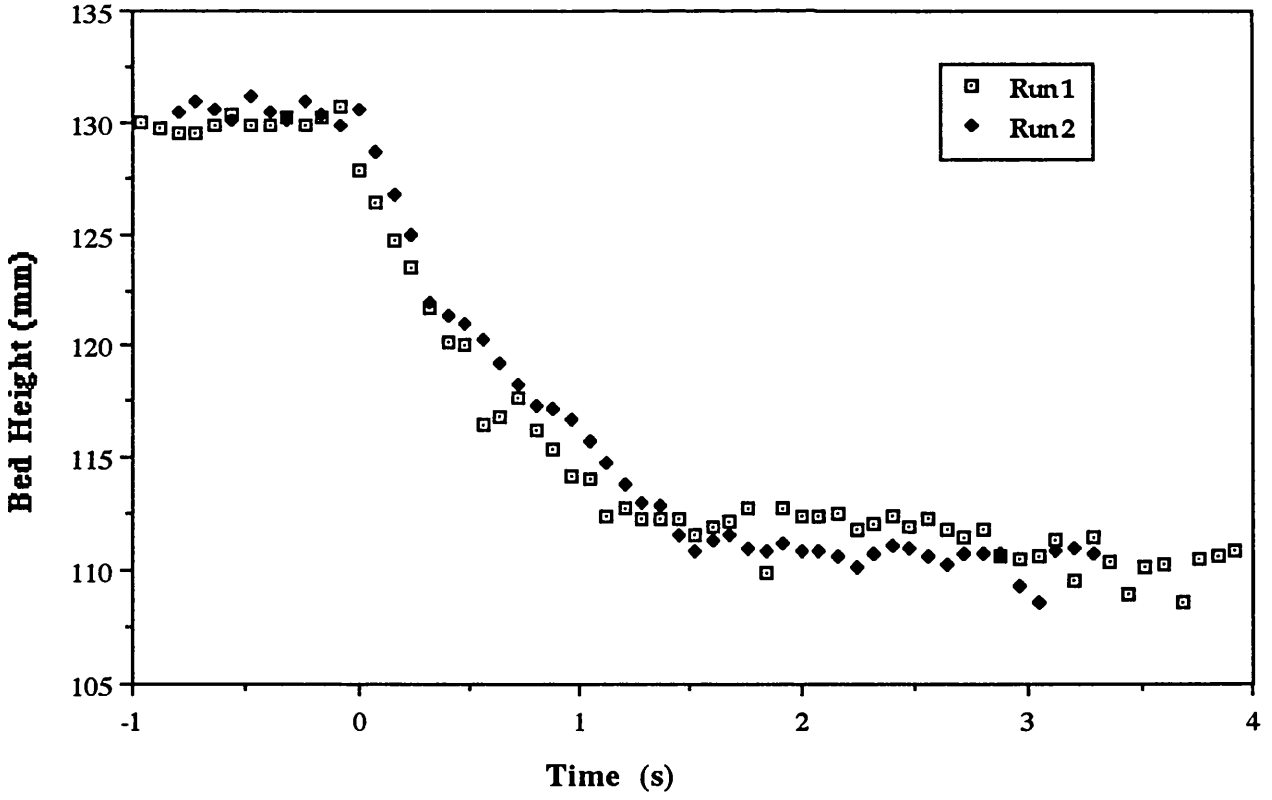

Fig. 4.4.14. Bed collapse of silica with 2.5% CAB-O-SIL.

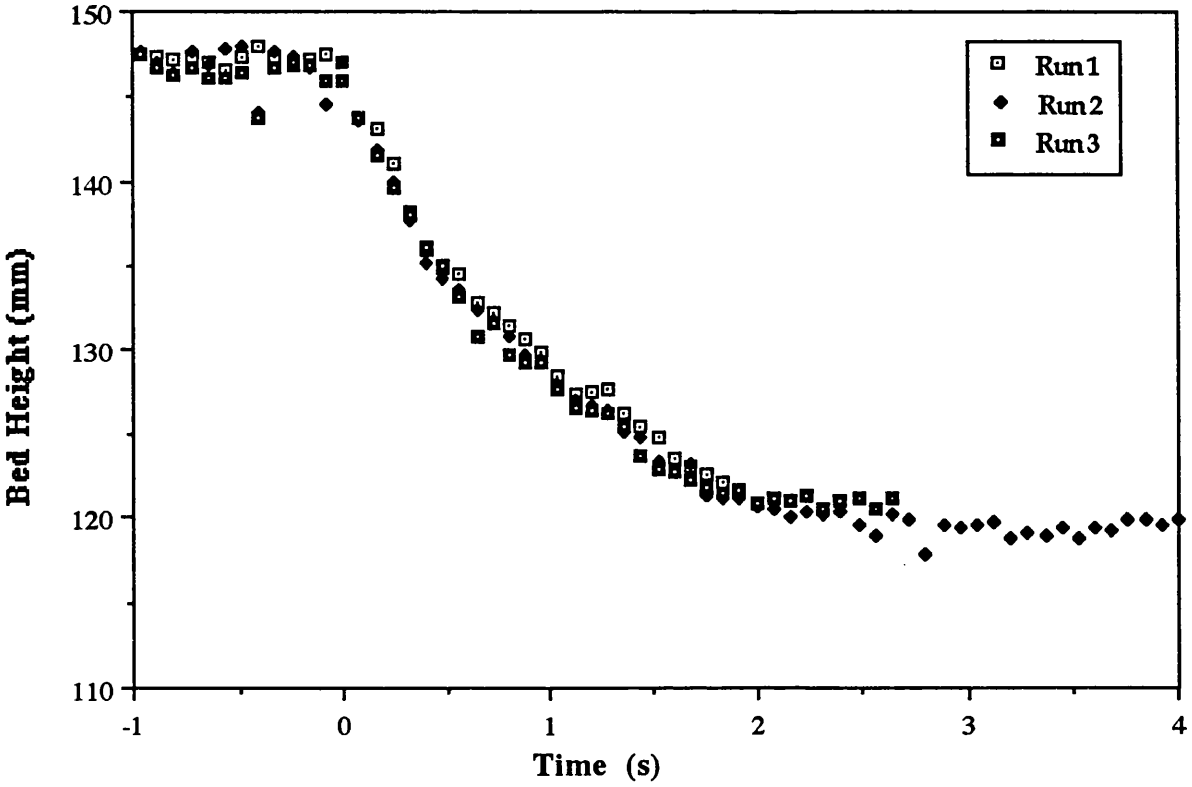

Fig. 4.4.15. Bed collapse of silica with 5% CAB-O-SIL.

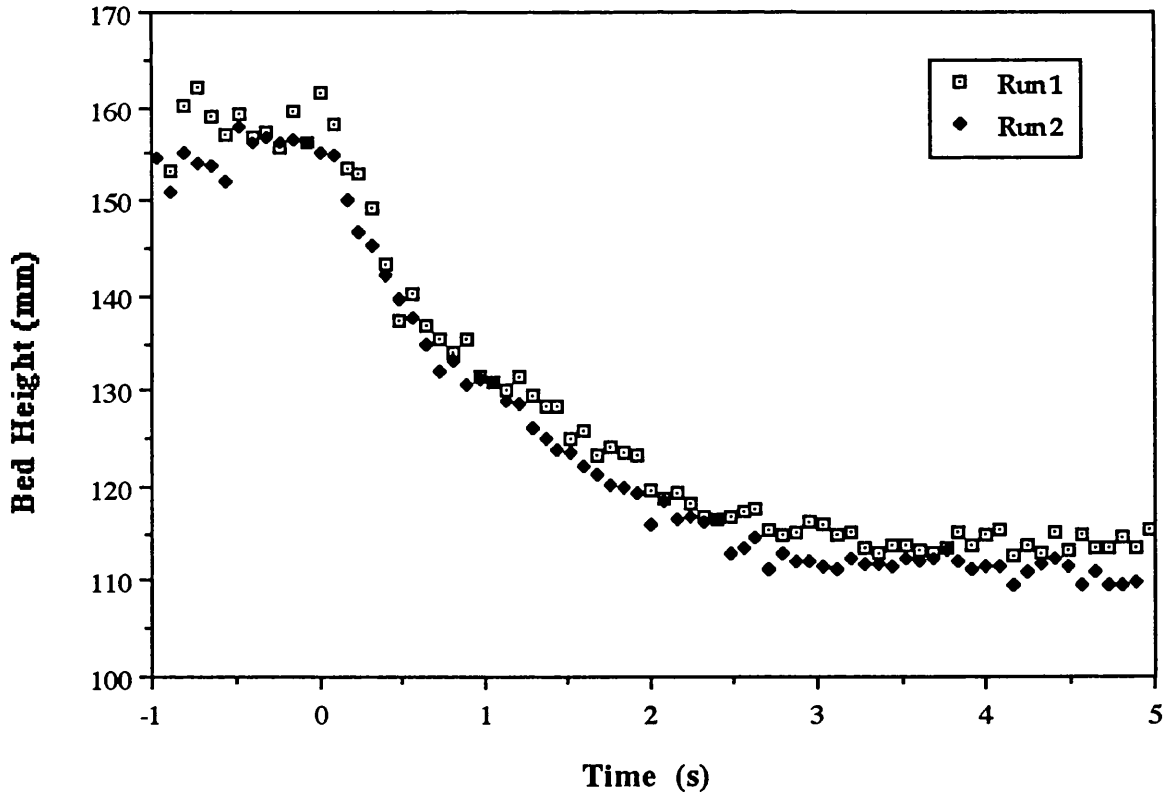

Fig. 4.4.16. Bed collapse of silica with 10% CAB-0-SIL.

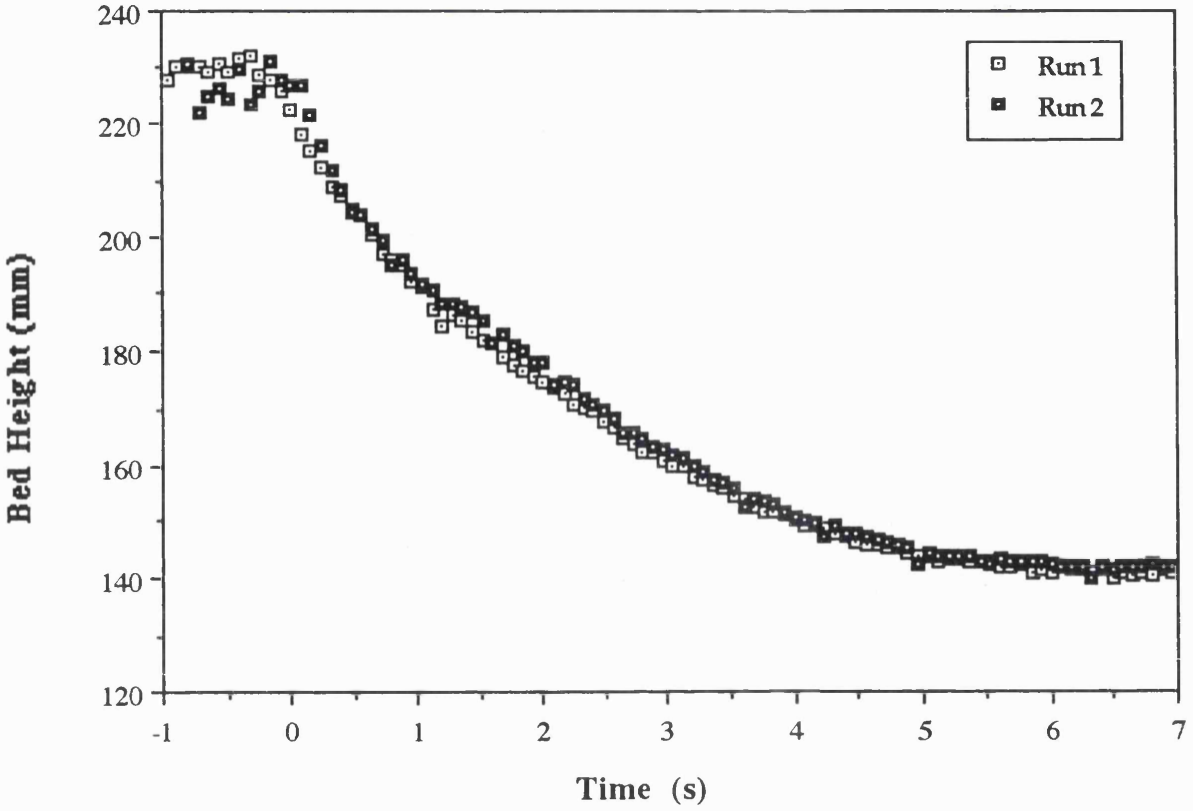

Fig. 4.4.17. Bed collapse of silica with 15% CAB-O-SIL.

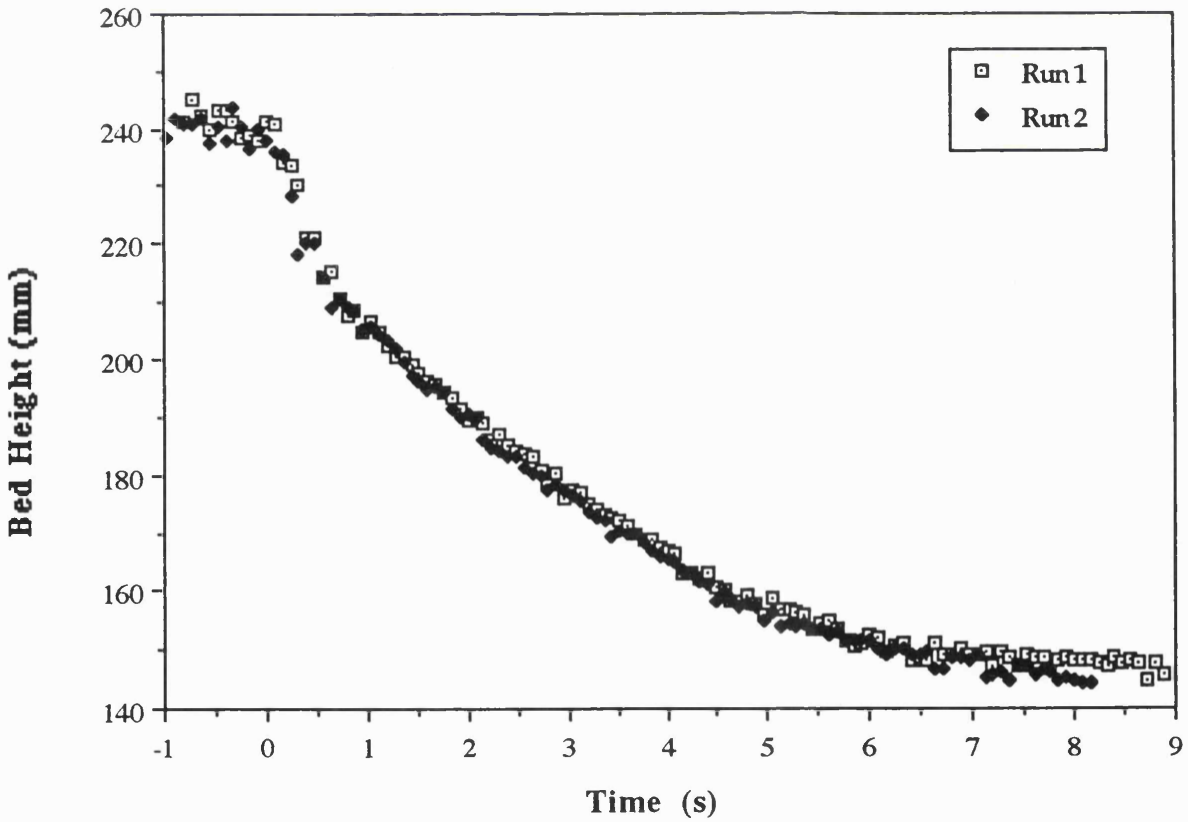

Table 4.4.3. Calculation of bed expansion and voidages for Silica with CAB–O–SIL.

CAB–O–SIL (wt%)	H_o (mm)	H_d (mm)	H_s (mm)	M (g)	Dense phase Expansion (%)	Expansion due to bubbles (%)	ε_s	ε_d
0	215.96	205.47	189.22	750	8.591	5.102	0.448	0.492
1	130.19	123.07	111.21	400	10.666	5.785	0.499	0.547
2.5	147.01	138.20	120.34	400	14.833	6.378	0.537	0.597
5	155.99	143.38	112.80	300	27.109	8.799	0.630	0.709
10	228.39	206.56	140.51	300	47.008	10.569	0.703	0.798
15	240.46	217.70	145.42	250	49.708	10.456	0.761	0.840

Fig. 4.4.18. Effect of CAB-O-SIL on different expansions of silica.

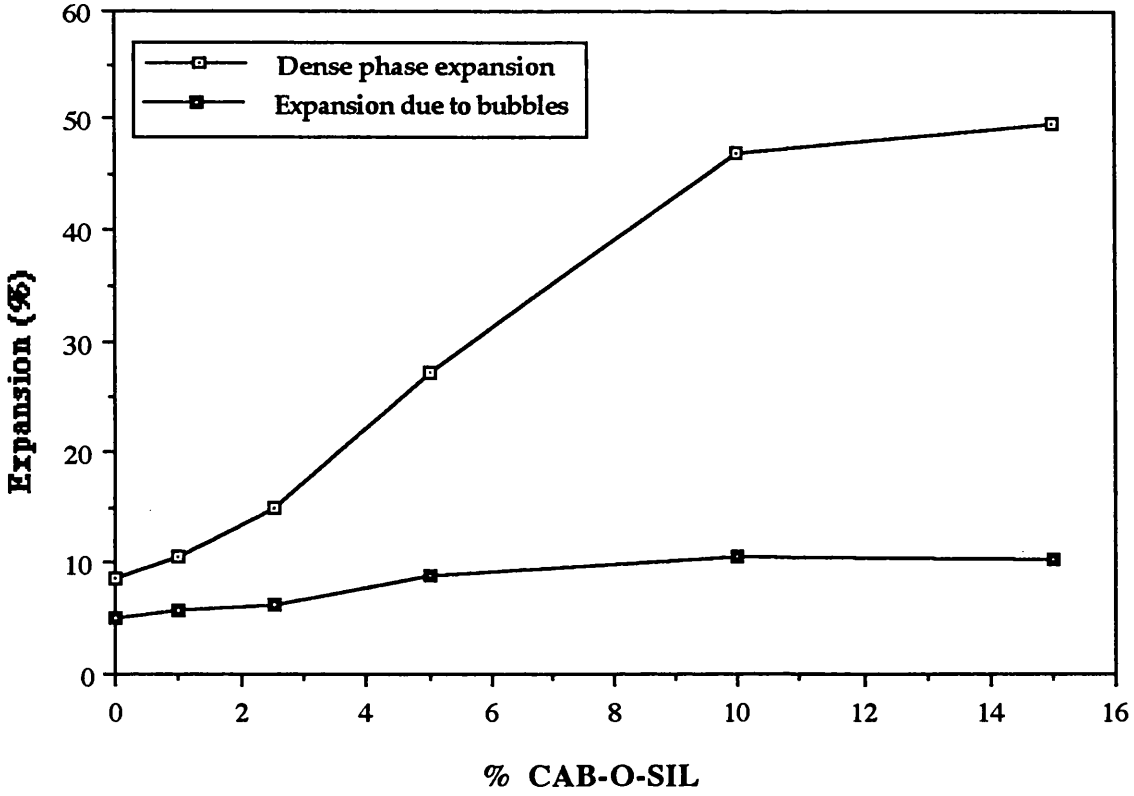

Fig. 4.4.19. Effect of CAB-O-SIL on different bed voidages of silica.

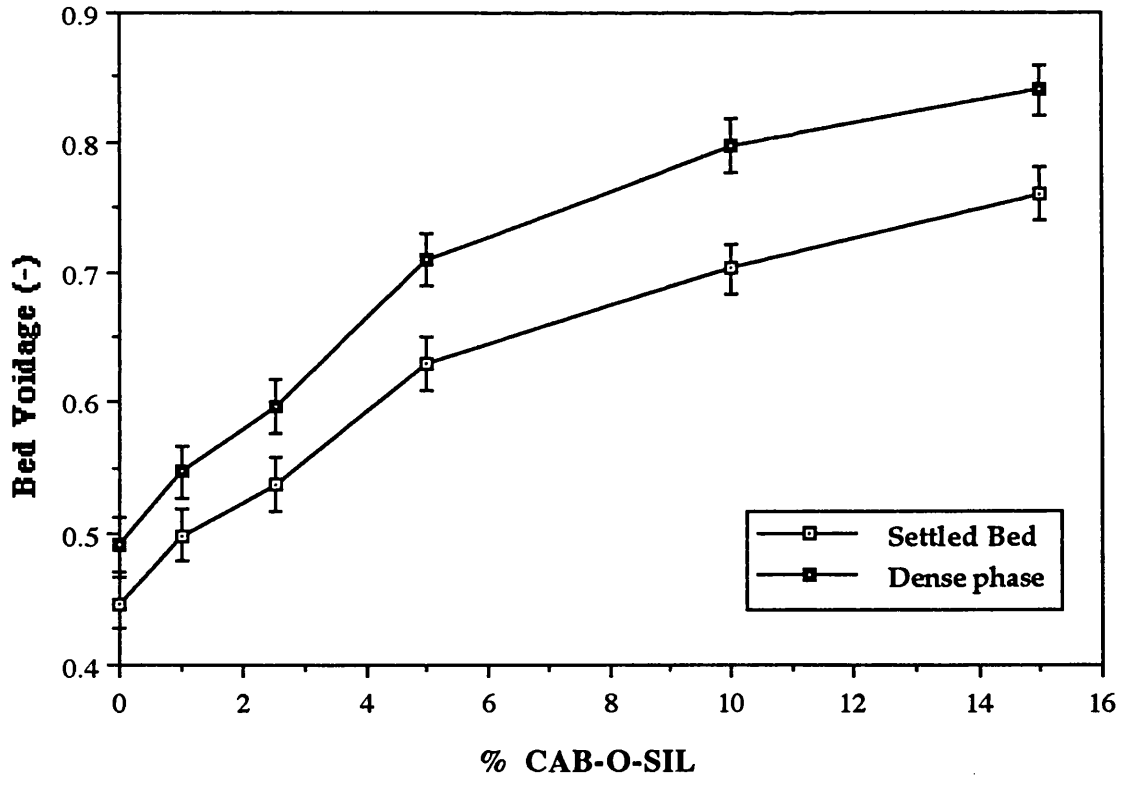

4.4.3. Discussions

Bed collapse curves showed that addition of CAB–O–SIL increased the deaeration time of FCC and silica mixtures. The deaeration velocity* of FCC and silica are shown in Fig. 4.4.20. The deaeration velocity of FCC blends were slightly smaller than silica but a similar trend was observed. The large deaeration velocity means that the air could escape more rapidly from the powder, allowing it to deaerate and settle faster. This could only be possible if the bed had a more porous structure. Therefore the deaeration velocity can be related to the porosity of the emulsion phase, the strength of interparticle networks and cohesion.

The voidage of the dense phase, ε_d, increased by addition of ultrafines but it was mainly due to the increase in the settled bed voidage, ε_s. It appeared that the fluidization properties of powders depended more on the concentration and type of ultrafines added and less on the host material.

Dense phase expansion of FCC and silica blends were in good agreement with the expansions found by simple fluidization experiments as shown in Figs. 4.4.21 and 4.4.22 which confirmed that the expansions observed during fluidization mainly occurred in the dense phase. The dense phase expansion of both FCC and silica increased significantly up to 10% CAB–O–SIL concentration and addition of another 5% of ultrafines did not improve this expansion. Considering that presence of ultrafines increased the cohesion of the bed, 10–15% additive was probably the optimum concentration for improving the fluidization behaviour of these material. Further addition of ultrafines increases the cohesion in the bed and would not probably produce

*Deaeration velocity is the slope of the linear part of the bed collapse curves.

any significant effect or might even reverse the improvements which requires further investigation.

Fig. 4.4.20. Effect of CAB-O-SIL on the deaeration velocity of FCC and silica.

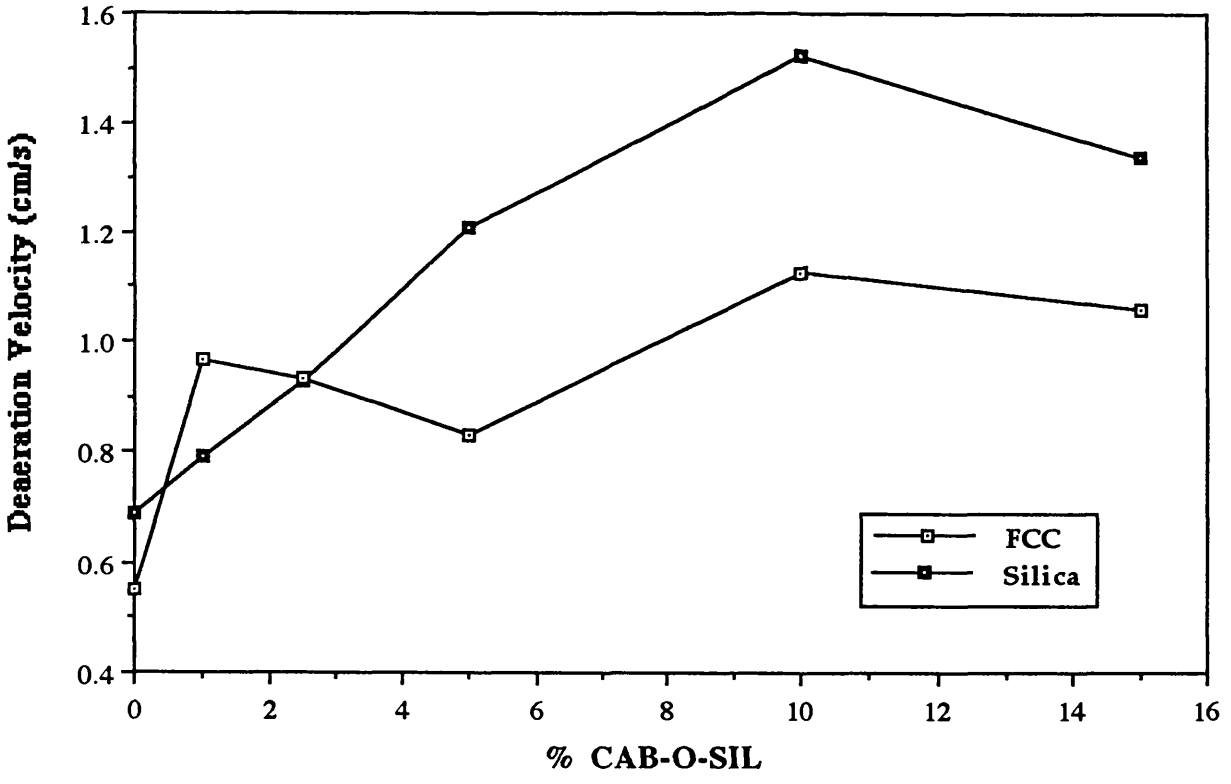

Fig. 4.4.21. Comparison of different expansions of FCC mixtures.

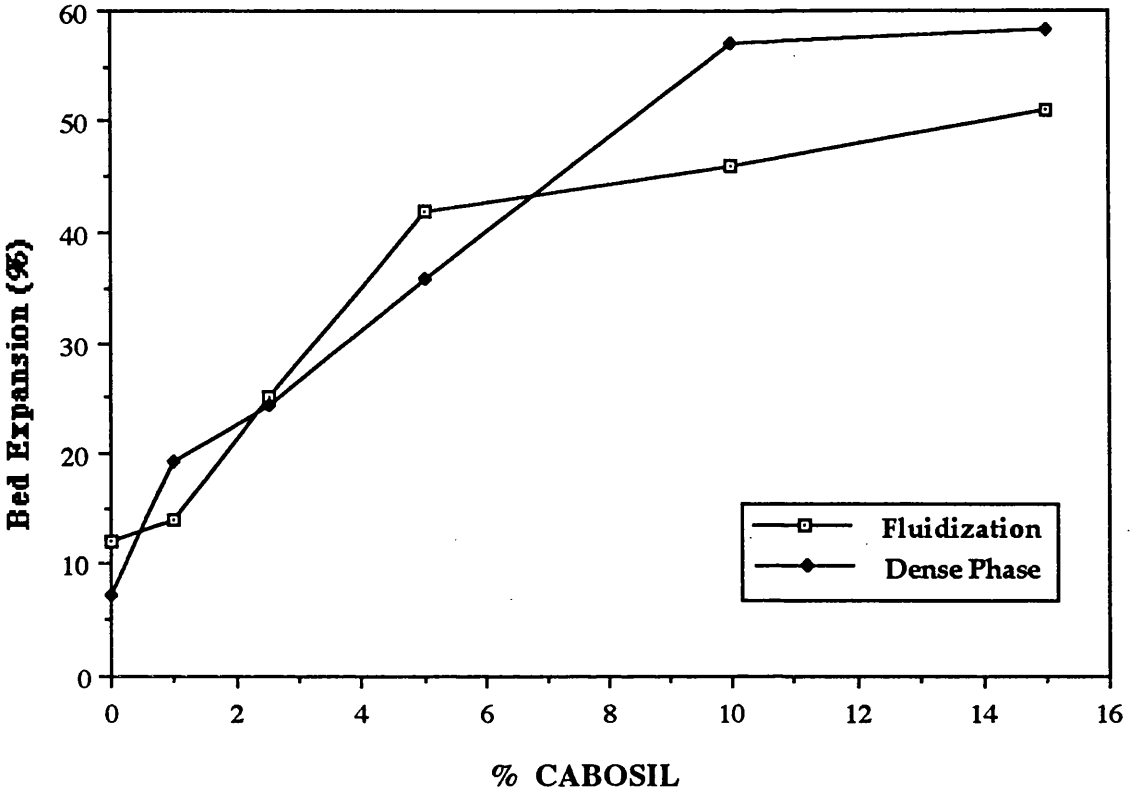

Fig. 4.4.22. Comparison of different expansions of silica mixtures.

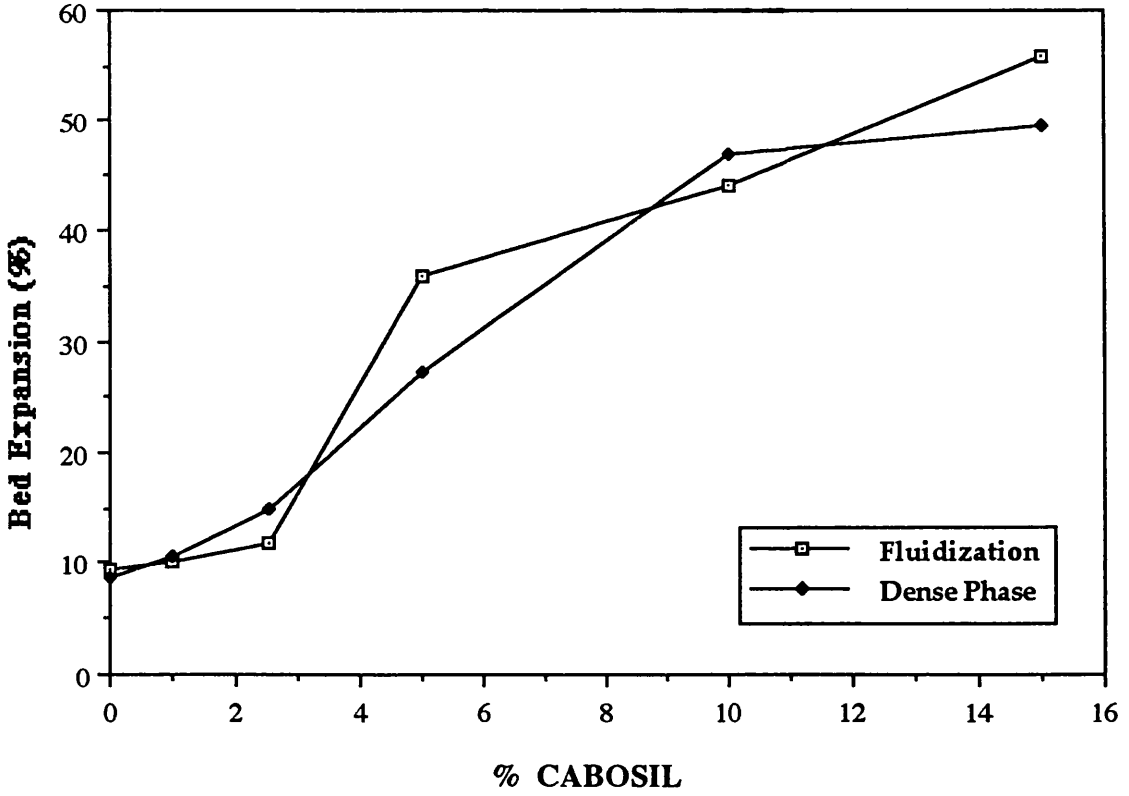

4.5. Stability of Fluidized Beds

In this section, the experimental data of bed voidage at incipient bubbling will be compared to different stability criteria discussed in section 2.8. The parameters that appear in these models include particle size and density of the host material, density and viscosity of the continuous phase, Richardson–Zaki indices n and U_t, bed height at incipient bubbling, H_{mb}, minimum bubbling velocity, U_{mb} and the loose packed voidage of the bed, ε_{lp}. Particle density and particle size of the host materials have already been determined (Table 3.1). U_{mb}, H_{mb} and ε_{lp} were experimentally measured (Tables 4.3.1 and 4.3.3). Other values like density and viscosity of the continuous phase, Richardson–Zaki indices and ΔP^*_{mb} should be determined. The method used for calculation of each parameter will be explained in the following sections. ΔP^*_{mb} will be explained in section 4.5.5 as it was used only in Reiling's model.

4.5.1. Density and Viscosity of Continuous Phase

As most of the ultrafines were segregated agglomerates and it was not possible to determine what fraction of it was attached to the host particles, it was assumed that all the additives were in the continuous phase. On this basis, the volume of the ultrafines could be found at the point of minimum bubbling in the following manner:

Let the height of the bed at minimum bubbling conditions be H_{mb}. Therefore the volume of the bed, V_t, is:

$$V_t = \frac{\pi}{4} D^2 H_{mb} \qquad (4.1)$$

where D is the bed diameter. Take the weight of the host material and its particle density as m_h and ρ_p, respectively. The volume of the host material is given by m_h/ρ_p and the volume of the continuous phase, V_{con}, can be found as:

$$V_{con} = Vt - m_h/\rho_p \qquad (4.2)$$

Take the weight of the additive and its bulk density as m_{add} and ρ_{add}, respectively. The volume occupied by the additive is then m_{add}/ρ_{add} and the volume fraction of the ultrafines in air, y will be:

$$y = \frac{V_{add}}{V_{con}} = \frac{m_{add}/\rho_{add}}{Vt - m_h/\rho_p} \qquad (4.3)$$

Average density of the continuous phase can be determined by using a linear equation as:

$$\rho = \rho_{add} \cdot y + \rho_{air} \cdot (1-y) \qquad (4.4)$$

Average viscosity of the mixture of air and CAB–O–SIL may be obtained using the empirical correlations suggested by Barnea and Mizrahi (1976):

$$\frac{\mu_m}{\mu_c} = \exp\left[2.5\frac{0.4\,\mu_c + \mu_d}{\mu_c + \mu_d}\left(y + y^{5/3} + y^{11/3}\right)\right] \qquad (4.5)$$

where μ_m, μ_c and μ_d are the viscosities of the mixture, the continuous phase and the dispersed phase, respectively.

Using the bulk density (70 kg/m^3) and the viscosity of CAB–O–SIL (0.166 Pa.s) in equations (4.4) and (4.5), the density, ρ, and viscosity, μ, of the continuous phase were calculated; the results are summarized in Tables 4.5.1 and 4.5.2 for FCC and silica mixtures, respectively. Fig. 4.5.1. shows that ρ increased sharply with additive concentration of up to 5% wt of CAB–O–SIL beyond which ρ remained fairly constant

Table 4.5.1. Calculation of fluid density and viscosity for mixtures of FCC and CABOSIL.

CAB–O–SIL (wt%)	Hmb, cm	Host mass, g	Additive mass, g	Host volume, cc	Additive volume, cc	Air volume, cc	y	$\rho \times 10^3$, g/cc	$\mu_m \times 10^4$, cP
0	16.5	1000	0	568.505	0	727.402	0	1.214	1.750
1	16.7	891	9	506.538	128.571	676.506	0.1597	12.199	2.943
2.5	20	829	21	471.148	303.571	796.077	0.2761	20.203	4.780
5	17.8	475	25	270.04	357.143	770.826	0.3166	22.993	5.787
10	20.1	270	30	153.496	428.571	996.583	0.3007	21.899	5.361
15	23.1	204	36	115.975	514.286	1184.010	0.3028	22.044	5.415

Note that particle density of FCC was 1759 kg/m^3 and bulk density of CABOSIL 70 kg/m^3.

Table 4.5.2. Calculation of fluid density and viscosity for mixtures of silica and CABOSIL.

CAB–O–SIL (wt%)	Hmb, cm	Host mass, g	Additive mass, g	Host volume, cc	Additive volume, cc	Air volume, cc	y	$\rho \times 10^3$, g/cc	$\mu_m \times 10^4$, cP
0	21.9	500	0	696.379	0	1023.64	0	1.214	1.750
1	17.6	400	4	556.468	57.654	768.178	0.0698	6.016	2.147
2.5	20.1	391	10	544.914	143.314	890.422	0.1386	10.750	2.720
5	22.5	285	15	396.671	214.143	1156.33	0.1563	11.962	2.904
10	30.9	270	30	375.844	428.343	1622.69	0.2088	15.579	3.573
15	34.4	212	38	295.843	535.5	1870.43	0.2226	16.524	3.783

Note that particle density of silica and 718 kg/m^3 and bulk density of CABOSIL 70 kg/m^3.

Fig. 4.5.1. Effect of CAB-O-SIL on the fluid density of continuous phase.

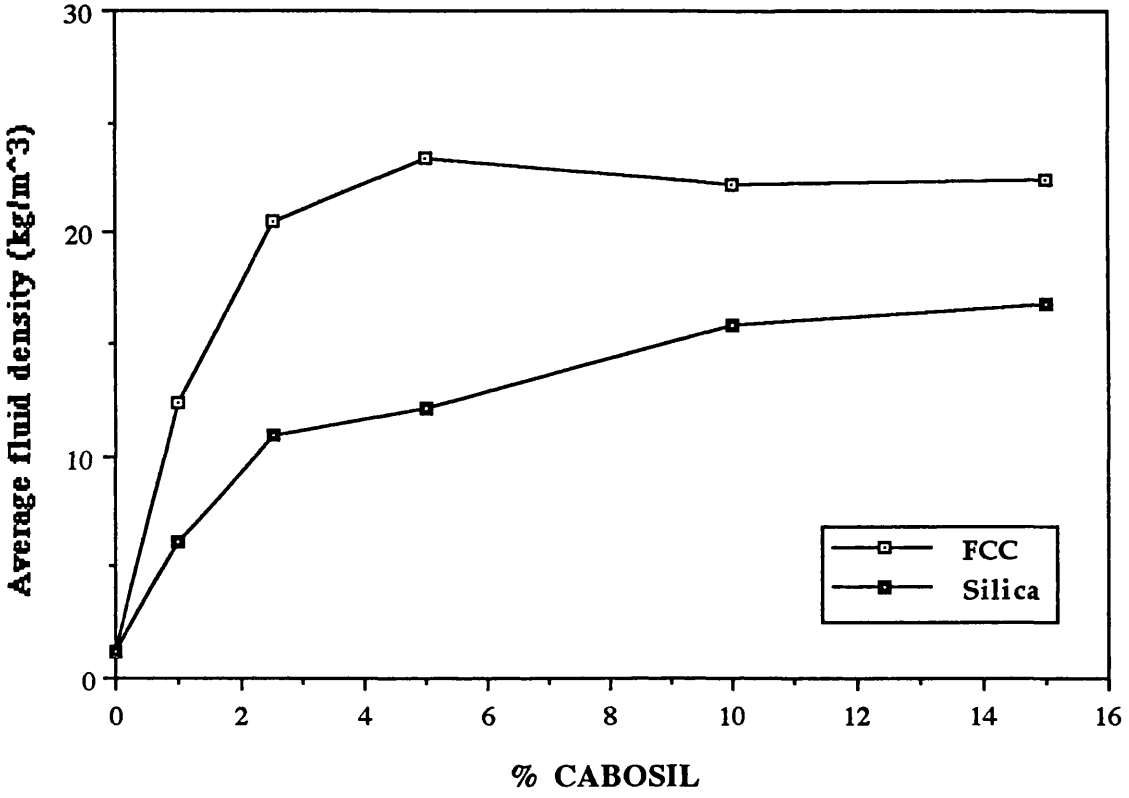

Fig. 4.5.2. Effect of CAB-O-SIL on the viscosity of continuous phase.

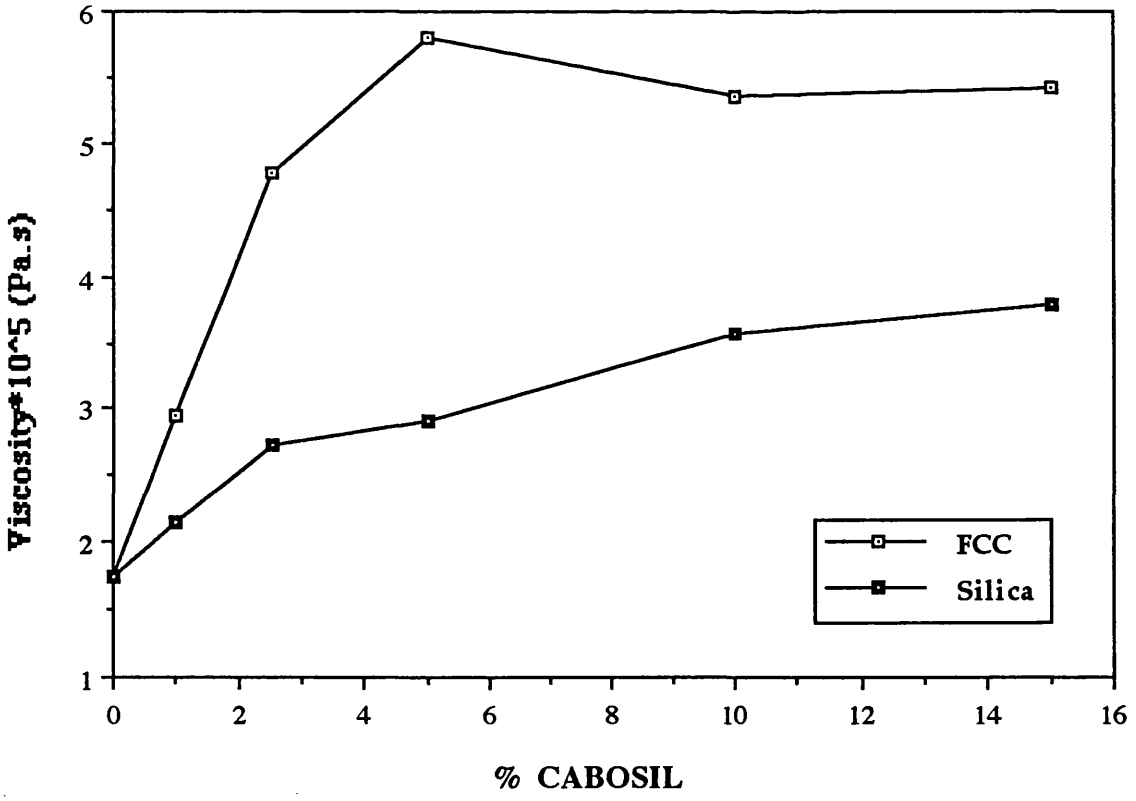

with further increase in CAB–O–SIL. Although the density increased by up to 16–20 times, it was still much lower than the particle density of the host materials (1759 and 718 kg/m^3 for FCC and silica, respectively).

Viscosity of the continuous phase increased as shown in Fig. 4.5.2. Maximum viscosity corresponded to FCC with 15% CAB–O–SIL as 5.415×10^{-5} Pa.s which was only three times as the viscosity of air, 1.75×10^{-5} Pa.s.

4.5.2. Richardson–Zaki Parameters

According to equation (2.34), Richardson–Zaki indices can be determined from a plot of logU versus logε for each sample:

$$\log U = n \log \varepsilon + \log U_t \qquad (2.34)$$

Therefore a plot of logU against logε is linear and n is the slope of the line while logU_t is the intercept on the logU axis corresponding to ε=1. For each sample, bed voidage at different velocities were calculated from the results of the fluidization experiments. As this equation is mainly valid for a homogeneous system, only the data between U_{mf} and U_{mb} were used. The best line was fitted to the data and the bed expansion index, n, and the terminal velocity, U_t, were determined. The results are summarized in Tables 4.5.3 and 4.5.4 which show that there was a good linear relationship between logU and logε.

The terminal velocity was also found using the calculated density and viscosity of the continuous phase together with Haider–Levenspiel's method (section 2.9) as well as Stoke's law, equation (2.27). The results are shown in Tables 4.5.5 and 4.5.6. It

Table 4.5.3. Richardson–Zaki parameters for FCC mixtures.

% CAB–O–SIL by weight	n	U_t, m/s	R^2 fit
0	5.719	0.2563	0.9584
1	6.109	0.1954	0.8430
2.5	6.334	0.1107	0.7225
5	14.374	0.3836	0.9501
10	32.65	0.6418	0.9755
15	25.07	0.172	0.9149

Table 4.5.4. Richardson–Zaki parameters for Silica mixtures.

% CAB–O–SIL by weight	n	U_t, m/s	R^2 fit
0	5.856	0.2215	0.9010
1	5.688	0.1851	0.8996
2.5	7.636	0.3825	0.9595
5	11.527	0.5712	0.9919
10	19.360	0.8306	0.9623
15	23.438	0.6414	0.9933

Table 4.5.5. Calculation of terminal velocity of FCC mixtures using Kunii–Levenspiel method and also Stoke's law.

% CAB–O–SIL by weight	d_p^*	U_t^*	U_t, m/s	U_t, m/s (Stoke's)
0	2.2895	0.2615	0.1541	0.1717
1	3.4863	0.5563	0.0836	0.1014
2.5	2.9806	0.4222	0.0532	0.0622
5	2.7381	0.3626	0.0446	0.0513
10	2.8354	0.3861	0.0479	0.0554
15	2.8227	0.383	0.0474	0.0548

Table 4.5.6. Calculation of terminal velocity of silica mixtures using Kunii–Levenspiel method and also Stoke's law.

% CAB–O–SIL by weight	d_p^*	U_t^*	U_t, m/s	U_t, m/s (Stoke's)
0	3.3349	0.5149	0.2251	0.2701
1	4.9501	0.9998	0.1606	0.2187
2.5	5.1190	1.0547	0.1242	0.1715
5	5.0752	1.0404	0.1166	0.1603
10	4.8187	0.9575	0.0962	0.1296
15	4.7285	0.9286	0.0914	0.1223

should be mentioned that Stoke's law holds only when $Re_t < 0.2$ which was not the case in either of the systems studied here.

Figs 4.5.3 and 4.5.4 compare the terminal velocities obtained by different techniques. Considering that the viscosity of the continuous phase did not change significantly and the density was very low comparing to the particle density of the host materials, despite its increase with ultrafine concentration, both Haider–Levenspiel and Stoke's law predicted that for a constant particle density, U_t should remain fairly constant. However, the values obtained by Richardson–Zaki equation, decreased initially but they then increased with additive concentration. The reason could be explained as below: When ultrafines were added to the bed, they formed a fluffy structure around the host material causing a decrease in the effective particle density of the host material. However, there was an upper limit to the amount of ultrafines that could be added to the Group A powder and beyond that limit segregated ultrafines appeared in the powder. The increase in the terminal velocity, was probably because of particle clustering or cross–linking in fine powders.

As the concentration of ultrafines increased in the bed, the difference between U_{mf} and U_{mb} increased, therefore more experimental data of logU and logε were available. Also, maximum bed voidage used in equation (2.27), ε_{mb}, increased with addition of CAB–O–SIL to the bed. Hence the extrapolation of the line to $\varepsilon = 1$ was subject to less error and the values found for terminal velocities should be valid.

The bed expansion index, parameter n, increased with additive concentration because the bed was stabilized and allowed to expand over a much wider range of bed height and porosity. The n values found in this work were different from the ones suggested by

Fig. 4.5.3. Terminal velocity of FCC using different methods.

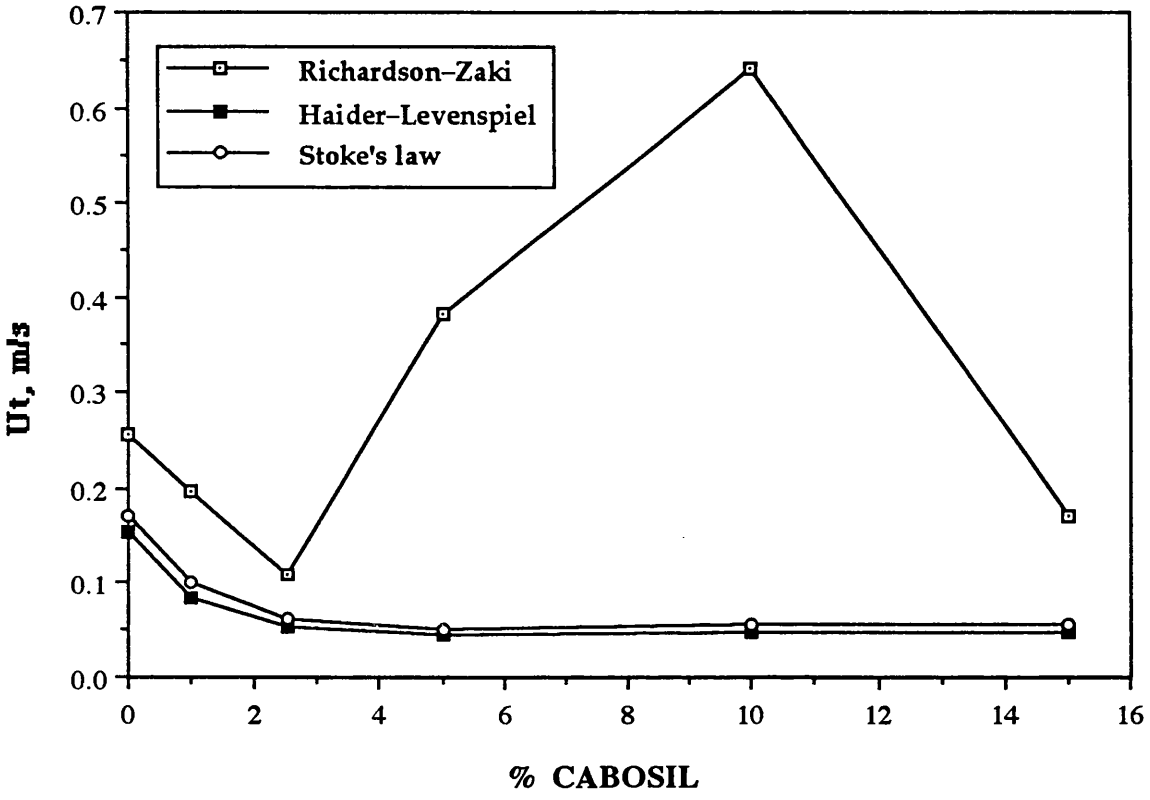

Fig. 4.5.4. Terminal velocity of silica by different methods.

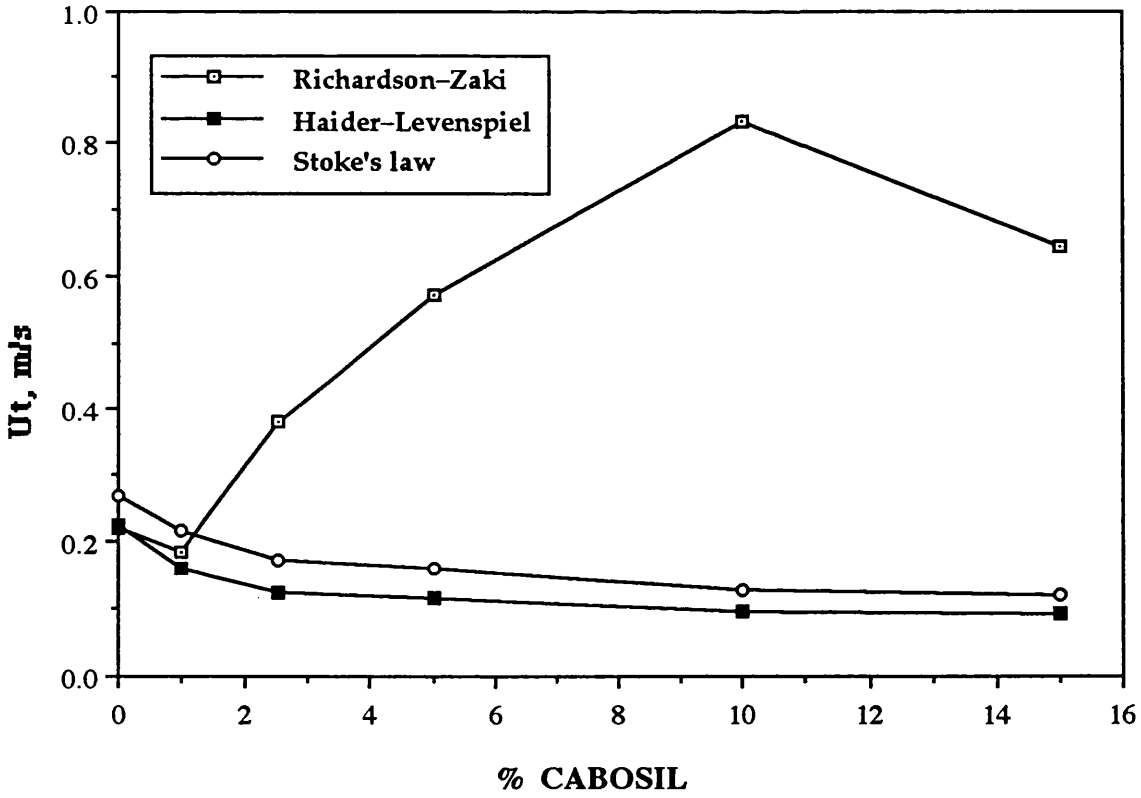

Richardson–Zaki (1954). But it should be considered that the original work of Richardson and Zaki was based on fluidization of *monosized* spherical particles in liquid–solid systems. Other researchers (Whitmore, 1957; Reiling, 1992) have already reported high values of n for gas–solid systems as already referred to in section 2.9.

4.5.3. Foscolo–Gibilaro's Model

Using the average fluid density and viscosity in Tables 4.5.1 and 4.5.2 and the Richardson–Zaki indices in Tables 4.5.3 and 4.5.4, the voidage at which transition from particulate to bubbling occurred, ε_b, according to Foscolo–Gibilaro's model (1984) was found using equation (2.26):

$$\frac{(gd_p)^{0.5}}{U_t}\left(\frac{\rho_p - \rho}{\rho_p}\right)^{0.5} \geq 0.56\, n\, (1-\varepsilon_b)^{0.5}\varepsilon_b^{n-1} \qquad (2.26)$$

The model predicted that as the concentration of ultrafines increased in the bed, the critical bed voidage ε_b should increase (Tables 4.5.7 and 4.5.8) which was in agreement with the experimental results. For FCC without any additive the predicted value of ε_b was 0.509 (Fig. 4.5.5) which increased to 0.859 for the sample containing 15% CAB–O–SIL. The voidage at which transition from particulate to aggregate occurred was found to be 0.580 for silica (Fig. 4.5.6) and increased to 0.810 for mixture of silica and 15% additive. The predicted values of ε_b were between 5–10% less than the experimental values as shown in Figs. 4.5.5 and 4.5.6.

When the values of terminal velocity found by Haider–Levenspiel's method were used together with the n values obtained from logU vs logε plots (Tables 4.5.3 and 4.5.4),

Fig. 4.5.5. Comparison of Foscolo–Gibilaro's model to the experimental values of bed voidage for FCC.

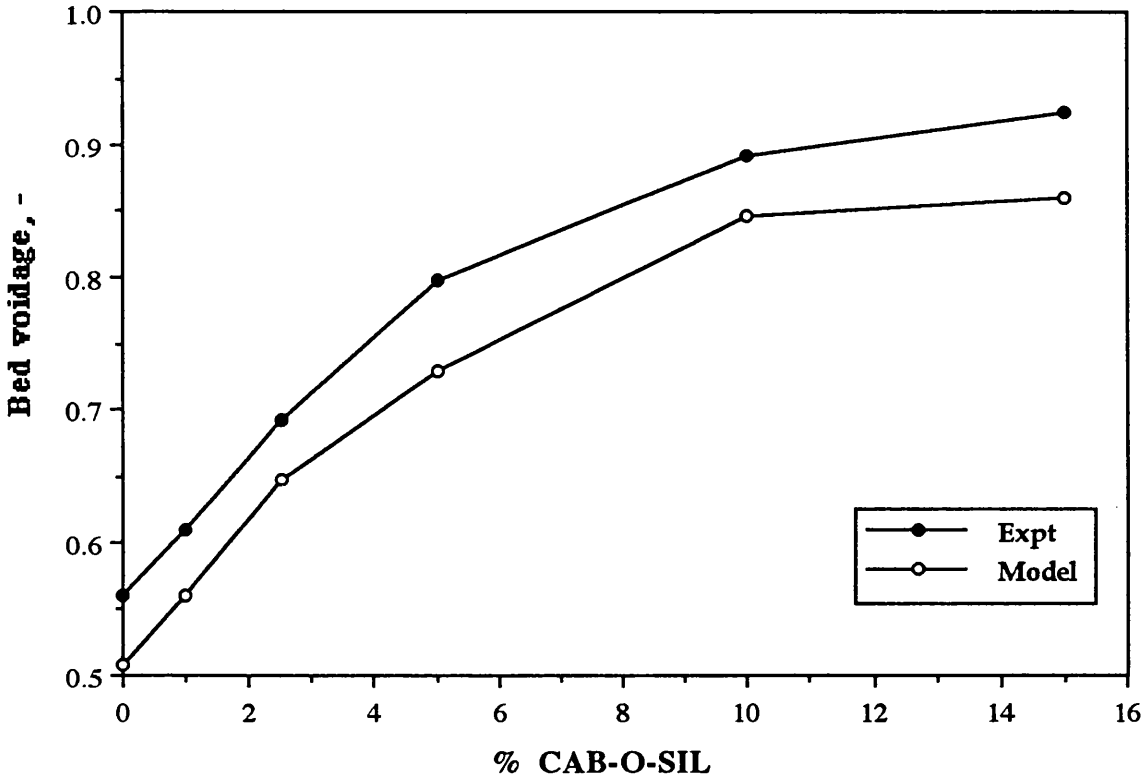

Fig.4.5.6. Comparison of Foscolo–Gibilaro's model to the experimental values of bed voidage for silica.

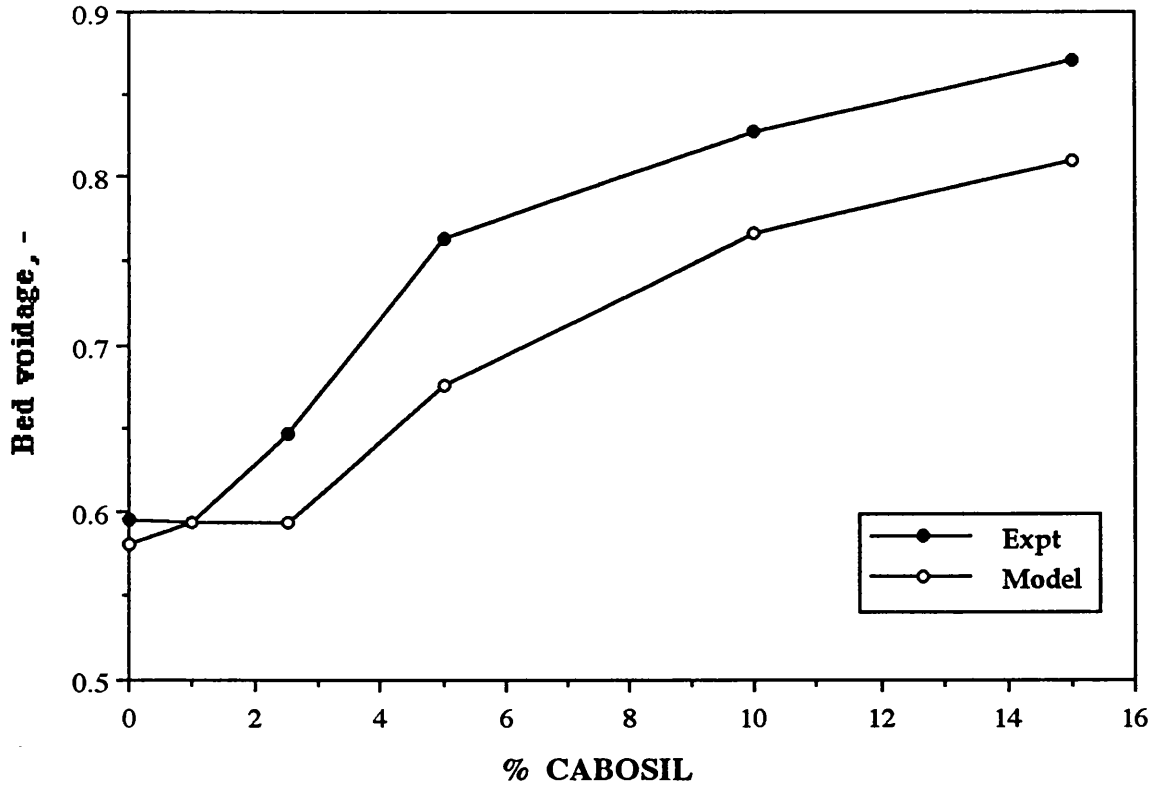

the ε_b for FCC was found to be 0.572 which was in good agreement with the experimental value of 0.561. The predicted bed voidage values increased with additive concentration except for the mixture containing 15% CAB–O–SIL. The drop at this point was due to the reduction of U_t found by Richardson–Zaki method. The bed voidage for silica was found to be 0.577 in this case, which was in good agreement with the experimental value of 0.595. Although there was a major difference between the terminal velocities found by different methods, changing U_t in Foscolo–Gibilaro's model did not lead to better agreement between predicted and experimental values of bed voidages which showed the importance of bed expansion index, n, comparing to U_t in the model.

Setting n equal to 4.8 and using U_t values obtained from both Richardson–Zaki and Haider–Levenspiel methods, the bed voidage at the transition point, ε_b, was found. The predicted values of ε_b were in general significantly less than the experimental data (Figs. 4.5.7 and 4.5.8). Values of n in the range suggested by Richardson–Zaki would provide unrealistically low values of ε_b, mainly in the range of 0.1–0.5.

For a range of n values, U_t was determined as shown in Figs. 4.5.9 and 4.5.10. Terminal velocity was found to be highly dependent on n for low concentrations of additives but as more ultrafines were added to the bed, the predicted terminal velocities remained fairly constant.

Table 4.5.7. Calculation of ε_b using Foscolo–Gibilaro model for FCC.

CAB–O–SIL (wt%)	Fluid density, kg/m^3	U_t, m/s (R–Z)	n	ε_b	ε_{mb}	$\frac{\varepsilon_b-\varepsilon_{mb}}{\varepsilon_{mb}}$ ×100	U_t, m/s (H–L)	ε_b	$\frac{\varepsilon_b-\varepsilon_{mb}}{\varepsilon_{mb}}$ ×100
0	1.214	0.2563	5.719	0.509	0.561	9.36	0.1541	0.572	1.91
1	12.199	0.1954	6.109	0.561	0.61	8.01	0.0836	0.686	12.48
2.5	20.203	0.1107	6.3344	0.650	0.692	6.14	0.0532	0.789	13.98
5	22.993	0.3836	14.374	0.728	0.797	8.61	0.0446	0.884	10.88
10	21.899	0.6418	32.65	0.846	0.892	5.17	0.0479	0.928	4.02
15	22.044	0.172	25.07	0.859	0.925	7.18	0.0474	0.919	–0.64

R–Z: Richardson–Zaki

H–L: Kunii–Levenspiel

Table 4.5.8. Calculation of ε_b using Foscolo–Gibilaro model for silica.

CAB–O–SIL (wt%)	Fluid density, kg/m^3	U_t, m/s (R–Z)	n	ε_b	ε_{mb}	$\frac{\varepsilon_b-\varepsilon_{mb}}{\varepsilon_{mb}}$ ×100	U_t, m/s (H–L)	ε_b	$\frac{\varepsilon_b-\varepsilon_{mb}}{\varepsilon_{mb}}$ ×100
0	1.214	0.2215	5.8561	0.580	0.5951	2.49	0.2251	0.577	3.00
1	6.016	0.1851	5.6875	0.593	0.5934	0.00	0.1606	0.612	–3.16
2.5	10.750	0.3825	7.6359	0.592	0.646	8.30	0.1242	0.719	–11.35
5	11.962	0.5712	11.5267	0.675	0.7636	11.63	0.1166	0.802	–5.08
10	15.579	0.8306	19.3601	0.766	0.8278	7.41	0.0962	0.876	–5.80
15	16.524	0.6414	23.438	0.810	0.8711	6.96	0.0914	0.895	–2.71

R–Z: Richardson–Zaki

H–L: Kunii–Levenspiel

Fig. 4.5.7. Predicted values of bed voidage for different terminal velocities using Foscolo–Gibilaro model (n= 4.8) for FCC.

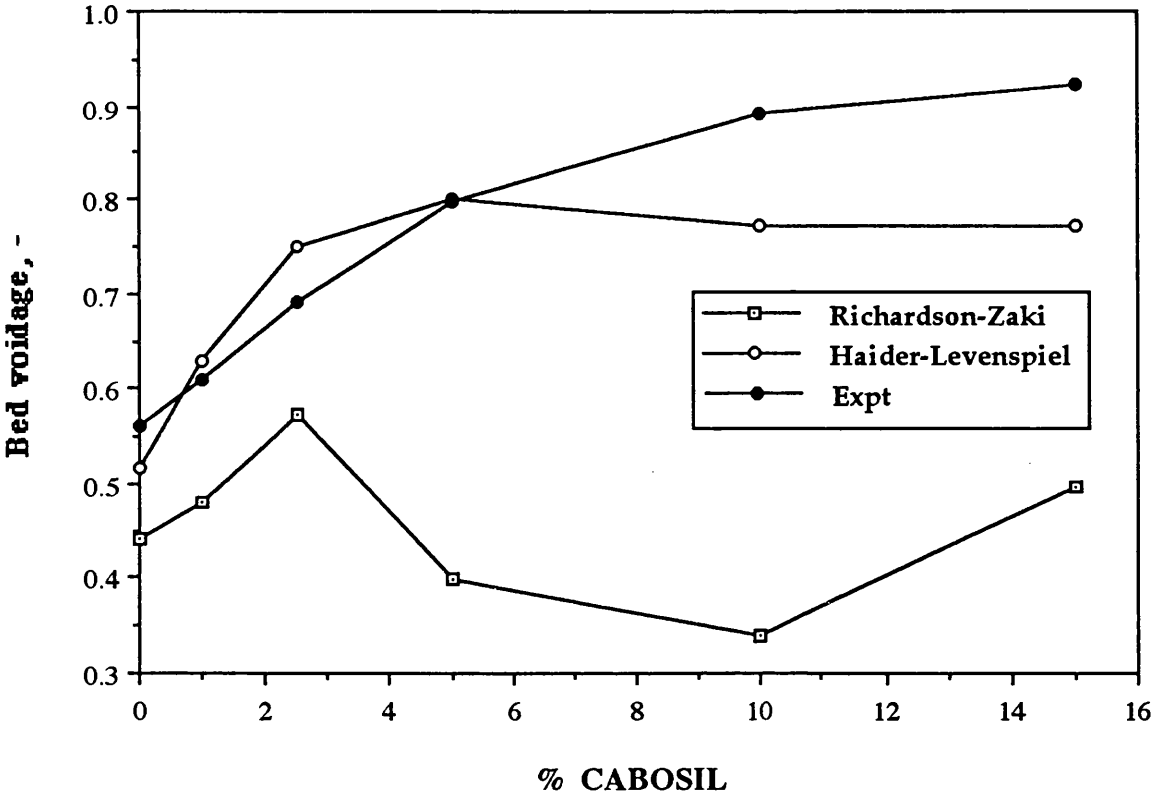

Fig. 4.5.8. Predicted values of bed voidage using different terminal velocities and Foscolo–Gibilaro model (n = 4.8) for silica.

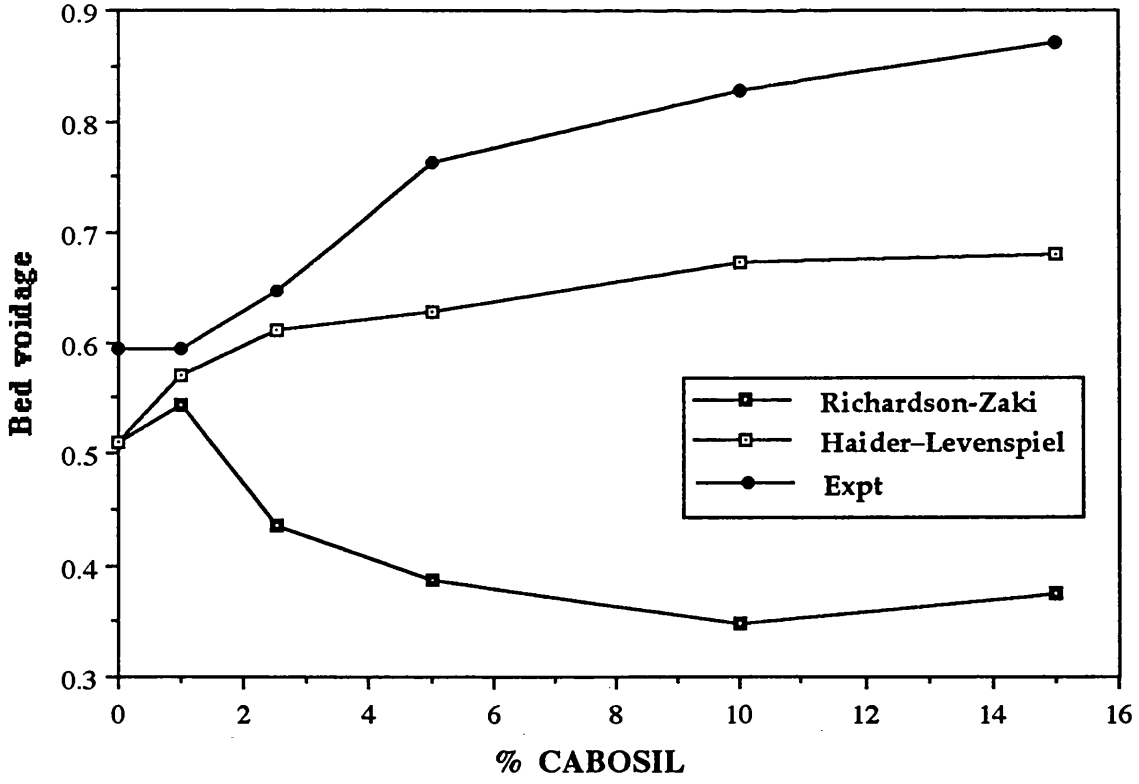

Fig. 4.5.9. Effect of n values on terminal velocities of FCC mixtures using Foscolo–Gibilaro's model.

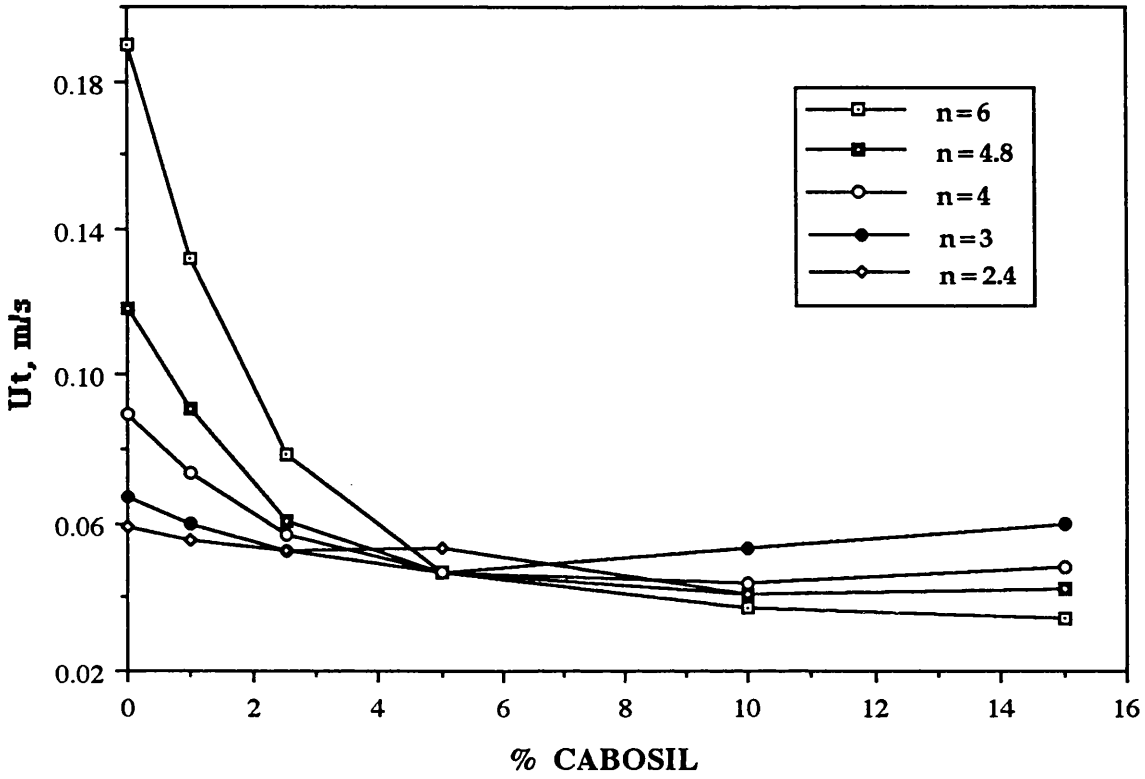

Fig. 4.5.10. Effect of n values on terminal velocities of silica mixtures using Foscolo–Gibilaro's model.

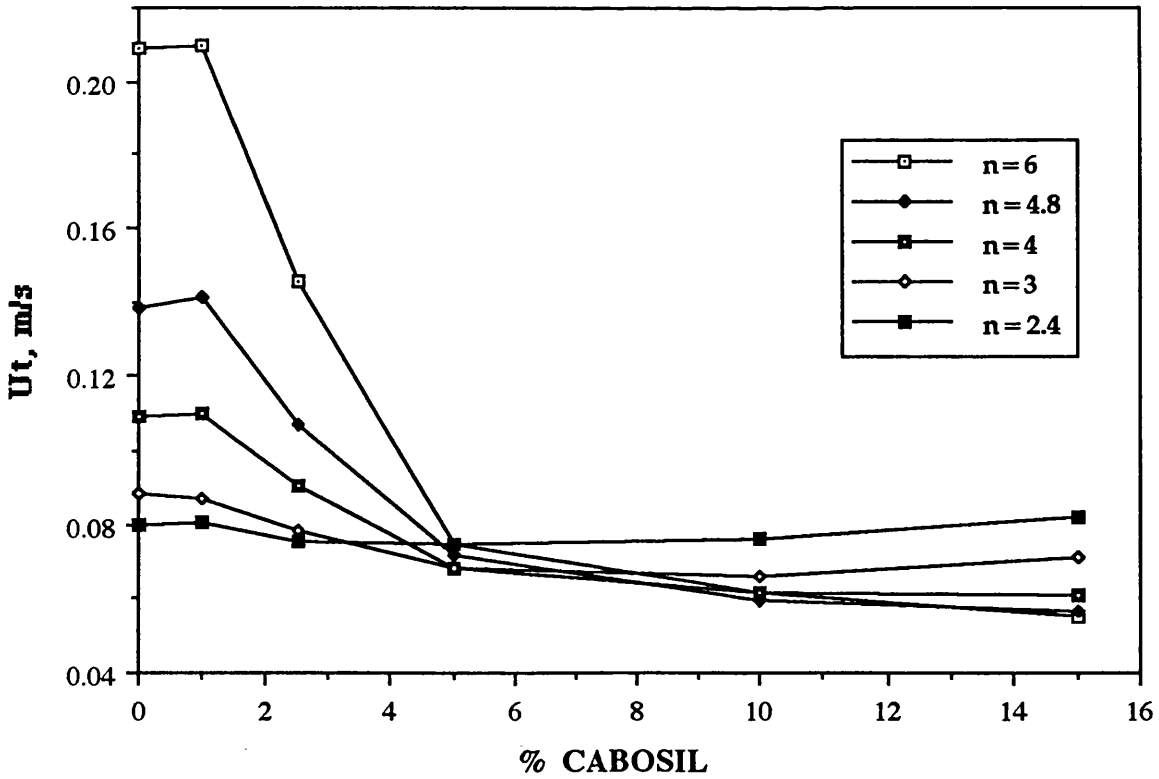

4.5.4. Mutsers–Rietema's Model

The density and viscosity of the continuous phase determined earlier together with the experimental minimum bubbling velocity, U_{mb}, were used in equation (2.23) and it was solved for ε:

$$N_F = \frac{\rho_d^3 d_p^4 g^2}{\mu^2 E} \leq \left\{\frac{150\,(1-\varepsilon)}{\varepsilon^2(3-2\varepsilon)}\right\}^2 \qquad (2.23)$$

The predicted values of bed voidage at the transition point according to Mutsers and Rietema (1977) slightly increased for FCC from 0.579 to 0.789 for the sample containing 15% CAB–O–SIL (Fig. 4.5.11). There was a good agreement between the experimental data in low concentrations of ultrafines and the predicted values (Table 4.5.9). As the additive concentration increased in the bed, the difference between the predicted values and ε_{mb} became more significant.

The model predicted a similar trend for silica as shown in Fig. 4.5.12. The bed voidage of silica at the transition point was found to be 0.580 which increased to 0.808 for the mixture of 15% CAB–O–SIL and silica. In this system, too, the difference between the predicted and experimental values of bed voidage were more significant at higher concentrations of ultrafines (Table 4.5.10). The viscosity of the continuous phase which is an important parameter in this model was found using an empirical equation suggested for liquids. As the concentration of ultrafines increased, the deviation between the true and calculated values of viscosity of the continuous phase increased which could be the reason for difference between the predicted and experimental bed voidages. Also the

Table 4.5.9. Calculation of ε_b using Mutsers–Ritema model for FCC.

CAB–O–SIL (wt%)	Fluid density, kg/m^3	Fluid viscosity, Ns/m^2 x 10^5	U_{mb}, m/s	ε_{mb}	ε_b	E, N/m^2 (at ε_b)	$\frac{\varepsilon_b-\varepsilon_{mb}}{\varepsilon_{mb}} \times 100$
0	1.214	1.750	0.0095	0.561	0.579	1.6073	–3.19
1	12.199	2.943	0.0095	0.61	0.648	1.0957	–6.29
2.5	20.203	4.780	0.0124	0.692	0.747	1.1014	–7.90
5	22.993	5.787	0.0120	0.797	0.766	0.9290	3.86
10	21.899	5.361	0.0180	0.892	0.805	1.6994	9.75
15	22.044	5.415	0.0155	0.925	0.789	1.3732	14.71

Table 4.5.10. Calculation of ε_b using Mutsers–Ritema model for silica.

CAB–O–SIL (wt%)	Fluid density, kg/m^3	Fluid viscosity, Ns/m^2 × 10^5	U_{mb}, m/s	ε_{mb}	ε_b	E, N/m^2 (at ε_b)	$\frac{\varepsilon_b-\varepsilon_{mb}}{\varepsilon_{mb}}\times 100$
0	1.214	1.750	0.0115	0.5951	0.580	1.6502	2.47
1	6.016	2.147	0.0095	0.5934	0.582	1.1168	1.86
2.5	10.750	2.720	0.014	0.646	0.6747	1.6716	–4.44
5	11.962	2.904	0.026	0.7636	0.7730	4.028	–1.24
10	15.579	3.573	0.0195	0.8278	0.7620	2.3549	7.95
15	16.524	3.783	0.026	0.8711	0.8077	3.5753	7.27

Fig. 4.5.11. Comparison of the experimental bed voidage to Mutsers–Rietema's model for FCC.

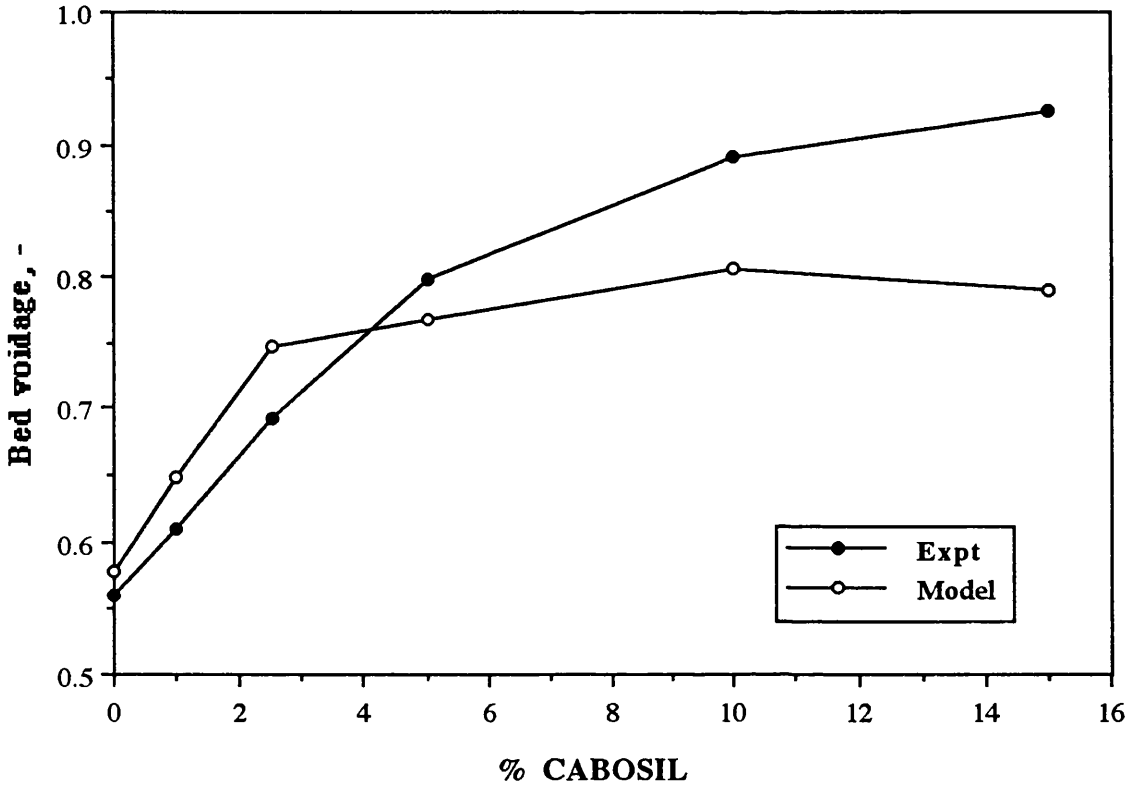

Fig. 4.5.12. Comparison of the experimental bed voidage to Mutsers–Rietema's model for silica.

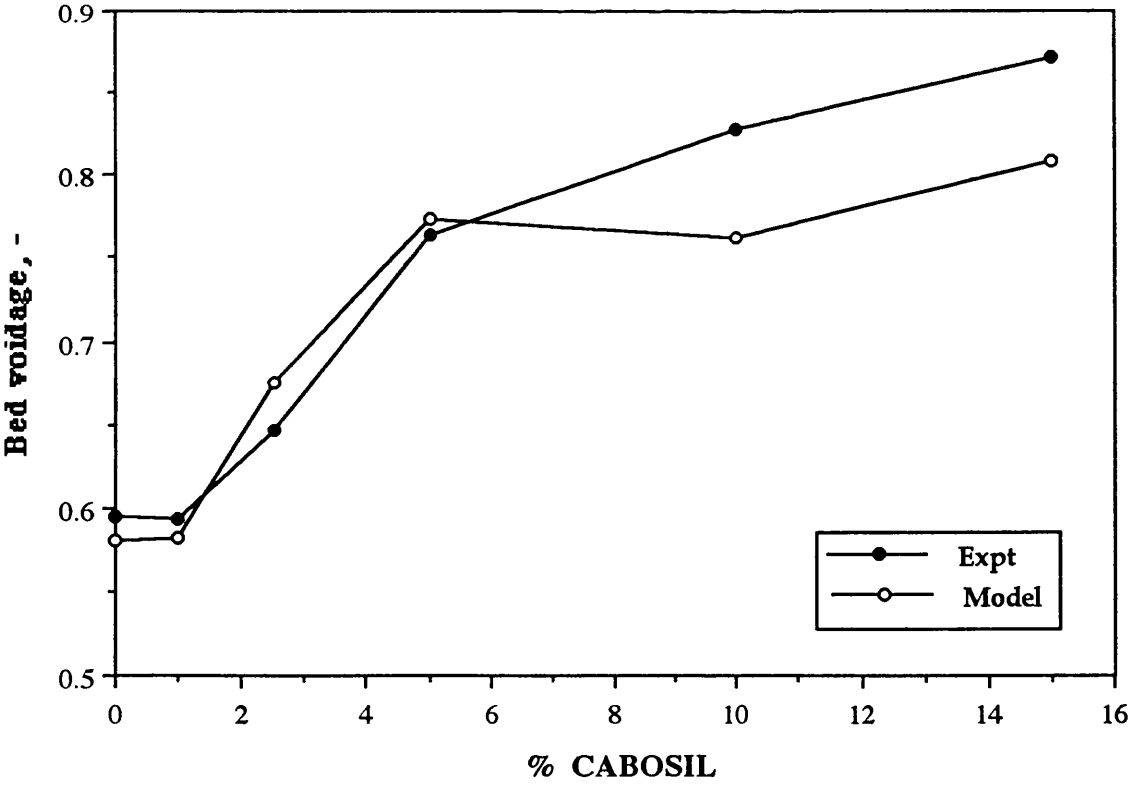

difference between U_{mf} and U_{mb} increased with concentration of ultrafines, therefore hydrodynamic forces should not be ignored in this model.

4.5.5. Reiling's model

The hypothetical pressure drop at incipient bubbling, ΔP^*_{mb} was found by extrapolating the bed pressure drop to U_{mb} as shown in Fig. 2.7. Using equation (2.35), the bed voidage at which transition from particulate to aggregate occurs can be found:

$$n\, U_t\, (1-\varepsilon)\, \varepsilon^{n-1} = \left[\frac{d_p . \Delta P^*_{mb}}{\rho_p . H_{mb}} \cdot \frac{\varepsilon_{lp}}{\varepsilon_{mb}\left(\varepsilon_{mb} - \varepsilon_{lp}\right)} \right]^{1/2} \qquad (2.35)$$

The parameters required in Reiling's model together with the results are shown in Tables 4.5.11 and 4.5.12. The model predicted the bed voidage at the transition point for FCC to be 0.540 (Table 4.5.11) and addition of 15% CAB–O–SIL would raise this voidage to 0.925. There was a good agreement between the experimental and predicted values as shown in Fig. 4.5.13.

The predicted critical bed voidage was 0.621 (Table 4.5.12) for silica which would increase up to 0.858 for the 15% blend. There was a good agreement between these values and the experimental data of ε_{mb} (Fig. 4.5.14); specially at higher concentrations of ultrafines the difference between the predicted and experimental values was negligible. Therefore, hydrodynamic forces and interparticle forces should both be considered in stability of fluidized beds. Using the terminal velocities obtained from Haider–Levenspiel's method increased the error in Reiling's model significantly.

Table. 4.5.11. Calculation of ε_b using Reiling's model for FCC.

CAB–O–SIL (wt%)	U_t, m/s	n	ΔP^*_{mb}, Pa	H_{mb}, m	ε_{mb}	ε_{lp}	ε	$\frac{\varepsilon_b-\varepsilon_{mb}}{\varepsilon_{mb}}\times 100$
0	0.2563	5.719	2276.22	0.165	0.561	0.336	0.540	–3.82
1	0.1954	6.109	1836.34	0.167	0.61	0.416	0.605	–0.82
2.5	0.1107	6.3344	2514.56	0.200	0.692	0.602	0.786	13.62
5	0.3836	14.374	1873.14	0.178	0.797	0.671	0.789	–0.97
10	0.6418	32.65	2333.13	0.201	0.892	0.811	0.894	0.18
15	0.172	25.07	1374.78	0.231	0.925	0.854	0.925	–0.06

Table 4.5.12. Calculation of ε_b using Reiling's model for silica.

CAB-O-SIL (wt%)	U_t, m/s	n	ΔP^*_{mb}, Pa	H_{mb}, m	ε_{mb}	ε_{lp}	ε	$\frac{\varepsilon_b-\varepsilon_{mb}}{\varepsilon_{mb}}\times 100$
0	0.2215	5.8561	871.908	0.219	0.595	0.440	0.621	4.34
1	0.1851	5.6875	580.683	0.176	0.593	0.496	0.654	10.26
2.5	0.3825	7.6359	695.544	0.201	0.646	0.546	0.659	1.97
5	0.5712	11.5267	1266.749	0.225	0.764	0.592	0.736	-3.59
10	0.8306	19.3601	2296.043	0.309	0.828	0.659	0.819	-1.05
15	0.6414	23.438	2059.472	0.344	0.871	0.705	0.858	-1.47

Fig. 4.5.13. Comparison of the experimental bed voidage to Reiling's model for FCC.

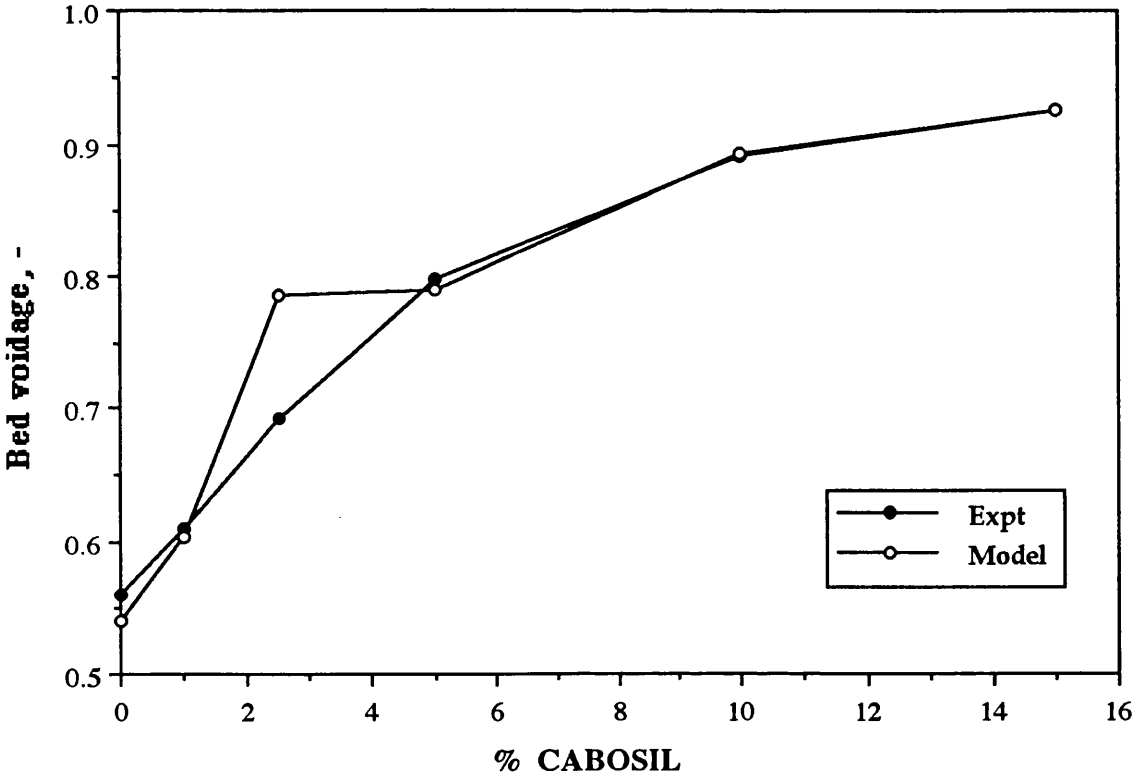

Fig. 4.5.14. Comparison of the experimental bed voidage to Reiling's model for silica.

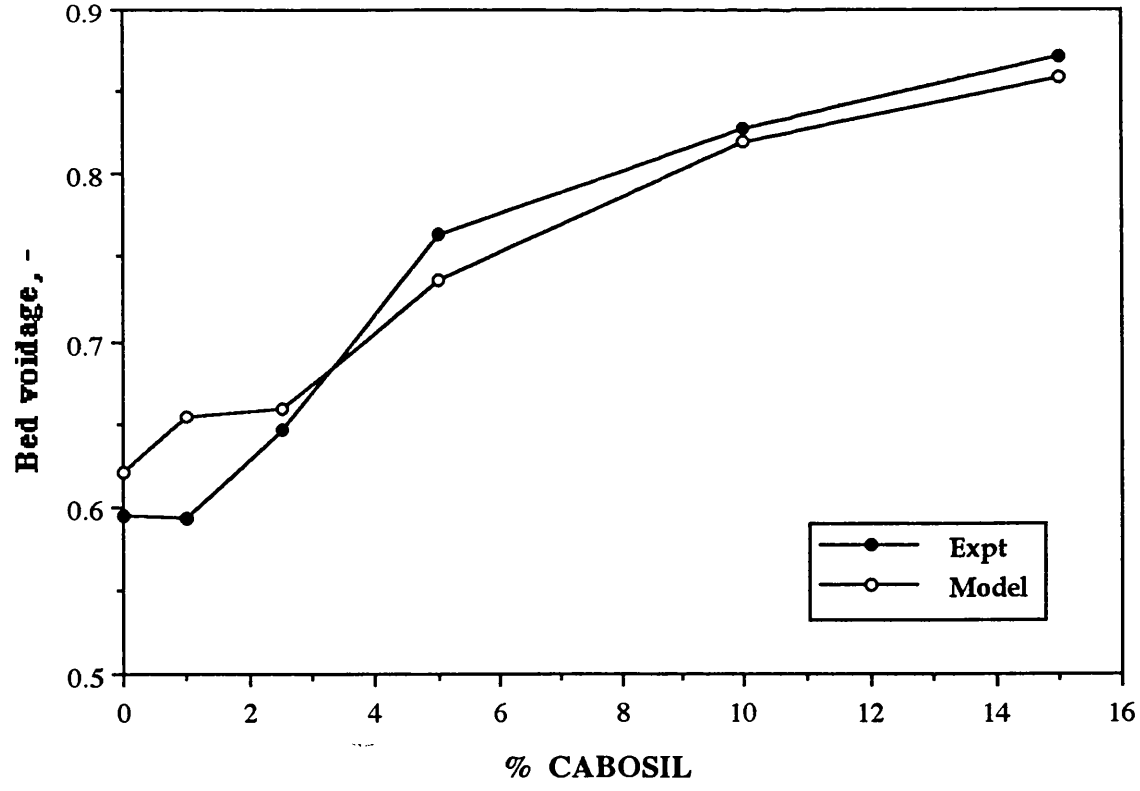

4.5.6. Discussions

Addition of ultrafines increased the bed expansion of Group A powders, therefore, the bed expansion index, n, increased. There was a good linear relationship between logU and logε. As the additive content in the bed increased, the maximum bed voidage, ε_{mb}, which was used in the plots of logU versus logε increased. Also more data points were available to be used in the plot, since bubbling was significantly delayed as a result of addition of CAB–O–SIL to the blends. Hence the extrapolation of the lines to $\varepsilon = 1$ was subject to less error.

Experimental values of n were larger than the recommended values of Richardson–Zaki (1954) but their original work was carried out on *monosized* particles, dissimilar to the blends investigated here.

Terminal velocity of the blends initially decreased which could be due to coverage of host particles by CAB–O–SIL leading to a smaller *effective* particle density. As more ultrafines were present in the blend, the terminal velocity increased which was probably because of particle clustering or cross–linking in fine powders.

The experimental values of bed voidage when transition from particulate to aggregate fluidization occurred, ε_{mb}, were compared to the predictions of three different models (Figs. 4.5.15 and 4.5.16). Predictions of Foscolo–Gibilaro's model, which is based only on the importance of hydrodynamics in the bed, were always below the experimental values by 5–12%. Therefore, according to this model, the systems should have been unstable. This model ignores the importance of interparticle forces which were found to increase by addition of ultrafines to the bed (see section 4.3).

The model of Mutsers–Rietema predicted ε_b to be in a fairly good agreement with the experimental results at low CAB–O–SIL concentrations and the systems were mostly predicted to be stable. However, at concentrations of 10–15% the predicted values were 8–15% lower than ε_{mb} which would imply unstability in fluidization. This model underestimates the hydrodynamic forces which become more important as U_{mb} increases with the concentration of ultrafines. Viscosity of the continuous phase which is an important parameter in this model, was calculated using an empirical method suggested for liquids. This can also affect the predicted values. Deviations of μ from the real values would probably increase as the concentration of the ultrafines increases.

There was a good agreement between the experimental values of ε_{mb} and the predicted values of Reiling's model which is based on the importance of interparticle forces as well as the hydrodynamics in the bed. There were no adjustable parameters in this model, therefore the uncertainty associated with the other two models in working out the properties of the continuous phase would not affect the results. In general, the agreement of this model with the experimental data was better than the other models.

Fig. 4.5.15. Comparison of experimental bed voidage with different predictions for FCC mixtures.

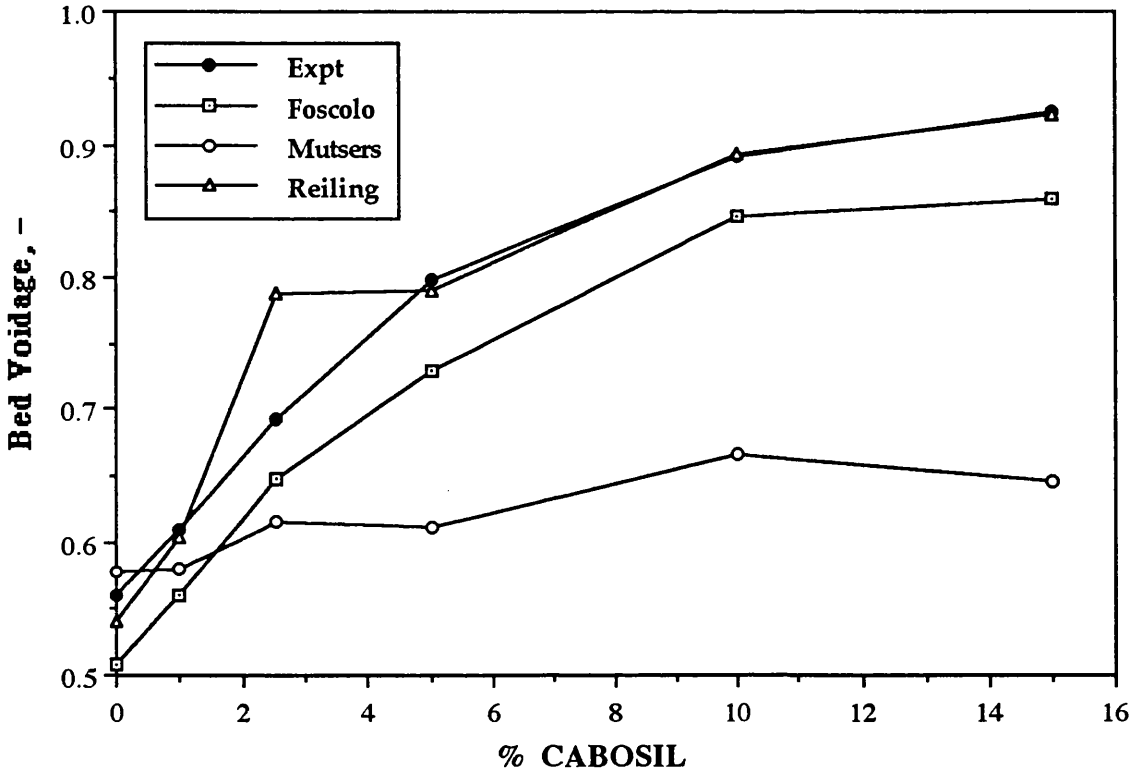

Fig. 4.5.16. Comparison of experimental bed voidage with different predictions for silica mixtures.

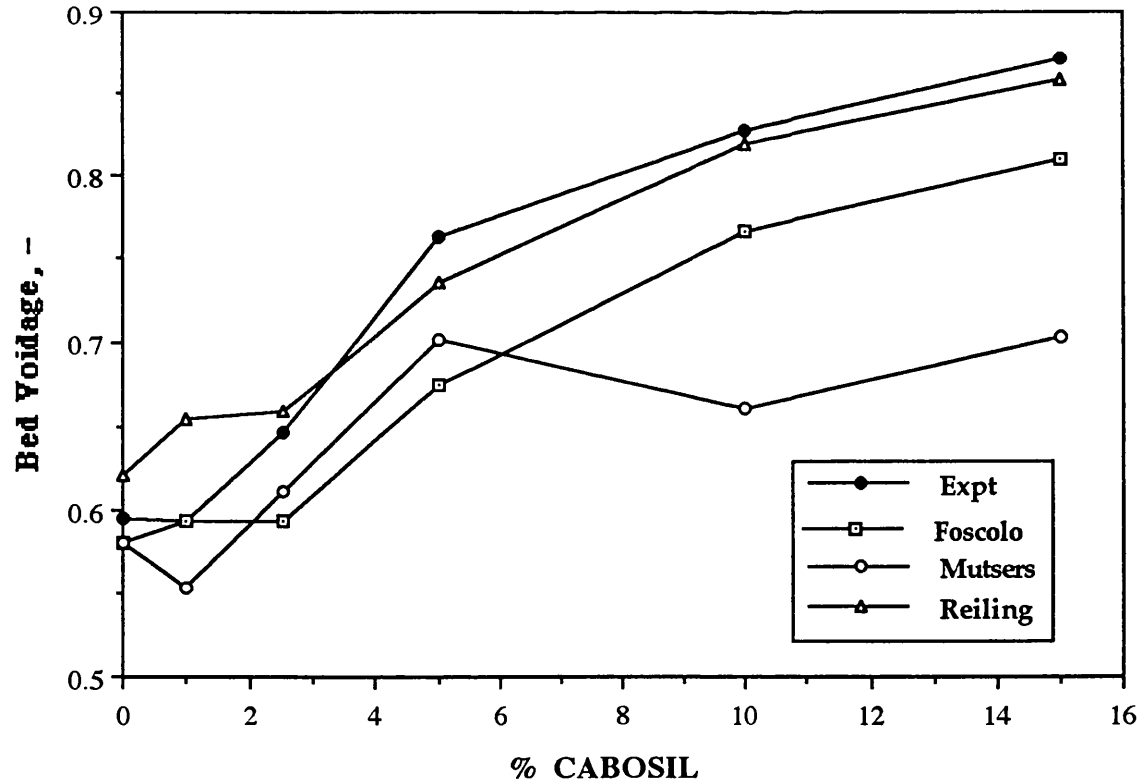

CHAPTER FIVE

CONCLUSIONS AND RECOMMENDATIONS FOR FURTHER STUDY

5.1. Conclusions

There appears to be a *saturation* limit where host particles are covered; beyond that limit ultrafines segregate from the bulk mixture and form agglomerates which are larger than their primary particle size but smaller than those of neat particles. This saturation limit is one of the physical properties of the host material and depends on the particle shape and the surface area of the host material not on its particle size. At low loadings, the Group C ultrafine particles appeared to prefer to adhere to and evenly coat the outer surfaces of the Group A host particles. The ultrafines interspersed themselves randomly on the surface of the host material. As the ultrafines content increased, the additives interacted with one another and formed agglomerates or secondary particles larger than their primary diameter. Eventually, the ultrafines form solid–solid bridges among themselves, giving rise to a cross–linked type particle network.

There was a fairly uniform distribution of the additives at the surface of the host material which suggested that ultrafines acted as bridges and did not merely fill the interparticle voids. There was not a significant change in the host surface coverage by additives between initial and final bed samples which showed that the force holding the additives to the host particles was stronger than the drag force applied by the fluid bed.

Reduction in the bulk density of FCC and silica mixtures by addition of CAB–O–SIL also confirmed that the ultrafines did not merely fill the interparticle voids. Rather they formed a particular network which resulted in a looser bed structure and an increase in the bed voidage. The change in the bulk density depended on the particle shape of the host material and ultrafines. The maxima in bulk density for kiesel–1 mixtures corresponded to 3% S1 fumed silica while the bulk density of kiesel–2 mixtures peaked at 1% CAB–O–SIL concentration. The change was due to more irregular shape of kiesel–1 particles comparing to kiesel–2.

Ultrafines could easily develop a negative charge by contact electrification. Therefore they tended to part and disperse evenly in mixtures but their contact during processes such as fluidization cannot be avoided. This could affect the fluidization of the material.

It appeared that the fluidization properties of powders depended more on the concentration and type of ultrafines added and less on the host material. The minimum fluidization velocity of FCC and silica blends decreased with addition of CAB–O–SIL to the bed. This was attributed to a decrease in the *effective* particle density of the host material as they were covered with additives. Addition of ultrafines resulted in the formation of a more porous bed structure which was more capable of holding the gas within itself and increased the U_{mb}. It should be noted that U_{mb} was always bigger than U_{mf}. Thus, a feature that is characteristic of Group A powders still remains even when they are mixed with a Group C powder.

Kieselguhr with different shapes demonstrated dissimilar fluidization behaviour which suggested that particle shape of the host material was an important factor as it would affect the network formed by ultrafines and host particles.

Since U_{mb} increased and U_{mf} decreased with addition of ultrafines, there was an increase in the excess interstitial gas flow which allowed the bed to expand further prior

to the onset of bubbling and gave rise to the large bed expansions. This is extremely advantageous in achieving better gas–solid contact. Considering that U_{mf} decreases with the bed diameter up to a limit (Rowe and Everett, 1972), the effect is more pronounced in larger columns providing that U_{mb} does not change with the bed size. CAB–O–SIL increased U_{mb}/U_{mf} by a factor of about 9 for FCC and silica blends. Therefore 9 times as much gas could pass through the emulsion phase before the onset of bubbling.

Normalized pressure drop increased in the bed which was an indication of an increase in the bed cohesion. This was not unexpected since ultrafines were cohesive Group C particles which would impart cohesion to the blend. However, as the concentration of ultrafines increases in the bed, a critical limit would be reached where the blend becomes too cohesive to show favourable fluidization behaviour. This confirms the existence of an optimum limit where further addition of ultrafines could reverse the desirable effects.

The elutriation loss decreased as ultrafine concentration increased in the bed which was due to the increase in cohesion and the formation of a particular bed structure which kept the particles together and prevented them from moving freely and/or leaving the bed.

Addition of CAB–O–SIL increased the deaeration velocity of FCC and silica mixtures. The large deaeration velocity means that the air could escape more rapidly from the powder, allowing it to deaerate and settle faster. This could only be possible for a bed with a more porous structure. Therefore the deaeration velocity can be related to the porosity of the emulsion phase, the strength of interparticle networks and cohesion.

Dense phase expansion of FCC and silica blends were in good agreement with the expansions found by simple fluidization experiments which confirmed that the expansions observed during fluidization mainly occurred in the dense phase. The dense phase expansion of both FCC and silica increased significantly up to 10% CAB–O–SIL concentration and addition of another 5% of ultrafines did not improve this expansion.

Addition of ultrafines increased the bed expansion of Group A powders, therefore, the bed expansion index, n, increased up to 25 which were larger than the recommended values of Richardson–Zaki. Terminal velocity of the blends initially decreased which could be due to coverage of host particles by CAB–O–SIL leading to a smaller *effective* particle density. As more ultrafines were present in the blend, the terminal velocity increased which was probably because of particle clustering or cross–linking in fine powders.

Comparing the experimental data to different stability models, showed that there was a better agreement between the experimental results and Reiling's model. The model considers interparticle forces as well as hydrodynamic effects in the bed which implied that these forces were both of importance in the stability of the bed.

5.2. Recommendations for Further Study

Considering that presence of ultrafines increased the cohesion of the bed, there is probably an upper limit for the amount of ultrafines that could be added to the blend which would improve the fluidization quality. Addition of ultrafines beyond that limit would change the behaviour of the blend from a Group A to a Group C. Experiments with higher additive concentrations should therefore be carried out to determine that limit.

Using ultrafines with distinct and different physical properties are recommended for further study to distinguish the important characteristics of additives in improving the quality of fluidization of different powders. Also further investigation is required to study the important factors in agglomeration and/or segregation of the additives from the powder blends.

Suspended bed technique could be employed to measure the interparticle forces in situ. Also the fluidized bed could be connected to an electrometer to detect the electrostatic charges, if any, and study their effects on the quality of fluidization.

APPENDIX A

DERIVATION OF REILING'S MODEL

The velocity of an elastic wave in any isothermal, compressible fluid is given as (Massey, 1979):

$$U_e = \sqrt{\frac{\delta P^*}{\delta \rho_b}} \qquad (A1)$$

where δP^* is the pressure drop across the wave and ρ_b is the density of the emulsion phase. This quantity represents the rate at which pressure changes with density in a gas–solid fluidized bed.

Assuming that the tensile strength of the emulsion phase at $U_o<U_{mb}$ is proportional to the viscous drag across the particles and also that the net pressure drop (excluding gravity) across any two vertical points in the bed is equal to the difference in tensile strength, (e.g. $\sigma_{t,\varepsilon}$ and $\sigma_{t,lp}$):

$$\sigma_{t,\varepsilon} - \sigma_{t,lp} = C\,(P_{lp} - P_{\varepsilon}) \qquad (A2)$$

where C is the proportionality constant and for an infinitesimal pressure disturbance δP^* can thus be given as:

$$C\,\delta P^* = \delta\sigma_{t,\varepsilon} \qquad (A3)$$

The pressure drop across a single layer of particles and the tensile strength at the horizontal stress plane is (Kono et al., 1987):

$$C^* = \frac{\text{interparticle forces across a single layer of particles}}{\text{drag force acting on a single layer of particle}} \qquad (2.31)$$

$$C^* = \frac{\delta\sigma_t}{\delta P^*} = \frac{(\sigma_{t,lp} - \sigma_{t,mb})}{\Delta P^*_{mb}} \cdot \frac{H_{mb}}{d_p} \qquad (2.32)$$

where $\sigma_{t,lp}$ is the tensile stress of the loose packed powder and ΔP^*_{mb} is the bed pressure drop at incipient bubbling velocity (see p.66). Note that C^* is a dimensionless quantity. The elastic wave velocity then follows from the analysis of Eq. A1:

$$U_e = \sqrt{\frac{dP^*}{d\rho_b}} = \sqrt{\frac{dP^*}{d\sigma_t} \cdot \frac{d\sigma_t}{d\varepsilon} \cdot \frac{d\varepsilon}{d\rho_b}} \qquad (A\,4)$$

The first term within the radical is given by the inverse of Eq.(2.32) or $1/C^*$. The second term follows from Rumpf's (1970) equation:

$$\left.\frac{d\sigma_t}{d\varepsilon}\right|_{\varepsilon_{mb}} = \frac{-\sigma_{t,mb}}{\varepsilon_{mb}(1-\varepsilon_{mb})} \qquad (A\,5)$$

The third term simply follows by taking the derivative of:

$$\rho_b = \rho_p\,(1-\varepsilon) \qquad (A6)$$

$$\frac{d\rho_b}{d\varepsilon} = -\rho_p \qquad (A\,7)$$

Substituting Eqs. (2.32), A5 and A7 in A4 and rearranging, gives the final expression for the elastic wave velocity:

$$U_e = \sqrt{\frac{\sigma_{t,mb}}{C^*\rho_p(1-\varepsilon_{mb})\varepsilon_{mb}}} \qquad (2.30)$$

Nomenclature and Abbreviations

a	Parameter in equations (3.9) to (3.12)
a_m	Measured value of a
a_t	True value of a
A	Bed cross–sectional area, m^2
b	Clearance in equation (3.3), m
b	parameter in equations (3.9) to (3.12)
b_m	Measured value of b
b_t	True value of b
C*	Proportionality constant, –
Co	Cohesion number, –
d_a	Diameter of sieve aperture, m
d_p	Particle size, m
d_p^*	Dimensionless particle size, –
$\bar{d}_{sm}$	Surface mean diameter as defined in equation (2.8), m
D	Bed diameter, m
E	Maximum sustainable particle surface field, V/m
E	Elasticity coefficient of the powder structure, N/m^2
E_{mb}	Elasticity coefficient at minimum bubbling conditions, N/m^2
F_c	Electrostatic force of adhesion, N
F_H	Capillary force of adhesion, N
F_M	Electromagnetic force of adhesion, N
F_u	Attraction force due to a difference in work functions, N
F_w	Van der Waals attraction force, N
g	gravitational acceleration, m/s^2
Ga_d	Gallilei number of the dense phase, –
h	Hardness of the solid, N/m^2

h_w	Lifshitz–van der Waals Constant, J
H	Bed height, m
H_d	Bed height of the dense phase, m
H_{mb}	Bed height at incipient bubbling velocity, m
H_{mf}	Bed height at minimum fluidization, m
H_o	Initial bed height, m
H_s	Bed height of settled bed, m
L	Height of material in the viscometer, m
m_{add}	weight of the additive in the bed, kg
m_h	weight of the host material, kg
n	Richardson–Zaki index, –
N	Rotation speed, rpm
N_F	Fluidization number, –
p	Degree of magnetization, N.m/A
ΔP	Bed pressure drop, Pa
ΔP^*_{mb}	Bed pressure drop at incipient bubbling velocity, Pa
q	Particle charge, C
Q	Volumetric gas flow rate, m^3/s
Q_B	Volumetric bubble flow rate, m^3/s
r_1	Radius of the inner cylinder in the viscometer, m
r_2	Radius of the outer cylinder in the viscometer, m
r_p	Particle resistivity, Ω.m
R	Particle radius, m
R_1	Particle radius, m
R_2	Particle radius, m
Re_t	Reynolds number for unhindered settling particle, –
t	Bed thickness, m
t	time, s

T	Torque, N.m
u	Velocity, m/s
U	Superficial velocity of the fluidizing gas, m/s
U^*	Dimensionless gas velocity, –
U_e	Elastic wave velocity, m/s
U_ε	Voidage propagation velocity, m/s
U_F	Minimum fluidization velocity of the fluid component, m/s
U_i	Superficial velocity corresponding to $\varepsilon = 1$, m/s
U_M	Minimum fluidization velocity of a completely mixed bed, m/s
U_{mb}	Minimum bubbling velocity, m/s
U_{mf}	Minimum fluidization velocity, m/s
U_{MS}	Minimum fluidization velocity of a partially mixed bed, m/s
U_P	Minimum fluidization velocity of the packed component, m/s
U_S	Minimum fluidization velocity of a completely segregated bed, m/s
U_S	Minimum slugging velocity, m/s
U_t	Particle terminal unhindered settling velocity, m/s
ΔU	Potential difference in equation (2.14), V
V_{add}	Volume of additive, m^3
V_{con}	Volume of continuous phase, m^3
V_t	Total bed volume, m^3
W	Total weight of the bed, kg
x	Mass fraction of particles, –
y	Volumetric fraction of additives in air, –
y	Distance, m
Z	Separation distance, m

Greek

γ	Surface tension of fluid, N/m

ε	Bed porosity, –
ε_b	Voidage at limiting bubbling conditions, –
ε_{cr}	Critical porosity, –
ε_e	Voidage of the stationary state, –
ε_{lp}	Porosity of the loose packed powder, –
ε_{max}	Maximum porosity, –
ε_{mb}	Voidage at minimum bubbling conditions, –
ε_{mf}	Porosity at minimum fluidization, –
ε_o	Permittivity of vacuum, F/m
ε_p	Permittivity of particle, F/m
θ	Characteristic relaxation time, t
μ	Fluid viscosity, Pa.s
μ_{add}	Viscosity of additive, Pa.s
μ_{air}	Viscosity of air, Pa.s
μ_o	Permeability of material, N/A^2
π	Constant, –
ρ	Fluid density, kg/m^3
ρ_{add}	Particle density of the additive, kg/m^3
ρ_{air}	Density of air, kg/m^3
ρ_d	Density of the dispersed phase, kg/m^3
ρ_g	Gas density, kg/m^3
ρ_p	Particle density, kg/m^3
$\sigma_{t,lp}$	Tensile stress of loose packed powder, Pa
$\sigma_{t,mb}$	Tensile stress of emulsion phase at incipient bubbling velocity, Pa
τ	Shear stress, Pa
ϕ	Sphericity factor, –

Abbreviations

BD	Bulk Density
HR	Hausner Ratio
RH	Relative Humidity
SD	Skeletal Density
TD	Tapped Density
TDH	Transport Disengaging Height

REFERENCES

Abrahamsen A R and Geldart D, 1980. Behaviour of Gas–Fluidized Beds of Fine Powders. Part II. Voidage of Dense Phase in Bubbling Beds. Powder Tech., **26**, 47–55.

Agbim J A, Nienow A W and Rowe P N, 1971. Interparticle Forces that Suppress Bubbling in Gas Fluidized Beds. Chem. Eng. Sci., **26**, 1293–1294.

Allen T, 1990. Particle Size Measurement, Chapman and Hall, 4th ed.

Ashton M D, Farley R, Valentin F H H, 1964. Improved Apparatus for Measuring Tensile Strength of Powders. J. of Sci. Instruments, **37**, 480–485.

Atkinson, K E; 1989. An Introduction to Numerical Analysis, 2nd ed., John Wiley & Sons, New York, p. 23–29.

Avedesian M M, 1977. Paper presented at Advances in Gas Fluidization Course, New Jersey.

Baerns M, 1966. Effect of Interparticle Adhesive Forces on Fluidization of Fine Particles. Ind. Eng. Chem. Fundam., **5**, 508–516.

Baeyens J, Geldart D and Wu S Y, 1992. Elutriation of Fines from Gas Fluidized Beds of Geldart A–type Powders; Effect of Adding Superfines. Powder Tech., **71**, 71–80.

Bailey A G, 1984. Electrostatic Phenomena during Powder Handling. Powder Tech., **37**, 71-85.

Baker C G J and Geldart D, 1978. An Investigation into the Slugging Characteristics of Large Particles. Powder Tech., **19**, 177–187.

Barnea E and Mizrahi J, 1976. On the Effective Viscosity of Liquid–Liquid Dispersions. Ind. Engng. Chem. Fundam. **15**, 120–125.

Baron T, Briens C L, Bergougnou M A,Hazlett J D 1987. Electrostatic Effects on Entrainment from a Fluidized Bed. Powder Tech., **53**, 55–67.

Boehme G, Krupp H, Rabenhorst H and Sandstede G, 1962. Adhesion Measurements Involving Small Particles. Trans. Inst. Chem. Eng., **40**, 252–259.

Briens C L, Bergougnou M A and Baron T, 1988. Prediction of Entrainment from Gas–Solid Fluidized Beds. Powder Tech., **54**, 183–196.

Briens C L, Bergougnou M A, Inculet I I, Baron T, Hazlett J D, 1992. Size Distribution of Particles Entrained from Fluidized Beds: Electrostatic Effects. Powder Tech., **70**, 57–62.

Brooks E F, 1991. Private communication.

Brooks E F and Fitzgerald T J, 1985. Aggregation and Fluidization Characteristics of a Fibrous Carbon. Paper presented at the 77th AIChE Annual Meeting, Chicago.

Brooks E F and Fitzgerald T J, 1986. Fluidization of Novel Tendrillar Carbonaceous Materials. in Fluidization V, Proc. of the 5th Eng. Found. Conf. on Fluidization, Eds. Ostergaard K and Sorensen A, Eng. Found., New York, 217–224.

Brunauer S, Emmett P H and Teller E, 1938. Adsorption of Gases in Multimolecular Layers. J. Amer. Chem. Soc., **60**, 309–319.

BS1796, 1952. Methods for the Use of British Standard Fine Mesh Sieves.

Buysman P J and Peersman G A L, 1967. Stability of Ceilings in a Fluidized Bed. Proceedings of the International Symposium on Fluidization, Ed. A H H Drinkenberg, Eindhoven, Netherlands Univ. Press, Amsterdam, 38.

Carman P C, 1937. Fluid Flow through Granular Beds. Trans. Inst. Chem. Eng., **15**, 150–166.

Carr J F and Walker D M, 1967. Annular or Ring Shear Cell. Powder Tech. **1**, 369–373.

Carr R L; 1970. Particle Behaviour Storage and Flow. Brit. Chem. Eng., **15** (12) 1541–1549.

Cartwright P, Singh S and Bailey A G, 1982. IAS-IEEE Annual Meeting, San Fransisco, **41A**, 1162–1166.

Chaouki J, Chavarie C, Klvana D, Pajonk G, 1985. Effect of Interparticle Forces on the Hydrodynamic Behaviour of Fluidized Aerogels. Powder Tech., **43**, 117–125.

Cheng D C H, 1968. The Tensile Strength of Powders. Chem. Eng. Sci., **23**, 1405–1420.

Cheremisinoff N P and Cheremisinoff P N, 1984. Hydrodynamics of Gas–Solid Fluidization, Gulf Publ. Co., Houston, Tx., 8–9; Jenike shear cell 46–49.

Coste J and Pechery P, 1977. 3rd Int. Cong. on Static Electricity, Grenoble, 4a–4f.

Coste J and Pechery P, 1981. Influence of Surface Profile in Polymer–Metal Contact Charging. J. of Electrostatics, **10**, 129–136.

D'Amore M, Donsi G and Massimilla L, 1979. The Influence of Bed Moisture on Fluidization Characteristics of Fine Powders. Powder Tech., **23**, 253–259.

Dahneke B, 1972. The Influence of Flattening on the Adhesion of Particles. J. Colloid and Interface Sci., **40**, 1–13.

de Groot J H, 1967. Scaling up of Gas–Fluidized Bed Reactors. In Proceedings of the International Symposium on Fluidization, Eindhoven, Netherlands Univ. Press, Amsterdam, 348.

de Vries R J, van Swaaij W P M, Mantovani C and Heykoop A;1972. Design Criteria and Performance of the Commercial Reactor the Shell Chlorine Process. Proc. 5th Eur. Symp. Chem. React. Eng., Elsevier, Amsterdam, B9–B59.

Donsi G and Massimilla L, 1973a. Bubble–Free Expansion of Gas–Fluidized Beds of Fine Particles. AIChE J., **19** (6) 1104–1110.

Donsi G and Massimilla L, 1973b. Particle to Particle Forces in Fluidization of Fine Powders. Proc. Cong. Int. sur la Fluid et ses Appl, Toulouse, France, Publ. Soc. de Chim. Ind., Malmaison, France, 41–52.

Dry R J, Christensen I N and Thomas G C, 1988. The Effect of Naturally-Occuring Interparticle Forces on the Fluidization Characteristics of Fine Iron Oxide Powders. Chem. Eng. Sci., **43** (5) 1033–1038.

Dry R J, Judd M R, Shingles T, 1983. Two Phase Theory and Fine Powders. Powder Tech., **34**, 213–223.

Dry R J, Judd M R, Shingles T, 1984. Bubble Velocities in Fluidized Beds of Fine, Dense Powders. Powder Tech., **39**, 69–75.

Dry R J and Potter O E, 1986. Improved Throughput and Gas–solids contact in a Fluidized Bed: The Concept of a Bubble Collector. Powder Tech., **46**, 13–22.

Duffin W J, 1990. Electricity and Magnetism. 4th ed., McGraw Hill, Berkshire, England, p. 85.

Dutta A and Dullea L V, 1990. A Comparative Evaluation of Negatively and Positively Charged Submicron Particles as Flow Conditioners for a Cohesive Powder. AIChE symposium series, **86** (276) 26–40.

Dutta A and Dullea L V, 1991. Effects of External Vibration and the Addition of Fibres on the Fluidization of a Fine Powder. AIChE symposium series, **87** (281) 38–46.

Ergun S, 1952. Fluid Flow through Packed Columns. Chem. Eng. Prog., **48** (2) 89–94.

Fayed M E and Otten L, 1984. Handbook of Powder Science and Technology, von Nostrand Reinhold Co., 396–397.

Finnerty R G, Maa J R, Vossler A M, Yeh H S, Crouse W W, Rice W J, 1969. Waves at Surface of Fluidized Beds. I. and E. C. Fund., **8** (2), 271–278.

Foscolo P U and Gibilaro L G, 1984. A Fully Predictive Criterion for the Transition between Particulate and Aggregate Fluidization. Chem. Eng. Sci., **39** (12) 1667–1675.

Gallo C F and Lama W L, 1976. J. of Electrostatics, **2**, 145–150.

Geldart D, 1973. Types of Gas Fluidization. Powder Tech., **7**, 285–292.

Geldart D, 1972. The Effect of Particle Size Distribution on the Behaviour of Gas Fluidized Beds. Powder Tech., **6**, 201–215.

Geldart D, 1986. Gas Fluidization Technology, Wiley, Chichester.

Geldart D and Abrahamsen A R; 1980. The Effect of Fines on the Behaviour of Gas Fluidized Beds of Small Particles. School of Powder Technology, University of Bradford, 453–460.

Geldart D and Baeyens J; 1984. The Design of Distributors for Gas–Fluidized Beds. Powder Tech., **42**, 67–78.

Geldart D, Cullinan J, Georghiades S, Gilvray D, Pope D J, 1979. The Effect of Fines on Entrainment from Gas Fluidized Beds, Trans. Inst. Chem. Eng., **57**, 269–275.

Geldart D, Harnby N, Wong A C, 1984. Fluidization of Cohesive Powders. Powder Tech., **37**, 25–37.

Geldart D and Pope D J, 1983. Interaction of Fine and Coarse Particles in the Freeboard of a Fluidized Bed. Powder Tech., **34**, 95–97.

Geldart D and Wong A C Y, 1987. Entrainment of Particles from Fluidized Beds of Fine Powders. AIChE Symp. Ser., **83** (255) 1–9.

Gibilaro L G, di Felice R and Waldram S P; 1985. The Effect of Interparticle Forces on the Stability of Fluidized Beds. Chem. Eng. Sci., **40** (12), 2379–2381.

Godard K E and Richardson J F, 1968. The Behaviour of Bubble–Free Fluidized Beds. Inst. Chem. Eng. Symp. Ser., **30**, 126–135.

Grace J R, 1986. Contacting Modes and Behaviour Classifications of Gas–Solid and Other Two–Phase Suspensions. Can. J. Chem. Eng., **64**, 353–363.

Grace J R and Sun G; 1991. Influence of Particle Size Distribution on the Performance of Fluidized Bed Reactors. Can. J. of Chem. Eng., **69**, 1126–1134.

Guedes de Carvalho J F R, 1981. Dense Phase Expansion in Fluidized Beds of Fine Particles: The Effect of Pressure on Bubble Stability. Chem. Eng. Sci., **36**, 413–416.

Gugnoni R J and Zenz F A, 1980. Particle Entrainment from Bubbling Fluidized Beds. Fluidization, Eds. J R Grace and J N Matsen, Plenum Press, New York, 501–508.

Haider A and Levenspiel O, 1989. Drag Coefficient and Terminal Velocity of Spherical and Non–Spherical Particles. Powder Tech., **58**, 63–70.

Harper W R, 1967. 'Contact and Frictional Electrification', OUP.

Harrison D, Davidson J F and de Kock J W, 1961. On the Nature of Aggregative and Particulate Fluidization. Trans. Inst. Chem. Eng., **39**, 202–211.

Hartley P A and Parfitt G D, 1984. An Improved Split–Cell Apparatus for the Measurement of Tensile Strength of Powders. J. Phys. E: Sci. Instrum., **17**, 347–349.

Harrison D, Grace J F; 1971. Fluidized Beds with Internal Baffles. in Fluidization, Eds. Davidson J F, Academic Press, New York.

Hartley P A, Parfitt G D and Pollack L B, 1985. The Role of the van der Waals Force in the Agglomeration of Powders containing submicron Powders. Powder Tech., **42**, 34–46.

Hollenbach A M, Peleg M and Rufner, R, 1982. Effect of Four Anticaking Agents on the Bulk Characteristics of Ground Sugar. J. Food Sci., **47**, 538–544.

Jackson R, 1963. The Mechanics of Fluidized Beds, Part I. The Stability of the state of Uniform Fluidization. Trans. Inst. Chem. Eng., **41**, 13–21.

Jean R H, Eubank R, Jiang P and Fan L S; 1990. On the Fluidization Behaviour of Polymeric Particles in Gas–Solid Fluidized Beds. AIChE Annual Meeting, Chicago, 1–26.

Jenike A W, 1961. Bulletin 108: Jenike Shear Cell. Univ. of Utah, Utah.

Jenike A W and Carson J W, 1987. Measurement Principles of Flowability of Powders. Adv. in Ceramics, **21**, Ceramic Powder Sci., The American Cer. Soc.

Jones D H, Schingles T, Kelley F T and Dry M E; 1980. Fluidization Promoters. U. S. Patent 4, 225, 531.

Jottrand R, 1952. An Experimental Study of the Mechanism of Fluidization. J. Appl. Chem., **2**, S17.

Jovanovic Z, Kimura S and Levenspiel O; 1992. Extended Abstracts for the AIChE Annual Meeting, Miami, 188h.

Koch W H and Licht W, 1977. New Design Approach Boosts Cyclone Efficiency. Chemical Engineering, 80–87.

Kokkoris A and Turton R, 1991. The Reduction of Attrition in Fluidized Beds by the Addition of Solid Lubricants. AIChE Symp. Series, **87** (281) 20–31.

Kono H O, Chiba S, Ells T S, Daniell P and Suzuki M, 1989. The Effect of Emulsion Phase Characteristics on Fluidization–Selection of Powder Properties. in Fluidization V, Proc. of the 5th Eng. Found. Conf. on Fluidization, Ed. K Ostergaard and A Sorensen, Eng. Found., New York, 143–150.

Kono H O, Chiba S, Ells T and Suzuki M, 1986. Characterization of the Emulsion Phase in Fine Particle Fluidized Beds. Powder Tech., **48**, 51–58.

Kono H O, Chiba S, Suzuki M, Daniell P and Ells T, 1985. The Effect of Interparticle Adhesion Force on Fluidization. AIChE Conf., Chicago, AIChE, NY, 1–17.

Kono H O, Ells T S, Chiba S, Suzuki M and Morimoto E, 1987. Quantitative Criteria for Emulsion Phase Characterization and for the Transition between Particulate and Bubbling Fluidization. Powder Tech., **52**, 69–76.

Kono H O, Huang C C, Morimoto E, Nakayama T and Hikosaka T, 1987. Segregation and Agglomeration of Type C Powders from Homogeneously Aerated Type A–C Powder Mixtures during Fluidization. Powder Tech., **53**, 163–168.

Kono H O, Huang C C and Xi M, 1988. Characterization of Fine Bulk Powders by Rheological Properties of the Gas–Powder Colloid Structure at Aerated Conditions. AIChE Symp. Series, Fluidization Eng. Fund. and Appl., **84** (262) 74–81.

Kono H O, Matsuda T, Huang C C and Tian D C, 1990. Agglomeration Cluster Formation of Fine Powders in Gas–Solid Two–Phase Flow. AIChE Symp. Series, **86** (276) 72–77.

Kono H O and Tian D C, 1992. Densification and Modification of Bulk Flow Properties of Ultrafine Powders in Fluidized Beds. Fluidization VII. Eds. O E Potter and D J Nicklin, Engineering Foundation, New York, 555–561.

Krupp H, 1967. Particle Adhesion, Theory and Experiment. Advances in Colloid and Interface Science, Eds. J T G Overbeek, W Prins, A C Zettlemoyer, Elsevier, Amsterdam, 116–239.

Kunii D and Levenspiel O, 1991. Fluidization Engineering, 2nd ed., Butterworths, Boston, p. 80–81.

Langbein D, 1969. J. of Adhesion, **1**, 237.

Lauga C, Chaouki D, Klvana D, Chavarie C, 1991. Improvement of the Fluidizability of Ni/SiO_2 Aerogels by Reducing Interparticle Forces. Powder Tech., **65**, 461–468.

Liu Y D and Kimura S, 1993. Fluidization and Entrainment of Difficult–to–fluidize Fine Powder Mixed with Easy–to–fluidize Large Particles. Powder Tech., **75**, 189–196.

Massey, B S; (1979). Mechanics of Fluids, 4th ed., Van Nostrand Reinhold, London.

Lowell S and Shields J E, 1984. Powder Surface Area and Porosity. 2nd ed., Chapman and Hall, London, p. 17–18, 217–218, 221–222.

Martin, P D, 1983. On the 'Particulate' and 'Delayed Bubbling' Regimes in Fluidization. Shorter Comm., Chem. Eng. Res. Des., **61**, 318–320.

Massimilla L and Donsi G, 1976. Cohesive Forces between Particles of Fluid Bed Catalysts. Powder Tech., **15**, 253–260.

Massimilla L, Donsi G, Zucchini C, 1972. The Structure of Bubble–Free Gas Fluidized Beds of Fine Fluid Cracking Catalyst Particles. Chem. Eng. Sci., **27**, 2005 –2015.

Matheson G L, Herbst W A, Holt P H, 1949. Characteristics of Fluid–Solid Systems. Ind. Eng. Chem., **41**, 1099–1104.

Merrick D and Highley J, 1974. Particle Size Reduction and Elutriation in a Fluidized Bed Process. AIChE Symp. Series, **70** (137) 366–378.

Meissner H P, Michaels A S and Kaiser R, 1964. Spontaneous Pelletization in Fine Powders. Ind. Eng. Chem. Proc. Des. and Dev., **3** (3) 197–201.

Molerus O, 1967. Hydrodynamische Stabilität des Fliessbetts. Chem. Ing. Tech., **39**, 341–348.

Mori S, Iwasaki N, Mizutani E and Okada T, 1992. Vibro–Fluidization of Two–Component Mixtures of Group C Particles. Proc. Fluidization VII. Eds. O E Potter and D J Nicklin, Engineering Foundation, New York, 571–578.

Mori S, Yamamoto A, Iwata S, Haruta T, Yamada I, Mizutani E, 1990. Vibro–Fluidization of Group C Particles and Its Industrial Applications. AIChE Symp. Series, **86** (276) 88–94.

Morooka S, Kusakabe K, Kobata A and Kato Y, 1988. Fluidization State of Ultrafine Powders. J. Chem. Eng. Japan, **21** (1) 41–46.

Murray J D, 1965. On the Mathematics of Fluidization. Part 1. Fundamental Equations and Wave Propagation. J. Fluid Mech., **21**, 465–493.

Mutsers S M P, 1977. PhD Thesis, Eindhoven University, The Netherlands.

Mori Y, Himeno N, Hijikata K and Miyauchi T; 1980. Effects of Vibrational Relaxation of Multi–Atomic Molecules on Stagnation Heat Transfer. Int. J. Heat and Mass Transfer, 23, 1625.

Mutsers S M P and Rietema K, 1977a. The Effect of Interparticle Forces on the Expansion of a Homogeneous Gas-Fluidized Bed. Powder Tech., **18**, 239–248.

Mutsers S M P and Rietema K, 1977b. Gas–Solid Fluidization in a Centrifugal Field; The Effect of Gravity on Bed Expansion. Powder Tech., **18**, 249–256.

Newton D, 1984. The Influence of Fine Particles on the Performance of a Fluidized Bed Reactor. PhD Thesis, University College London.

Nienow A W and Chiba T, 1985. Fluidization of Dissimilar Material. in Fluidization, Eds. Davidson J F, Clift L and Harrison D, Academic Press, Second edition, 357–381.

Nienow A W, Rowe P N and Chiba T, 1978. Mixing and Segregation of a Small Proportion of Large Particles in Gas Fluidized Beds of Considerably Smaller Ones. AIChE sym. series, **74** (176) 45–53.

Oltrogge R D, 1972. Gas Fluidized Beds of Fine Particles. PhD Thesis, Univ. of Michigan.

Ormiston R M, Mitchell F R G and Davidson J F, 1965. The Velocities of Slugs in Fluidized Beds. Trans. Inst. Chem. Eng., **43**, 209–216.

Pacek A W and Nienow A W, 1990. Fluidization of Fine and Very Dense Hard–Metal Powders. Powder Tech., **60**, 145–158.

Pell M and Jordan S P; 1988. Effects of Fines and Velocity on Fluid Bed Reactor Performance. Fluidization Engineering; Fund. and Appl., AIChE Symp. Ser., **84** (262), 68–73.

Piepers H W, Cottaar E J E, Verkooijen A H M and Rietema K, 1984. Effects of Pressure and Type of Gas on Particle–Particle Interaction and the Consequences for Gas–Solid Fluidization Behaviour. Powder Tech., **37**, 55–70.

Pigford R L and Baron T, 1965. Hydrodynamic Stability of a Fluidized Bed. Ind. Eng. Chem. Fundam., **4**, 81–87.

Reiling V G, 1992. The Effects of Ultrafine Particles on Powder Cohesion and Fluidization. PhD Thesis, Case Western Reserve University.

Richardson J F and Meikle R, 1961. Sedimentation and Fluidization; Part III. The Sedimentation of Uniform Fine Particles and of Two–Component Mixtures of Solids. Trans. Inst. Chem. Eng., **39**, 348–356.

Richardson J F and Zaki W N, 1954. Sedimentation and Fluidization; Part I. Trans. Inst. Chem. Eng., **32**, 35–53.

Rietema K, 1967. Application of Mechanical Stress Theory to Fluidization. In Proceedings of the International Symposium on Fluidization, Ed. A H H Drinkenberg, Eindhoven, Netherlands Univ. Press, Amsterdam, 154–175.

Rietema, 1973. The Effect of Interparticle Forces on the Expansion of a Homogeneous Gas–Fluidized Bed. Chem. Eng. Sci., **28**, 1493–1497.

Rietema K, 1984. Powders, What Are They? Powder Tech., **37**, 5–23.

Rietema K, 1991. The Dynamics of Fine Powders. Elsevier Science, England, p. 135–136.

Roscoe K H, 1953. Proc. 3rd Int. Conf. Soil Mechanics I, **2**, 186.

Rowe P N, Everett D J, 1972. Fluidized Bed Bubbles Viewed by X-rays; Part II. The Transition from Two to Three Dimensions of Undisturbed Bubbles. Trans. Inst. Chem. Eng., **50**, 49–54.

Rowe P N, Foscolo P U, Hoffman A C and Yates J G, 1982. Fine Powders Fluidized at Low Velocity of Pressures up to 20 Bar with Gases of Different Viscosity. Chem. Eng. Sci., **37**, 1115–1117.

Rowe P N, Nienow A W and Agbim A J, 1972b. The Mechanisms by which Particles Segregate in Gas Fluidized Beds– Binary Systems of Near-Spherical Particles. Trans. Inst. Chem. Eng., **50**, 310–323.

Rowe P N, Nienow A W and Agbim A J, 1972c. A Preliminary Quantitative Study of Particle Segregation in Gas Fluidized Beds – Binary Systems of Near Spherical Particles. Trans. Inst. Chem. Eng., **50**, 324–333.

Rowe P N, Partridge B A, Cheyney A G, Henwood G A and Lyall E, 1965. The Mechanisms of Solids Mixing in Fluidized Beds. Trans. Inst. Chem. Eng., **43**, 271–286.

Rooney N M and Johanson L N; 1962. Factors Affecting Fluidized Bed Quality. Chem. Eng. Prog. Symp. Ser., **58** (38), 28.

Rowe P N, Santoro L and Yates J G; 1978. The Division of Gas between Bubble and Interstitial Phases in Fluidized Beds of Fine Powders. Chem. Eng. Sci., **33**, 133–140.

Rowe P N and Yacono C X R, 1978. The Bubbling Behaviour of Fine Powders when Fluidized. Chem. Eng. Sci., **31**, 1179.

Rumpf H, 1970. Zur Theorie der Zugfestigkeit von Agglomaraten bei Kraftübertragung an Kontaktpunkten, Chem. Ing. Tech., **42**, 538–840.

Seville J P K and Clift R, 1984. The Effect of thin Liquid Layers on Fluidization Characteristics. Powder Tech., **37**, 117–129.

Shimizu M, Fukuoka H and Fukuhira M; 1991. Japan Kokai Tokyo Koho, 3–60410 and 3–60411; U. S. Patent 5073358.

Steeneken P A M, Woortman A J J, Gerritsen A H, Poort H, 1986. The Influence of Flow Conditioners on Some Mechanical Properties of Potato Starch Powder. Powder Tech., **47**, 239–246.

Streeter V L and Wylie E B, 1985. Fluid Mechanics. 8th ed., McGraw Hill, USA, p. 379–380.

Sun G and Grace J R; 1990. The Effect of Particle Size Distribution on the Performance of a Catalytic Fluidized Bed Reactor. Chem. Eng. Sci., **45** (8), 2187–2194.

Trawinski H, 1951. Zur Hydrodynamik Aufgewirbelter Partikelschichten. Chem. Ing. Tech., **23**, 416–419.

Trawinski H, 1953. Entmischung Gasdurchströmter Partikelschichten und deren Zusammenhang mit der Wirbelschichtzähigkeit. Chem. Ing. Tech., **25**, 201–203.

Toomey R D and Johnstone H F, 1952. Gaseous Fluidization of Solid Particles. Chem. Eng. Prog., **48**, 220–226.

Tsubaki J and Jimbo G, 1984. Theoretical Analysis of the Tensile Strength of a Powder Bed. Powder Tech., **37**, 219–227.

Turton R and Clark N N, 1987. An Explicit Relationship to Predict Spherical Particle Terminal Velocity. Powder Tech., **53**, 127–129.

van Swaaij W P M; 1985. Chemical Reactors. In Fluidization, Eds. Davidson J F, Clift R and Harrison D, 2nd ed., Academic Press, London, p. 598–600.

Verloop J and Heertjes P M, 1970. Shock Waves as a Criterion for the Transition from Homogeneous to Heterogeneous Fluidization. Chem. Eng. Sci., **25**, 825–832.

Visser J, 1976. in Surface and Colloid Interface Science, Ed. E Matijevic, Vol 8, Wiley, New York.

Visser J, 1989. An Invited Review: van der Waals and Other Cohesive Forces Affecting Powder Fluidization. Powder Tech., **58**, 1–10.

Wallis G B, 1969. One Dimensional Two–Phase Flow, McGraw Hill, New York.

Welty J R, Wicks C E and Wilson R E, 1984. Fundamentals of Momentum, Heat, and Mass Transfer. 3rd ed., John Wiley & sons, New York, p. 98–99.

Wen C Y and Yu Y H, 1966. A Generalized Method for Predicting the Minimum Fluidization Velocity. AIChE J., **12**, 610–612.

Whitmore R L, 1957. The Relationship of the Viscosity to the Settling Rate of Slurries. J. Inst. Fuel, **30**, 238–242.

Yang Z, Tung Y and Kwauk M, 1985. Characterizing Fluidization by the Bed Collapsing Method. Chem. Eng. Comm., **39**, 217–232.

Yates J G, 1983. Fundamentals of Fluidized–bed Chemical Processes, Butterworths, London, pp. 4–16, 37–38.

Yates J G and Newton D; 1986. Fine Particle Effects in Fluidized Bed Reactors. Chem. Eng. Sci., **41**, 801.

Yates J G, Rowe P N and Cheesman D J, 1984. Gas Entry Effects in Fluidized Bed Reactors. AIChE J., **30** (6) 890–894.

Yokoyama T, Fuji K and Yokoyama T, 1982. Measurement of the Tensile Strength of a Powder Bed by a Swing Method Measuring Instrument. Powder Tech., **32**, 55–62.

York P, 1975. The Use of Glidants to Improve the Flowability of fine Lactose Powder. Powder Tech., **11**, 197–198.

Zenz F A, 1957. Influence of Particle Size Distribution on Fluidization Characteristics. Petr. Refiner, **36**, 261.

Zenz F A, 1984. Observations Leading to a Suggested 'Catalyst Size Formulation' Enhancing Fluidity and Contacting Effectiveness.

Zenz F A and Weil N A, 1958. A Theoretical–Empirical Approach to the Mechanism of Particle Entrainment from Fluidized Beds. AIChE J., **4** (4) 472–479.

Zenz F A; 1968. Bubble Formation and Grid Design. IChemE Symp.Ser.: Inst. Chem. Eng., London, No. 30, 55–58.